

N 70 25301

NASA CR102609

PROPULSION DIVISION

STABILITY CHARACTERIZATION OF ADVANCED INJECTORS

[REDACTED] Final Report on Phase I of
Contract NAS 8-20672

Prepared for

MARSHALL SPACE FLIGHT CENTER
Huntsville, Alabama

Report 20672-PI **[REDACTED]** F

25 October 1968

CASE FILE
COPY



AEROJET-GENERAL CORPORATION

SACRAMENTO, CALIFORNIA



STABILITY CHARACTERIZATION OF
ADVANCED INJECTORS

Final Report on Phase I of
Contract NAS 8-20672

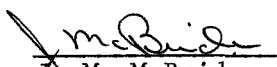
Prepared for

MARSHALL SPACE FLIGHT CENTER
Huntsville, Alabama

Report 20672-PIF

25 October 1968

Approved


J. M. McBride
Project Manager


C. B. McGough
Program Manager



AEROJET-GENERAL CORPORATION
A SUBSIDIARY OF THE GENERAL TIRE & RUBBER COMPANY

Report 20672-PIF

TABLE OF CONTENTS

	<u>Page</u>
I. Introduction	1
II. Summary	2
A. Summary of Program	2
B. Task I: Analytical Model Development	3
C. Task II: Annular Thrust Chamber Assembly Tests	5
D. Task III: Transverse Excitation	7
III. Conclusions	10
IV. Experimental Tasks	13
A. Test Apparatus	13
B. Test Procedure	20
C. Test Results	28
V. Analytical Tasks	34
A. Annular Thrust Chamber Analysis	34
B. Staged Combustion Model	38

FIGURE LIST

	<u>Figure No.</u>
Annular Thrust Chamber Assembly on Test Stand C-6	1
Transverse Excitation Chamber with Lid Removed	2
High Injection Density Annular Triplet Injector Schematic	3
Low Injection Density Triplet Injector Schematic	4
Annular Coaxial Injector Schematic	5
Annular Coaxial Injector	6
Annular Thrust Chamber Assembly	7
Excitation Chamber Triplet Injector Insert Schematic	8
Transverse Excitation Chamber Assembly Schematic	9
Isometric Drawing of Test Stand C-6	10
View of C-6 Test Stand and Intensifiers	11
Typical Start Transient Record of an Annular Coaxial Test on Test Stand C-6	12
Flow Schematic for Test Stand C-6	13
Transverse Excitation Chamber on Test Stand J-1	14
Flow Schematic for Test Stand J-1	15
Typical Start Transient for a Transverse Excitation Chamber Test on Test Stand J-1	16
Initial Pulse Amplitude $P_c = 1000$ psia	17
Initial Pulse Amplitude $P_s = 2500$ psia	18
High Frequency Stability Results - All Injectors at 900 P_c 1200 psia	19
High Frequency Stability Results - All Injectors at 2400 P_c 2700 psia	20
Impingement - Velocity Ratio Function Versus $VRSin\phi$ for Impinging Coaxial Element	21
Frequency Response Characteristics of Triplet Injectors	22
Effect of Pressure on Non-Coaxial Elements	23
Tangential Mode Acoustic Frequencies for Annular Chambers	24
Staged Combustion Model	25
Effect of Pressure on Impinging Coaxial Injectors	26

Report 20672-PIF

FIGURE LIST (cont.)

	<u>Figure No.</u>
Case I, Orifice Diameter Versus Stability	27
Case II, Orifice Diameter Versus Stability	28
Computer Program Flow Schematic	29
Computer Program flow Schematic	30
Data Package Computer Deck Organization	31
Annular Combustion Computer Input Parameters	32
Annular Chamber Computer Input Parameters	33
Cylindrical Chamber Computer Input Parameters	34
n, τ Plots	35
n, τ Plots	36
n, τ Plots	37

TABLE LIST

	<u>Table No.</u>
Comparison of Coaxial Elements, NAS 8-11741 and NAS 8-20672	1
Coaxial Injector Design Characteristics	2
Comparison of Triplet Injector Designs	3
Engine Nozzle Design Parameters	4
Design Features of Excitation Chamber Injectors	5
Acoustics Frequencies of Excitation Chamber	6
Excitation Chamber Nozzle Throat Width	7
Steady State and Stability Test Results	8
Excitation Engine Performance Data Summary	
11-Element Triplet Injector	9
Transverse Excitation Chamber High Frequency Data	10
Bessel Function Value ($S_{v\eta}$) for Tangential Modes in Annular Chambers $_{ann}$	11

NOMENCLATURE

P	Pressure
u	Mach number
ψ	Radial dependence of pressure
θ	Tangential dependence of pressure
R'	Ratio of inner radius to outer radius
γ	Ratio of specific heats
A	Area of nozzle
s	Laplace variable
z	Axial distance
c	Speed of sound
n	Interaction index
R	Mixture ratio
α	Longitudinal nozzle admittance coefficient
\dot{m}	Mass flow rate
τ	Time lag
ρ	Density
L	Length of chamber
Z	Orifice resistance
G	Flow admittance
B	$\frac{1 + \alpha \bar{u}}{1 - \alpha \bar{u}}$
P	$n(1 - e^{-s\tau})$
F	Defined by Equation 7
$A_{v\eta}, B_{v\eta}, C_{v\eta}$	Distribution coefficients
C_1, C_2	Constants
$S_{v\eta}$	Separation constant
Subscripts:	
x	oxidizer
f	fuel
p	primary
s	secondary
t	turbine

I. INTRODUCTION

The purpose of Phase I of this program was to determine the stability characteristics of various injectors using high combustion chamber pressures with the cryogenic propellants, hydrogen and oxygen. Coaxial injectors for the most part were characterized under previous programs at Aerojet, NASA, and other government subcontractors. The remaining design feature to be evaluated on the coaxial injector was the effect of injection density on combustion stability. This effect was evaluated during the test portion of this program in an annular combustion chamber.

Combustion stability correlations based on Sensitive Time Lag Theory require an accurate definition of theoretical considerations. Consequently, part of the investigation necessary to advance current knowledge in combustion stability was the advancement of Sensitive Time Lag Theory. A refinement to the basic theory was the addition of terms to account for higher combustion chamber Mach numbers and an extension of the current model to include the toroidal or annular combustors.

As part of the experimental program an experimental tool, the "Transverse Excitation Chamber," was designed and the feasibility of using this tool to measure the frequency sensitivity of a particular injector demonstrated.

Many preliminary designs were evaluated prior to the selection of the designs fabricated and tested on this program.

Phase I was scheduled for 12 months of technical effort, but was extended to 15 months to include additional hardware fabrication.

II. SUMMARY

A. SUMMARY OF PROGRAM

The stability characteristics of two injection concepts to be used in advanced injectors for high chamber pressure, hydrogen/oxygen systems were determined on this phase of the program. The two injection concepts tested were: coaxial with central oxidizer and 30° included angle fuel impingement; and triplet injectors with 60° included angle oxidizer-fuel-oxidizer pattern. Analytical model developments were advanced for the Sensitive Time Lag Theory, and a research tool termed "Transverse Excitation Chamber" was demonstrated.

Analytical model developments included expansion and refinement of the existing Sensitive Time Lag model to include annular combustion chambers and initiation of analyses to include feed system coupled pressure oscillations as encountered with the staged combustion system.

The second major task consisted of testing injector patterns in an annular thrust chamber. Injectors designed and fabricated for this task included one coaxial and two versions of one basic triplet element pattern. The coaxial injector was patterned after an injector tested on Contract NAS 8-11741, except that the injection density (total propellant flow rate per projected injector face area) was nearly doubled. The triplet injectors were patterned after a design being considered for NASA's Advanced Cryogenic Rocket Engine. The major difference between the two versions of this injection pattern is that one has nearly twice the injection density of the other. Seven tests on the coaxial injector were made under this task. Two triplet injectors were also fabricated.

The third major task consisted of the design, development, and demonstration of a research tool, the "Transverse Excitation Chamber." This combustor is a variable angle sector chamber that can be varied from 9 to 36°

II, A, Summary of Program (cont.)

and is used to determine the relative sensitivity of injection elements to instability. Six tests conducted with this combustion chamber yielded preliminary results on its effectiveness as a research tool.

A detailed analysis of combustion stability data obtained during the testing of this program is included in this report, and correlations with results from tests conducted on other programs were made. Considerable injector design studies were conducted on this program.

B. TASK I: ANALYTICAL MODEL DEVELOPMENT

1. Annular Combustor Analysis

Analytical tasks on this program included the extension of the basic Sensitive Time Lag model for cylindrical combustion chamber to include annular chambers. A preliminary analysis for the gas-generator-fed staged combustion system was also made.

The analysis for the annular combustion chamber fits into the basic framework of the cylindrical chamber analysis; a few minor modifications are required. In the general solution of the pressure perturbation equation by using separation of variables technique the solution is:

$$P_o = P_o(z) \psi_o(r) \theta_o(\theta)$$

Three ordinary differential equations for $P_o(z)$, $\psi_o(r)$ and $\theta_o(\theta)$ are obtained.

The solution for the annular combustion chamber case is concerned with the solution of $\psi_o(r)$. The differential equation for $\psi_o(r)$ is a Bessel equation of the form: $\psi_{\nu\eta}(r) - AJ_{\nu}(S_{\nu\eta} \cdot r) + BY_{\nu}(S_{\nu\eta} \cdot r)$

II, B, Task I: Analytical Model Development (cont.)

where: J_v = Bessel function of the first kind
 Y_v = Bessel function of the second kind
 $S_{v\eta}$ = the transverse mode number

By considering the cylindrical chamber case and the inner wall for the annular case separately and solving these two relationships simultaneously one obtains the following result:

$$J'_v(S_{v\eta}) Y'_v(S_{v\eta} R) - J'_v(S_{v\eta} R) Y'_v(S_{v\eta}) = 0$$

The solution of this equation defines the transverse acoustic mode number, $S_{v\eta}$, for annular chambers. This equation has been solved in published literature and values of $S_{v\eta}$ are listed. Annular combustion chambers will alter the frequency of the transverse mode from the cylindrical case.

The configuration of the exhaust nozzle affects the nozzle admittance coefficient in much the same manner as for the cylindrical combustion chamber nozzle. The analysis for the annular nozzle is different primarily in the determination of the local contraction ratio. This is accomplished in the computer program by inputting both the inner and outer radii of the chamber and throat.

2. Staged Combustion Model

The system selected for the staged combustion model consists of (1) propellant feed system, (2) primary combustor, (3) secondary combustor, and (4) a turbine. The approach taken was to assume that the engine design parameters are given. The instability zones are then calculated for the secondary combustor, for assumed values of the primary combustion parameters (n_p, τ_p) and the total time lag of the hot gas τ_{FS} . The shift of the instability zones as these combustion parameters are varied shows the nature of the interaction between the two combustors.

II, B, Task I: Analytical Model Development (cont.)

The first-order analysis involves the following assumptions: the propellants are incompressible, the feed lines are short, the combustion is concentrated at the injector, and mean chamber Mach numbers are small.

As a general result of this analysis, it has been observed that the total time lag is from 6 to 10 times larger than the sensitive time lag. Consequently, for frequencies of interest to high frequency instability, the effects of the feed system terms will tend to average over the finite length of the combustion zone. Since the total time lag includes the time required for atomization, vaporization, mixing, and heating of the propellants, some interaction is likely in high pressure engines -- particularly in the secondary combustor.

C. TASK II: ANNULAR THRUST CHAMBER ASSEMBLY TESTS

Annular thrust chamber assembly hardware consisted of three major components: (1) injector with attached axial centerbody, (2) combustion chamber, and (3) annular nozzle. Of the injectors designed for the annular combustion chamber, three were fabricated and one tested. A 600-element triplet injector to deliver 60,000 lb thrust with a total propellant weight flow of 180 lb/sec was fabricated, and a 200-element triplet injector to deliver 20,000 lb thrust with 60 lb/sec total propellant weight flow was also fabricated. To evaluate the effect of injection density on stability a 54-element coaxial injector was designed, fabricated, and tested for comparison with injectors previously built on Contract NAS 8-11741.

The combustion chamber and centerbody were ablatively cooled and both centerbody and chamber converged to form a throat. Two pyrotechnic igniters, three pulse guns, eight high-frequency pressure transducers and three static pressure transducers were located on the combustion chamber.

Report 20672-PIF

II, C, Task II: Annular Thrust Chamber Assembly Tests (cont.)

Tests were conducted at mixture ratios from 4 to 6 and chamber pressures of from 1500 to 2500 psia at a constant propellant weight flow of 180 lb/sec.

Each instability pattern observed during the annular testing was nearly identical in its form and was initiated by the 20-grain charge, using a tangential pulse gun. The peak-to-peak overpressures of these instabilities ranged from 800 to 2000 psi. The frequency was approximately 2500 Hz, depending on the acoustic velocity value for each test condition.

Test No. 7, using 200°R hydrogen, experienced -- in addition to its high-frequency instability -- a low-frequency (500 Hz) oscillation which attained an amplitude of 750 psi. Except for one brief occurrence of a low frequency (100 Hz and 100 psi) instability on Test No. 3, there was no other indication of a coupling between the feedlines and the combustion process. It should be pointed out that the large pressure drops across the injector face due to the small orifice design result in significant hydraulic resistances in the circuit.

The effect of chamber Mach number was evaluated in this series of tests by comparing results with test results from Contract NAS 8-11741. The two Mach numbers used were 0.176 and 0.29.

This verification of the Mach number as an important correlating parameter, together with the work of NASA's Lewis Research Center, has led to the selection of six design parameters as being important in combustion stability evaluations. These parameters are functionally related by the following formula:

II, C, Task II: Annular Thrust Chamber Assembly Tests (cont.)

$$f_s = 4550 \left(\frac{M_c}{d_i} \right)^{0.15} \frac{(P_c/P_{\text{critical}})^{1/3}}{F}$$

where:	f_s	=	Sensitive frequency (Hz)
	M_c	=	Chamber Mach Number
	d_i	=	Injection orifice diameter of least volatile propellant, inches
	P_{critical}	=	Critical pressure of least volatile time controlling propellant, psia
	P_c	=	Chamber pressure, psi
	F	=	Function of the velocity ratio and impingement angle. This function is not defined for the nonimpinging showerhead coaxial element.

This formula may be used by a designer in his preliminary work to develop an injector configuration whose sensitive frequency is displaced from the first tangential acoustic mode of the thrust chamber. These first order estimates may then be combined with the analytical results of the sensitive time lag computer program to obtain a more detailed engine configuration. Of prime importance is the overall trends which may be observed from changes in any of the six design parameters.

D. TASK III: TRANSVERSE EXCITATION CHAMBER TESTING

The concept of a transverse excitation was originated at Aerojet on a Company-sponsored Independent Research and Development program to evaluate transverse modes of pressure oscillation (tangential instabilities) and simulate the pressure/velocity effects as experienced in a rocket combustion chamber. The transverse excitation chamber tested on this program is described in the following paragraphs.

II, D, Task III: Transverse Excitation Chamber Testing (cont.)

The excitation chamber consisted of three principal parts: (1) chamber, (2) nozzle, and (3) injector inserts. The chamber is a 36° sector of a circle 2-1/4 inches in height. The 36° sector of the 30-inch radius results in a fundamental acoustic frequency in the transverse mode at 1800 Hz. The smallest chamber angle was 9°, which results in a chamber acoustic frequency of 7000 Hz. The height of the chamber (2.17) inches limits the associated acoustic frequency to greater than 13,000 Hz. A single chamber design was used and the chamber angle was varied by inserting steel wedges in the combustion zone to achieve the desired angle. The O-ring-sealed chamber lid is removable to facilitate various injection concepts; ablative liners and throats were used to protect the areas most vulnerable to erosion.

Two triplet injectors were designed and fabricated for testing. One was an 11-element triplet, and the other was a three-element triplet similar to the 11-element triplet design in all but the orifice diameters. The purpose of the larger orifice size was to determine the effect of orifice diameter or thrust per element on combustion stability. Only the 11-element injector inserts were tested during this program.

Testing of the transverse excitation chamber was conducted to measure the growth rates of spontaneous instabilities or decay rates of pulsed pressure perturbations.

Mixture ratios of around 4 and chamber pressures of 1300 to 1400 psi were evaluated during the test series. Two of the three valid tests (in three tests the fuel valve was inoperative) attained these conditions and both experienced spontaneous instabilities. One test exhibited a growth rate of 650 db/sec, while the other test had two distinct growth periods. The first, occurring at the onset of the instability, had a 600 db/sec rate, while the second growth period came after thermal ignition of the 40 grain pulse charge had disrupted the initial instability. Its growth rate was 330 db/sec.

II, D, Task III: Transverse Excitation Chamber Testing (cont.)

From the data obtained, the indication is that over the frequency range of 3000 to 4500 Hz the triplet element has a peak response at 3300 Hz at the specified steady state conditions. This peak response frequency, when related to τ by the relationship

$$\tau = \frac{1}{2f}$$

compares favorably with previous correlations of τ for this type of injector.

III. CONCLUSIONS

1. The use of combustion chamber Mach number as a stability correlating factor was examined and was found to have a relatively minor effect which appears to be related to the sensitive frequency as follows:

$$f_s = 4550 \left(\frac{M_c}{d_i} \right)^{0.15} \frac{(P_c/P_{crit})^{0.33}}{F}$$

f_s	=	Sensitive frequency
M_c	=	Chamber Mach Number
d_i	=	Injection orifice diameter of least volatile propellant (inches)
P_{crit}	=	Critical pressure of least volatile propellant (psia)
P_c	=	Chamber pressure, (psia)
F	=	Function of the velocity ratio and impingement angle

2. For the annular chamber tests, all recorded high frequency instabilities were pure first tangential modes pulsed at a comparatively low shock level (20 grains). This indicates that, for the operating parameters, the combustion process was close to its spontaneous oscillation regime.

3. The incidence of pure modes rather than the mixed modes noted with previous tests with a cylindrical chamber indicates a higher value for the sensitive time lag (τ) and, correspondingly, a lower sensitive frequency value (since $\tau = \frac{1}{2f}$). This conclusion is logical when the annular chamber design is considered. Placing the centerbody in the injector has two effects: (1) the centerbody acts as an effective barrier against the radial modes, and (2) the integrated effect of propellant injection (mass distribution) is over larger radial distances -- or in a zone of greater tangential acoustic mode sensitivity.

III, Conclusions (cont.)

4. The fact that lower pulse charges triggered instability does not necessarily indicate a reduction in pressure interaction index (the sensitive time lag term, n). This apparent increased combustion sensitivity could be due to the fact that pure modes are initiated at lower n values than are the combined modes. In fact it is analytically theorized that the pressure interaction index, n , was approximately the same for both the cylindrical and the annular chamber coaxial injection test phases (that is equal to approximately 0.5).

5. The excitation chamber has potential as a stability rating tool which will give many inexpensive tests and will evaluate many single parameter characteristics of an injection pattern. A complete spectrum of frequencies can be evaluated; short duration tests are adequate to evaluate an injector. Injector modules are inexpensive and easily replaced; the removable chamber lid permits testing of long injection elements (i.e., tubelet or HIPERTHIN), servicing of the combustion chamber protective coating, and removal and replacement of wedge inserts.

6. It is recommended that dynamic high frequency transducers be flush mounted for proper wave description.

7. It is recommended that the transverse excitation chamber as a research tool be used extensively to evaluate the effect on combustion stability of the various injection parameters (i.e., injection velocities, velocity ratio, fuel temperature orifice chambers, injection distribution, etc.) on a variety of injection concepts (i.e., triplets, quadlets, coaxial, HIPERTHIN, etc.). These tests should serve as a single parameter variation test and should evaluate a range of design and test conditions to determine optimum operating conditions for combustion stability and performance for a given injector design.

III, Conclusions (cont.)

8. It is recommended that a limited number of verification tests be conducted using conventional cylindrical or annular combustion chambers to evaluate the injectors tested in the transverse excitation chamber in pulse rated stability tests. These tests should serve as demonstration tests to determine correlations between conventional injectors and excitation chamber results.

IV. EXPERIMENTAL TASKS

A. TEST APPARATUS

1. General

The stability characteristics of advanced injection concepts were evaluated on this program by two methods: full-scale annular thrust chamber assemblies and subscale single-parameter evaluations in a transverse excitation chamber. The ablatively cooled full-scale hardware was tested with a coaxial injector for an average test duration of 2.0 sec, developing a nominal thrust of 65,000 lb. Triplet injectors were also designed and fabricated for testing in the annular hardware. The subscale excitation chamber hardware was designed specifically to determine the frequency response characteristics of selected injection elements on a single design parameter variation basis. Because of particular design features of the excitation chambers, the thrust level was lower for the high-frequency testing (minimum 2000 lb) and higher for the lower frequencies (maximum 8000 lb). Figure 1 shows the full-scale annular hardware mounted on the test stand with the center body cone attached. Figure 2 shows the excitation chamber with the lid removed and one of the wedges installed. Detailed descriptions of each system and test hardware are given in the following paragraphs.

2. Full-Scale Annular Thrust Chamber Assembly

The full-scale annular thrust chamber assembly consisted of three major components: (1) injector with attached axial center body, (2) combustion chamber, and (3) annular nozzle. Hot gas joints on this assembly were sealed by thin Durabola gaskets placed between serrated sealing surfaces.

IV, A, Test Apparatus (cont.)

a. Injectors

Three injectors were designed and fabricated for the annular combustion chamber, and one was tested. The unit tested was a 54-element coaxial injector of the same element design as the 54-element coaxial injector tested in the 14.0 inch-diameter cylindrical hardware under NAS 8-11741. Seven pulse tests were conducted. A 600-element triplet injector was also designed and fabricated and is shown conceptually in Figure 3. It is rated at 60,000 lb thrust with 180 lb/sec total weight flow of propellant. A second triplet injector, using the same injection element design but containing only 200 triplet elements and delivering approximately 20,000 lb thrust with 60 lb/sec total weight flow of propellant, was also designed and fabricated. A conceptual drawing of this injector is shown in Figure 4.

(1) 54-Element Coaxial Injector

Testing of coaxial injectors on NAS 8-11741 and results from other test programs yielded data to permit evaluation of the size aspects of the coaxial element and the impinging versus nonimpinging patterns. The remaining parameter requiring evaluation was the effect of chamber Mach number and injection density. Using the same element design and impingement angle as used on the 54-element, the 14-inch-diameter cylindrical injector of last year's NAS 8-11741 contract permitted direct correlation between it and the annular high injection density injector parameters. A comparison of the 54-element cylindrical injector and the 54-element annular injector is shown in Table 1.

IV, A, Test Apparatus (cont.)

Design details for the coaxial injector fabricated on this task (Figures 5 and 6) and the design test condition used in computing the design data are shown in Table 2.

(2) High Injection Density Triplet Injector

The injector is composed of 600 triplet elements having an injection density of 3 lb/sec-in.². The triplet elements are drilled in a radial ray arrangement around an annulus conforming to the annular chamber envelope. There are 48 raised bars around the annulus. The fuel orifices are central and are located in the center of the raised bars. The two rows of oxidizer orifices on either side of the fuel bar are located 0.197 inches below the fuel orifice exit plane. The raised fuel bar has a truncated triangular cross section. The pattern and manifold arrangement are shown in Figure 3. The remaining high injection density triplet injector design parameters are listed in Table 2, for comparison with those of the low injection density triplet.

There is a provision for four baffles (one every 90 degrees) to protect the face from erosion by spinning tangential modes of instability. The baffles are held in place by bolts and are replaceable. The oxidizer orifices are fed by slots which receive propellant from a flooded annular back plate. Propellant is supplied to the annulus through eight holes connecting the annulus to the central oxidizer supply line. Fuel is fed to the orifices by 48 radially drilled holes which are supplied by an outer annulus. The annulus is filled by six tubes connected to the main fuel supply line.

(3) Low Injection Density Triplet Injector

The low injection density triplet injector has the same size orifices and element geometry as the above described injector. The flow rate, thrust and number of elements have been reduced by 2/3 that of the 600 triplet injector. The design of the two injectors is compared in Table 3.

IV, A, Test Apparatus (cont.)

The fuel orifices are fed by radial holes connected to an outer annulus. The annulus is supplied by six tubes connected to the main fuel line. The oxidizer orifices are fed by radially drilled holes which are plug welded at the outer circumference to prevent intermanifold leakage. The radial tubes are fed from an inner annulus by means of connecting holes. A central line supplies oxidizer to the annulus through eight equally spaced holes.

b. Chamber

An annular thrust chamber was used so that the chamber acoustic frequency would be in a suitable range while increasing the injection density. It also allowed the determination of combustor configuration effect on combustion stability. Information obtained for a previous program (Contract NAS 8-11741) allowed determination of the effects of a cylindrical chamber on combustion stability using a comparable coaxial type injector element at lower injection density. The annular chamber was assembled by placing a flanged cylinder over the center body attached to the injector. The chamber was kept cool by the use of 1/2-inch-thick ablative sleeves on both the outer and inner diameters of the annulus. The chamber can be seen assembled on the test stand in Figure 1. The internal chamber dimensions are as follows:

Chamber inside diameter	=	10.50 in.
Center body outside diameter	=	6.14 in.
Chamber effective length	=	15.25 in.

Two igniters, three pulse guns, eight high-frequency transducers, and three static pressure transducers are located on the combustion chamber as shown in Figure 7.

IV, A, Test Apparatus (cont.)

The chamber and center body ablative liners made a smooth transition into an ablative annular throat by using nozzle inserts held in place by flanged housings. Chamber pressures of 1500 and 2500 psia were obtained by maintaining a constant flow rate and changing the throat area. The center body throat diameter remained constant; the throat diameter of the insert attached to the outer chamber nozzle housing was varied to achieve two chamber pressures. A center body nozzle extension of graphite was used to attain a uniform expansion with minimum nozzle losses, thereby providing accurate performance measurements. A photograph of the chamber and nozzle mounted on the test stand viewed from the nozzle end is shown in Figure 1. The pertinent nozzle design parameters are outlined in Table 4.

3. Transverse Excitation Chamber

The concept of a transverse excitation was originated at Aerojet on a Company-Sponsored Independent Research and Development program to study transverse modes of pressure oscillation (tangential instabilities) and simulate the pressure/velocity effects as experienced in a rocket combustion chamber. The transverse excitation chamber tested on this program is described in the following paragraphs.

a. Injectors

Two triplet element patterns were designed and fabricated for testing in the transverse excitation chamber. One was an 11-element triplet, and the other was a three-element triplet similar to the 11-element triplet design in all but the orifice diameters. The purpose of the larger orifice size was to determine the effect of orifice diameter or thrust per element on combustion stability. Only the 11-element injector inserts were tested during Phase I. A conceptual drawing of the two injectors is shown in Figure 8. A summary of the injector design features is listed in Table 5.

IV, A, Test Apparatus (cont.)

The injector inserts are interchangeable modules that offer fabrication economics and test program versatility. Injectors that would not fit into the 1.8-in.-diameter bore can be inserted from the lid side, then connected to the manifold. The inserts are sealed by two O-rings seated in circumferential grooves. A port at the base of the insert allows insertion of a fast response thermocouple to monitor fuel manifold temperature.

b. Combustion Chamber

The excitation chamber consisted of three principal parts: (1) chamber, (2) nozzle, and (3) injector inserts. The chamber is a 36° sector of a circle 2-1/4 inches in height. A drawing of this chamber is shown in Figure 9. The 36° sector of the 30-inch radius results in a fundamental acoustic frequency in the transverse mode at 1800 Hz. The smallest chamber angle was 9° , which results in a chamber acoustic frequency of 7000 Hz. The height of the chamber (2.17 in.) limits the associated acoustic frequency to greater than 13,000 Hz.

Originally, the variation in frequency was to be obtained by varying the chamber length to determine acoustic amplitude growth or decay rate for various chamber frequencies. Test results from an Aerojet Independent Research and Development program indicated that chamber losses, the relationship of the combustion distance to the acoustic field amplitude, and the physical location of the pulse gun to the combustion front greatly affected the response characteristics of the multiple-length (36° included angle) combustion chambers. To overcome the disadvantages of multiple-length combustion chambers, a single chamber 30 in. long and having a 36° included angle was used. The frequency of the acoustic mode was varied by changing the angle in the chamber, using various wedges inside the chamber to block part of the combustion zone. Undrilled blank injector inserts seal the injector bores blocked by the wedge. The frequencies associated with the wedges and the included chamber angle are listed in Table 6.

IV, A, Test Apparatus (cont.)

The O-ring sealed chamber lid is removable to facilitate repairs and inspection. The combustion chamber wall was protected by a flame sprayed zirconium oxide coating 0.020 to 0.040 in. thick.

Ablative liners were bonded to the chamber with room-temperature vulcanizing silicone rubber RTV-60. They were located in the nozzle end of the chamber and covered half of the distance between the nozzle and injector face. The liners served to protect the steel from the hot erosive combustion products and were used only in the nozzle end to avoid acoustic losses due to the highly absorptive ablative material.

The nozzles are composed of a housing and ablative inserts. The nozzle throat and exit planes are rectangular in section to avoid transition pieces. The outside envelope of the nozzle insert is cylindrical with the exception of a molded key. The nozzle ablative insert is designed to be made from a common mold and is bonded into the nozzle housing using RTV-60. The housing, in turn, is bolted onto the chamber and sealed by an O-ring. The throat width for each of the eight nozzles is shown in Table 7.

IV, Experimental Tasks (cont.)

B. TEST PROCEDURE

The 60K thrust annular chamber tests were conducted on the C-6 test stand and the subscale (excitation chamber) tests were conducted on test stand J-1.

A total of 13 tests were conducted for this investigation; seven were made using the 60K annular thrust chamber and coaxial injector hardware. The other six tests were performed on the transverse excitation chamber. These latter tests used a triplet injector pattern (O-F-O). High-frequency data were satisfactorily recorded on all valid tests.

Both series of tests were designed to operate at nominal mixture ratios of from 4 to 6 and at velocity ratios of from 3.5 to approximately 10. Chamber pressures of 1500 and 2500 psia were to be attained on the TCA tests, whereas facility limitations dictated a maximum excitation chamber pressure in the 1500 psi range.

During the steady-state portion of each test, perturbations were introduced into the chamber in an attempt to disturb the combustion process. Three pulses (20, 40, and 80 grain charges) were used for the annular chamber tests; a 40-grain pulse was used to perturb the excitation chamber tests.

1. Full-Scale Testing (60K Annular Chamber)

a. General

The duration of all tests was scheduled for 2 seconds. Three pulse charges were fired at 100 millisecond intervals. The 2-second duration allowed pulsing to take place during the last portion of the test so that a reliable value for specific impulse (I_g) could be determined from data during

IV, B, Test Procedure (cont.)

the early part of the test. Sufficient high frequency, low frequency, and static instruments were used to establish the thermodynamic properties of the propellants and the combustion characteristics within the chamber.

b. Test Stand

An isometric drawing of test stand C-6 is shown in Figure 10. A picture of the test stand showing the intensifier layout can be seen in Figure 11. The intensifiers are a positive expulsion device which allows the propellants to be supplied to the engine at high pressure using a relatively low pressure inert gas. The pressure is intensified by amplifying force through an in-line axial piston having a large diameter gas input and a small diameter propellant output. The intensifier's output is 6000 psi from an input of 1700 psi. The propellant capacity of the oxidizer and fuel intensifiers is 80 and 250 gallons, respectively. The intensifier piston is restricted from traveling the full distance to avoid damaging the head end.

The amount of propellant flowing to the engine was regulated by a servo control system. The function of the servo is to adjust the opening of the flow control valve upstream of the injector to maintain a preset manifold pressure that is input to the servo system by the transducer measuring injector pressure. An orifice is provide in each propellant line downstream of the flow control valve. The orifice functions to decouple low-frequency instabilities initiated in the feed lines. The engine is held immobile by the stand structure, designed to withstand a maximum reaction thrust of 100,000 lb.

c. Chill and Fill Procedure

Hydrogen propellant consumption was minimized by a combination of a vacuum jacket, which acts as insulation, and a LN_2 heat exchanger wrapped around the propellant end of the intensifier. Liquid nitrogen was

IV, B, Test Procedure (cont.)

flowed through the tubes until a temperature of 140°R was monitored. At that time, the LN_2 was then purged from the heat exchanger tubes and liquid hydrogen introduced through the vacuum-jacketed run lines to the intensifier until the system reached liquid hydrogen temperature ($\sim 35^{\circ}\text{R}$). The LH_2 temperature was monitored at the intensifier vent, the system was considered chilled down, full, and ready for testing. Oxidizer was serviced in a similar manner as the fuel by first filling through the insulated propellant lines, then topping off propellant through the intensifier vent.

The injector was prechilled by flowing LN_2 through the fuel circuit downstream of the thrust chamber flow control valve. Temperature was monitored at the injection orifice by high response thermocouples; when LN_2 temperature was detected, the system was considered sufficiently chilled.

Gaseous hydrogen (200°R) was obtained by filling the intensifier with a predetermined amount of LH_2 , then injecting gaseous hydrogen from an auxiliary supply. The mixture of gaseous and liquid hydrogen was then allowed to reach thermal equilibrium before firing.

To produce a smoother start and reduce the possibility of ignition spikes (overpressures), the oxidizer and fuel propellant valves were programmed to produce an oxidizer-rich mixture ratio.

d. Test Sequence

The test firing countdown was started after the fill and chill had been completed. A test duration of 2 seconds was scheduled for each test. The test duration time is defined as the interval between FS-1 and FS-2. Fire switch one (FS-1) was operated manually, initiating timers which sequenced valves, igniters, pulse guns, and FS-2. Ignition was accomplished by two

IV, B, Test Procedure (cont.)

pyrotechnic igniters which had burn durations of 0.75 sec at 14.7 psi. The start was oxidizer rich to reduce the possibility of ignition spikes (overpressures). The start was accomplished by programming the oxidizer and fuel propellant valve opening times and rates so that, as soon as the valves reached approximately 80% of the scheduled full-open position, the servo controller system was activated. The smooth transition into steady-state operation was verified by the record shown in Figure 12. The three pulse guns were fired at 0.10 second intervals starting at 1.6 seconds. An indication of the steady-state specific impulse could be obtained from test data before the time the pulse guns fired. Fire Switch Two (shutdown) could be activated by any one of five methods:

- (1) Thrust chamber pressure switch
- (2) Combustion stability monitor
- (3) Oxygen or full 70% limit switch
- (4) Duration timer
- (5) Manual override

The sequencer FS-2 command resulted in the opening of all bleeds and vents (except run tank vent) and the closure of all other valves. Purges were opened manually prior to FS-1 and were checked by system pressure until system pressure decayed to a predetermined level, at which point they began to flow until closed manually.

e. Instrumentation

A schematic of the C-6 test stand flow and instrumentation diagram is shown in Figure 13. The instrumentation used to monitor engine high-frequency fluctuations and their location is shown in Figure 7. The types of instrumentation used are discussed below.

IV, B, Test Procedure (cont.)

(1) Pressure Measurement

There are eight Model 352A Photocon pressure transducers located in the chamber wall. The transducers are located in three axial planes and four circumferential positions. The locations allow determination of the phase, amplitude, and damping rate of pressure waves in the chamber. Planes A, B, and C are located at distances of 4.625, 7.925, and 12.125 inches from the injector face, respectively. All three planes had transducers located at 30 and 120° from top dead center. In addition, Plane A had two located at 210 and 270° from top dead center. The transducers were mounted within 0.100 inch of the half-inch ablative liner, as shown in Section A-A of Figure 7. Five orifices drilled through the 1/2-inch thick ablative liner at each Photocon location allowed chamber pressure oscillation to be sensed. Pressure perturbations were introduced by firing two pulse charges through ports in the chamber wall, which were aimed tangential to the center body diameter. The location of the ports is shown in Figure 7.

Static pressure transducers were located in the injector inlet lines to measure injector pressure. Static chamber pressure transducers were used to measure chamber pressure at three locations on the chamber; at the injector face and 4.62 and 7.925 in. from the face.

(2) Temperature Measurement

A platinum resistive temperature transducer and high-response copper-constantan (C-C) thermocouples were used to monitor propellant temperature at the injector entrance. Copper-constantan thermocouples were also located in the fuel manifold to monitor temperature prior to injection. The rate of volumetric displacement of propellant in the intensifiers was determined by means of a potentiometer attached to the intensifier piston shaft. The density of the propellant was obtained from appropriate equations of state. Flow rate was then calculated as the product of time rate of change of intensifier volume and propellant density.

IV, B, Test Procedure (cont.)

2. Excitation Chamber Testing

a. General

The duration of all tests was scheduled for 0.8 to 1.5 sec. A single pulse charge was fired at 50 milliseconds prior to FS-2. Sufficient high frequency, low frequency, and static instruments were used to establish the thermodynamic properties of the propellants and the combustion characteristics within the chamber.

b. Test Stand

The excitation engine was tested on Test Stand J-1. A picture of the engine mounted on the stand is shown in Figure 14 and a schematic flow and instrumentation diagram for Test Stand J-1 is shown in Figure 15. Propellant was supplied to the engine by means of an 80-gallon oxidizer intensifier and a 100-gallon-capacity pressurized fuel tank. The oxidizer intensifier (propellant end only) and run lines were glass fiber insulated. The fuel tank and run lines were vacuum jacketed to prevent excessive heat loss. The oxidizer intensifier is similar in construction and operation to the one used for full-scale tests, as described in Section III,B,1,b. The spherical fuel tank had a 3500-psi upper pressure limit and was pressurized by hydrogen gas supplied from a cascade. A steady flow rate was maintained by servo control, shown schematically in Figure 15. The servo system controlled flow rate by adjusting the flow of the pressurizing gas into the fuel tank and oxidizer intensifier to provide a constant set pressure at the thrust chamber valves. An orifice was located just downstream of the oxidizer valve to decouple low frequency instabilities associated with the feed lines. The fuel tank pressure rating of 3500 psi precluded placement of an orifice in the fuel side since the sum of the chamber and injector pressure drops nearly equaled the total available head. The stand mount was designed for 100,000 pounds of thrust and could, therefore, easily accept the 2000 to 8000 pound thrust the excitation chamber could deliver.

IV, B, Test Procedure (cont.)

c. Chill and Fill Procedure

The two systems were chilled down by introducing the propellants into their respective tanks until liquid conditions were monitored in the vent stack. Vacuum jacket intensifier and run lines and an insulated oxidizer propellant system prevented excessive propellant consumption by reducing heat losses. The fuel manifold was cooled externally by a LN_2 jacket.

d. Test Procedure

There were only minor differences between the excitation and full-scale engine test procedures discussed in Section III,B,1,d. A test duration of 0.750 seconds was established after Test -002. The short duration was to minimize hardware damage. The shutdown parameters were the same as for the full-scale engine except for the combustion stability monitor (CSM). The shortness of the duration made a CSM function needless since the oxidizer and fuel valve closing times were of the same order of magnitude as the duration. The oxidizer valve was opened first, followed by the fuel valve opening, to result in an oxidizer lead so that chamber overpressure could be avoided. A start transient of a typical test is shown in Figure 16.

The single 10-grain pulse gun was fired at FS-2. By so doing, a spontaneous instability would be allowed, and the time that elapsed while the valves closed was sufficient to determine decay or growth values.

e. Instrumentation

The parameters necessary to evaluate the experimental characteristics to determine the combustion stability of advanced injectors included propellant flow rate, pressure, temperature, and amplitude and frequencies of chamber pressure oscillations. A schematic of the J-1 test stand flow and instrumentation is shown in Figure 15.

IV, B, Test Procedure (cont.)

(1) Pressure Measurement

There was one Model 352A Photocon transducer located in the chamber wall and one located in the chamber lid. Both transducers were located approximately 1-1/2 inches from the injector face, and the water-cooled face of the transducer was flush with the combustion chamber wall. The Photocon transducers were used to measure oscillatory pressure. Pressure perturbations were introduced by firing a 10-grain pulse charge into the combustion chamber using a squib-initiated Mod V pulse gun. The location of the pulse gas ports are shown in Figure 9.

Static pressure transducers were used to measure injector pressure. Two static chamber pressure transducers, connected in parallel, were located approximately 1 in. from the injector face and were used to measure chamber pressure.

(2) Temperature Measurement

A platinum resistive temperature transducer and a high-response copper-constantan (C-C) thermocouple were used to monitor propellant temperature at the injector entrance. Six fast response C-C thermocouples were located in the fuel manifold to monitor temperature prior to injection.

(3) Flow Measurement

The rate of volumetric displacement of oxidizer in the intensifier was determined by a potentiometer attached to the intensifier piston. Oxidizer flow rate was then calculated as the product of intensifier volumetric time rate of change and propellant density. Fuel flow rate was measured with a turbine-type flowmeter. A schematic of the instrument locations is shown in Figure 15.

IV, Experimental Tasks (cont.)

C. TEST RESULTS

1. Annular Thrust Chamber

A total of 7 tests were conducted with the annular thrust chamber using the coaxial injector pattern (Figure 5).

Each instability pattern observed during the annular testing was nearly identical in its form and was initiated by the 20-grain charge, using a tangential pulse gun. The peak-to-peak overpressures of these instabilities ranged from 800 to 2000 psi. The frequency was approximately 2500 Hz, depending on the acoustic velocity value for each test condition.

Test No. 7, using 200°R hydrogen, experienced--in addition to its high-frequency instability--a low-frequency (500 Hz) oscillation which attained an amplitude of 750 psi. Except for one brief occurrence of a low-frequency (100 Hz and 100 psi) instability on Test No. 3, there was no other indication of coupling between the feedlines and the combustion process. It should be pointed out that the large pressure drops across the injector face due to the small orifice design result in significant hydraulic resistances in the circuit.

Though the amplitudes of the higher frequency instabilities were large, there was no evidence of erosion taking place across the injector face which was protected by a ZrO_2 coating. The ablative liner of the chamber did exhibit a "scallop" effect around its periphery approximately 2 to 3 inches down from the injector face. The orifices in the heat shield on the high-frequency transducers were partially plugged by the molten ablative material; however, the data recorded by the transducers were not seriously compromised. The eight transducers spaced around the chamber indicate the instability was a standing first tangential mode.

IV, C, Test Results (cont.)

In addition to pressure data, a thorough temperature distribution was made across the entire feed system. Six high-response thermocouples were placed in the fuel circuit at the point of injection into the chamber to allow accurate density values to be calculated. These values were then used to determine the propellant injection velocity from the measured flow rates. Temperature measurements were also made in the manifolds, propellant lines, and into the intensifier using both high-response thermocouples and resistance temperature transducers.

Flow measurement data were improved over last year's program. Two devices were installed on both the oxidizer and fuel intensifiers to measure piston velocities. One device, a rotary potentiometer spool, gave good data on the fuel circuit but inconsistent results on the oxidizer side. This is due to the larger displacement of the fuel piston (6 to 8 feet) versus approximately 2 feet of oxidizer piston travel, giving greater sensitivity to displacement measurement errors. A second experimental velocity measuring device consisted of a slider mechanism riding along a calibrated wire and yielding an analog output signal. Data from it were sporadic but nonetheless did, at times, closely correlate with the rotary potentiometer.

As a check on both types of devices, analytical calculations were made using the temperature data, feed system pressure drops, and experimental hydraulic resistance values.

The major difference in this year's test program versus the Phase II work on Contract NAS 8-11741 was the use of higher chamber Mach number resulting from the use of an annular chamber (e.g., lower contraction ratio). Two Mach numbers were used, 0.176 and 0.29 (vs a previous range of 0.02 to 0.14), to define the correlative effect of this parameter.

IV, C, Test Results (cont.)

Combined modes were common in the Phase II testing; however, only pure first tangential modes were recorded in the current testing. All unstable tests exhibited high peak-to-peak amplitudes ranging from 40 to 90% of chamber pressure, each being triggered by the 20-grain pulse charge. The initial pressure wave resulting from this charge varied considerably (100 to 1000 psi) from test to test, yielding the same random spread as seen on the Phase II testing (Figures 17 and 18).

Referring to Figures 19 and 20, the mixture ratio vs velocity ratio plots, it may be seen that the unstable points fell within the spontaneous instability zones plotted from last year's work. Due to the limited number of tests fired, this could signify either a rightward shifting (higher MR) of the stability zones or a larger pulsed instability zone. It should be noted that, since the annular chamber instabilities were triggered by a small charge (20 grain), the combustion sensitivity was close to its spontaneous zone. Forty to sixty grains were needed in the Phase II testing to trigger the instabilities.

The following correlation equation was obtained from an analysis of the LOX/LH₂, coaxial injection test data obtained by AGC (NAS-8-11741, Phase II), PWA, and LeRC. From the multitude of design and performance parameters available, six variables were selected which, from empirical results, could best be correlated to the observed high frequency instability, f_s .

The Mach number (e.g. mean chamber gas velocity) and the orifice diameter, d_i , of the least volatile propellant were found to have an effect approximately proportional to the 1/7 power.

Chamber pressure was related to the sensitive frequency by the 1/3 power in cases when its value was lower than the vaporization pressure of oxygen. Increasing the pressure above this value did not directly effect the frequency.

IV, C, Test Results (cont.)

The test results also correlated the velocity ratio and the impingement angle to the sensitive frequency. Physically, a high degree of droplet breakup caused both by a large absolute fuel velocity and it's respective radial component directed normal to the central (oxidizer stream) would result in a shorter time lag, τ , (e.g., higher frequency, f_s). A large central oxidizer velocity would act to resist this breakup causing the opposite effect (larger τ and lower frequency) to occur.

The intent of this year's annular chamber/coaxial injector program was to validate the effect of Mach No. by treating larger values (0.176 and 0.29).

This verification of the Mach number as an important correlating parameter, together with the results of Phase II testing and the work of LeRC, has led to the following correlation equation:

$$f_s = 4550 \left(\frac{M_c}{d_i} \right)^{0.15} \frac{(P_c/P_{\text{critical}})^{1/3}}{F}$$

f_s	= Sensitive frequency (Hz)
M_c	= Chamber Mach number
d_i	= Injection orifice diameter of least volatile propellant, inches
P_{critical}	= Critical pressure of least volatile (time controlling) propellant, psia
P_c	= Chamber pressure, psia
F	= Function of the velocity ratio and impingement angle. This function is not defined for the nonimpinging showerhead coaxial element. (Figure 21).

IV, C, Test Results (cont.)

This formula may be used by a designer in his preliminary work to develop an injector configuration whose sensitive frequency is displaced from the first tangential acoustic mode of the thrust chamber. These first order estimates may then be combined with the analytical results of the sensitive time lag computer program to obtain a more detailed engine configuration. Of prime importance is the overall trends which may be observed from changes in any of the six design parameters. An example problem using the above equation to make both a preliminary and final design study is presented in Section V, Application of Results.

Admittedly further testing and research into the physico/chemical kinetics of high chamber pressure/ $\text{LO}_2\text{-H}_2$ combustion may lead to the correlation of additional parameters and/or an adjustment (exponential) of each term. Also certain parameters may only be correlative over a definite range (much as chamber pressure appeared to have an effect only when below oxygen's vaporization pressure).

2. Transverse Excitation Chamber

This series of tests was conducted to demonstrate the capability of the excitation chamber to characterize injector elements. This type of information is needed to rate stability of a particular injector design and/or a variation of operating conditions.

Mixture ratios of around 4 and chamber pressures of 1300 to 1400 psi were evaluated during the test series. Two of the three valid tests (three tests had an inoperative fuel valve) attained these conditions and both experienced spontaneous instabilities. One test exhibited a growth rate of 650 db/sec, while the other test had two distinct growth periods. The first, occurring at the onset of the instability, had a 600 db/sec rate, while the second growth period came after thermal ignition of the 40 grain pulse charge had disrupted the initial instability. Its growth rate was 330 db/sec.

IV, C, Test Results (cont.)

Pressure, temperature, and flow rate measuring devices all gave satisfactory data. Some damage to the high-frequency pressure transducer was caused by the instability; however, it did not invalidate the data.

Tables 9 and 10 summarize the recorded valid performance data together with the stability results.

From the data obtained, the indication is that over the frequency range of 3000 to 4500 Hz the triplet element shown in Figure 3 has a peak response at 3300 Hz (see Figure 22) at the specified steady state conditions. This peak response frequency, when related to τ by the relationship

$$\tau = \frac{1}{2f}$$

compares favorably with previous correlations of τ (Figure 23) for this type of injector. This correlation was developed during Phase II of Contract NAS 8-11741.

V. ANALYTICAL TASKS

A. ANNULAR THRUST CHAMBER ANALYSIS

1. Annular Combustion Chamber

The analysis for annular combustion chambers fits into the basic framework of the cylindrical chamber analysis with only a minor modification. This modification is the direct result of a boundary condition at the inner wall of the annular chamber. A brief description of the analysis is contained in the following paragraphs.

In the solution of the characteristic equation for the cylindrical chamber, the pressure perturbation, P' , was solved by assuming a solution of the infinite series form

$$P' = P_0 + P_1 + P_2 + \dots P_n$$

Using an order of magnitude analysis on the general perturbation equations permitted the separation of the general equations into equations for P_0 , P_1 , etc., where it was assumed that $P_1 = 0 (P_0 \cdot u_e)$ --that is, one order of magnitude less than P_0 by virtue of the product of P_0 and the steady state Mach number u_e -- $P_2 = 0 (P_0 \cdot u_e^2)$, and $P_n = 0 (P_0 \cdot u_e^n)$. The solution for P_0 considered terms of $O(1)$ with the result that P_0 represents the solution of the acoustic equations in a no flow, no combustion system.

The P_0 equations were solved by using the separation of variables technique:

$$P_0 = P_0(Z) \psi_0(r) \theta_0(\theta) \quad (1)$$

V, A, Annular Thrust Chamber Analysis (cont.)

and resulted in three ordinary differential equations for

$$P_o(Z), \psi_o(r), \text{ and } \theta_o(\theta).$$

The modification to the cylindrical chamber analysis imposed by the annular analysis presents itself in the solution of $\psi_o(r)$. The discussion hereafter will be concerned with $\psi_o(r)$.

The differential equation for $\psi_o(r)$ is the classic Bessel equation which results in the following general solution:

$$\psi_{v\eta}(r) = C_1 J_v(S_{v\eta} \cdot r) + C_2 Y_v(S_{v\eta} \cdot r) \quad (2)$$

where J_v is the Bessel function of the first kind, Y_v is the Bessel function of the second kind, and $S_{v\eta}$ (where v specified the order of the Bessel equation) is the transverse acoustic mode number. Specifically, this means that at all chamber walls

$$\frac{d\psi_v}{dr} = 0$$

Applying this condition to (2) yields

$$\psi'_v = 0 = J'_v(S_{v\eta} \cdot r_c) + \frac{C_2}{C_1} Y'_v(S_{v\eta} \cdot r_c) \quad (3)$$

at the outer wall, $r_c = 1$, equation (3) reduces to

$$J'_v(S_{v\eta}) + \frac{C_2}{C_1} Y'_v(S_{v\eta}) = 0 \quad (4)$$

V, A, Annular Thrust Chamber Analysis (cont.)

For the cylindrical chamber case, equation (4) reduces to

$$J'_v(s_{v\eta}) = 0 \quad (5)$$

since B must be zero because Y_v becomes infinite at $r = 0$. The solution of equation (5) serves to define the transverse acoustic mode number, $S_{v\eta}$, for cylindrical combustion chambers.

The annular chamber has its inner wall located in the range $0 < R' < 1$. Therefore, for the inner wall, equation (3) is written.

$$J'_v(S_{v\eta} \cdot R') + \frac{C_2}{C_1} Y'_v(S_{v\eta} \cdot R') = 0, \text{ @ } r = R \quad (6)$$

whereas at the outer wall, $r = 1$ and equation (4) is still applicable.

Solution of (4) and (6) simultaneously yields

$$J'_v(S_{v\eta}) Y'_v(S_{v\eta} R') - J'_v(S_{v\eta} R') Y'_v(S_{v\eta}) = 0 \quad (7)$$

The solution of equation (7) defines the transverse acoustic mode number, $S_{v\eta}$, for annular chambers. Fortunately, equation (7) has been solved in Reference (29) and the values of $S_{v\eta}$ are listed as a function of R' where $R' = R_i/R_o$ on Table 11.

Thus the use of an annular chamber will alter the frequencies of the transverse modes. The extent of the alteration is illustrated in Figure 24. In addition, radial injection distribution effects will be minimized by the use of the annular chamber so that in most cases the distribution coefficients $A_{v\eta}$, $B_{v\eta}$, and $C_{v\eta}$ can be assumed as unity.

V, A, Annular Thrust Chamber Analysis (cont.)

2. Annular Exhaust Nozzle

The configuration of the exhaust nozzle effects the nozzle admittance coefficients that are used in the boundary condition imposed by the analysis at the chamber/nozzle interface.

The annular exhaust nozzle analysis does not differ significantly from the cylindrical nozzle analysis. The only difference is in the determination of the local contraction ratio as a function of the z-coordinate for input into the isentropic relationship

$$\frac{A(Z)}{A_{th}} = \frac{1}{u(z)} \left[\frac{2}{\gamma+1} \left\{ 1 + \frac{\gamma-1}{2} u^2(z) \right\}^{\frac{\gamma+1}{2(\gamma-1)}} \right]$$

to define the local Mach number, $u(z)$. This is accomplished in the computer program by specifying the inner and outer radii of the annular chamber and throat. A detailed discussion of the computer model which includes the annular chamber analysis can be found in Appendix B.

V, Analytical Tasks (cont.)

B. STAGED COMBUSTION MODEL

The high frequency staged-combustion stability analysis has been completed for the simplified engine system in which the effects of oscillations on liquid propellant injection rates are neglected. The oscillatory flow of fuel-rich combustion products from the primary combustor is included, and provides the dynamic coupling between the two combustors. The simplified analysis is directed toward the study of these coupling effects. In the first version of the analysis, complications which have been studied previously--such as axially distributed combustion and exhaust nozzle shape--are not considered. Similarly, to bring out the coupling effects more clearly, the turbine is replaced by a simple orifice. All of these features can be added to the model, but introduce complications that will obscure the results.

The system considered is represented schematically in Figure 25. The approach taken to the solution is to assume that the engine design parameters are given. Then instability zones are calculated for the secondary combustor, for assumed values of the primary combustion parameters (n_p, τ_p), and for the total time lag of the hot gas τ_{fs} . The shift of the instability zones as these combustion parameters are varied shows the nature of the interaction between the two combustors. An alternative approach would be to solve for the instability zones for the primary combustor, assuming values of the secondary combustion parameters. A closed-form solution is impossible because of the presence of a set of simultaneous, nonlinear, algebraic equations, requiring an iterative solution.

For purpose of analysis, the engine system can be divided into four parts: (1) the propellant feed system, (2) the primary combustor, (3) the secondary combustor, and (4) the turbine. The first-order analysis involves the following assumptions: the propellants are incompressible, the feed

V, B, Staged Combustion Model (cont.)

lines are very short, the combustion is concentrated at the injector end of each combustor, and the mean chamber Mach numbers are small. Although there are many significant interactions between low and high frequency types of instability, initially the two will be treated separately.

To simplify the analysis it is assumed that the Mach number of the mean gas flow through the combustion chambers is small, that the perturbations of all flow properties about their steady-state values are small, and that the combustion is concentrated at the injector face. Then the perturbations are governed by the linear wave equation:

$$\frac{d^2}{dz^2} \left(\frac{P'}{\bar{P}} \right) - \frac{s^2}{c^2} \left(\frac{P'}{\bar{P}} \right) = 0 \quad (8)$$

where the unsteady pressure is of the form $P(z, \tau) = \bar{P} + P'(z)e^{s\tau}$

The boundary condition at the injector face, that is at the downstream side of the combustion front, can be written as

$$\frac{u'}{\bar{u}} + \frac{P'}{\bar{P}} = \frac{R}{R+1} \frac{\dot{m}_x}{\bar{m}_x} e^{-s\tau_x} + \frac{1}{R+1} \frac{\dot{m}_f'}{\bar{m}_f} e^{-s\tau_f} + n(1-e^{-s\tau}) \frac{P'}{\bar{P}} \quad (\text{at } z = 0) \quad (9)$$

At the chamber exit, the boundary condition can be written in terms of an admittance coefficient:

$$\frac{u'}{\bar{u}} = \alpha \frac{p'}{\bar{p}}, \quad \text{at } z = L \quad (10)$$

where α is the complex, dimensionless admittance coefficient, which determines the phase and amplitude of the wave reflection. For $\alpha = 0$, the reflection is that from a solid wall; $\alpha = 1$ corresponds to no reflection (waves propagating

V, B, Staged Combustion Model (cont.)

downstream only); and $\alpha = \infty$ corresponds to reflection from an open end, at which the pressure is kept constant. For rocket chambers, α lies between 0 and 1, and for short, supercritical nozzles, $\alpha = \frac{\gamma-1}{2}$. In general, α is dependent on both nozzle geometry and frequency.

The injector boundary condition includes both propellant feed and combustion dynamic response contributions. For generality, each of the bipropellants is assumed to have its own total time lag τ_t . However, if the propellants are well mixed in the process of injection, a better assumption would be a common total time lag. For simplicity, in the high frequency response of the combustion, a single sensitive time lag is assumed, since the processes involved are more likely to occur after the propellants have been mixed. The form of the combustion response is that developed by Crocco, in which the parameters are the sensitive time lag τ , which is related to the frequencies at which oscillations can occur, and the interaction index n , a measure of the magnitude of the combustion response to a disturbance.

The general solution of equation (8) is

$$\frac{P'}{\bar{P}}(z) = C_1 e^{\frac{sZ}{c}} + C_2 e^{-\frac{sZ}{c}} \quad (11)$$

for which the velocity perturbation is given by

$$\frac{\gamma u'}{\bar{u}}(z) = C_2 e^{-\frac{sZ}{c}} - C_1 e^{\frac{sZ}{c}} \quad (12)$$

Substituting these expressions into the boundary conditions, equations (9) and (10), yield the combustion chamber equation

$$\bar{u} - \bar{u}\gamma(F + \hat{P}) = \frac{1 - B e^{\frac{2sL}{c}}}{1 + B e^{\frac{2sL}{c}}} \quad (13)$$

V, B, Staged Combustion Model (cont.)

where

$$F = \frac{R}{R+1} \frac{\bar{P}}{\bar{m}_x} \frac{\dot{m}'_x}{P'} e^{-s\tau_x} + \frac{1}{R+1} \frac{\bar{P}}{\bar{m}_f} \frac{\dot{m}'_f}{P'} e^{-s\tau_f} \quad (14)$$

$$\text{and} \quad B = \frac{1+\alpha\bar{u}}{1-\alpha\bar{u}}, \quad \hat{P} = n (1-e^{-s\tau})$$

In considering the feed system effects it is convenient to make use of a flow admittance, G , defined by

$$G = \frac{\dot{m}'}{P'}$$

For incompressible flow, and assuming that the feed lines are very short, the admittance at the downstream end of a feed line, G_2 , can be expressed in terms of the admittance at the upstream end, G_1 , by the relation

$$G_2 = \frac{G_1}{1-Z_1 G_1}$$

where $Z_1 = 2 (\bar{P}_1 - \bar{P}_2) / \bar{m}$. If the line originates in a propellant tank, the equation simplifies to

$$G_2 = -\frac{1}{Z_1} = -\frac{\bar{m}}{2\Delta P}$$

for cases in which the lines are too long to neglect wave effects, or the propellant compressibility must be considered, the relation between the admittances becomes much more complicated and is dependent on frequency. Such complications, which can have a significant influence on the stability, will be introduced into the analysis at a later time.

A schematic diagram of a simplified staged-combustion engine is shown in Figure 25. For the present, we consider the turbine to be a short length of line with a pressure drop, with an admittance coefficient at the entrance α_p , to be specified. Applying the combustion chamber and feed line relations to the components of the engine system results in the following set of simultaneous equations:

V, B, Staged Combustion Model (cont.)

Initial feed line sections:

$$G_{fp} = -\frac{1}{Z_f} = -\frac{\bar{m}_f}{2\Delta P_f}$$

$$G_{x1} = -\frac{1}{Z_{x1}} = -\frac{\bar{m}_x}{2\Delta P_{x1}}$$

At the tee in the oxidizer line:

$$G_{x1} = G_{x2} + G_{x3}$$

Primary combustor injector:

$$G_{xp} = \frac{G_{x2}}{1 - Z_{x2} G_{x2}}$$

Primary combustor:

$$\bar{u}_p - \gamma \bar{u}_p (F_p + \hat{P}_p) = \frac{1 - B_p e^{\frac{2sL_p}{c_p}}}{1 + B_p e^{\frac{2sL_p}{c_p}}}$$

$$F_p = \frac{\bar{P}_p}{\bar{m}_p} [G_{xp} e^{-s\tau_{xp}} + G_{fp} e^{-s\tau_{fp}}]$$

$$\hat{P}_p = n_p (1 - e^{-s\tau_p})$$

V, B, Staged Combustion Model (cont.)

Turbine inlet:

$$G_{pe} = \frac{\bar{m}_p}{\gamma \bar{P}_p} (1 + \alpha_p)$$

$$\text{where } \bar{m}_p = \bar{m}_{xp} + \bar{m}_{fp}$$

Secondary combustor injector:

$$G_{fs} = \frac{G_{pe}}{1 - Z_t G_{pe}}$$

$$G_{xs} = \frac{G_{x3}}{1 - Z_{x3} G_{x3}}$$

Secondary combustor:

$$\bar{u}_s - \gamma \bar{u}_s [F_s + P_s] = \frac{1 - B_s e^{\frac{2sL_s}{c_s}}}{1 + B_s e^{\frac{2sL_s}{c_s}}}$$

$$F_s = \frac{\bar{P}_s}{\bar{m}_s} [G_{xs} e^{-s\tau_{xs}} + G_{fs} e^{-s\tau_{fs}}]$$

$$\hat{P}_s = n_s (1 - e^{-s\tau_s})$$

$$B_s = \frac{1 + \alpha_s(s) \bar{u}_s}{1 - \alpha_s(s) \bar{u}_s}$$

V, B, Staged Combustion Model (cont.)

In general, it has been observed that the total time lag is about 6 to 10 times larger than the sensitive time lag. Thus, for frequencies of interest to high frequency instability, the effects of the feed system terms will tend to average out over the finite length of the actual combustion zone. However, since the total time lag includes the times required to accomplish the processes of atomization, vaporization, mixing, and heating of the propellants, some interaction is likely in high pressure engines, particularly in the secondary combustor.

The most successful approach to the solution of the perturbation equations for high frequency instability has been to consider the relations between the system parameters that must hold in the case of neutral oscillations, the "stability limit" relations. The generalized frequency, $s = \lambda + i\omega$, includes both a real part λ , which is the amplification factor, and an imaginary part $i\omega$, where ω is the oscillation frequency. To obtain the stability limit conditions, the real part λ is set equal to zero. The system equations can then be reduced to a single complex characteristic equation, which indicates that the occurrence of instability involves both a gain and a phase condition. It has been found convenient to select two of the combustion parameters, and to solve for these parameters as function of the frequency and of the other system parameters.

TABLE 1
COMPARISON BETWEEN COAXIAL ELEMENTS USED FOR
CONTRACTS NAS 8-11741 AND NAS 8-20672

Contract NAS 8-	11741 (past)					20672 (present)
	I	II	III	IV	V	
Injector Characteristics:						
Task number						--
Number of elements	54	54	108	54	54	54
Oxidizer orifice diameter, in.	0.230	0.256	0.169	0.130	0.071	0.224
Fuel annulus width, in.	0.033	0.034	0.015	0.033	0.034	0.028
Oxidizer injection area, in.	2.22	2.74	2.23	0.716	0.211	2.13
Injection area ratio	0.984	0.748	1.02	3.06	9.74	0.943
Design mixture ratio range	4-6	4-6	4-6	1-2	1-2	4-6
Injection density, lb/sec-in. ²	0.2-1.1	0.6-1.1	0.3	0.3-0.6	0.1-0.3	3.0
Chamber configuration	Cylindrical					Annular

Report 20672-PIF

TABLE 2

SUMMARY OF FULL-SCALE COAXIAL INJECTOR DESIGN CHARACTERISTICS

Number of elements		54
Thrust per element (F/el)	lb	1200
Mixture ratio (MR)		5.5
Chamber pressure (P_c)	lb/in. ²	2500
Injection density (\dot{w}/A_j)	lb/sec-in. ²	3.15
Total flow rate (\dot{w}_T)	lb/sec	180
Oxidizer flow rate (\dot{w}_o)	lb/sec	152
Fuel flow rate (\dot{w}_f)	lb/sec	27.6
Injector velocity ratio (v_f/v_o)		3.5
Oxidizer velocity (v_o)	ft/sec	150
Fuel velocity (v_f)	ft/sec	525
Fuel temperature (TFJ)	°R	80
Pressure drop across oxidizer orifice (ΔP_o)	psid	350
Pressure drop across fuel orifice (ΔP_f)	psid	260
Oxidizer orifice diameter (D_o)	in.	0.224
Fuel orifice diameter		
Inside	in.	0.283
Outside	in.	0.339
Annulus width normal to flow	in.	0.035
Orifice included impingement angle (α_i)	°	60

Note: This injector is schematically shown in Figure 5 and a photograph of the injector is included as Figure 6.

TABLE 3

TRIPLET INJECTOR COMPARISON

<u>Parameter</u>	<u>High Inj Density</u>	<u>Low Inj Density</u>
Injection density, lb/sec-in. ²	3.0	1.0
Number of elements	600	192
Total flow rate, lb/sec	≈ 180	≈ 60
Mixture ratio	5.5	5.5
Orifice exit velocity, ft/sec		
(a) Fuel	700	700
(b) Oxidizer	200	200
Orifice diameter, in.		
(a) Fuel	0.047	0.047
(b) Oxidizer	0.040	0.040
Impingement angle, °	30	30
Impingement height above face, in.	0.348	0.433
Fuel bar height above oxidizer orifice plane, in.	0.197	0.250
Number of radial fuel bars	48	24
Fuel temperature, °R	80	80
Fuel coolant, %	8	8

Report 20672-PIF

TABLE 4

FULL-SCALE ENGINE NOZZLE CONFIGURATION

<u>Parameter</u>	<u>Units</u>	<u>Magnitude of Parameter at Chamber Pressure of</u>	
		<u>1500 psia</u>	<u>2500 psia</u>
Throat diameter (D_t)			
OD	in.	9.290	8.480
ID	in.	7.090	7.090
Exit diameter (D_e)			
OD	in.	11.010	10.200
ID*	in.	5.400	5.400
Throat area (A_t)	in. ²	28.3	17.0
Exit area** (A_e)	in. ²	95.2	81.8
Area ratio (A_e/A_t)		3.36	4.81
Entrance angle (β) (center body and chamber nozzle inserts)	°	50	50
Expansion angle (α) (center body and chamber nozzle inserts)	°	15	15

*With carbon extension nozzle detached.

**With carbon extension nozzle attached; i.e., if attached, center body
nozzle exit diameter = 0.

TABLE 5

EXCITATION CHAMBER TRIPLET ELEMENT INJECTOR CONFIGURATION

<u>Parameter</u>	<u>Units</u>	<u>Magnitude</u>	
Number of elements	--	3	11
Thrust per element (F/el)	lb	370	100
Impingement incidence angle	°	30	30
Mixture ratio		5.5	5.5
Total flow rate (\dot{w})	lb/sec	3	3
Oxidizer flow rate (\dot{w}_o)	lb/sec	2.54	2.54
Fuel flow rate (\dot{w}_f)	lb/sec	0.46	0.46
Oxidizer orifice diameter (D_o)	in.	0.0755	0.0400
Fuel orifice diameter (D_f)	in.	0.0885	0.0470
Fuel coolant orifice diameter (D_{fc})	in.	0.026	0.026
Percent fuel coolant	%	4.7	4.7
Oxidizer velocity (V_o)	ft/sec	190	190
Fuel velocity (V_f)	ft/sec	665	665
Velocity ratio (V_f/V_o)		3.5	3.5
Fuel temperature (T_f)	°R	80	80

Report 20672-PIF

TABLE 6

EXCITATION ENGINE CHAMBER CHARACTERISTICS

<u>Wedge Dash Number</u>	<u>Number of Inserts</u>	<u>Fundamental Frequency, Hz</u>	<u>Included Chamber Angle, °</u>
No wedge	7	2000	36.0
-1	5	2800	25.2
-3	4	3500	19.8
-5	3	4500	14.5
-7	2	7000	9.0

Report 20672-PIF

TABLE 7

EXCITATION ENGINE NOZZLE GEOMETRY

<u>Nozzle Dash Number</u> <u>Chamber Pressure</u>		<u>No. of Injector Inserts</u>	<u>Propellant Flow Rate, lb/sec</u>	<u>Nozzle Throat Width*, inches</u>	
<u>1500 psia</u>	<u>2500 psia</u>			<u>1500 psia</u>	<u>2500 psia</u>
-17	-9	7	21	1.470	0.885
-19	-11	5	15	1.050	0.630
-21	-13	4	12	0.840	0.505
-11	-15	3	9	0.630	0.380
-15	-23	2	6	0.380	0.230

*The throat height is a constant 2.250 inches.

TABLE 8
STEADY STATE AND STABILITY TEST RESULTS

OPERATING CONDITION PARAMETERS										STABILITY PARAMETERS				
Test No.	Time, sec.	Mixture Ratio	Velocity Ratio	Chamber Pressure, psia	Hydrogen Temperature, °R	Avg. Mach No.	High Frequency		Cause SP. or P.	Grain Size/ Pulse Ampl.	Stability	Low Frequency		REMARKS
							Frequency, Hz	Amplitude, psi (peak-to-peak)				Frequency, Hz	Amplitude, psi (peak-to-peak)	
001	1.016 1.210 1.604 (FS-2)	6.05 5.86 6.62	3.44 3.61 3.14	1575 1532 1417	83.4 82.9 80.6	0.29		2400	800	*P	20/960	*S	--	
002	1.140 1.575 1.944 (FS-2)	5.82 5.96 SEE REMARKS	3.39 3.27	1425 1467 1378	75.5 76.5 76.6	0.29		2450	1300	P	20/250	S	--	Oxidizer flow measurement erratic at FS-2.
003	0.970 1.140 1.495 1.577 1.655 2.004 (FS-2)	3.94 3.70 4.06 3.55 3.27 3.20	16.50 16.06 13.01 16.14 17.14 14.39	1413 1454 1422 1445 1445 1454	98.3 99.0 94.1 94.1 104.5 89.5		N O R E C O R D S					U S	100 --	Ox. valve malfunctioned.
004	0.996 1.475 1.596 (FS-2)	5.92 4.57 5.78	3.47 4.10 3.18	2345 2395 2494	96.9 80.1 79.4	0.176		2500	1000	IT	20/1000	S	--	Ox. valve malfunctioned. Average data used.
005	SEE REMARKS	4.88	26.37	1456	172.0		N O R E C O R D S			S		--	--	
006	0.900 1.186 1.245 (FS-2)	3.39 3.72 3.76	6.13 4.84 4.76	2285 2302 2221	102.5 78.5 77.8	0.176		2700	2000	IT	20/225	S	--	
007	0.900 1.086 1.462 (FS-2)	6.53 6.93 7.15	6.73 6.75 7.01	1221 1419 1317	113.5 107.8 173.4	0.177	S E E R E M A R K S			P	20/100	U U	500 500	High frequency pressure instruments substituted during tests. The data (wave forms) recorded were similar to the previous unstable tests.

*P = Pulsed, S = stable, Q = unstable

TABLE 9

EXCITATION ENGINE PERFORMANCE DATA SUMMARY
11-ELEMENT TRIPLET INJECTOR

Parameter	Unit	Test Number 1100-D02-OM-OXX					
		01	02	03	04	05	06
Date tested	X/X/196X	12/20/7	12/21/7	1/10/8	1/11/8	1/11/8	1/11/8
Duration (t_t)	sec	0.509	1.050	--	--	0.595	0.675
Throat area (A_t) (3)	in. ²	1.42	1.42	1.908	1.908	1.908	1.908
Chamber pressure (P_c)	psia	--	950	--	--	1390	1370
Flow rate (\dot{w})							
a. Total	lb/sec	--	9.80	--	--	11.49	12.40
b. Oxidizer	lb/sec	--	9.20	--	--	9.01	9.71
c. Fuel	lb/sec	--	0.60	--	--	2.48	2.68
Mixture ratio (MR)		--	15.30	--	--	3.64	3.62
Velocity ratio (VR)		--	4.60	--	--	8.66	13.3
Injection temperature (T_j)							
a. Oxidizer	°R	--	200	--	--	213	213
b. Fuel	°R	--	200	--	--	151	231
Characteristic velocity (c^*)	ft/sec	--	4800	--	--	7614	6790
% Theo c^*	%	--	80	--	--	92.1	84.4
No. of injector inserts		3	3	4	4	4	4
Chamber angle	°	14.5	14.5	19.8	19.8	19.8	19.8
Sample time	sec	--	0.5-1.2	--	--	0.55-0.60	0.55-0.60
Test remarks		(1)	(1)	(2)	(2)	(4)	(4)

Notes: (1) Tests were unsatisfactory due to extreme flow oscillations.
 (2) Hydrogen valve failed to open.
 (3) Prefire measured value.
 (4) Satisfactory test.

TABLE 10
TRANSVERSE EXCITATION CHAMBER HIGH FREQUENCY DATA

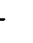
Test No.	Time, sec	Mixture Ratio	Velocity Ratio	Chamber Pressure, psia	Hydrogen Temperature, °R	Frequency, Hz	Amplitude, psi (Peak-to-Peak)	Mode	Cause	Growth Rate, db/sec	Remarks
002	Steady-State Averages	12.50	4.60	959	200	--	--	--	--	--	
005	0.358	--	--	--	--	--	--	--	--	--	Thermal ignition of 40-grain pulse.
	0.400	--	--	1250	--	3450	120	Δ IT	* SP	650	
	0.520	3.77	10.33	1361	200	3360	140	IT	SP	650	
	0.560	3.70	8.97	1374	160	3350	170	IT	SP	650	
	0.595 (FS-2)	3.57	8.35	1378	140	3300	170	IT	SP	650	
	0.640	3.89	6.84	1380	120	3300	170	IT	SP	650	
006	0.304	--	--	--	--	--	--	--	--	--	
	0.490	3.70	15.88	1347	316	--	--	--	--	--	
	0.510	3.76	15.04	1353	295	3300	210	IT	SP	600	
	0.570	3.59	13.53	1353	225	3260	300	IT	SP	600	
	0.640	3.61	10.35	1382	178	3150	256	IT	SP	600	
	0.652	3.57	10.14	1387	167						
	0.669	3.51	9.78	1395	162						
	0.675 (FS-2)	3.51	9.78	1395	160						
	0.730	3.85	7.92	1387	140	3025	190	IT	SP	330	40-grain charge knocks out instability temporarily.
	0.900	4.43	6.51	1378	128	2900	190	IT	SP	330	

* SP - Spontaneous instability
Δ IT - First tangential mode

Table 10

TABLE 11
 BESSEL FUNCTION VALUE $(S_{\nu\eta})_{\text{ann}}$ FOR TANGENTIAL MODES IN ANNULAR CHAMBERS

Annular Chamber Geometry		Tangential Modes					
$\frac{(\text{Radius}) \text{ Inner}}{(\text{Radius}) \text{ Outer}}$		<u>1T</u>	<u>2T</u>	<u>3T</u>	<u>4T</u>	<u>5T</u>	<u>6T</u>
0.910	$(S_{\nu\eta})_{\text{ann}} =$	1.04802	2.09602	3.14401	4.19197	5.23989	6.28778
0.833		1.092	2.1846	3.27672	4.368	5.4588	6.5496
0.667		1.209	2.412	3.61	4.80	5.98	7.14
0.500		1.35	2.68	3.98	5.18	6.34	7.45
0.400		1.41	2.85	4.10	5.27	6.40	7.5
0.333		1.54	2.91	4.17	5.31	6.42	7.5
0.286		1.60	2.99	4.18	5.31	6.42	7.5
0.250		1.64	3.00	4.18	5.31	6.42	7.5
0.222		1.67	3.02	4.18	5.31	6.42	7.5
0.200		1.70	3.025	4.18	5.31	6.42	7.5

NOTE: 1. Figure  gives the frequency ratio viz. $\frac{(S_{\nu\eta})_{\text{annular}}}{(S_{\nu\eta})_{\text{cylindrical}}}$ for different chamber geometries.

2. Calculation of annular chamber tangential frequencies

$$\left[f = \frac{a(S_{\nu\eta})_{\text{annular}}}{2\pi\sqrt{O}} \right]$$

Reference: Bridge and Angrist, "Math. of Computation, 16, 78," April 1962.

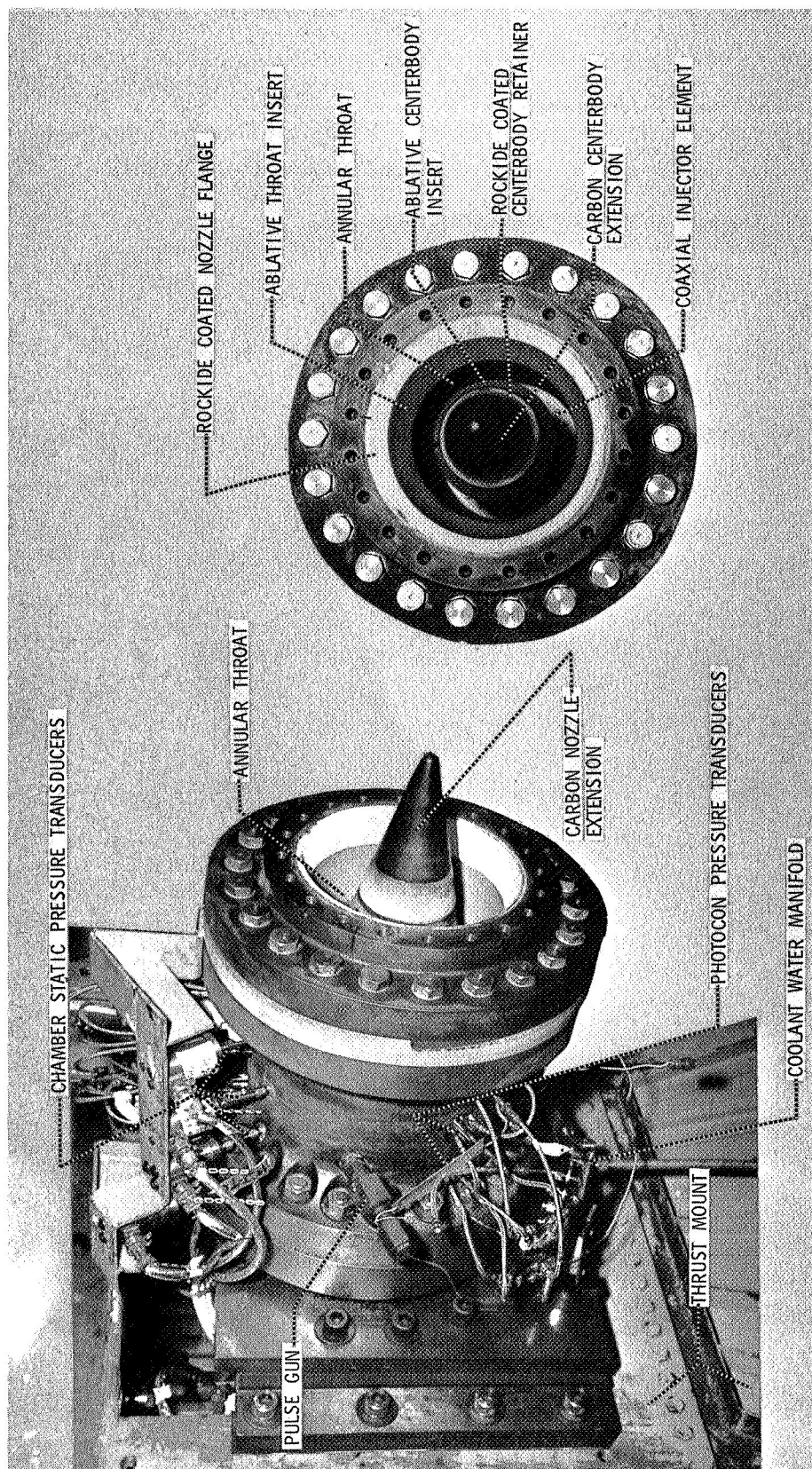
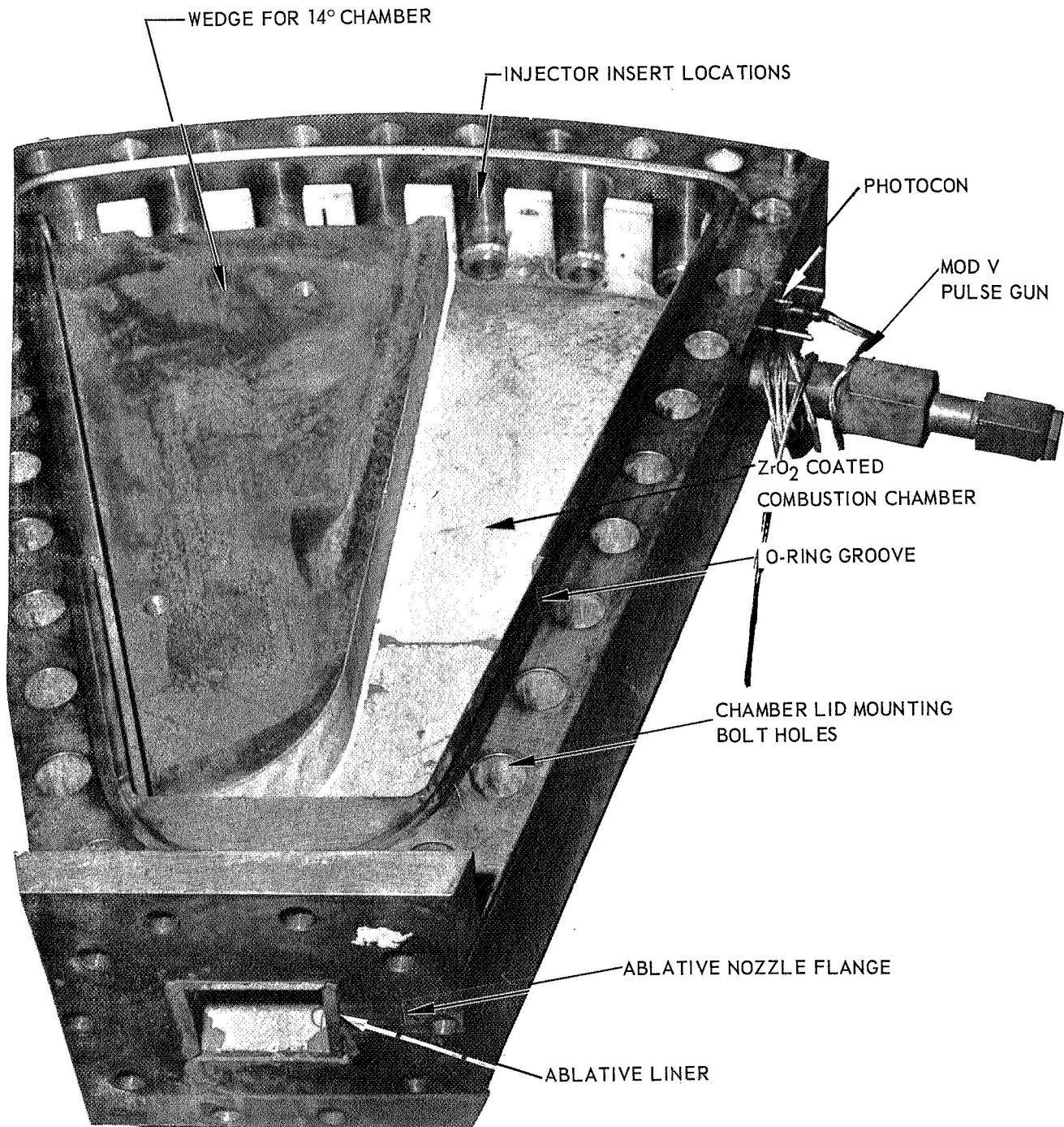


Figure 1

Annular Thrust Chamber Assembly on Test Stand C-6



Transverse Excitation Chamber with Lid Removed

Figure 2

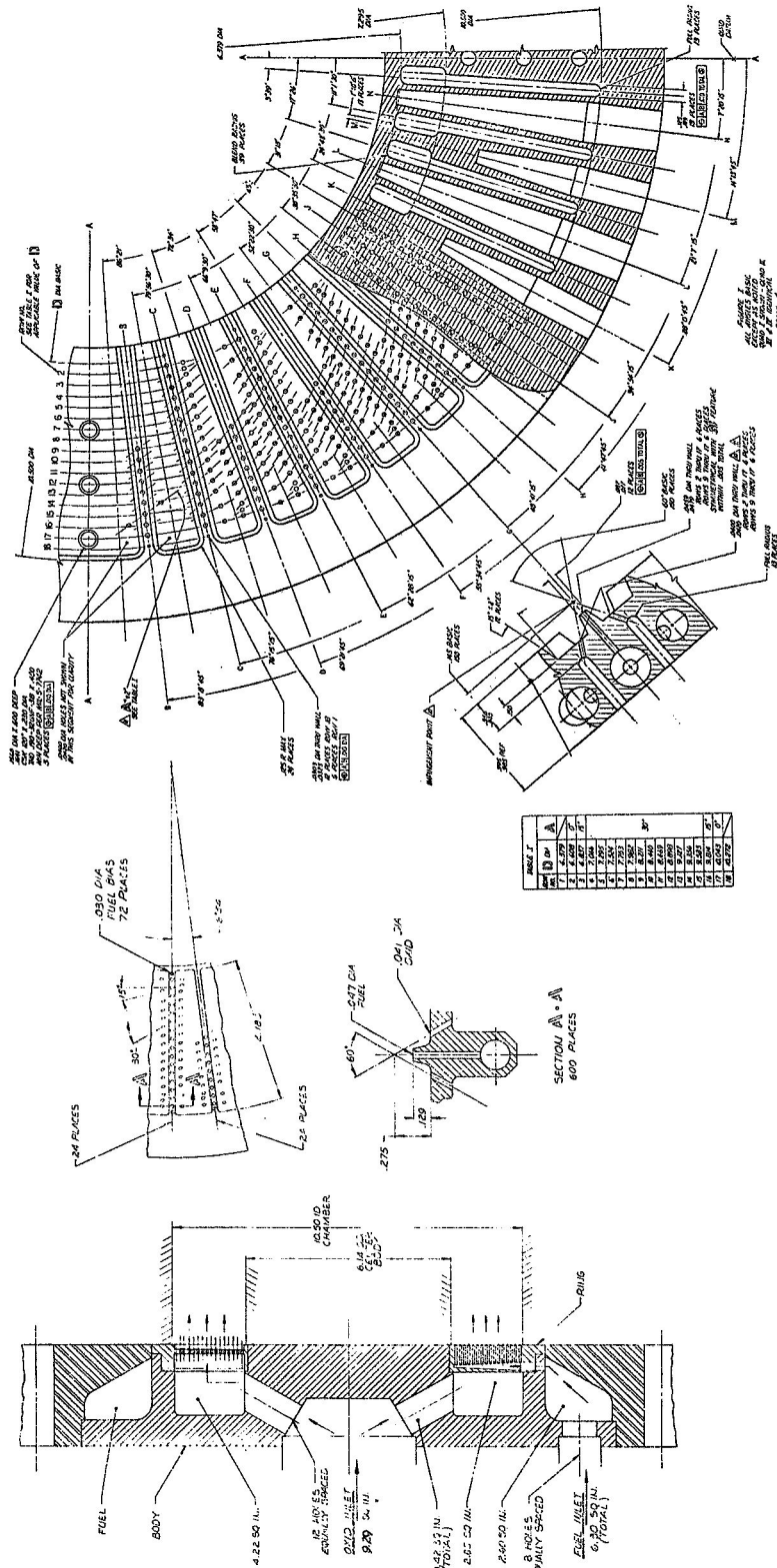


Figure 3

High Injection Density Annular Triplet Injector Schematic

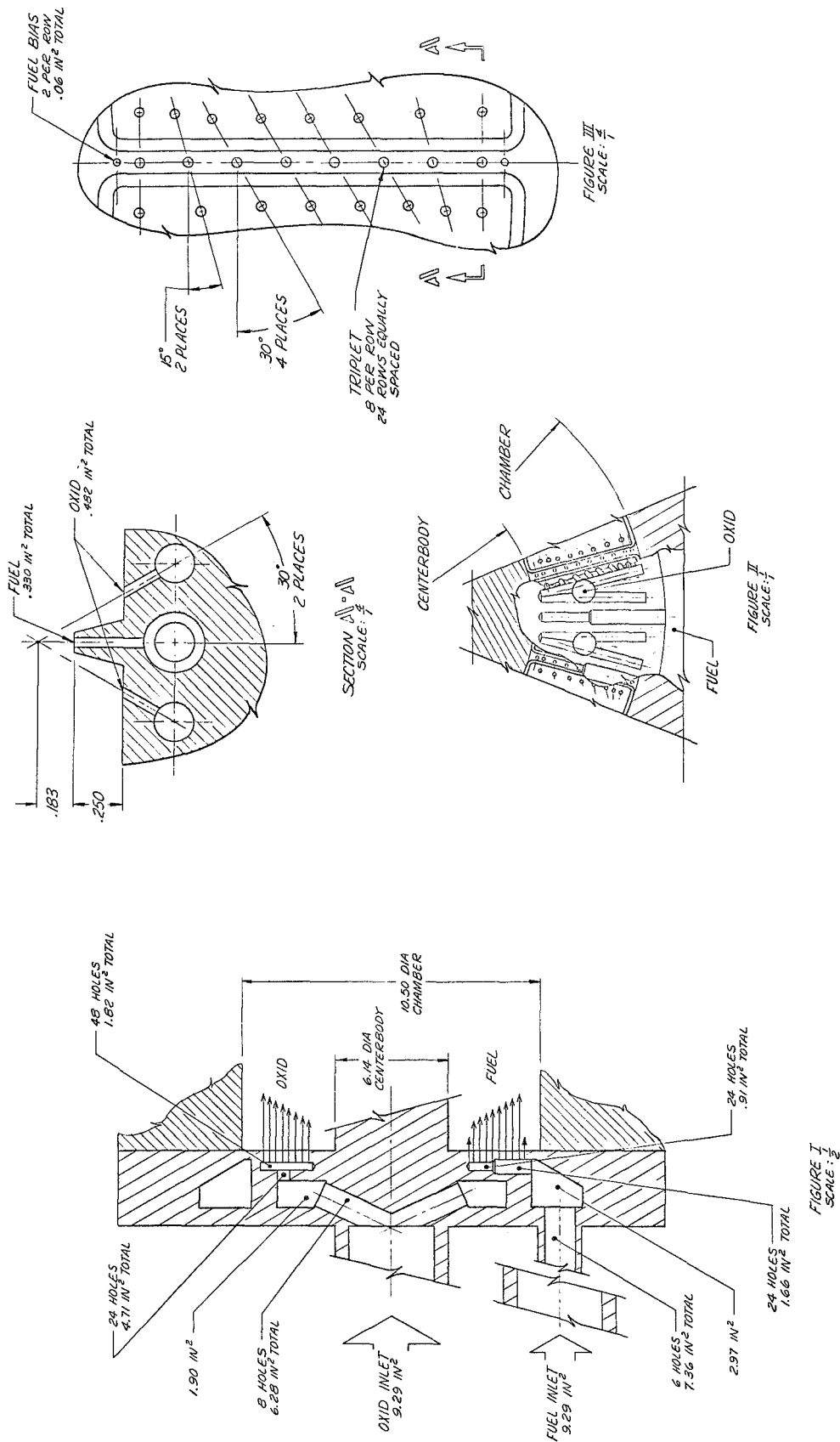
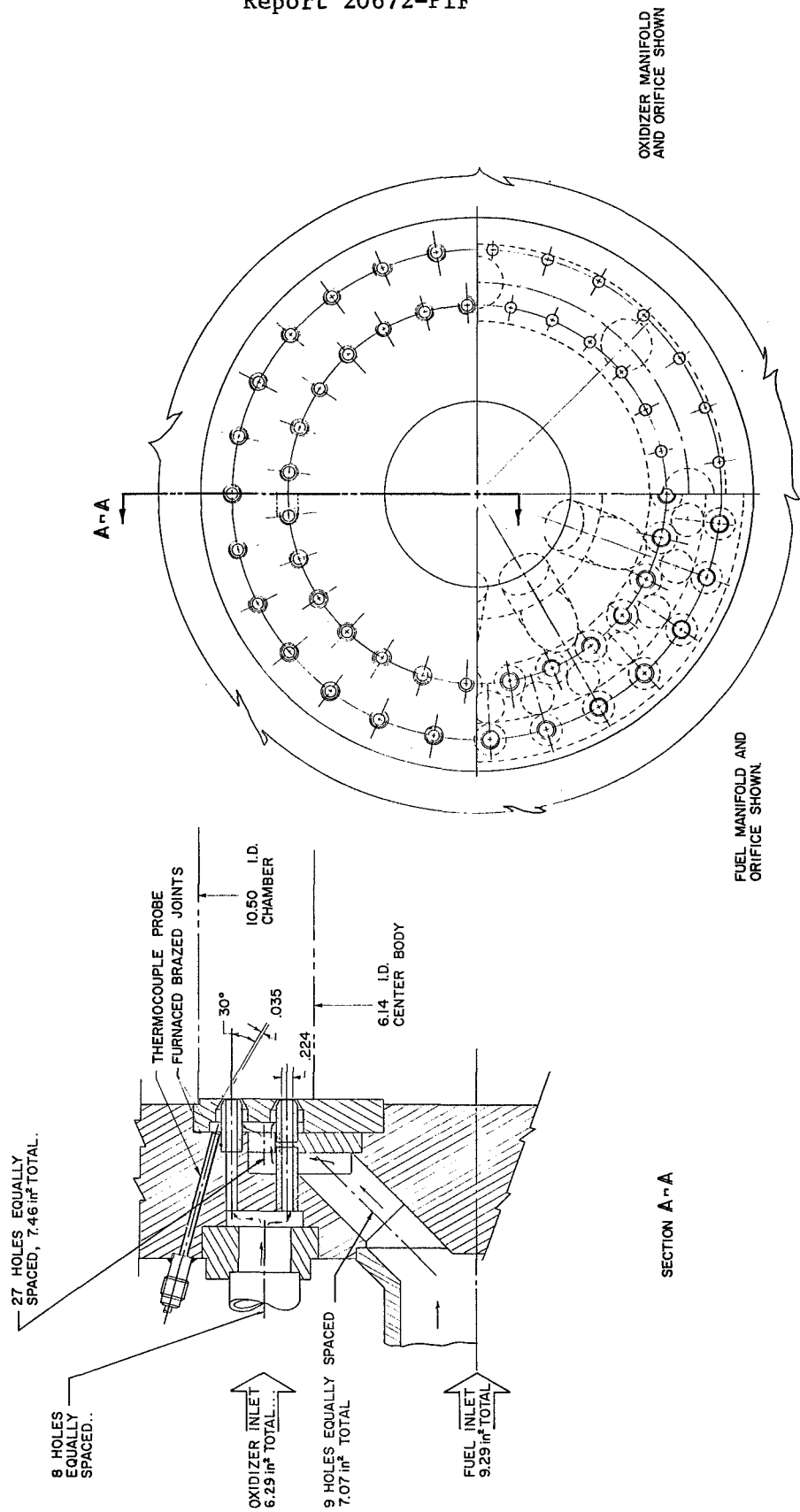


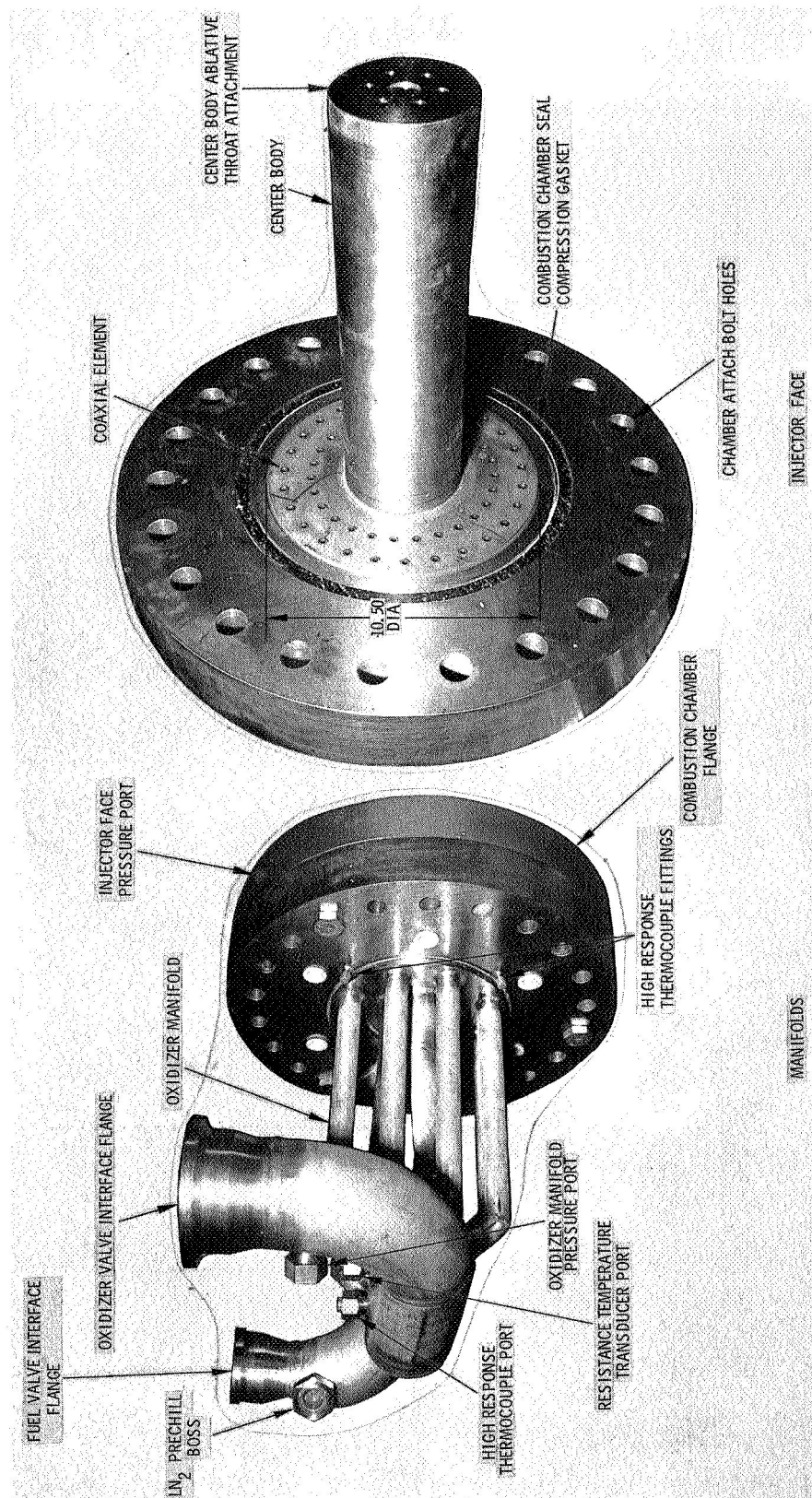
Figure 4

Low Injection Density Triplet Injector Schematic



Annular Coaxial Injector Schematic

Figure 5



Annular Coaxial Injector

Figure 6

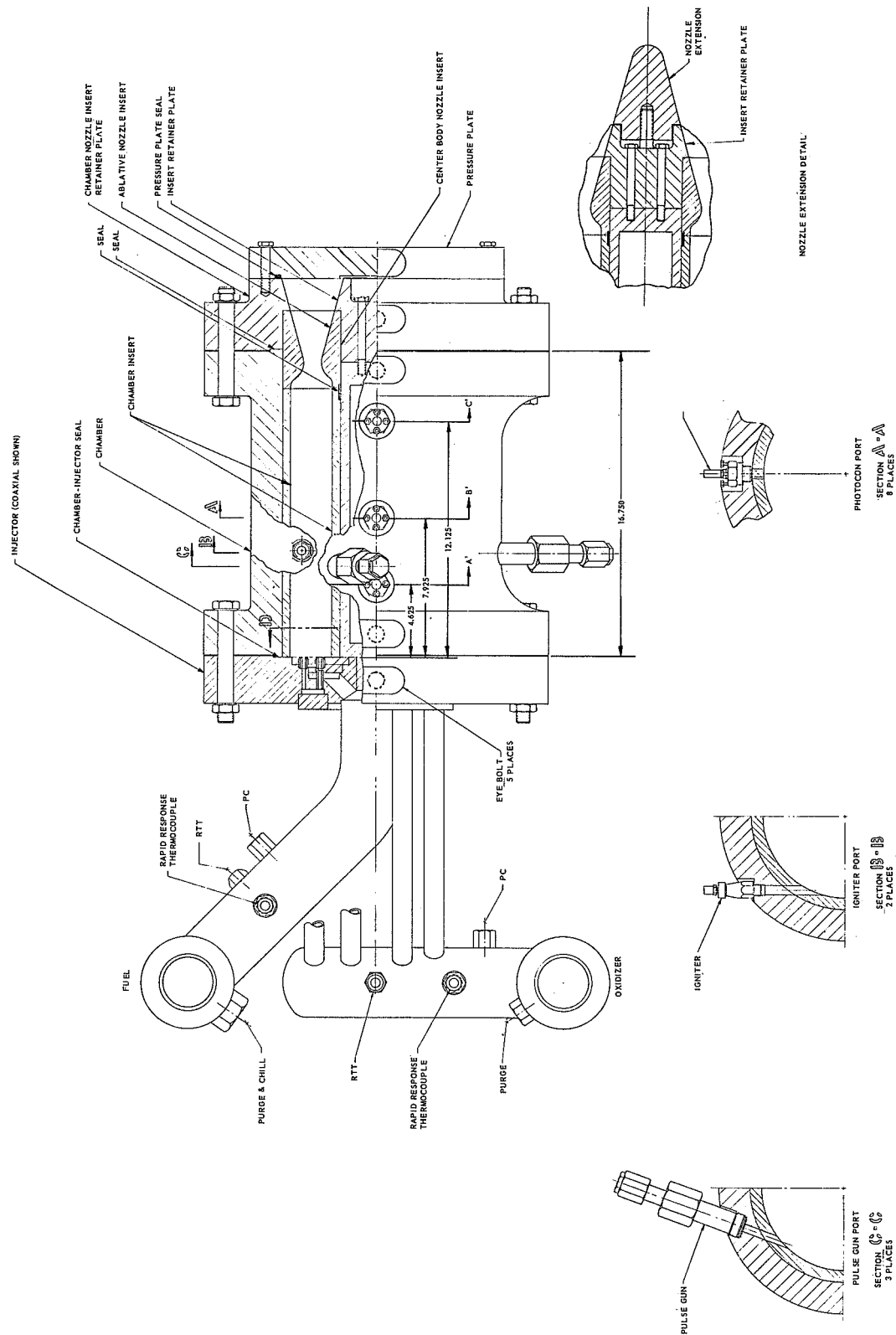
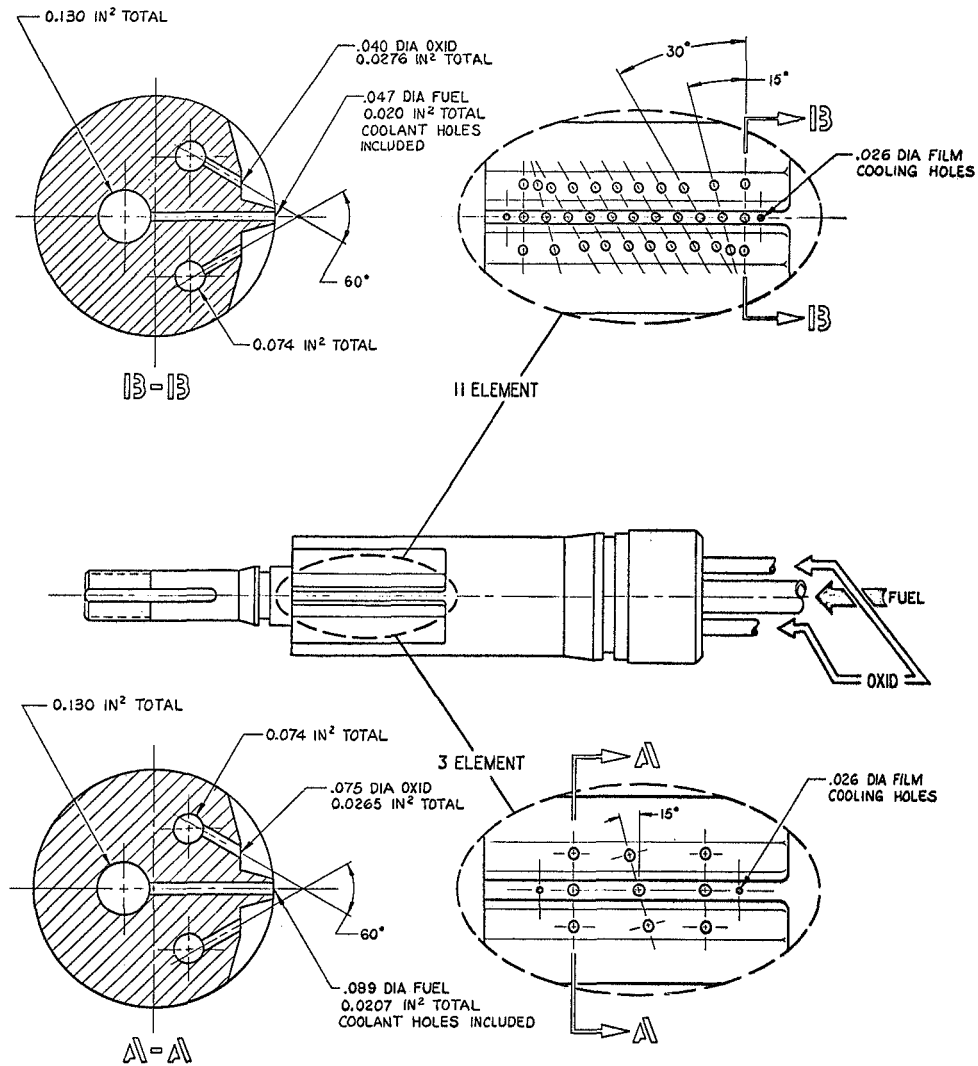


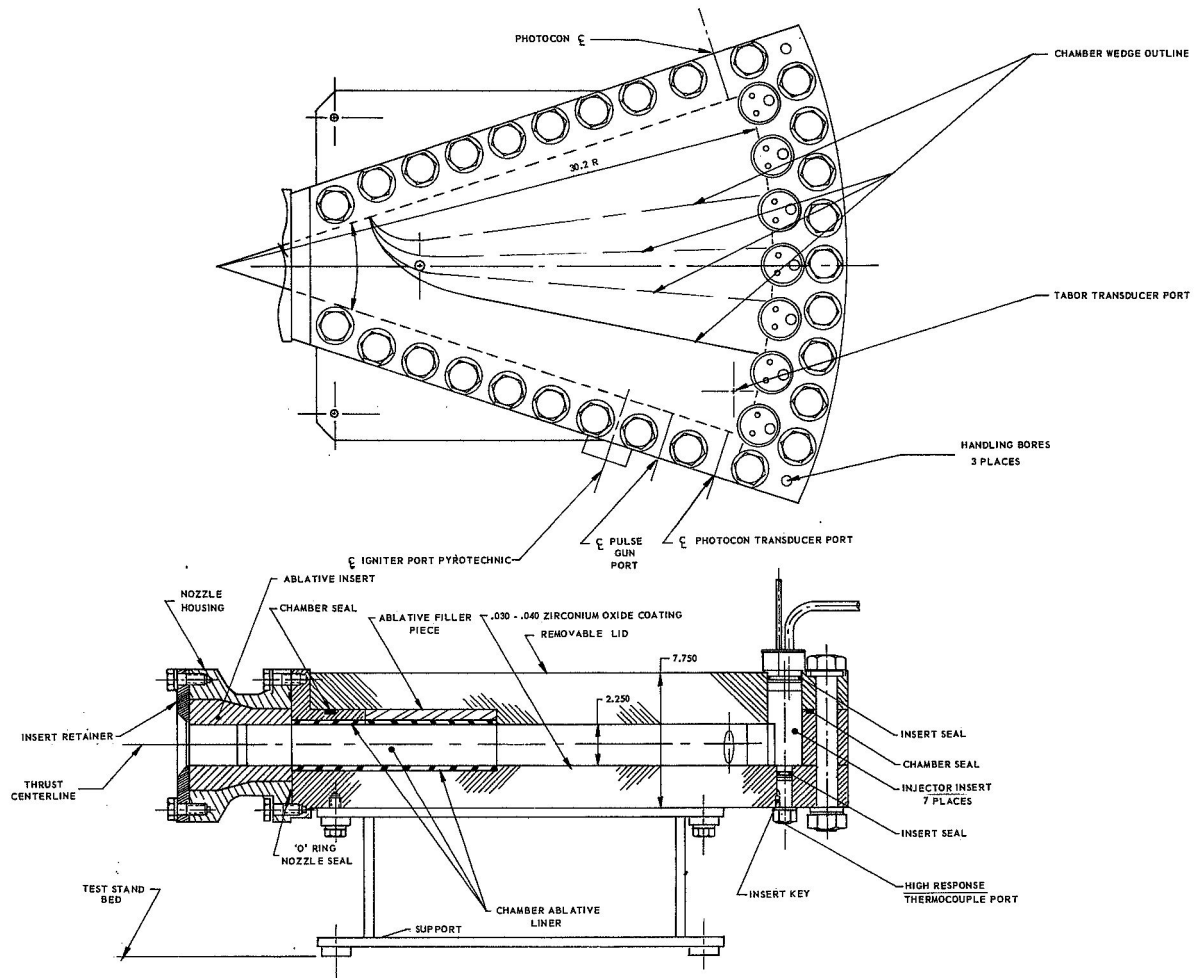
Figure 7

Annular Thrust Chamber Assembly



Excitation Chamber Triplet Injector Insert Schematic

Figure 8



Transverse Excitation Chamber Assembly Schematic

Figure 9

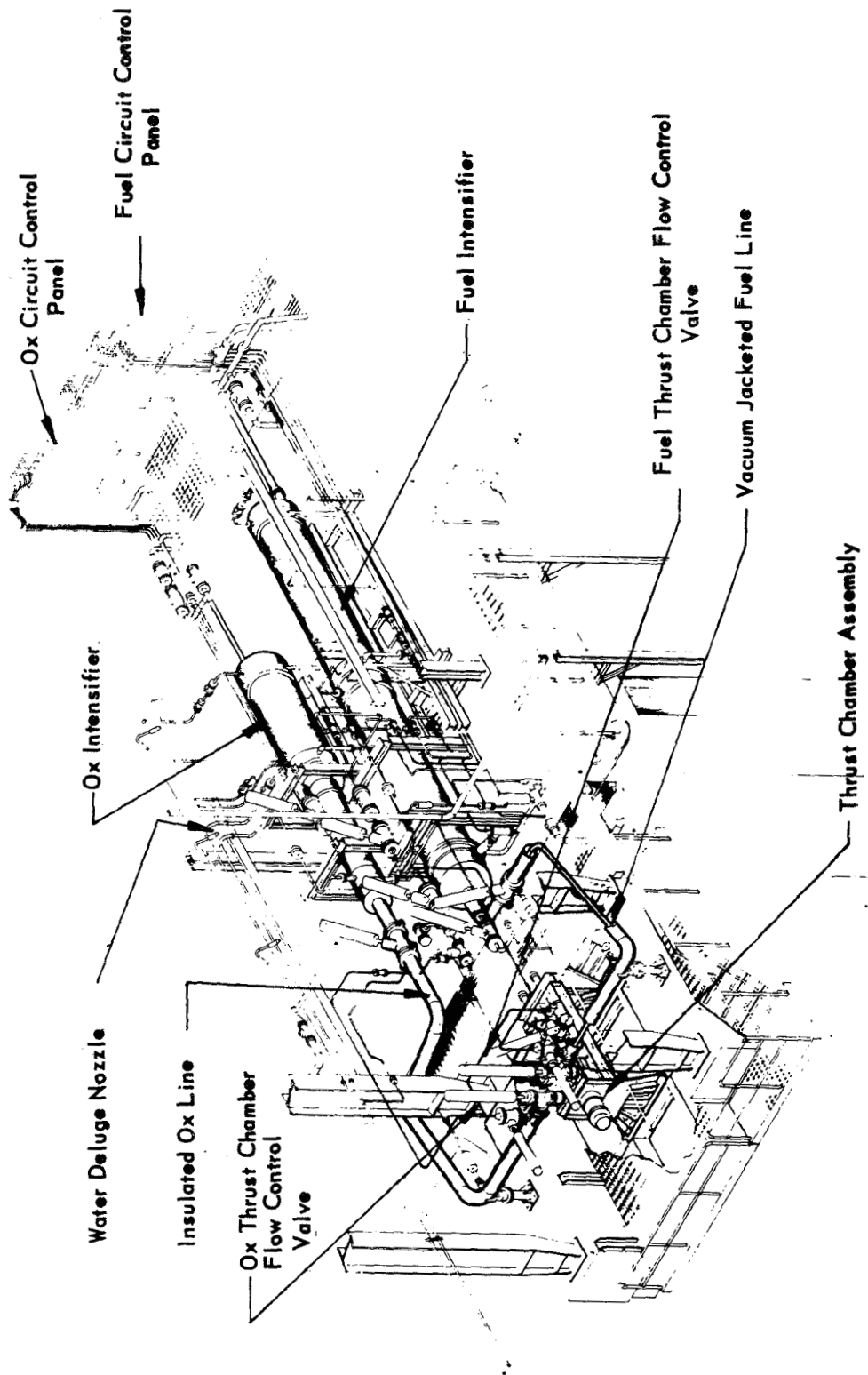


Figure 10

Isometric Drawing of Test Stand C-6

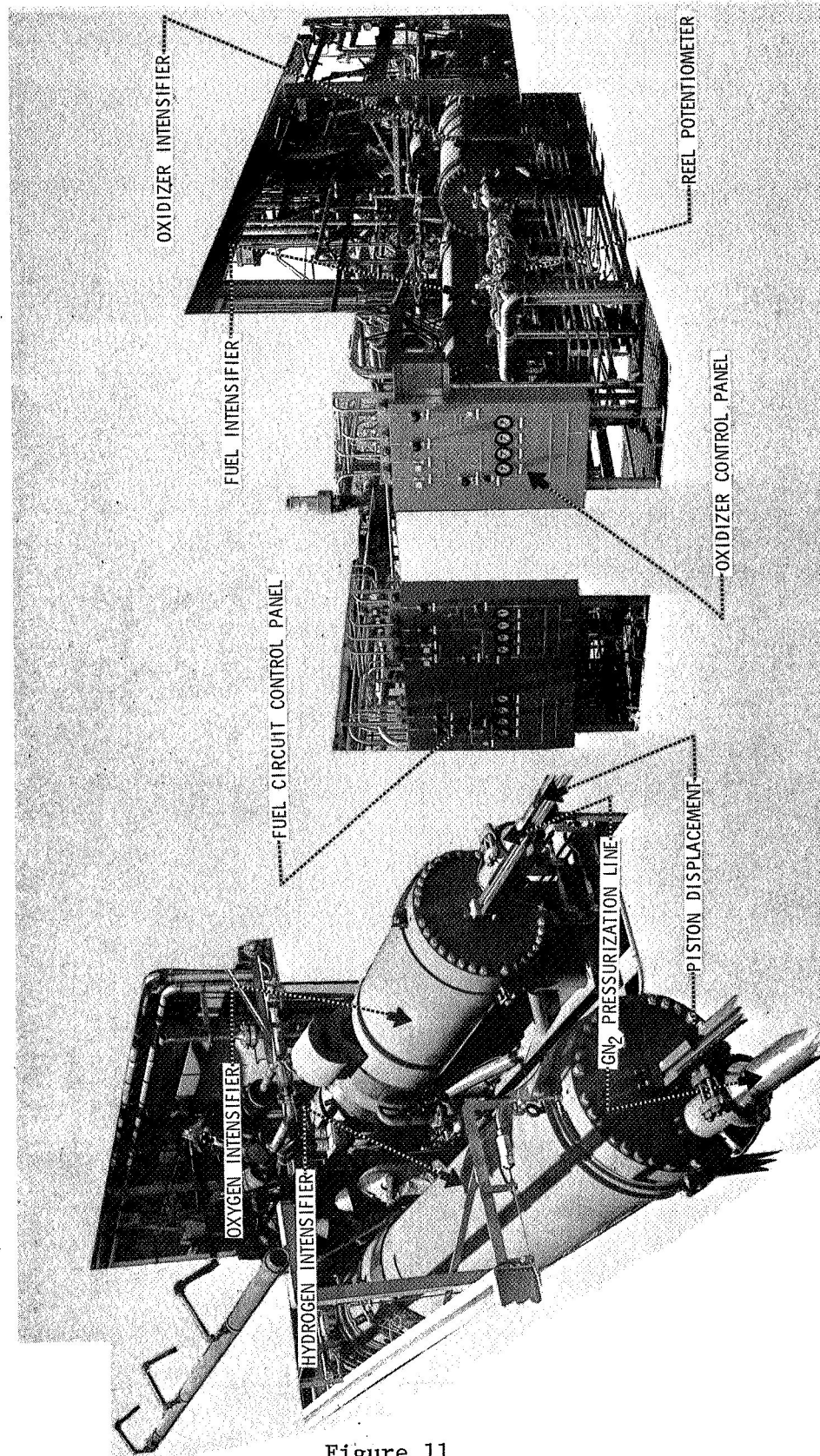


Figure 11

View of C-6 Test Stand and Intensifiers

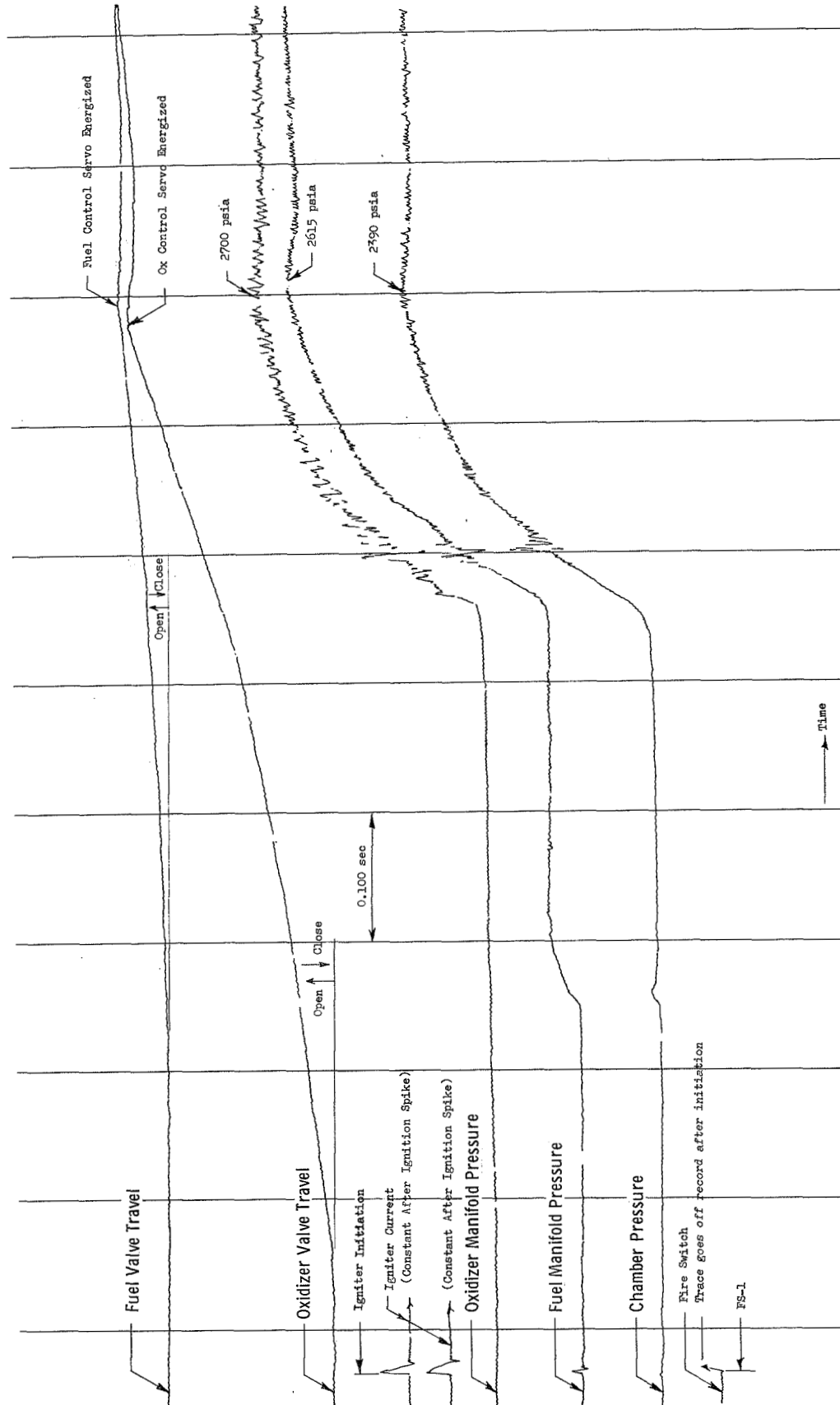


Figure 12

Typical Start Transient Record of an Annular Coaxial
Test on Test Stand C-6

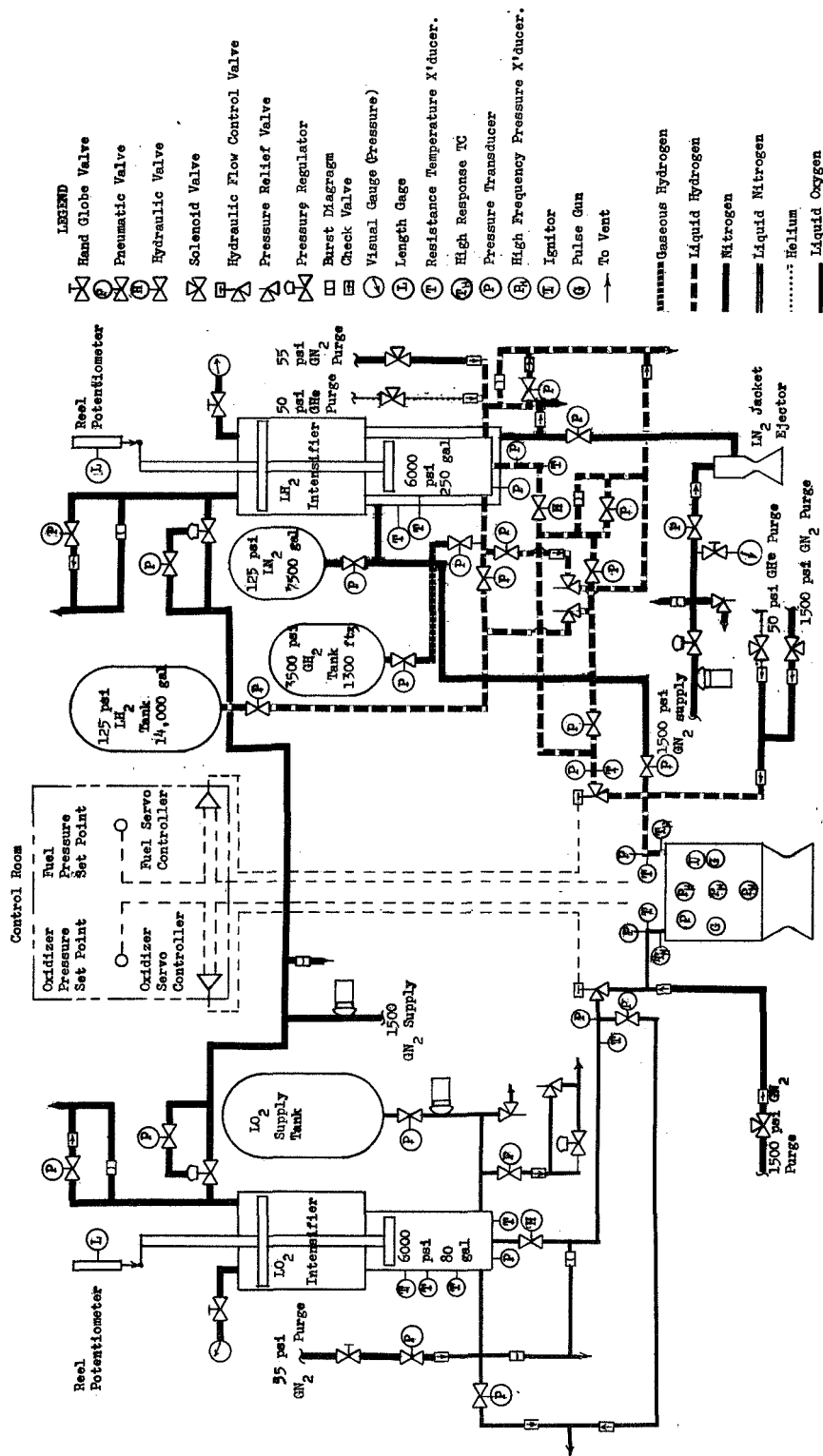
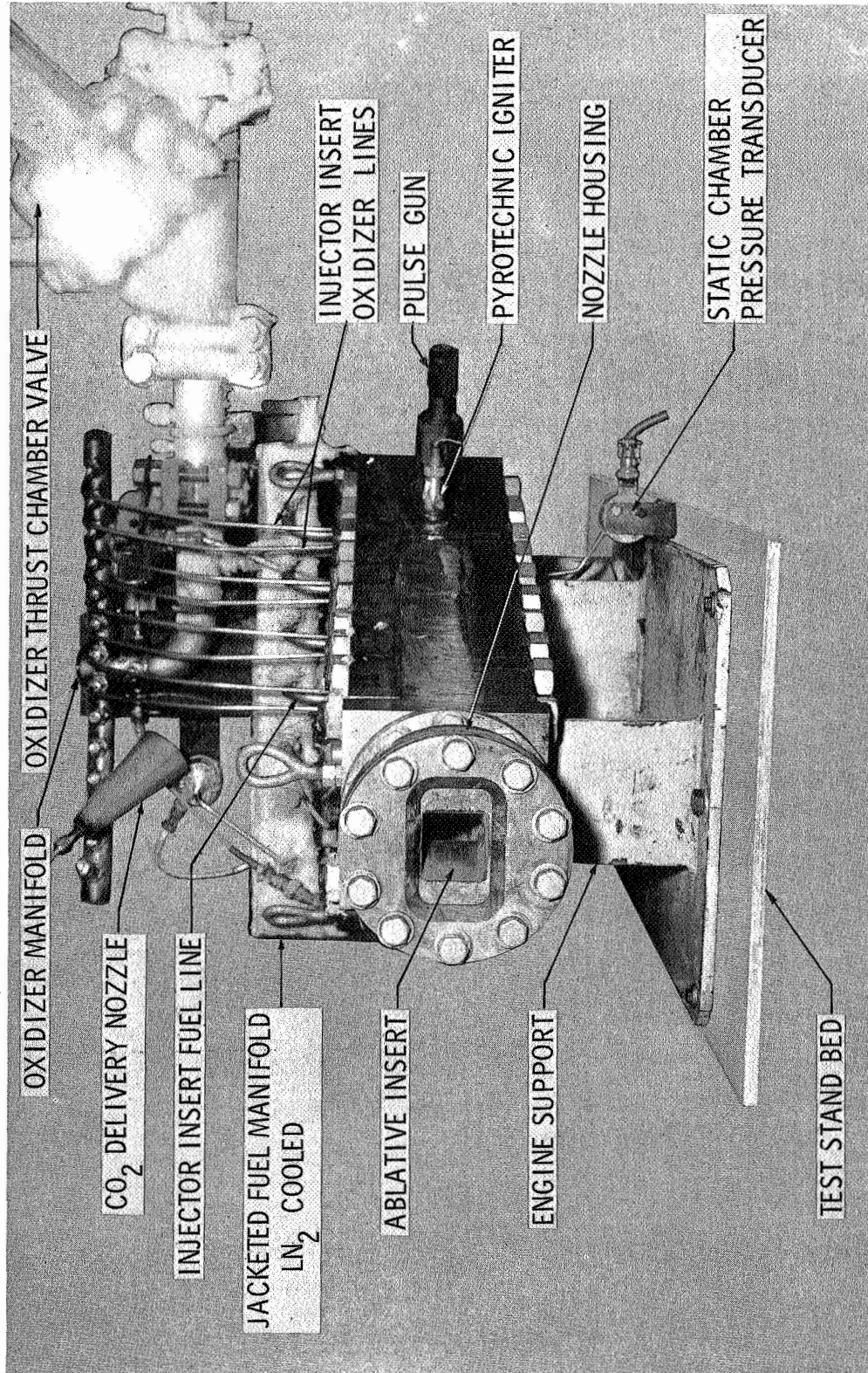


Figure 13



Transverse Excitation Chamber on Test Stand J-1

Figure 14

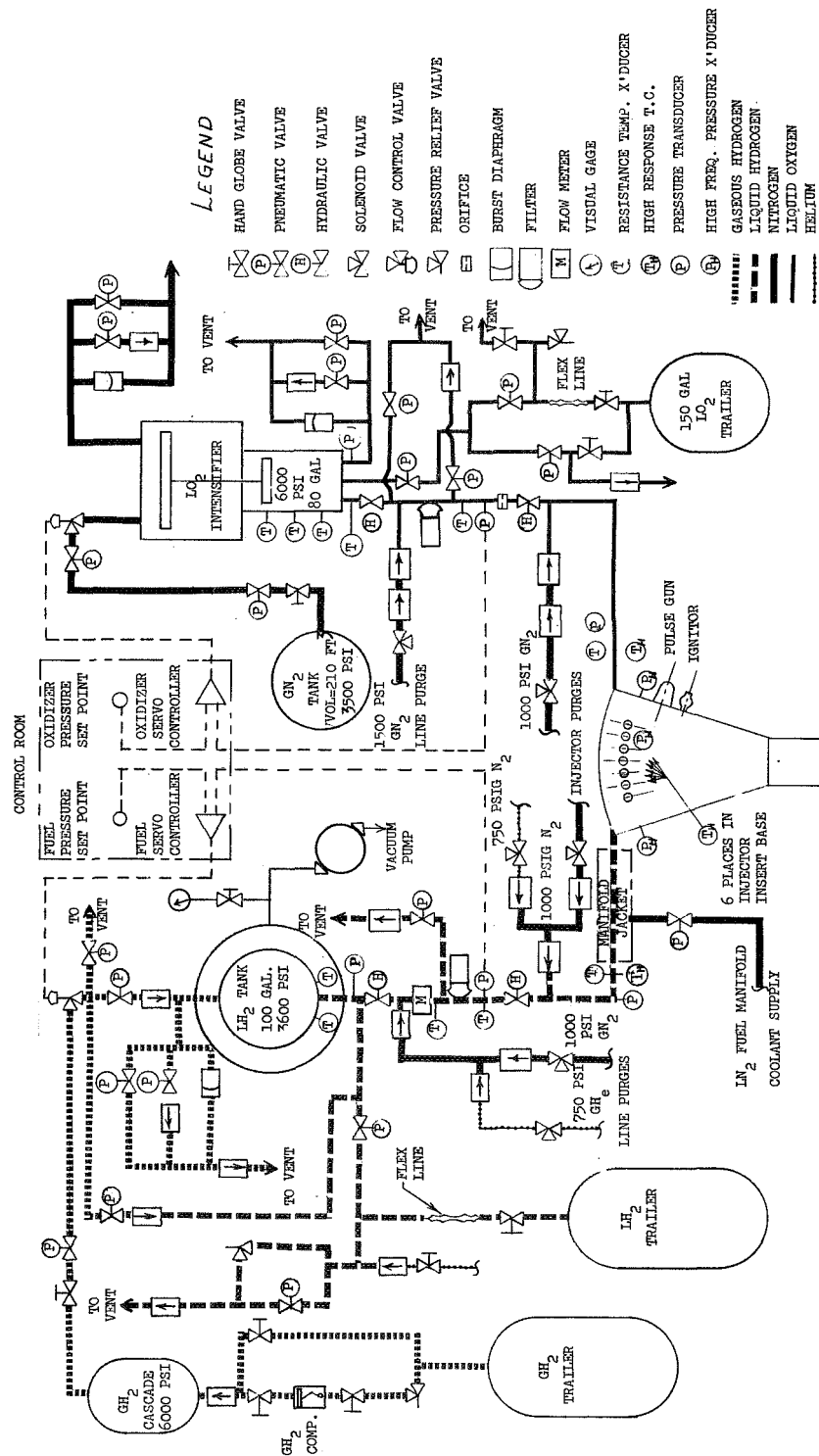


Figure 15

Flow Schematic for Test Stand J-1

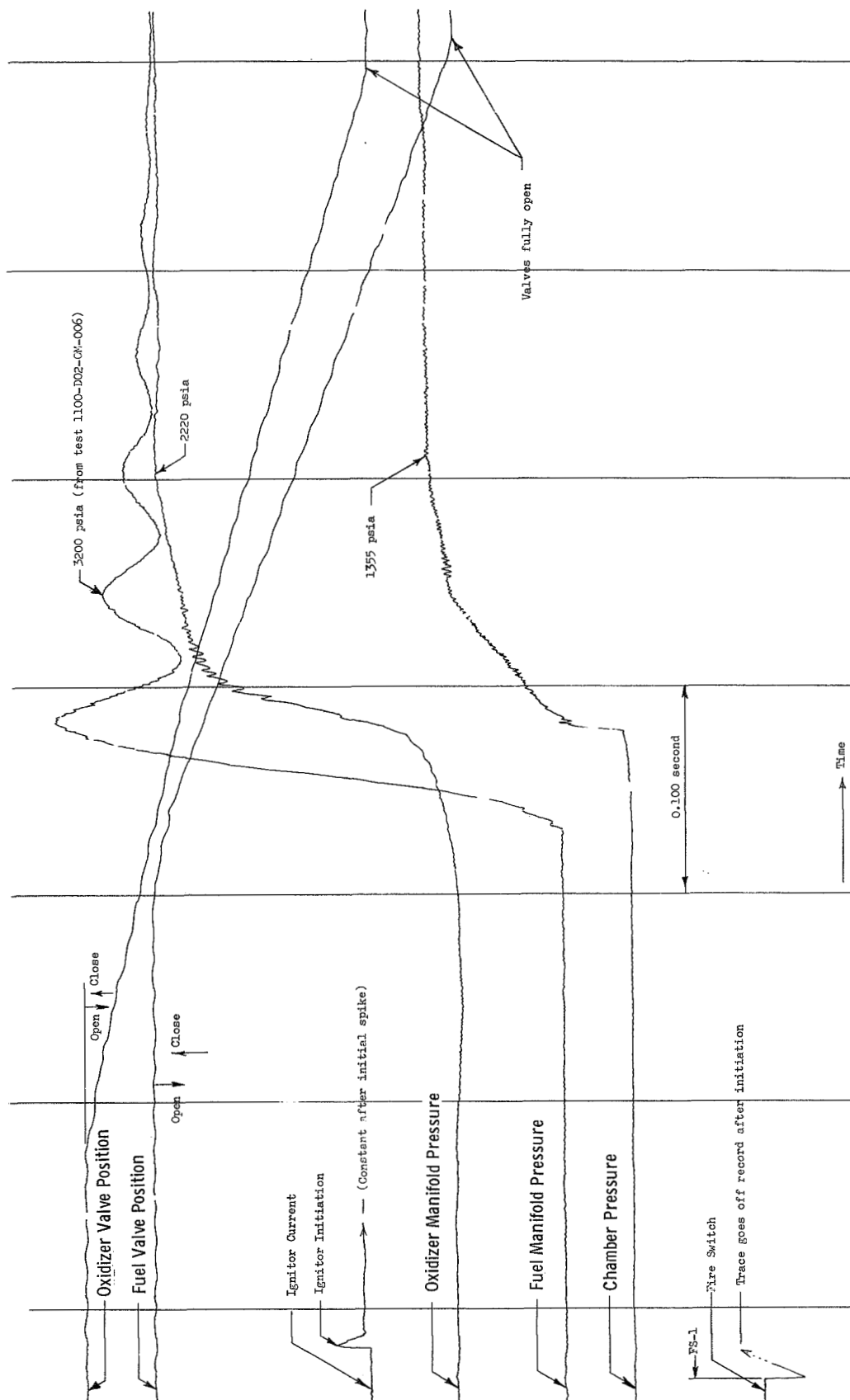


Figure 16

Typical Start Transient for a Transverse Excitation
Chamber Test on Test Stand J-1

```

X---STABILITY RETURNS AFTER PULSE DAMPS
O---PULSED INSTABILITY
+---INSTABILITY RETURNS AFTER PULSE DAMPS
□---PULSE SHIFTS MODE
◇---PULSED INSTABILITY ANNULAR CHAMBER

```

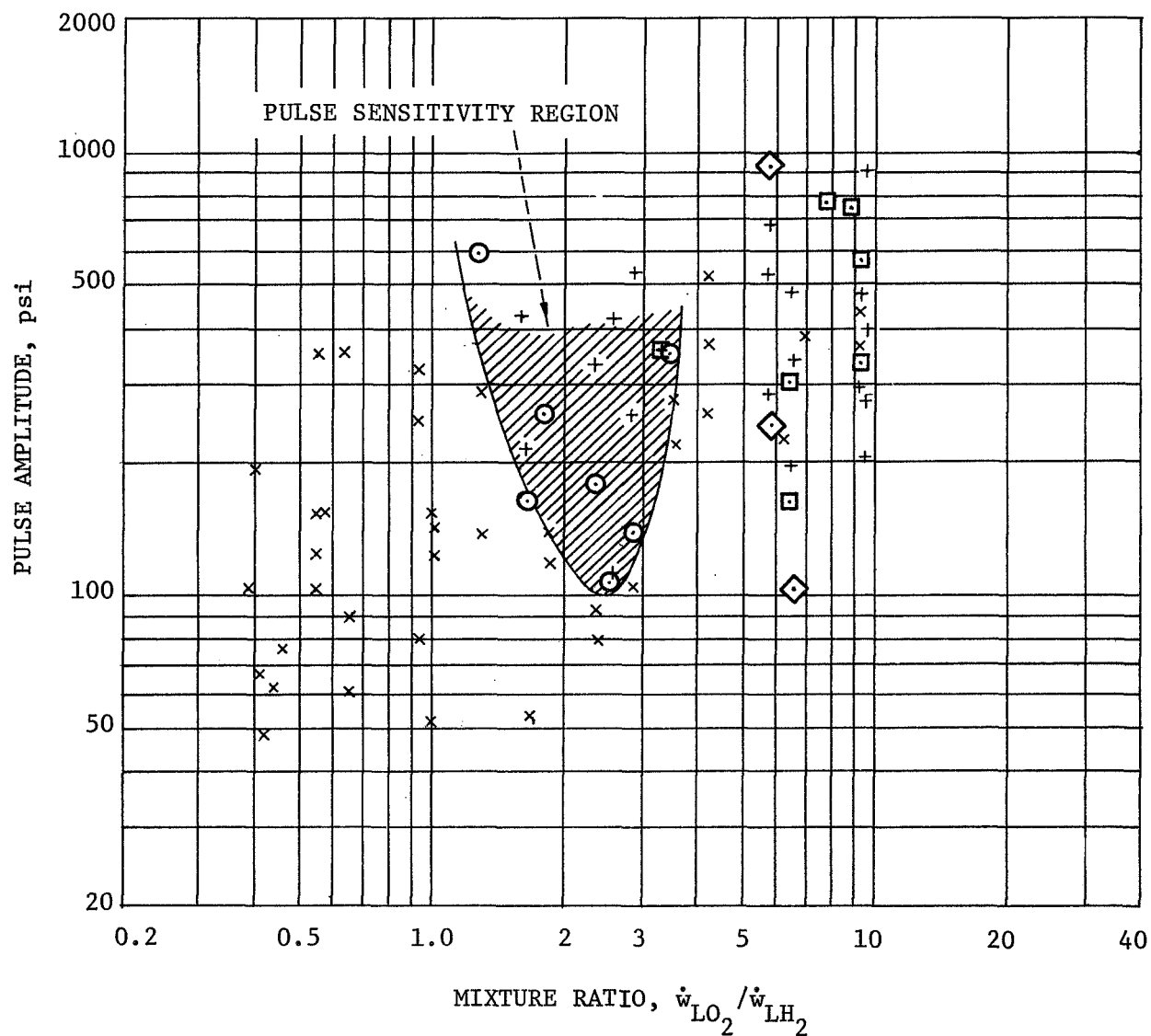
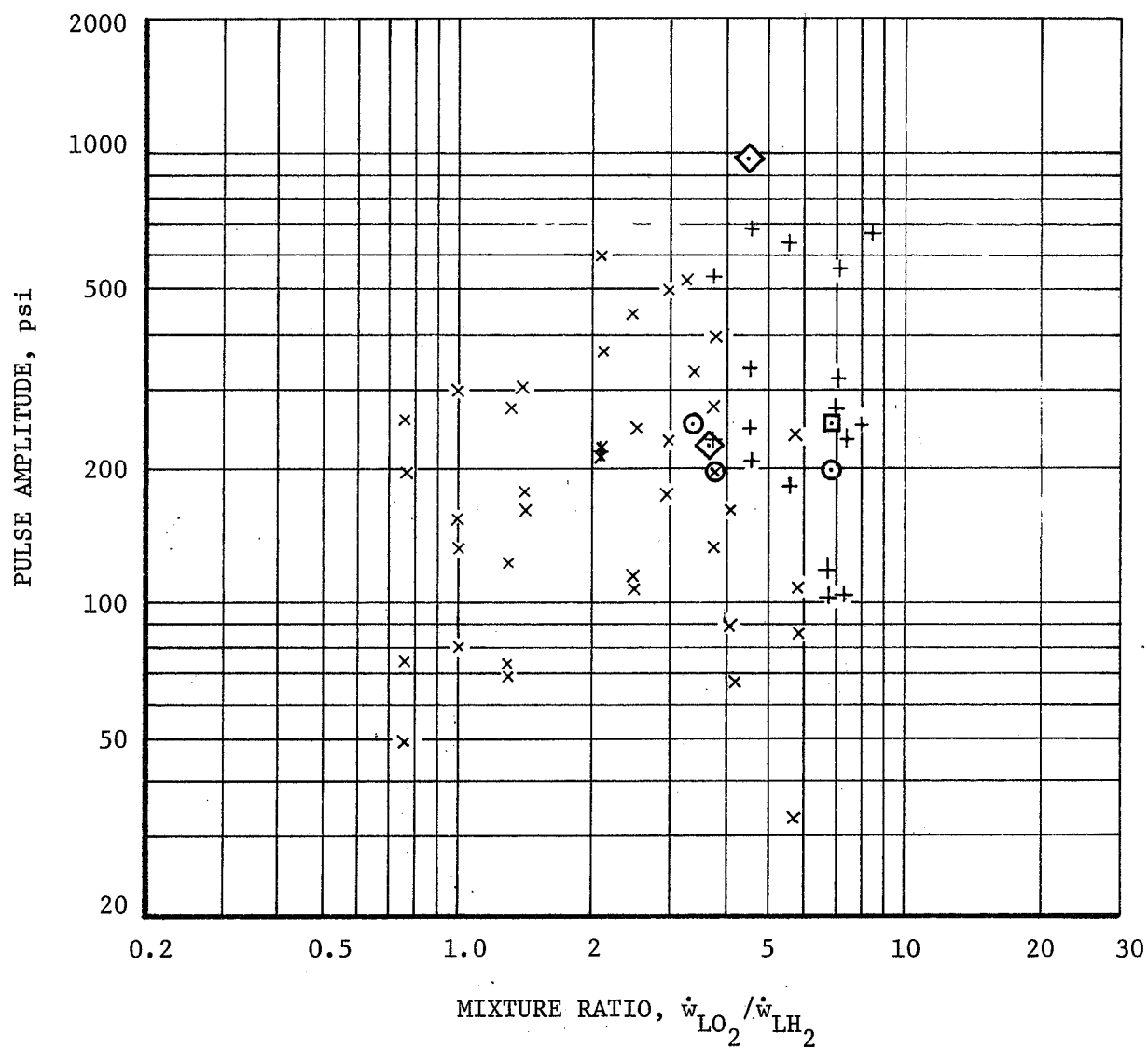
Initial Pulse Amplitude $P_c = 1000$ psia

Figure 17

LEGEND:

- ×---STABILITY RETURNS AFTER PULSE DAMPS
- PULSED INSTABILITY
- +---INSTABILITY RETURNS AFTER PULSE DAMPS
- PULSE SHIFTS MODE
- ◇---PULSED INSTABILITY ANNULAR CHAMBER

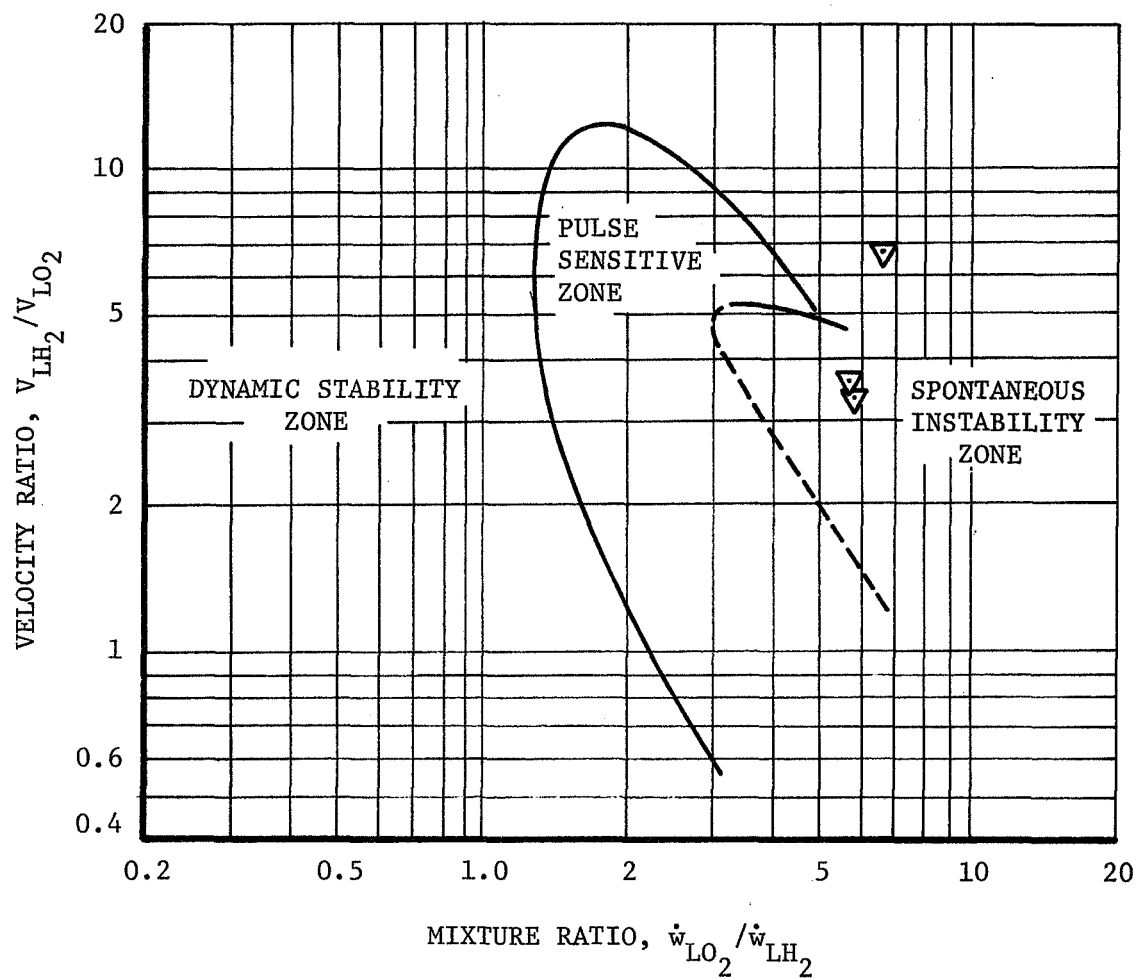


Initial Pulse Amplitude $P_s = 2500$ psia

Figure 18

WHERE:

▽---PULSED INSTABILITY ANNULAR CHAMBER



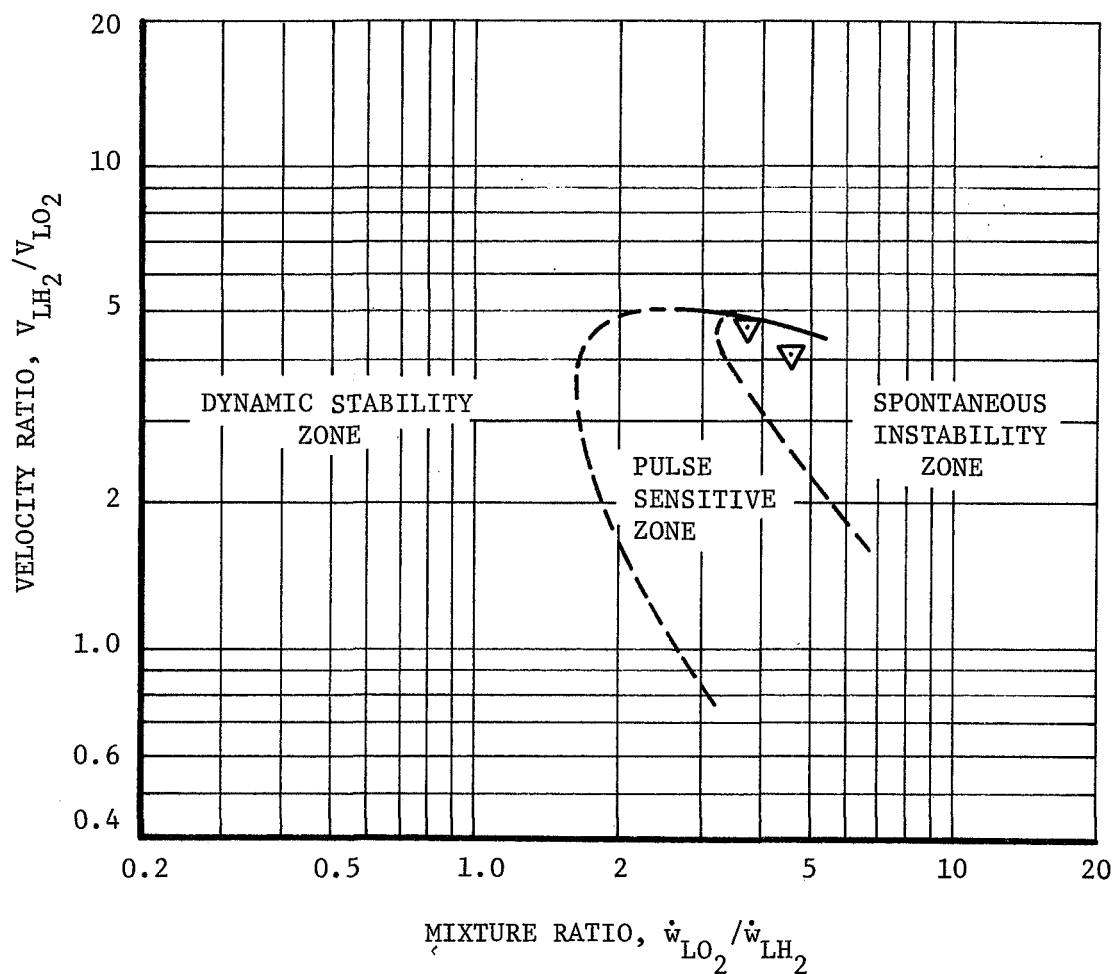
NOTE: CURVES TAKEN FROM AGC HiPc CYLINDRICAL CHAMBER TESTING.

High Frequency Stability Results - All Injectors at
900 Pc 1200 psia

Figure 19

WHERE:

▽--- PULSED INSTABILITY ANNULAR CHAMBER



NOTE: CURVES TAKEN FROM AGC HiPc CYLINDRICAL CHAMBER TESTING.

High Frequency Stability Results - All Injectors at
2400 Pc 2700 psia

Figure 20

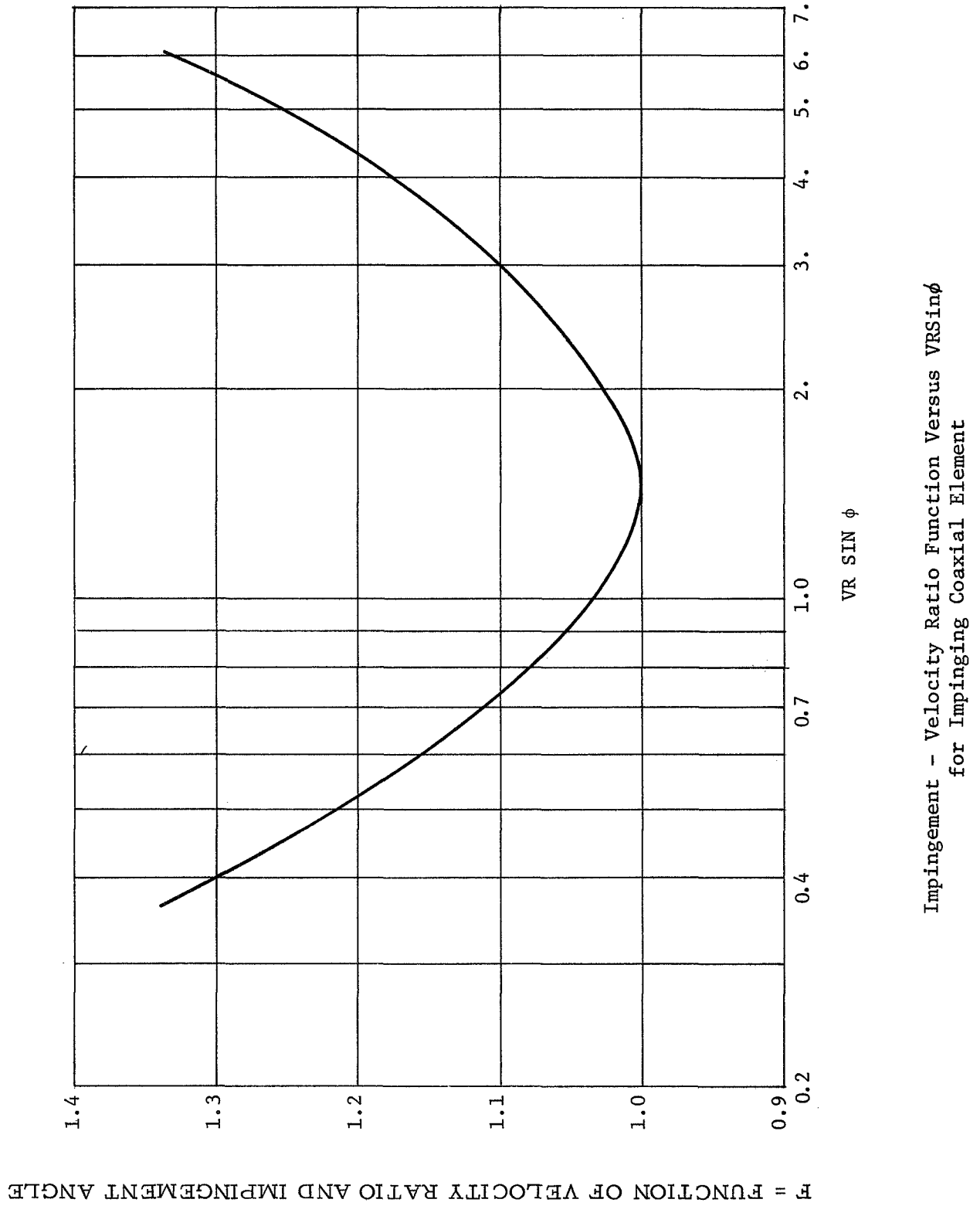


Figure 21

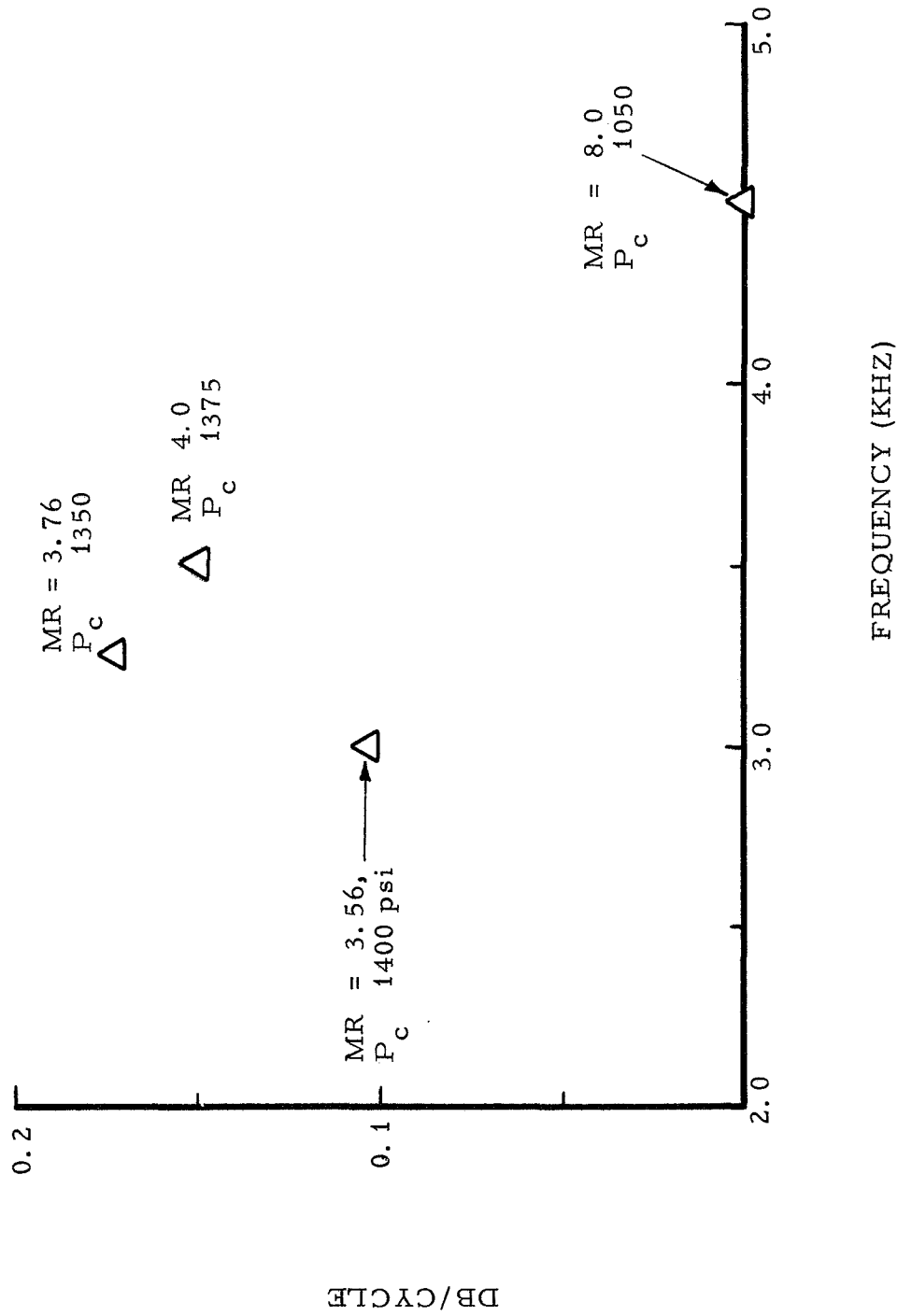


Figure 22

Frequency Response Characteristics of Triplet Injectors

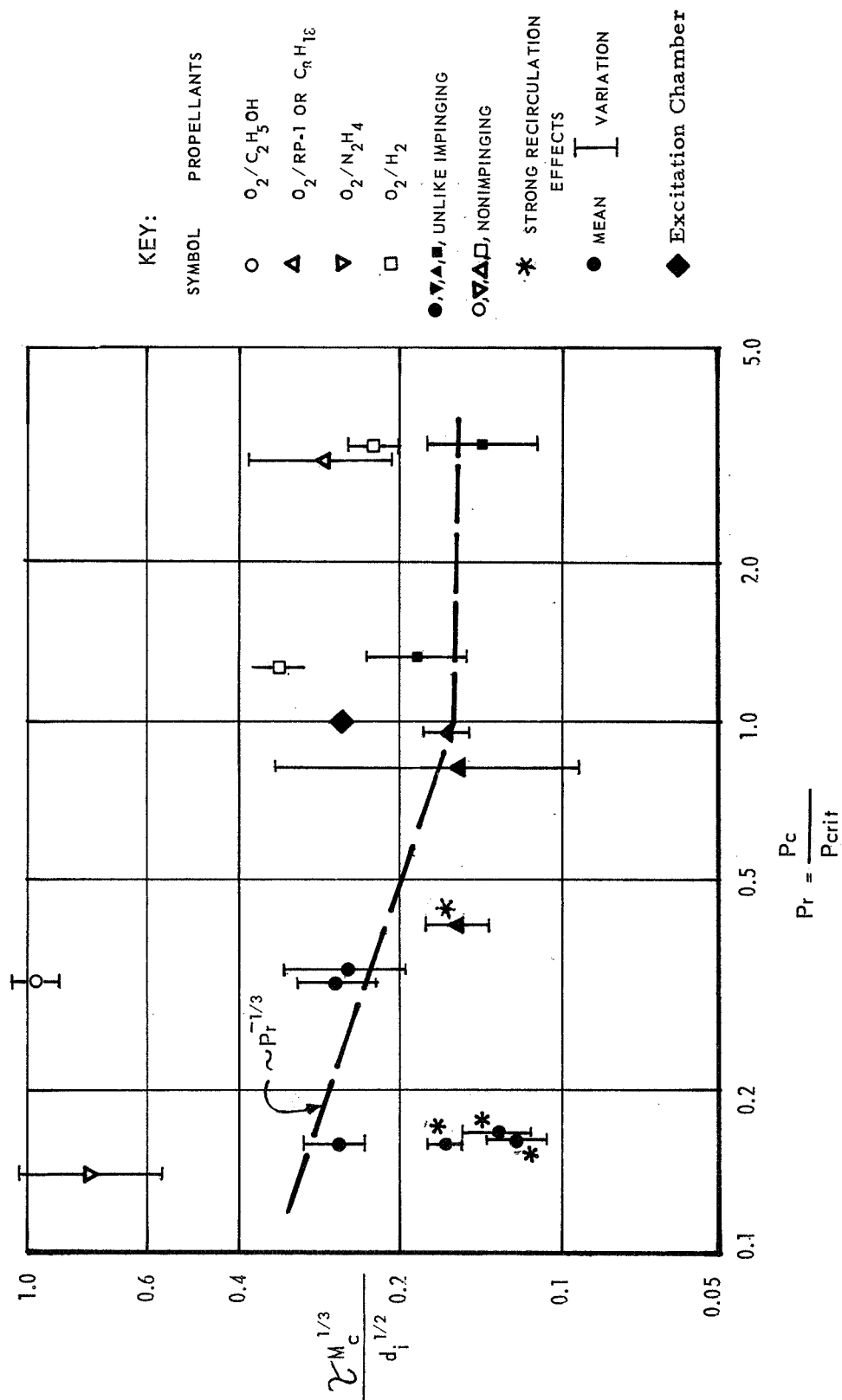
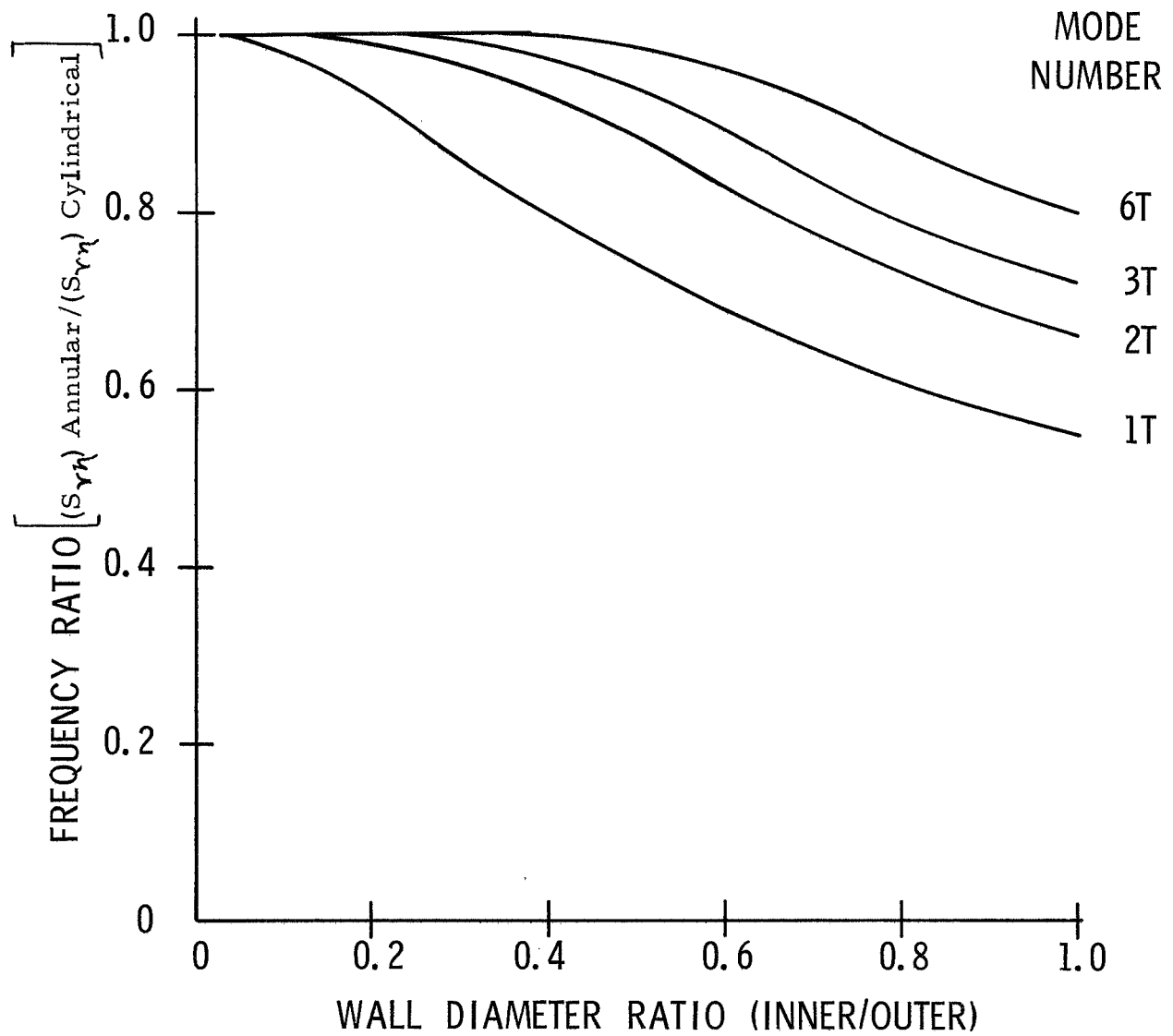


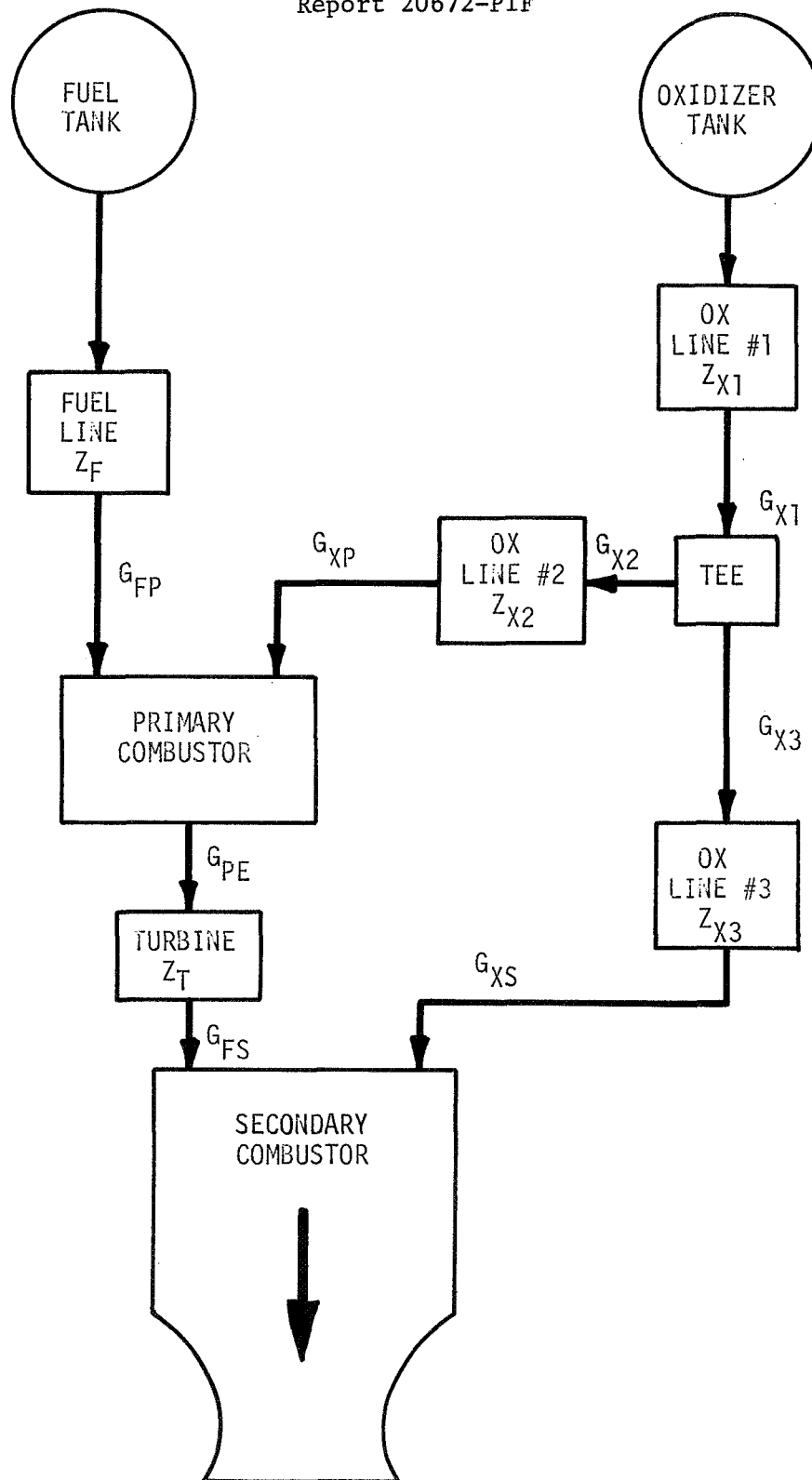
Figure 23

Effect of Pressure on Non-Coaxial Elements

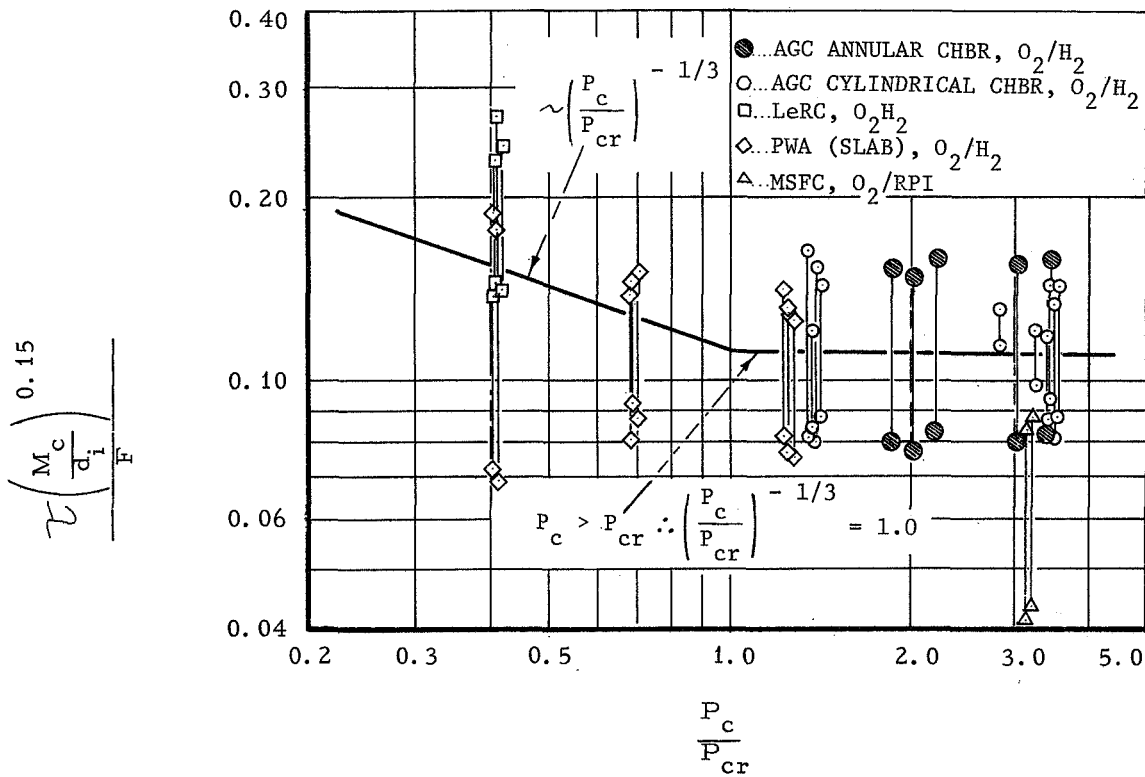


Tangential Mode Acoustic Frequencies for Annular Chambers

Figure 24



Staged Combustion Model



$$\frac{1000}{2 f_s} = \tau = 0.11 (d_i/M_c)^{0.15} (P_c/P_{cr})^{-1/3} F \quad (P_c \leq P_{cr})$$

$$= 0.11 (d_i/M_c)^{0.15} F \quad (P_c \geq P_{cr})$$

WHERE:

f_s = SENSITIVE FREQUENCY, hz

τ = TIME LAG, msec

d_i = INJECTION ORIFICE DIA (LEAST VOLATILE PROPELLANT), in.

P_{cr} = CRITICAL PRESSURE (LEAST VOLATILE PROPELLANT), psia

P_c = CHAMBER PRESSURE, psia

M_c = CHAMBER MACH NO.

VR = VELOCITY RATIO

ϕ = PROPELLANT IMPINGEMENT ANGLE

F = FUNCTION OF VELOCITY RATIO AND IMPINGEMENT ANGLE

Effect of Pressure on Impinging Coaxial Injectors

Figure 26

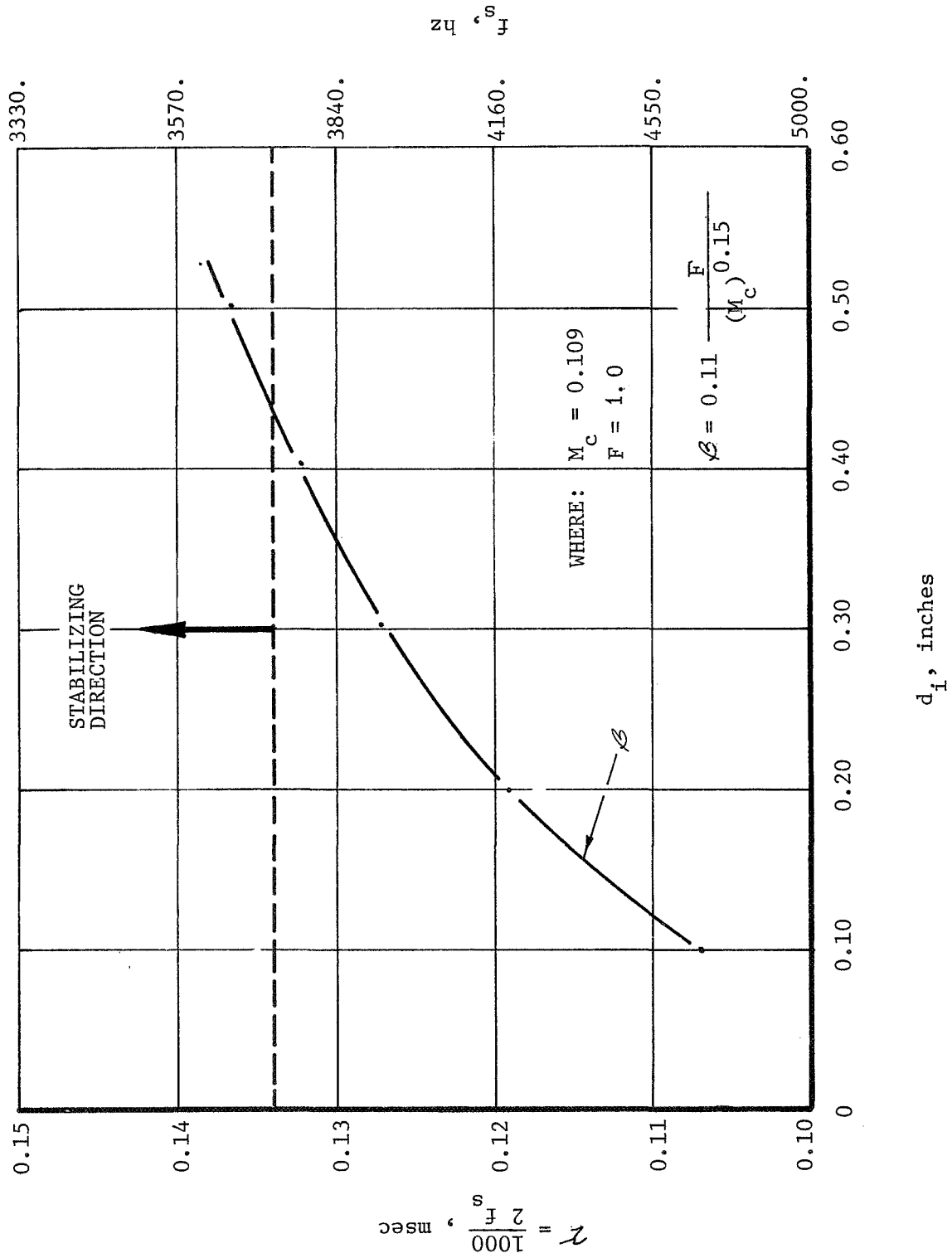


Figure 27

Case I, Orifice Diameter Versus Stability

Injector Coaxial (1132014)
Chamber Annular (1132000)
Propellants LOX/LH₂
Pc 1500 M.R. 4.0

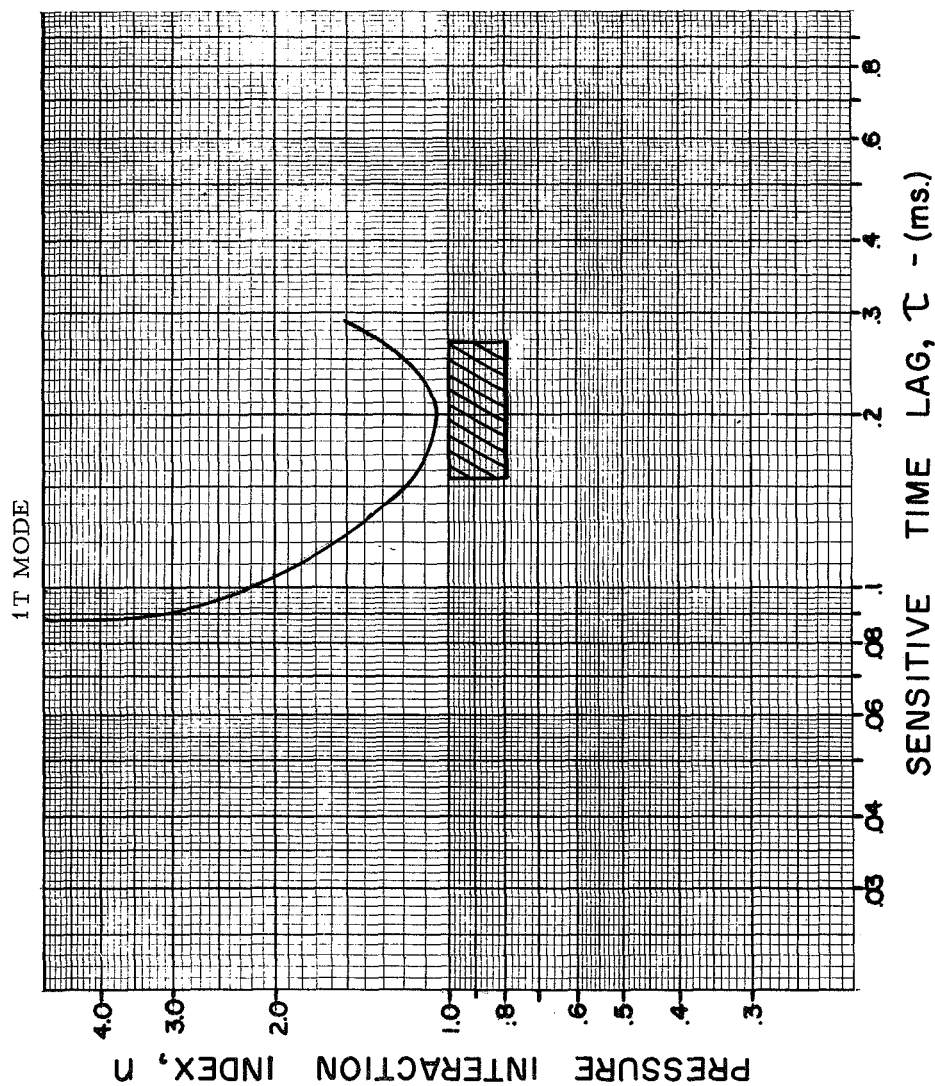
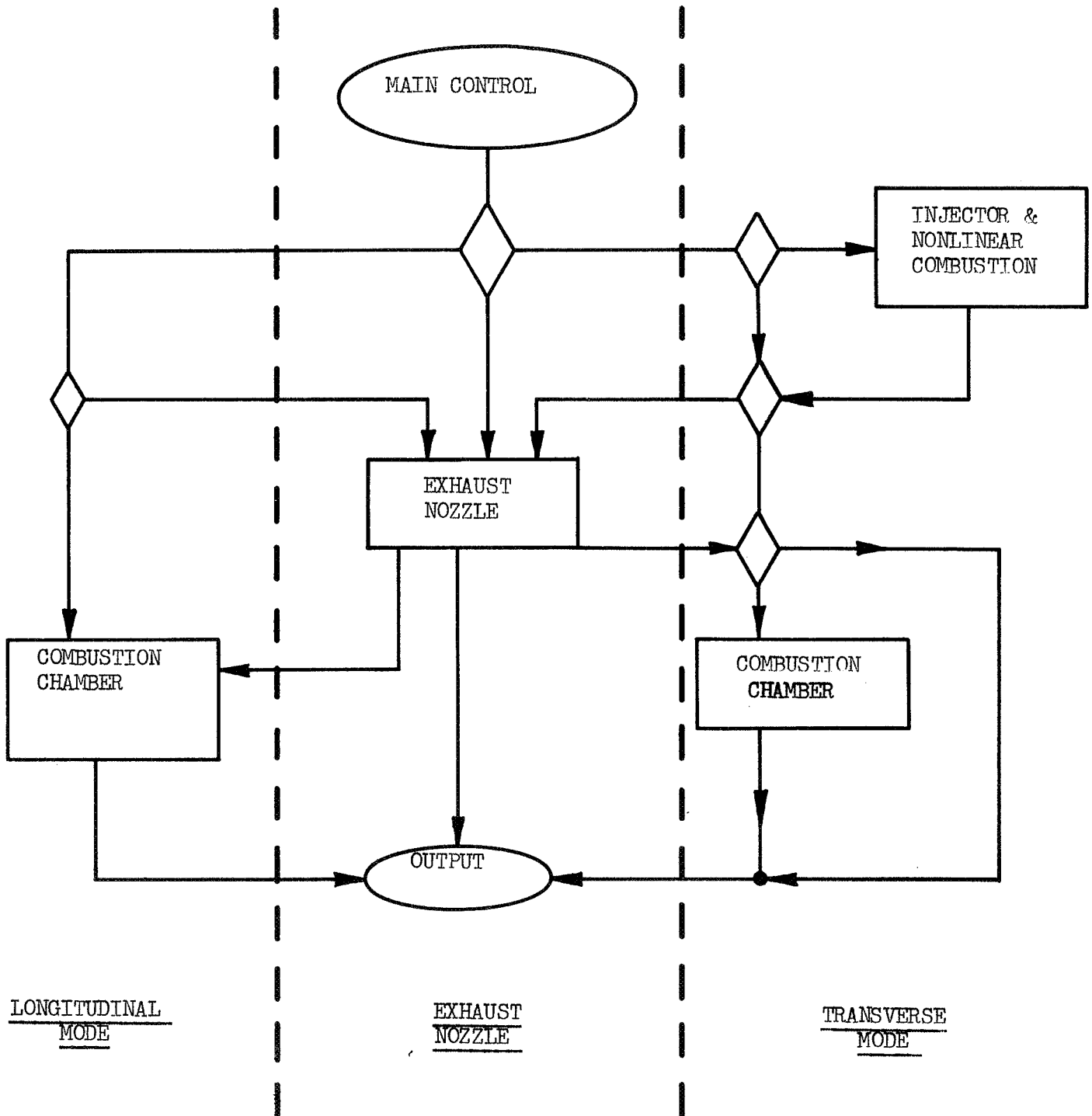


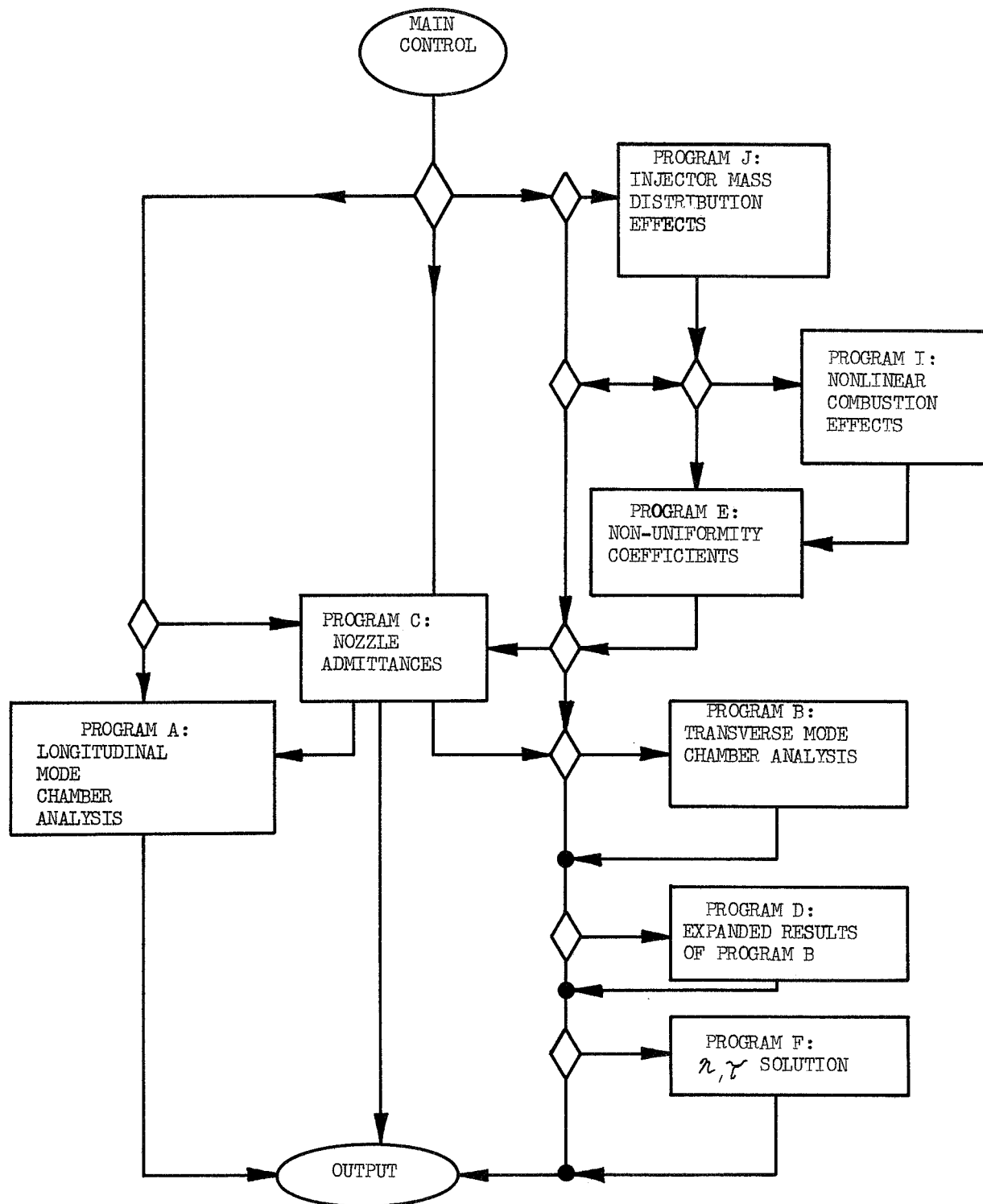
Figure 28

Case II, Orifice Diameter Versus Stability



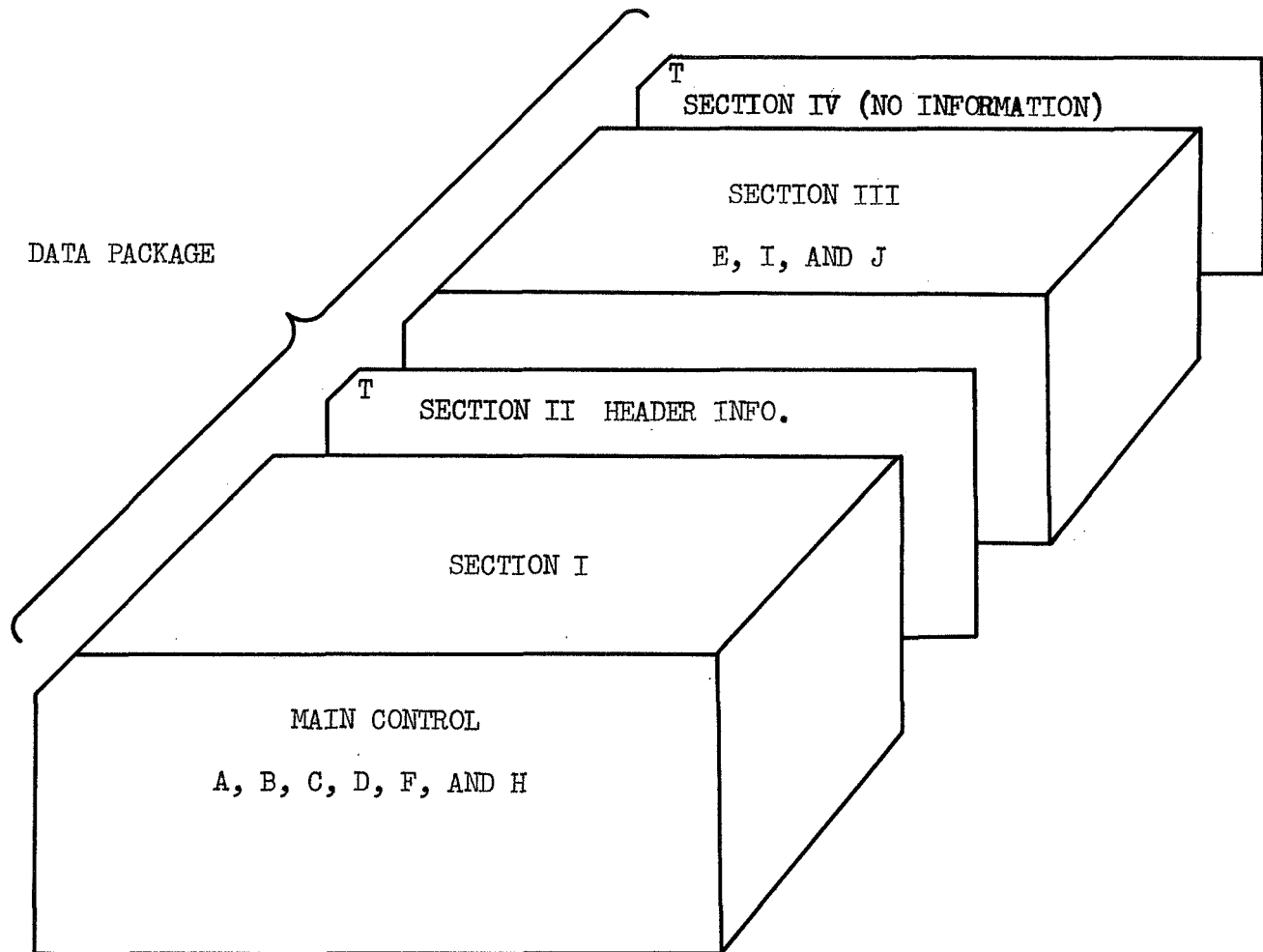
Computer Program Flow Schematic

Figure 29



Computer Program Flow Schematic

Figure 30



IF SECTION III IS NOT USED, SECTION IV MUST NOT BE USED.

Data Package Computer Deck Organization

Figure 31

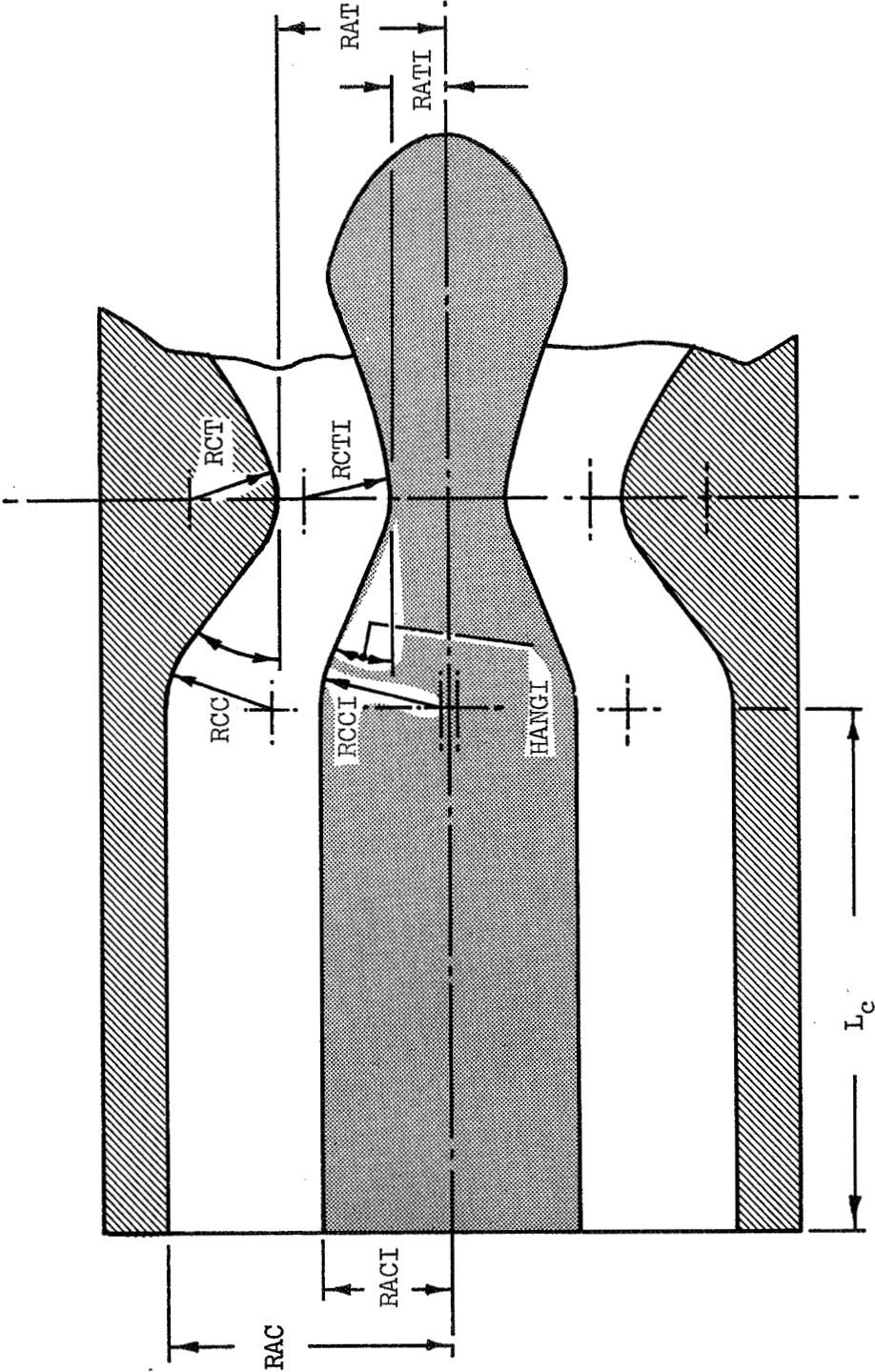
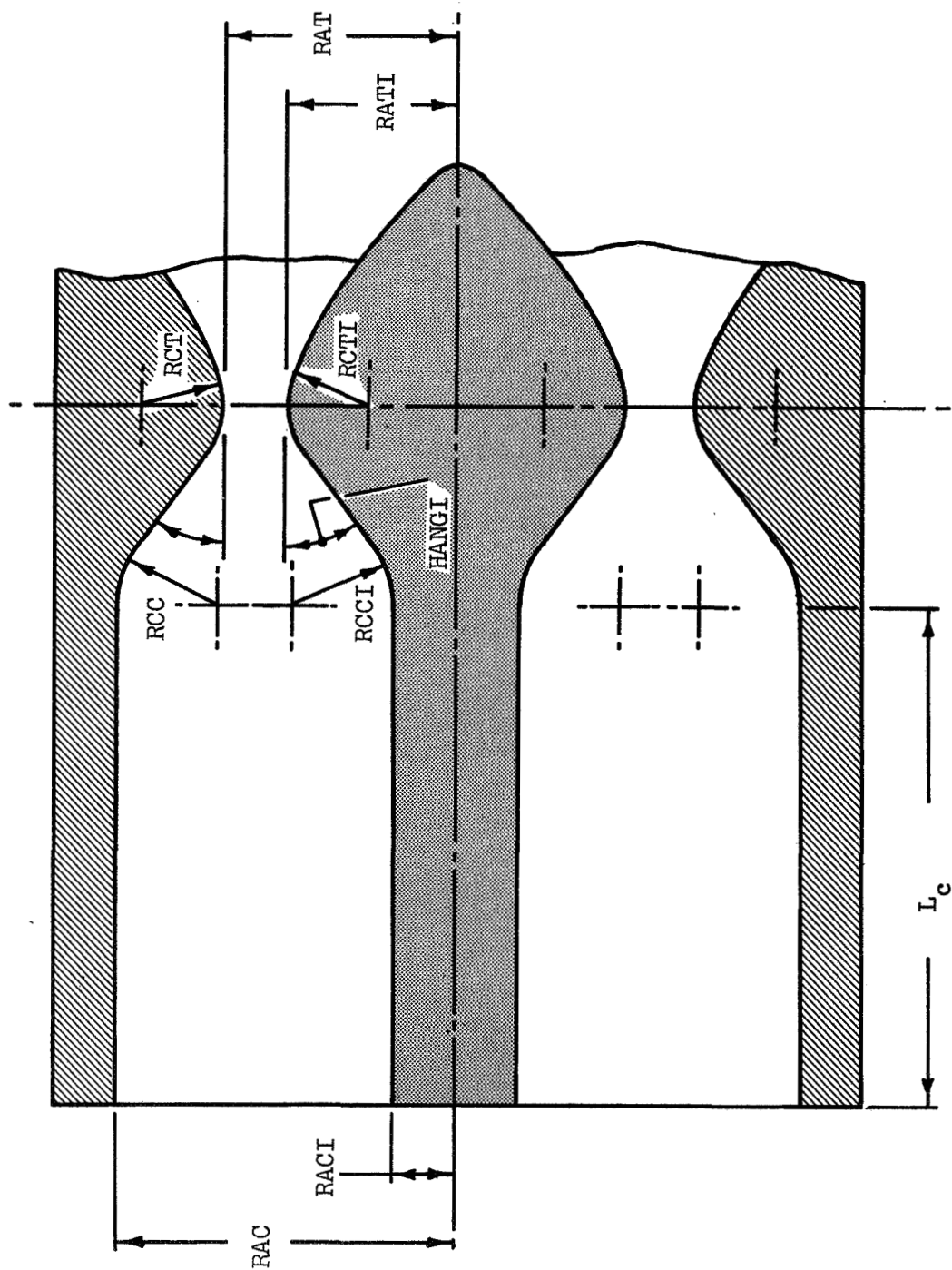
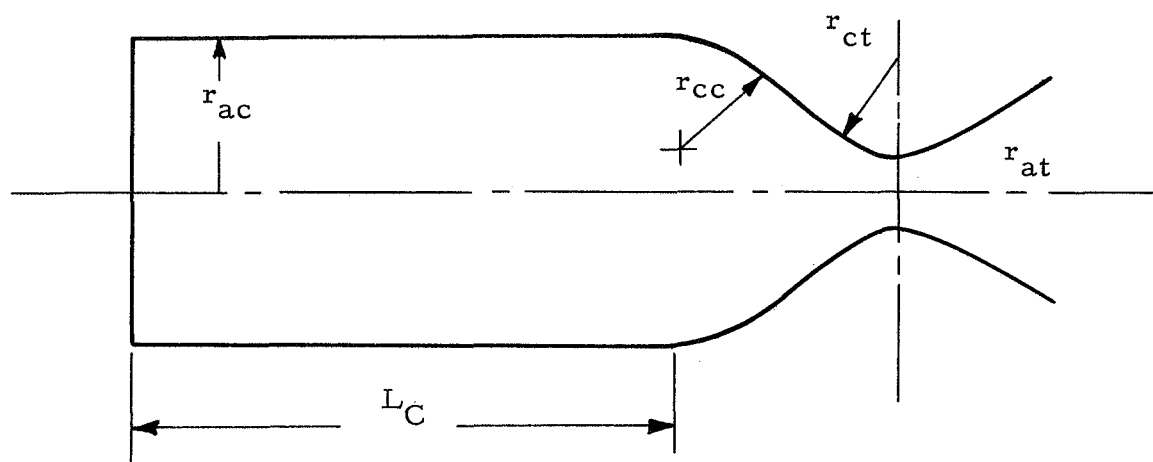


Figure 32



Annular Chamber Computer Input Parameters

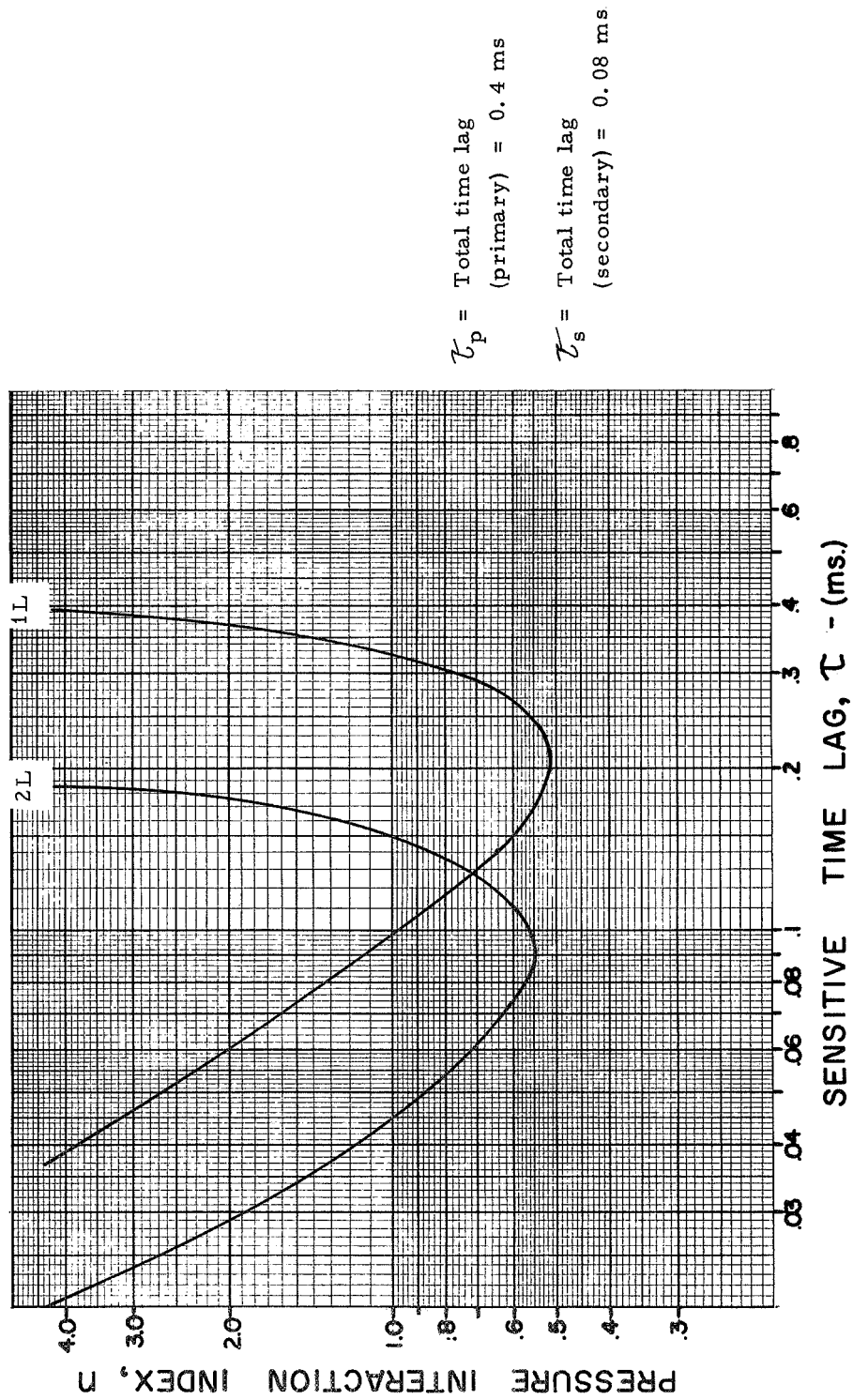
Figure 33



$$\begin{aligned}
 L_C &= 14.8, \text{ in.} \\
 r_{ac} &= 6.4, \text{ in.} \\
 r_{cc} &= 3.0, \text{ in.} \\
 r_{ct} &= 7.16, \text{ in.} \\
 r_{at} &= 3.58, \text{ in.} \\
 \alpha &= 15.0^\circ
 \end{aligned}$$

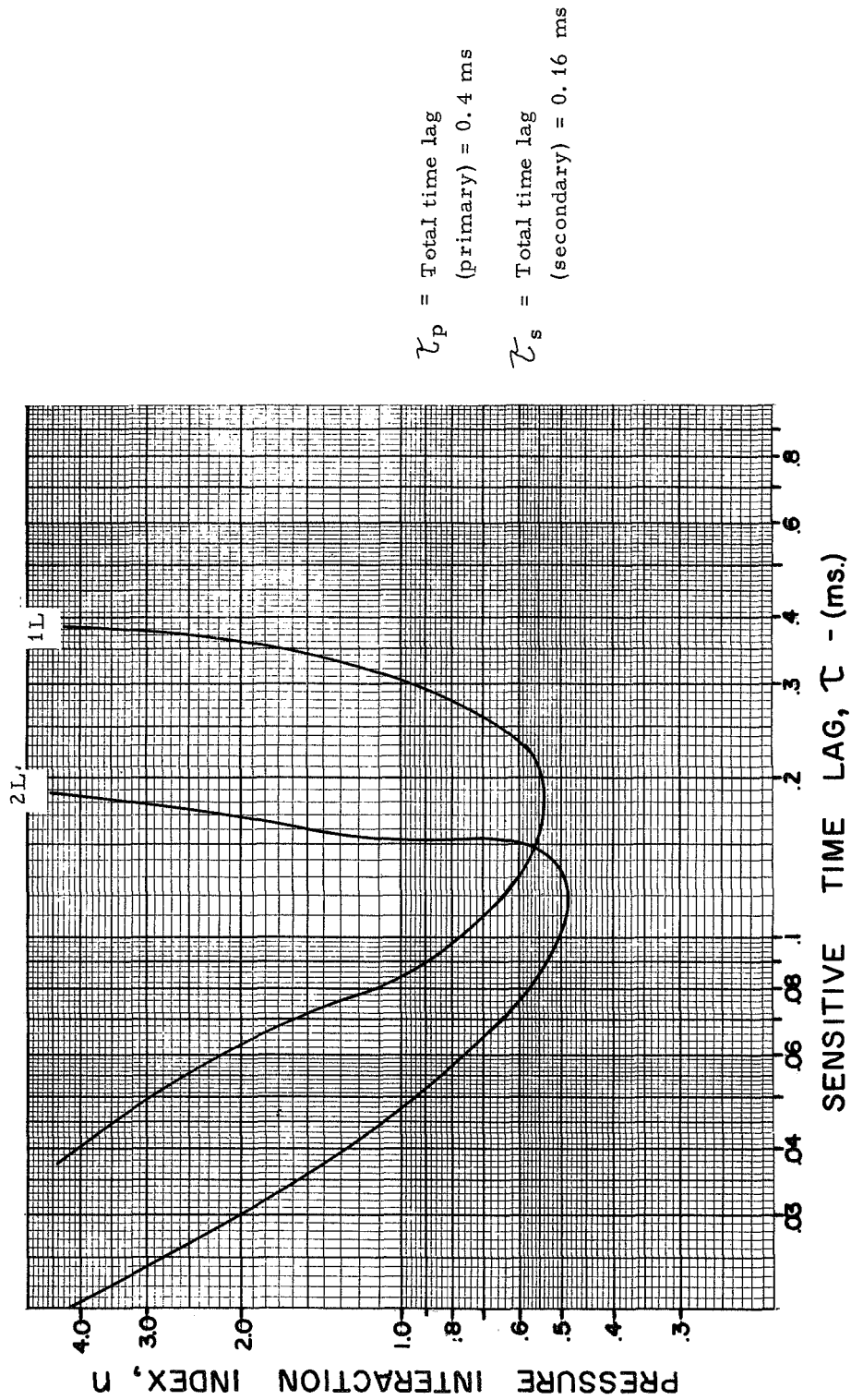
Cylindrical Chamber Computer Input Parameters

Figure 34



n, τ Plots

Figure 35

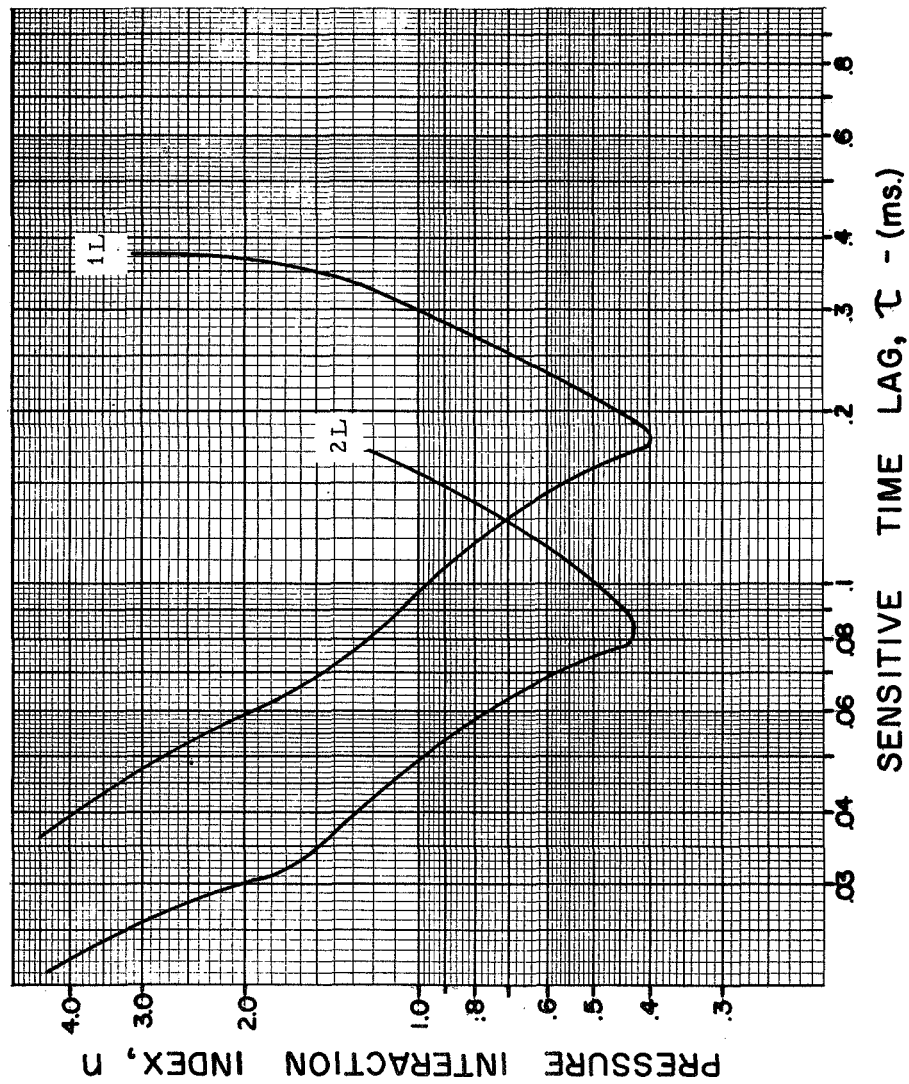


τ_p = Total time lag
(primary) = 0.4 ms

τ_s = Total time lag
(secondary) = 0.16 ms

n, τ Plots

Figure 36



τ_p = Total time lag
(primary) = 0.4 ms

τ_s = Total time lag
(secondary) = 0.3 ms

n, τ Plots

Figure 37

APPENDIX A

PRELIMINARY DESIGN DETAILS;
DETAILED TEST RESULTS

TABLE OF CONTENTS

	<u>Page</u>
I. Injector Design Studies	1
II. Task IIA - Primary Combustor High Frequency Stability Characteristic	1
A. General	1
B. Injector Design Characteristics	2
III. Task IIB - Secondary Combustor High Frequency Stability Characterization	3
A. General	3
B. Secondary Injector Design Characteristics	4
IV. Task III - Low Frequency Stability Characterization	5
A. General	5
B. Injector Design Characteristics	6
V. Task IV - High Injection Density Injectors	8
A. General	8
B. Injector Design Characteristics	8
VI. Full Scale Test Results on the Annular Coaxial Injector	9
A. Test 1100-D01-OM-001 (Satisfactory Test)	9
B. Test 1100-D01-OM-002 (Satisfactory Test)	9
C. Test 1100-D01-OM-003 (Satisfactory Test)	10
D. Test 1100-D01-OM-004 (Satisfactory Test)	11
E. Test 1100-D01-OM-005 (Unsatisfactory Test)	11
F. Test 1100-D01-OM-006 (Satisfactory Test)	11
G. Test 1100-D01-OM-007 (Satisfactory Test)	11
VII. Test Results of Transverse Excitation Chamber Testing	12
A. Test 1100-D02-OM-001, 10/20/67 (Unsatisfactory Test)	12
B. Test 1100-D02-OM-002, 10/20/67 (Unsatisfactory Test)	13
C. Tests 1100-D02-OM-003 and 004 (Fuel Valve Malfunction)	14
D. Test 1100-D02-OM-005 (Satisfactory Test)	15
E. Test 1100-D02-OM-006 (Satisfactory Test)	15

FIGURE LIST

	<u>Figure</u>
Coaxial Injector for Annular Gas Generator	1
Triplet (small Element) Injector for Annular Gas Generator	2
Triplet (Large Element) Injector for Annular Gas Generator	3
Concentric Sheet Injector for Annular Gas Generator	4
Four Injection Concepts for Staged Combustion System	5
Coaxial Injector for Trombone Engine	6
Triplet (Small Element) for Trombone Engine	7
Triplet (Large Element) for Trombone Engine	8
Concentric Sheet Injector for Trombone Engine	9
54-Element Triplet Injector for Annular Thrust Chamber Assembly	10
108-Element Triplet Injector for Annular Thrust Chamber Assembly	11
432-Element Triplet Injector for Annular Thrust Chamber Assembly	12
Concentric Sheet Injector for Annular Thrust Chamber Assembly	13
Damaged Injector Inserts from Test 002	14
Damaged Excitation Chamber	15
Damaged Injector Inserts from Tests 005 and 006	16

I. INJECTOR DESIGN STUDIES

The basic Contract NAS 8-20672 "Stability Characterization of Advanced Injectors" contained four discrete tasks. Task I was the continuation of analytical model development based on Sensitive Time Lag Theory. Task II consisted of determining the tangential high frequency response characteristics of gas generator assemblies, and the stability characteristics of staged combustion secondary injectors. Task III contained an evaluation of the longitudinal high frequency response characteristics of gas generator injectors. Task IV consisted of determining the effect of injection density on the stability of coaxial injection elements.

Designs were made for each of the injectors for the tasks mentioned above. Revisions to the basic contract excluded the fabrication and testing of injectors and components on Tasks II and III; these designs are discussed in this section. Task I did not include design of hardware and remained unchanged throughout the contract; Task IV remained, the hardware and test results are discussed in the text of this report. The designs presented were finalized after a study of injector parameters such as: injection density, pressure drop, orifice size, number of elements, scaleability and element distribution. These designs will be presented in the order of the respective contract tasks.

II. TASK IIA - PRIMARY COMBUSTOR HIGH FREQUENCY STABILITY CHARACTERISTIC

A. GENERAL

The primary combustor investigation was to be performed with an annular gas generator assembly (GGA) consisting of: 1) an 11.0 in. O.D. and a 9.25 in. I.D. annular combustion chamber, 2) two annular nozzles to allow two chamber pressure variations, and 3) an injector delivering liquid oxygen and liquid hydrogen. The annular configuration was to encourage the tangential mode of the high frequency instability. Design test operating conditions were:

II, A, General (cont.)

1. MR = 0.5 to 1.0
2. P_c = 2500 and 4000 psia
3. \dot{w}_T = 60 lb/sec

B. INJECTOR DESIGN CHARACTERISTICS

Four types of injectors were designed and are shown in Figures 1, 2, 3, and 4:

1. Coaxial
2. High thrust per element triplet
3. Low thrust per element triplet
4. Concentric ring

Each injector had the following common design features.

Oxidizer velocity	= 150 ft/sec
Fuel velocity	= 525 ft/sec
Velocity ratio	= 3.5
Injector face area	= 28 in.

II, B, Injector Design Characteristics (cont.)

TABLE 1
TASK IIA ANNULAR GAS GENERATOR INJECTOR FEATURES

<u>Parameter</u>	<u>Injector Type</u>			
	<u>Coaxial</u>	<u>Triplet</u>	<u>Triplet</u>	<u>Concentric Ring</u>
Number of elements	18	18	72	10
Orifice size a) Fuel (in.)	0.416 OD Annulus	0.243 dia.	0.125 dia.	0.045 wide
b) Ox (in.)	0.175 dia.	0.175 dia.	0.086 dia.	0.023 wide
Oxidizer slot diameter (in.)	-	-	-	10.12
Impingement angle (deg)	Nonimpinging or 30	30	30	30
Element array	Circumferential	Radial	Radial	Circumferential
Manifold method a) Fuel	**	**	**	**
b) Ox	*	*	*	*

*Flooded annulus

**Drilled hole connected to flooded annulus

III. TASK IIB - SECONDARY COMBUSTOR HIGH FREQUENCY STABILITY CHARACTERIZATION

A. GENERAL

The secondary combustor investigation required a liquid/liquid primary combustor to produce the fuel rich gas for the gas/liquid secondary combustor. The primary or gas generator combustor was a 6 in. diameter cylindrical injector selected from Task III; these gas generator injectors will be discussed in Section IV of this Appendix. An orifice between the primary and secondary combustor simulates turbine pressure drops and also decouples low frequency interactions between the two combustion chambers.

III, A, General (cont.)

An 18 in. diameter to 14 in. diameter transition piece joined the cylindrical primary combustor to the annular secondary combustor. The fuel rich gas generator supplied gas at 1400°F - 1800°F to a secondary combustor which was designed to operate at a MR of 5.5, and a P_c of 1000 or 2500 psia and deliver 60,000 lb of thrust.

B. SECONDARY INJECTOR DESIGN CHARACTERISTICS

Four types of injectors (Figure 5) were designed for the secondary combustor: (1) coaxial, (2) high thrust per element spray bar, (3) low thrust per element spray bar and, (4) concentric ring. Manifolding was similar for all four units. Design and operating characteristics for these secondary injectors were:

- | | |
|-----------------------|------------|
| 1. Oxidizer velocity | 150 ft/sec |
| 2. Fuel velocity | 525 ft/sec |
| 3. Velocity ratio | 3.5 |
| 4. Total flow rate | 180 lb/sec |
| 5. Injector face area | 90 in. |

III, B, Secondary Injector Design Characteristics (cont.)

TABLE 2
TASK IIB SECONDARY COMBUSTOR INJECTOR FEATURES

<u>Parameter</u>	<u>Coaxial</u>	<u>Injector Type</u>		<u>Concentric Ring</u>
		<u>Spray Bar</u>	<u>Spray Bar</u>	
Number of elements	14	4	16	1
Orifice size				
a) Fuel (in.)	0.786 OD	0.723 wide	0.723 wide	0.51 wide outer 0.69 wide inner
b) Oxidizer (in.)	0.224 dia.	0.224 dia.	0.112 dia.	0.112 wide
Oxidizer slot diameter (in.)	-	-	-	11.5
Impingement angle (deg)	Non- impinging	Non- impinging	Non- impinging	30
Element array	Circum- ferential 2 rows	Radial	Radial	Circumferential
Manifold method				
a) Fuel	*	*	*	*
b) Oxidizer	**	**	**	**

*Flooded back

**Tube fed by outer annulus

IV. TASK III - LOW FREQUENCY STABILITY CHARACTERIZATION

A. GENERAL

This hardware was to evaluate the longitudinal modes of high frequency instability of various gas generator injectors in a variable length combustion chamber and then use the best candidate injector on Task IIB. The TCA consisted of a 6 in. diameter injector in a 6 in. diameter water-cooled,

IV, A, General (cont.)

variable-length chamber and an ablative nozzle. Test conditions used for the design were the same for the annular gas generator described in Section II.

MR = 0.5 to 1.0
 P_c = 1,000 and 2,500 psia
Injection density = 3 lb/sec. in.²
 \dot{w}_T = 60 lb/sec

B. INJECTOR DESIGN CHARACTERISTICS

Four injectors (6 in. diameter) as shown schematically in Figures 6, 7, 8, and 9 were designed for the 6-in.-diameter cylindrical gas generator. The injector types were as follows:

1. Coaxial
2. High thrust per element triplet
3. Low thrust per element triplet
4. Concentric ring

Each had the following design features:

Injection density	2.1 lb/sec-in. ²
Oxidizer velocity	150. ft/sec
Fuel velocity	525 ft/sec
Velocity ratio	3.5
Injector face area	28 in.

IV, B, Injector Design Characteristics (cont.)

A comparison of injection pattern design features is presented in Table 3.

TABLE 3
TASK III GAS GENERATOR INJECTOR PATTERN DESIGN FEATURES

	<u>Injector Type</u>			
	<u>Coaxial</u>	<u>Triplet</u>	<u>Triplet</u>	<u>Concentric Ring</u>
Number of elements	18	18	72	2
Orifice size				
a) Fuel (in.)	0.416 OD x 0.238 ID	0.242 dia.	0.122	4 at 0.045 wide
b) Ox (in.)	0.175 dia.	0.175 dia.	0.086	2 at 0.023 wide
Oxidizer slot diameter in.	-	-	-	3.54 outer 2.14 inner
Impingement angle (deg)	Non- impinging	30	30	30
Element array	Circum- ferential 2 rows	Skewed to radial ray	Circum- feren- tial 2 skewed rows	Circumferential 2 rows
Manifold method				
a) Fuel	*	*	*	***
b) Oxidizer	**	* + tubes	** + tubes	II

*Flooded back plate

**Flooded annulus

***Flooded annulus and drilled holes

V. TASK IV - HIGH INJECTION DENSITY INJECTORS

A. GENERAL

The purpose of this task was to study the effect of injection density and Mach number on combustion stability. The coaxial and triplet injectors designed and fabricated for the test program reported in Section V,A, of this report were designed as part of this task. The combustion chamber was an annular configuration formed from a cylindrical combustion chamber with a 10.50-in. inside diameter and a center plug with a 6.14-in. outside diameter. Test conditions are the same as those described in Section V,A, and are summarized as follows:

MR = 5.5
P_c = 1500, 2500 psia
Inj. Density = 3.15 lb/sec in.²
 \dot{w}_T = 180 lb/sec

B. INJECTOR DESIGN CHARACTERISTICS

In addition to the injector fabricated on this task, four other injectors were designed. Conceptual drawings of these designs are shown in Figures 10, 11, 12, and 13. The injectors include the following type:

1. 54-Element Triplet
2. 108-Element Triplet
3. 432-Element Triplet
4. Concentric Sheet

V, B, Injector Design Characteristics (cont.)

These injectors had the following design features in common:

Oxidizer velocity	- 150 ft/sec
Fuel velocity	- 525 ft/sec
Fuel temperature	- 80°R
Oxidizer ΔP	- 350 psi
Fuel ΔP	- 260 psi
Oxidizer include impingement angle	- 60°

VI. FULL SCALE TEST RESULTS ON THE ANNULAR COAXIAL INJECTOR

A. TEST 1100-D01-OM-001 (SATISFACTORY TEST)

This test was planned to operate at a chamber pressure of 1500 psia at a MR of 4.0 for 2.0 seconds utilizing S/N -1 chamber and a -1 nozzle ($A_t = 28.3 \text{ in.}^2$) and a coaxial injector. The actual test was conducted at a P_c of 1430 psia and a MR of 6.24. The test was short in duration (1.60 seconds) because a voltage surge occurred when the first pulse gun was fired, which activated FS-2. Corrective action was taken by installing a larger resistor in the pulse charge electrical circuit. Slight erosion of the ablative liner was noted after this test; the final throat area was 32 in.^2 . No streaking was noted; however, increased ablation and erosion were noted near the injector face. Three Photocon pressure transducers were damaged during the test. There was a 20% overpressure at start indicating a moderate start.

B. TEST 1100-D01-OM-002 (SATISFACTORY TEST)

This test was planned to operate at a $P_c = 1500 \text{ psia}$, $MR = 6$, and fuel temperature = 80°R for a 2.0 second duration. There was no hardware changed after Test 001 except for replacement of the damaged Photocon pressure

VI, B, Test 1100 D01-OM-002 (Satisfactory Test) (cont.)

transducers. Actual average operating conditions of the test were $P_c = 1244$ psia, $MR = 5.58$ $T_f = 126^\circ R$; the test went to full duration (1.94 sec). Thermal damage was noted on four Photocon transducers and the center body nozzle extension was missing after the test. Although the overall dimensional ablation of the liner was small, it was noted that the chamber had eroded a leak path in back of the ablative liner from the igniter port to the interface of the liner with the nozzle insert. The nozzle of an expended igniter was burned off and the threads were damaged. The damaged combustion chamber was removed from the stand for repair. A review after test indicated all pulse guns fired. There was a 30% overpressure at start indicating a moderately hard start.

C. TEST 1100-D01-OM-003 (SATISFACTORY TEST)

A new chamber and nozzle were installed on the coaxial injector. Modifications were made to the Photocon port configuration to alter the thermal conditions causing damage to the instruments. This change consisted of drilling a 0.312-in.-diameter hole in the liner (centered with the Photocon transducer) and gasketing the Photocon so as to produce a gap between the instrument pressure plate and the ablative liner of 0.100 ± 0.030 inches. This change permitted greater distribution of the thermal flux to the pressure transducer.

This test was planned to operate at $P_c = 2500$ psia, $MR = 6.0$, and $T_f \approx 80^\circ R$ for 2.0 seconds. The test was of full duration (2.0 seconds) but operating conditions were not achieved because of a valve actuation malfunction which caused the valves to open only 10%. The resultant chamber operating conditions were 465 psia at a MR of 3.73, with fuel temperature $113^\circ R$; all pulse guns fired. There was no evidence of damage after the firing; normal dimensional ablation was noted.

VI, Full Scale Test Results on the Annular Coaxial Injector (cont.)

D. TEST 1100-D01-OM-004 (SATISFACTORY TEST)

This test was a repeat of the operating conditions of Test 003 ($P_c = 2500$, $MR = 6.0$ and $T_f \approx 80^\circ R$). The control system was altered for this test to reduce the P_c overshoot and thus soften the start and increase in valve actuation pressure to prevent malfunction as in Test 003. The hydrogen valve sequence was charged to ramp partially open before being controlled by the downstream injector pressure. The change resulted in the chamber pressure overshoot being held to under 2%. The test conditions which resulted were: $P_c = 2400$, $MR = 5.77$ and $T_f = 108^\circ R$. The duration was less than 2 seconds because the combustion stability monitor signaled shutdown. Two Photocon transducers were damaged and required replacement. Light dimensional ablation was noted.

E. TEST 1100-D01-OM-005 (UNSATISFACTORY TEST)

The test conditions were $P_c = 2500$ psia, $MR = 4.0$ and $T_f \approx 80^\circ R$. The prefire throat area was 19.45 square inches. Because of a malfunction, the valves failed to open the required amount. The malfunction resulted in a test duration of 1.10 seconds.

F. TEST 1100-D01-OM-006 (SATISFACTORY TEST)

This test was a repeat of the prior test conditions, ($P_c = 2500$, $MR = 4.0$ and $T_f \approx 80^\circ R$). The hydraulic pressure which actuates the thrust chamber valves was again increased to assure valve opening. The test was conducted at a chamber pressure of 2320 psia, MR of 3.79 and a fuel temperature of $125^\circ R$. The duration was shortened by a decrease in chamber pressure which activated the thrust chamber pressure switch at 1.25 seconds. The final throat area was 19.45 in.^2 and after firing it was 20.20 in.^2 . No streaking was observed.

VI, Full Scale Test Results on the Annular Coaxial Injector (cont.)

G. TEST 1100-D01-OM-007 (SATISFACTORY TEST)

This test was the final one on the coaxial injector. Planned operating conditions were: $P_c = 1500$ psia, $MR = 6.0$ and $T_f = 200^\circ R$. Because of the decreased density of "warm" hydrogen the duration was set at 1.46 seconds. The test was shut down by the fuel depletion switch. The actual conditions were: $P_c = 1440$ psia, $MR = 9.53$ and $T_f = 200^\circ R$. The prefire throat area was 20.20 square inches and increased to 22.25 square inches. Nominal dimensional ablation was noted.

VII. TEST RESULTS OF TRANSVERSE EXCITATION CHAMBER TESTING

A. TEST 1100-D02-OM-001, 10/20/67 (UNSATISFACTORY TEST)

Test hardware included a S/N 002 chamber with three eleven-element injector inserts with the corresponding -5 wedge and -11 nozzle. The planned test operating conditions were: $P_c = 1500$ psia, $MR = 6.0$, $T_f \approx 80^\circ R$ for a 0.80 sec duration.

The test was conducted at a P_c of 960 psia and an estimated MR of 10.0. The actual value of MR was not obtained from test data because of severe flow fluctuations in both fuel and oxidizer systems. The test duration was 0.509 sec. Malfunction sequence circuitry signaled FS-2 when P_c failed to exceed 1,000 psi. The fuel temperature at the injector was $400^\circ R$. The narrow opening at the throat (0.630 in. wide by 0.250 in. high rectangular slot) and the 30 in. distance to the injector face made hardware inspection difficult. Evidence of slag on the wedge and a darkening of the injector face indicated that a slight erosion had occurred. A survey of the test data indicated a fairly soft start (no pressure spike), but the flow had not reached steady state.

VII, A, Test 1100-D02-OM-001, 10-20-67 (Unsatisfactory Test)(cont.)

The following changes were made before proceeding to the next test:

1. Oxidizer and fuel valve opening times were increased to reduce flow oscillations.
2. Duration time was increased to allow hydrogen temperature in the fuel manifold to reach a constant value.
3. The minimum P_c kill parameter was reduced to 1000 psia to 700 psia to prevent malfunction shutdown due to low initial P_c .
4. Fuel tank pressure was increased to obtain higher fuel flow to compensate for higher propellant temperatures in the fuel manifold.

B. TEST 1100-D02-OM-002, 10/20/67 (UNSATISFACTORY TEST)

The same hardware used for Test 001 was used for Test 002. The following conditions were desired; $P_c = 1500$ psia, $MR = 6.0$, fuel temperature $\approx 80^\circ\text{F}$. The test was conducted at a chamber pressure of 1000 psia for a duration of 1.050 sec.

The average fuel temperature was 250°R . Inspection of the hardware after the test indicated that severe erosion had occurred at the face of the injector. The oxidizer orifices of the central injector were totally eroded away exposing the oxidizer manifold, and the fuel orifices were eroded until only tubes remained where the central fuel post was. A view of the injectors after removal from the chamber is shown in Figure 14. Removal of the lid revealed that both the lid and chamber cavity were similarly eroded (Figure 15); damage to the wedge was slight. A review of the oscillograph record indicated that the oxidizer orifices burned out at FS-2. The flow oscillations were not

Report 20672-PIF, Appendix A

VII, B, Test 1100-D02-OM-002, 10/20/67 (Unsatisfactory Test) (cont.)

as severe as those of Test 001 and were damped by 0.8 sec. Although the fuel temperature was decreasing with time, the rate was insufficient to approach the desired H_2 temperature conditions within the practical test duration. The changes in the test setup which were made after Test 001 improved operating conditions but did not totally eliminate the propellant transport problem. Prior to the next test the following changes were made:

1. An orifice was placed in the oxidizer line to harden the system and reduce the flow oscillations due to manifold pressure surge.
2. The manifold volume was reduced and a jacket to cool the remaining manifold with liquid nitrogen was added.
3. The system was balanced for a $MR = 4.0$ test using the temperature of liquid N_2 in the jacket around the fuel manifold as the expected fuel temperature.

C. TESTS 1100-D02-OM-003 and 004 (FUEL VALVE MALFUNCTION)

S/N 001 chamber was assembled with a -3 chamber wedge and a -21 nozzle. This configuration included four injector inserts in a 19.8° chamber. Operating conditions included an MR of 4.0 with an expected fuel temperature of $150^\circ R$ at the injector and a P_c of 1500 psia.

Both tests were unsatisfactory due to a malfunctioning fuel valve. The malfunction was at first thought to be insufficient hydraulic actuation pressure; however, the problem continued after system changes were made to accommodate a 30% increase in actuation pressure. After Test 004 the problem was found to be a frozen actuation discharge line which was immediately rerouted.

VII, Test Results of Transverse Excitation Chamber Testing (cont.)

D. TEST 1100-D02-OM-005 (SATISFACTORY TEST)

The test was conducted using chamber S/N 001 having a 19.8° chamber angle, a -3 wedge and a -21 nozzle insert. Four -3 injector inserts were used which had 11 triplet elements per injector. The planned test conditions were: $P_c = 1500$ psia, fuel temperature at the injector = 150°R and $\text{MR} = 4.0$ with a test duration of 0.75 sec. The flow oscillation problem encountered in the first two tests was overcome by the increase in valve opening time and placement of an orifice in the fuel line. The nitrogen jacket on the fuel manifold allowed a lower fuel injection temperature to be attained (110°R compared to 315°R for the same time from FS-1 on Test 002). The engine was shutdown at 0.595 seconds by the timed thrust chamber pressure switch. Actual operating conditions were as follows: $P_c = 1390$ psia, $\text{MR} = 3.64$, and $T_{fJ} = 110^\circ\text{R}$.

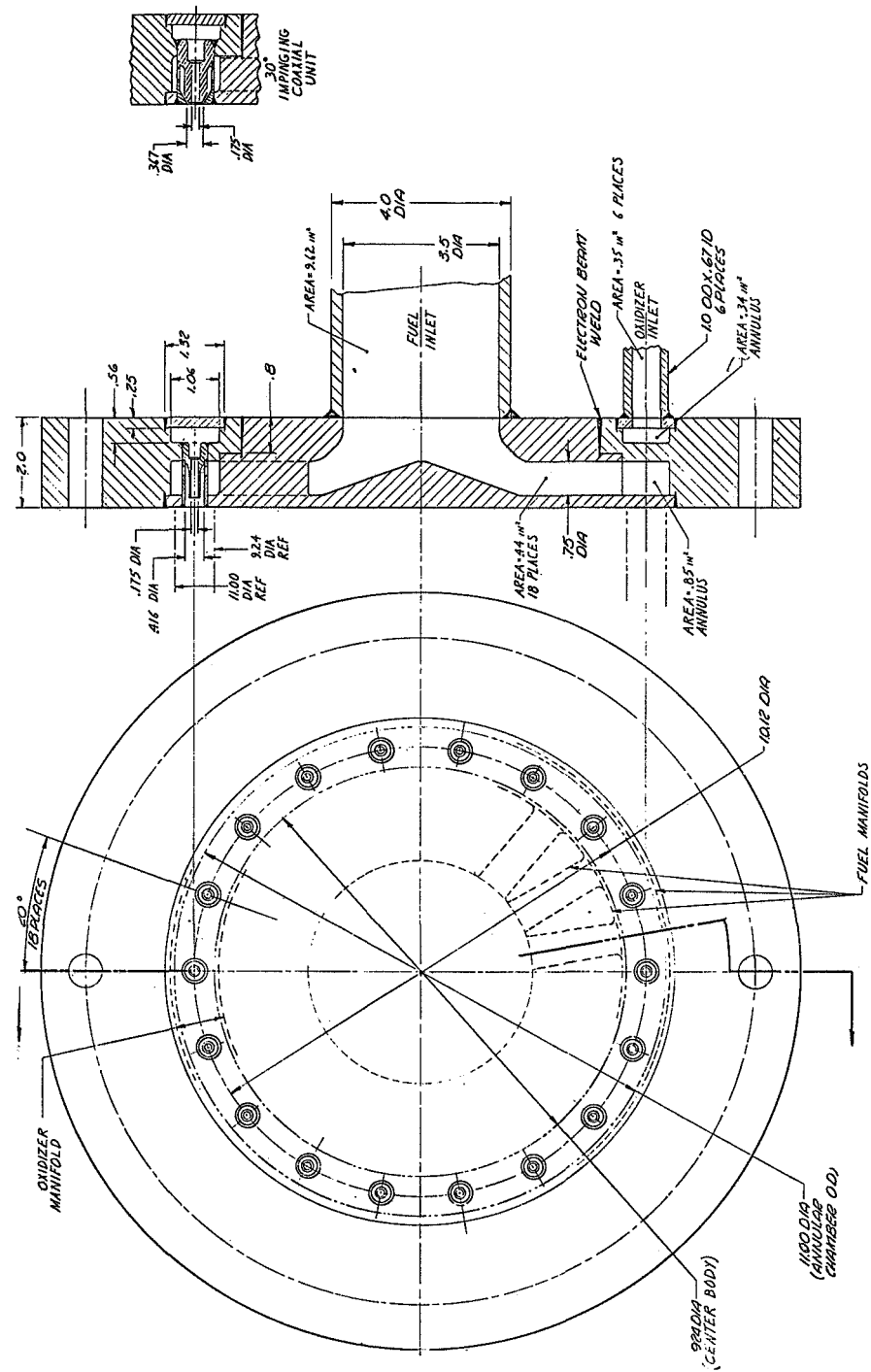
Inspection of the hardware after the test indicated that erosion had taken place on the face of the injector inserts; therefore, two of the four injectors were replaced. The two with the most severe face erosion were located in the center of the chamber and thus would be subjected to the greatest transverse velocity effects. This was also the case with the damage noted after Tests 001 and 002. A photo of the injectors after Test 005 is shown in Figure 16 in the same order as removed from the excitation chamber. The two outboard injectors were retained for Test 006 and the two center injectors were replaced. The chamber was not damaged and was ready for retesting as soon as the injector inserts were replaced.

E. TEST 1100-D02-OM-006 (SATISFACTORY TEST)

The hardware used for this test was the same as was used for Test 005, except that the two center injector inserts were replaced. The planned test conditions were as follows: $P_c = 1500$ psia, $\text{MR} = 5.0$ and $T_{fJ} = 150^\circ\text{R}$ with a test duration of 0.7 seconds. The engine was shut down at 0.675 sec by the

VII, E, Test 1100-D02-OM-006 (Satisfactory Test) (cont.)

FS-2 timer. The actual operating conditions for the test were: $MR = 3.62$, $P_c = 1370$ psia and $T_{fJ} = 150^\circ R$. After FS-2 a Photocon pressure transducer burned out, allowing a hot gas flow path which subsequently eroded the transducer port. Erosion of injectors similar to that experienced during Test 005 was observed, and these injectors are shown in Figure 16b in the same order as removed from the excitation chamber.



Coaxial Injector for Annular Gas Generator

Figure 1

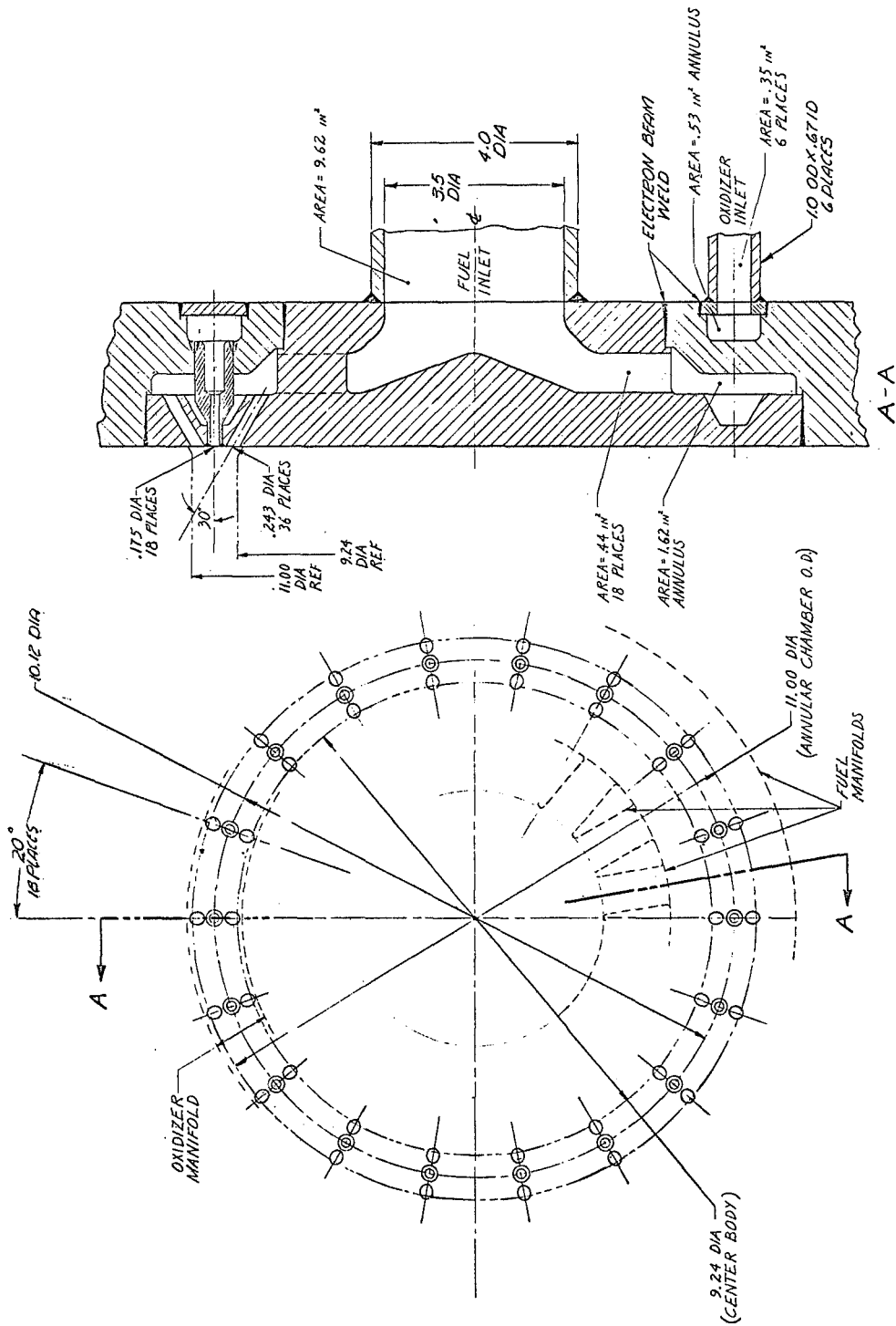
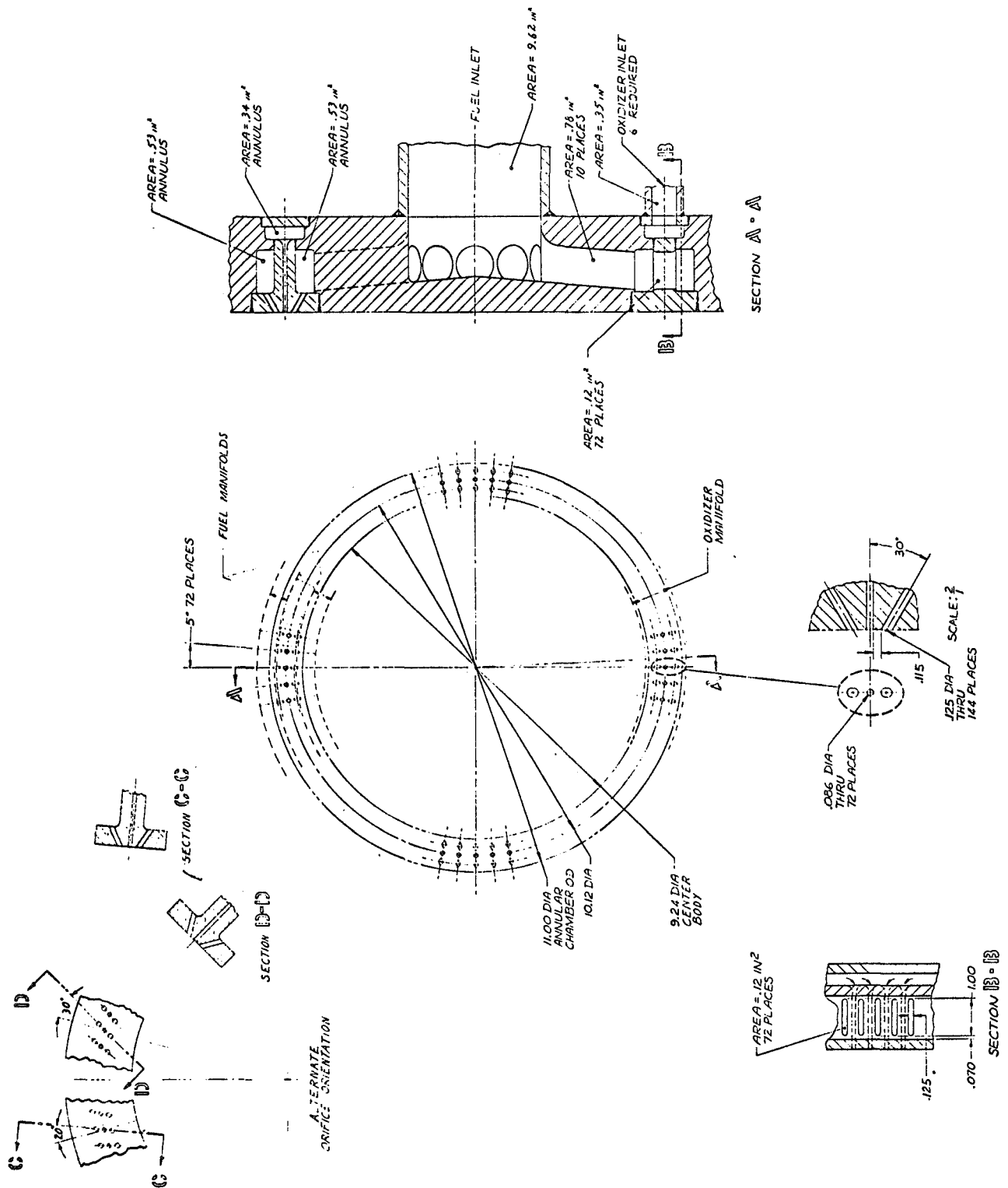


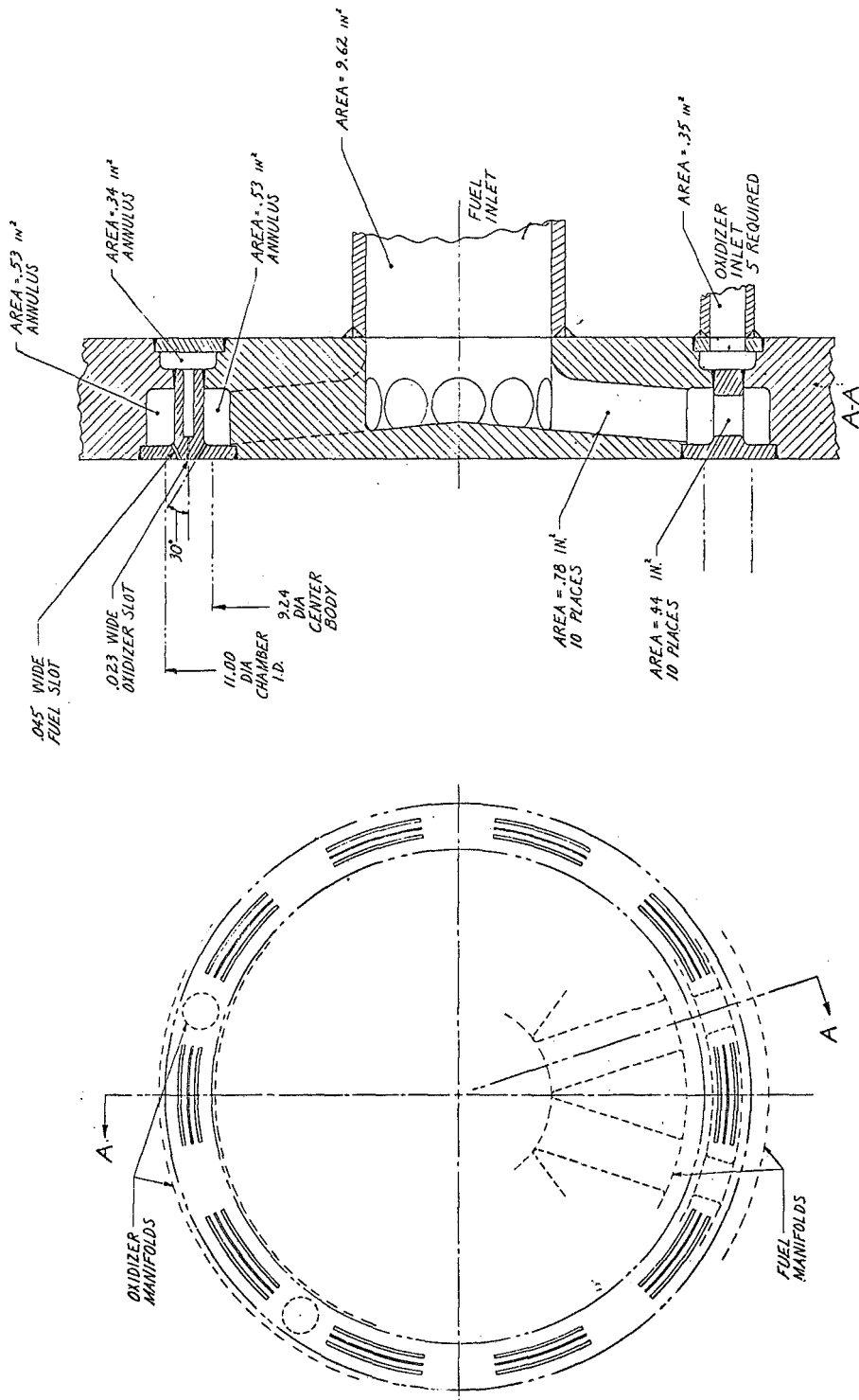
Figure 2

Triplet (small Element) Injector for Annular Gas Generator



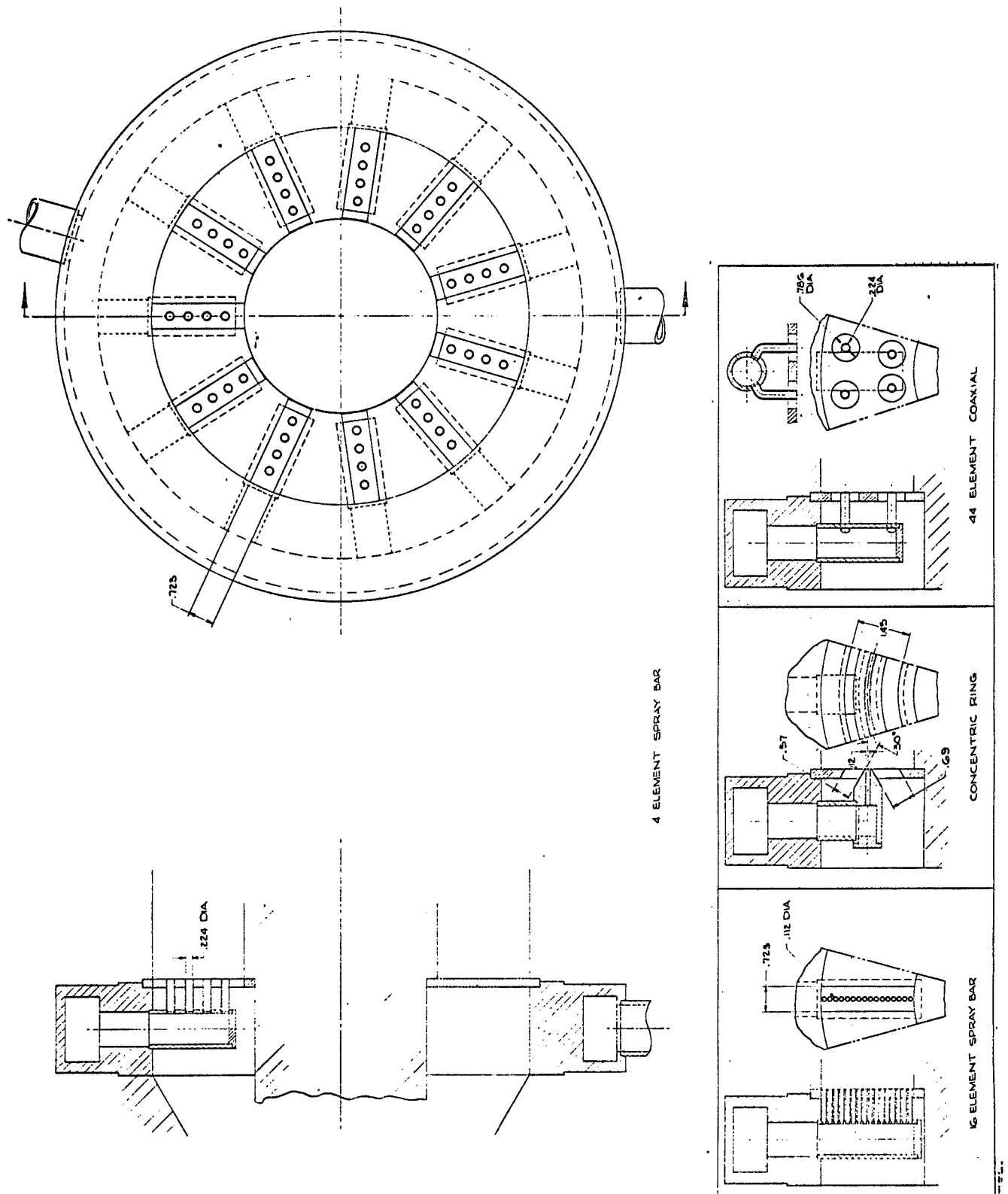
Triplet (Large Element) Injector for Annular Gas Generator

Figure 3



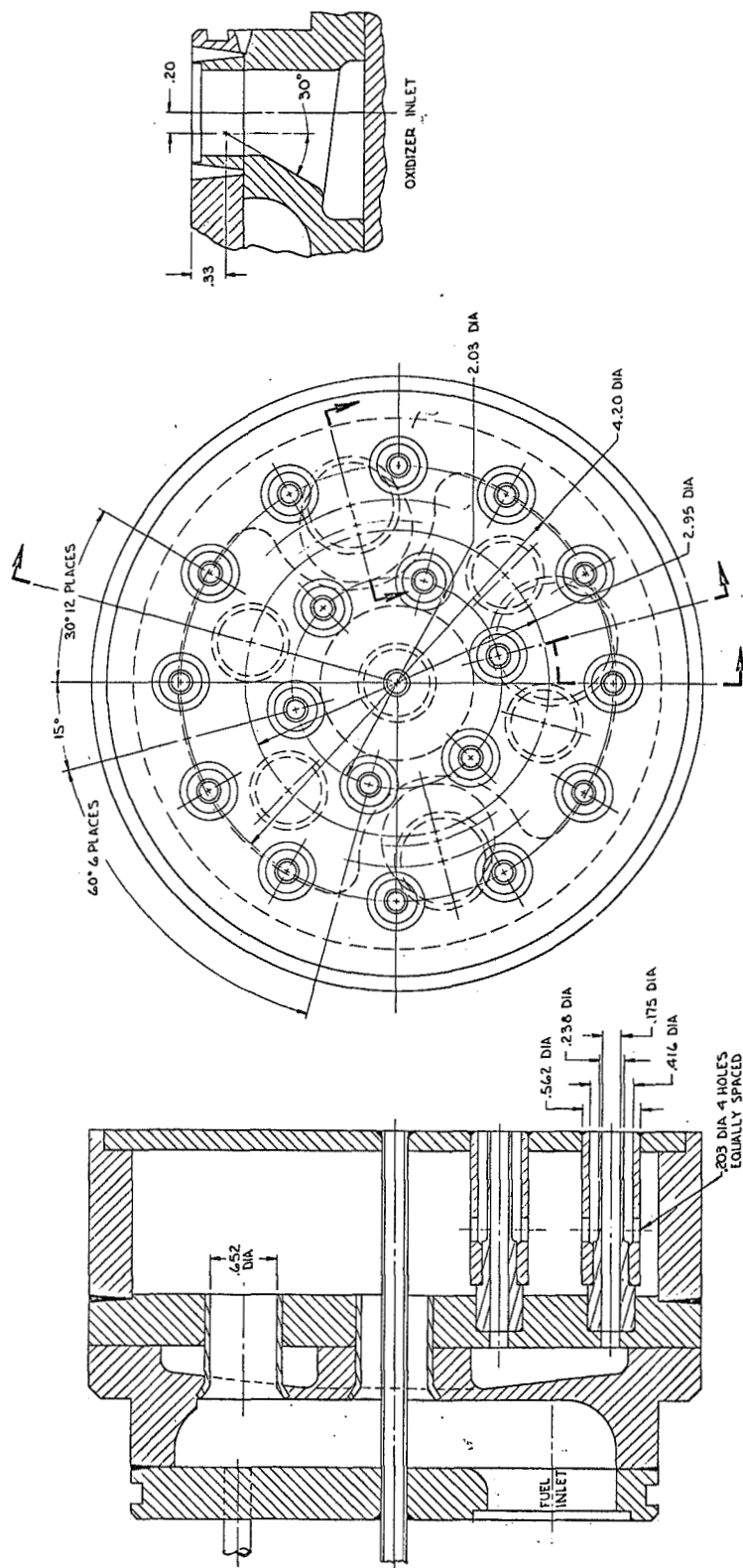
Concentric Sheet Injector for Annular Gas Generator

Figure 4



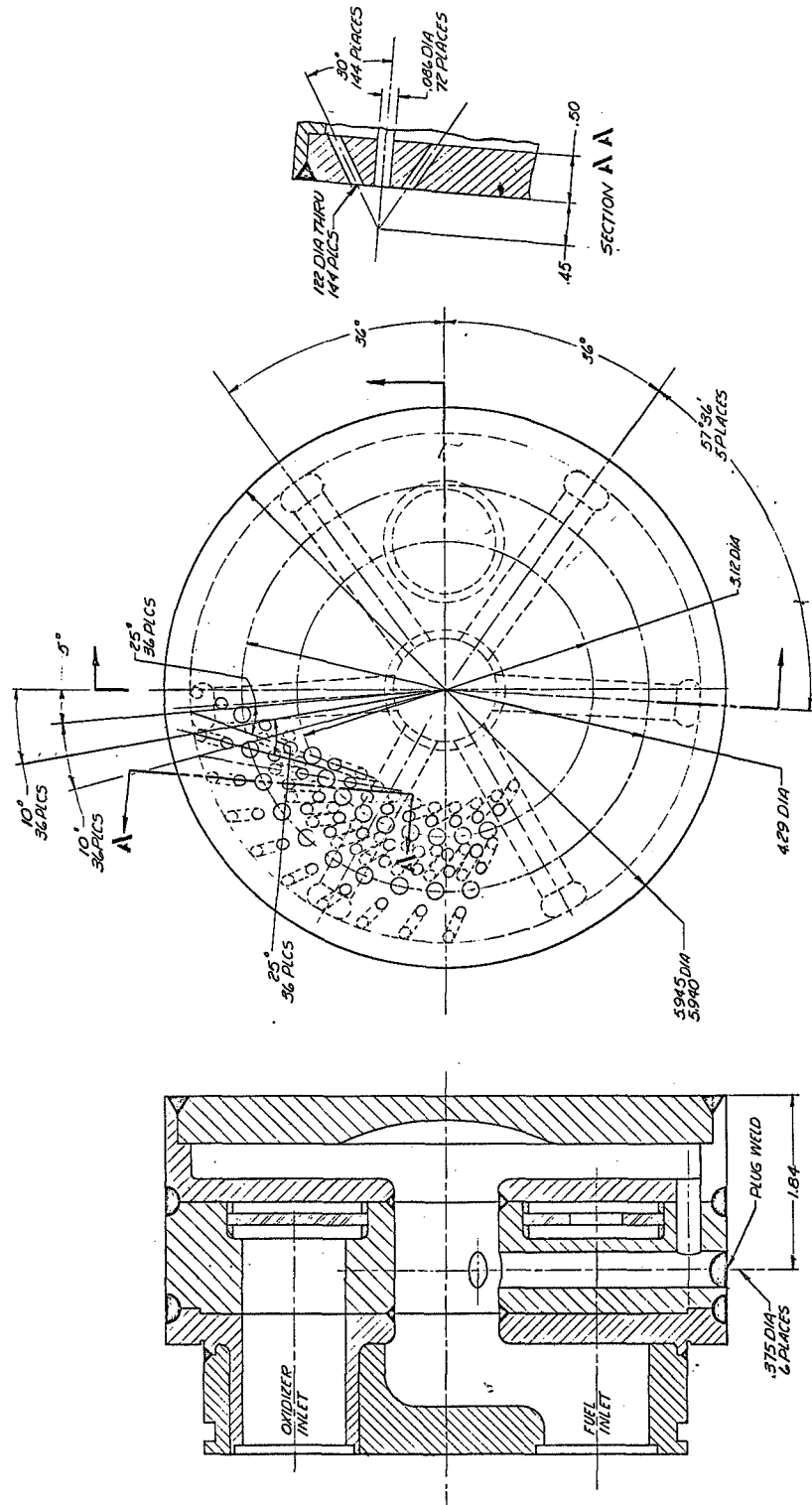
Four Injection Concepts for Staged Combustion System

Figure 5



Coaxial Injector for Trombone Engine

Figure 6



Triplet (Small Element) for Trombone Engine

Figure 7

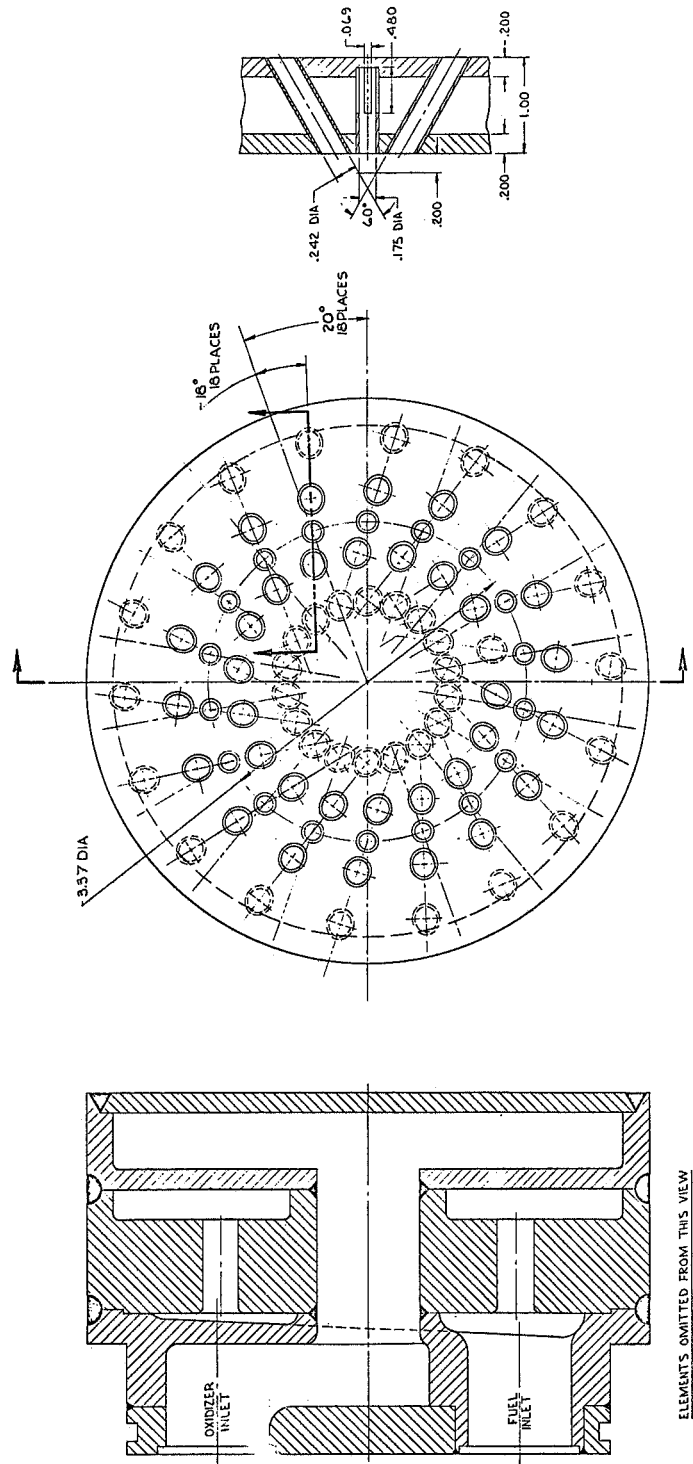
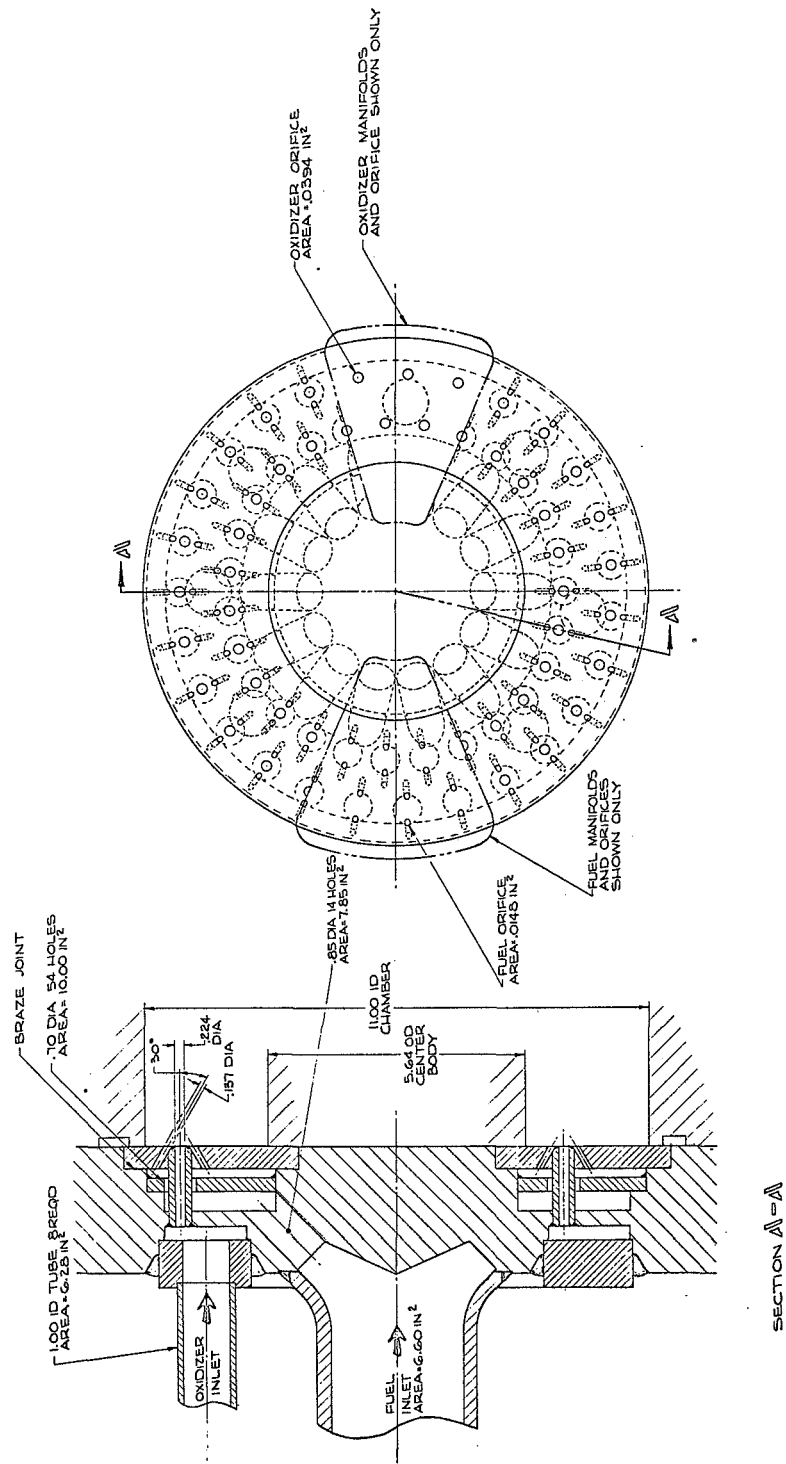


Figure 8

Triplet (Large Element) for Trombone Engine



54-Element Triplet Injector for Annular Thrust Chamber Assembly

Figure 10

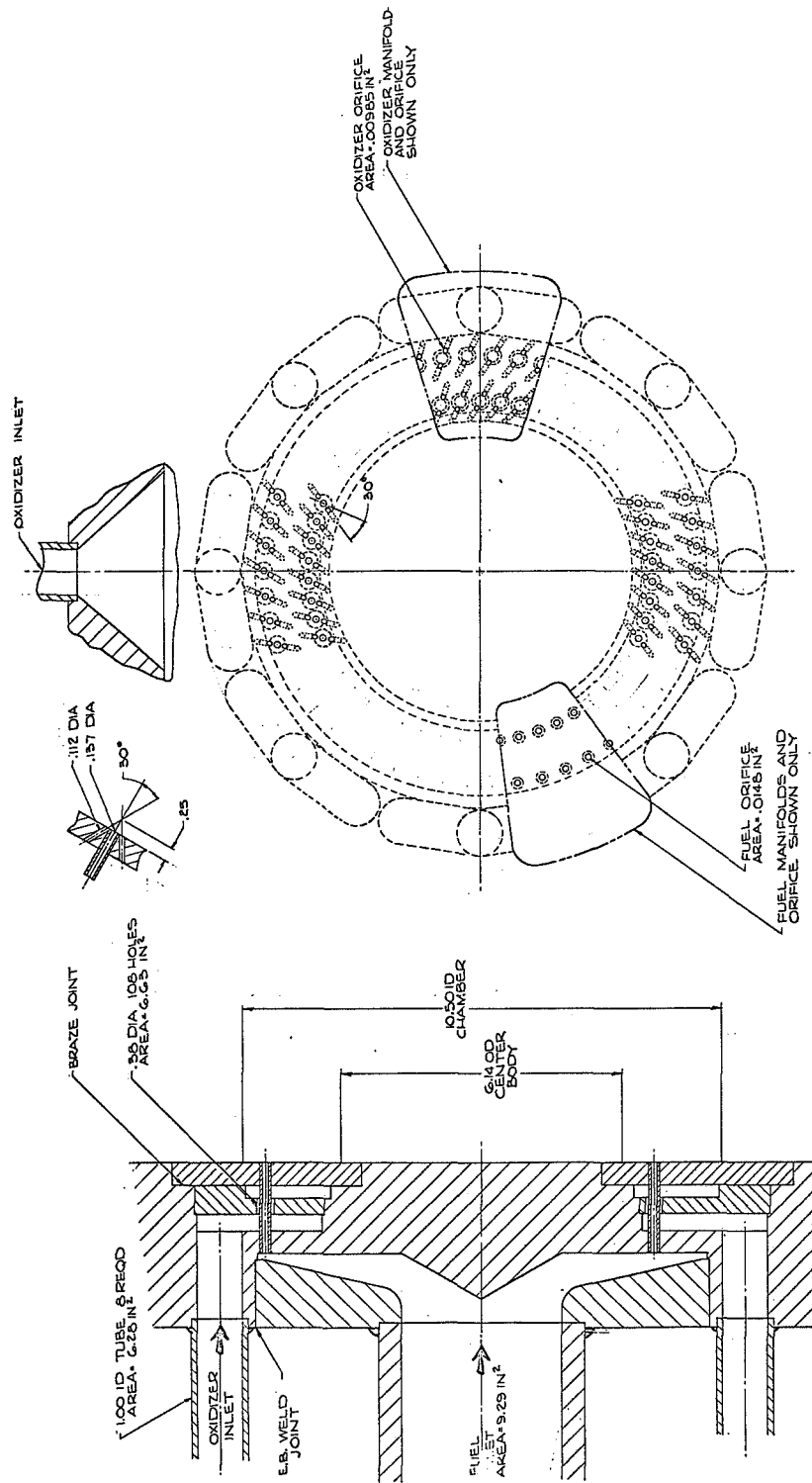
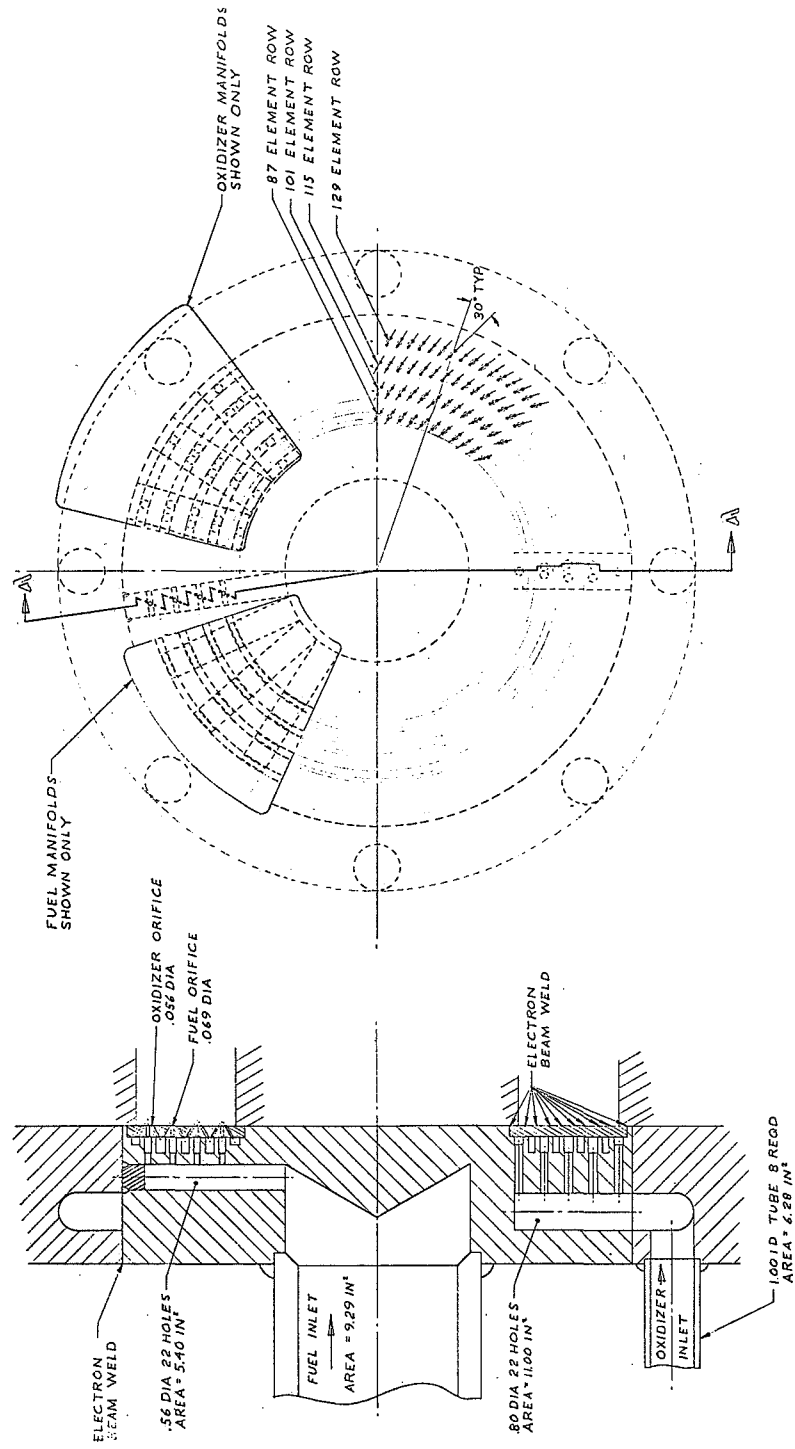


Figure 11



432-Element Triplet Injector for Annular Thrust Chamber Assembly

Figure 12

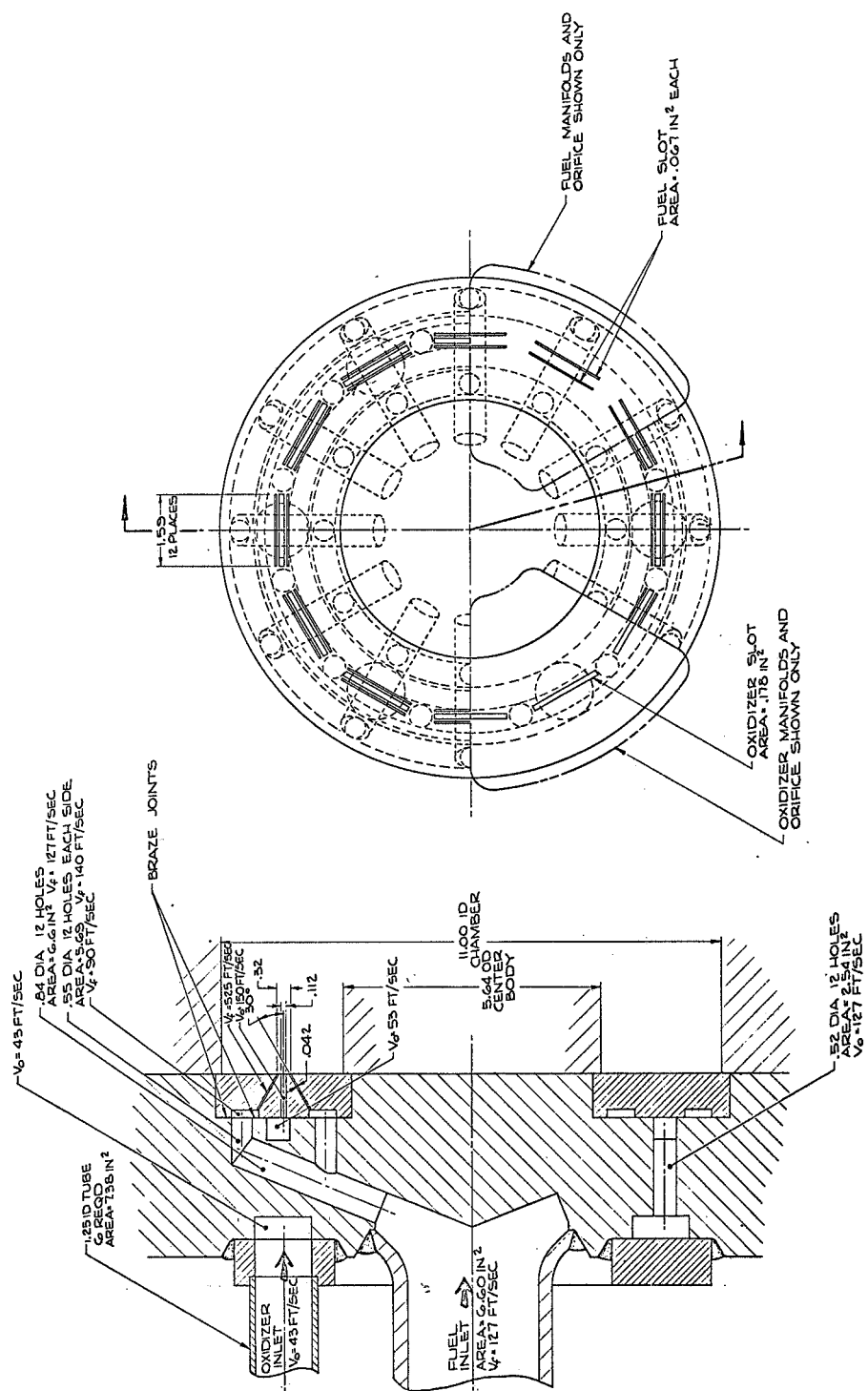
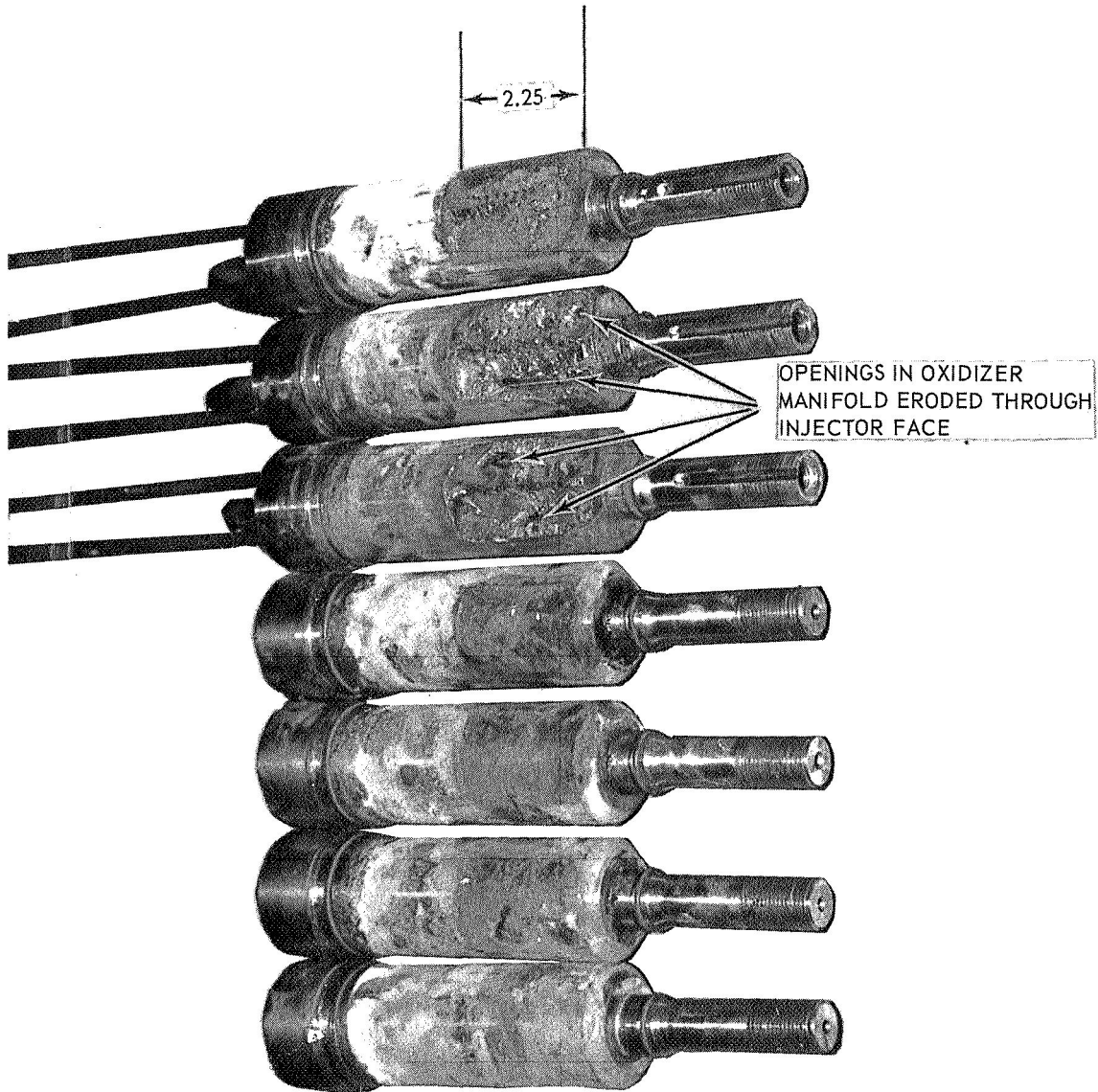


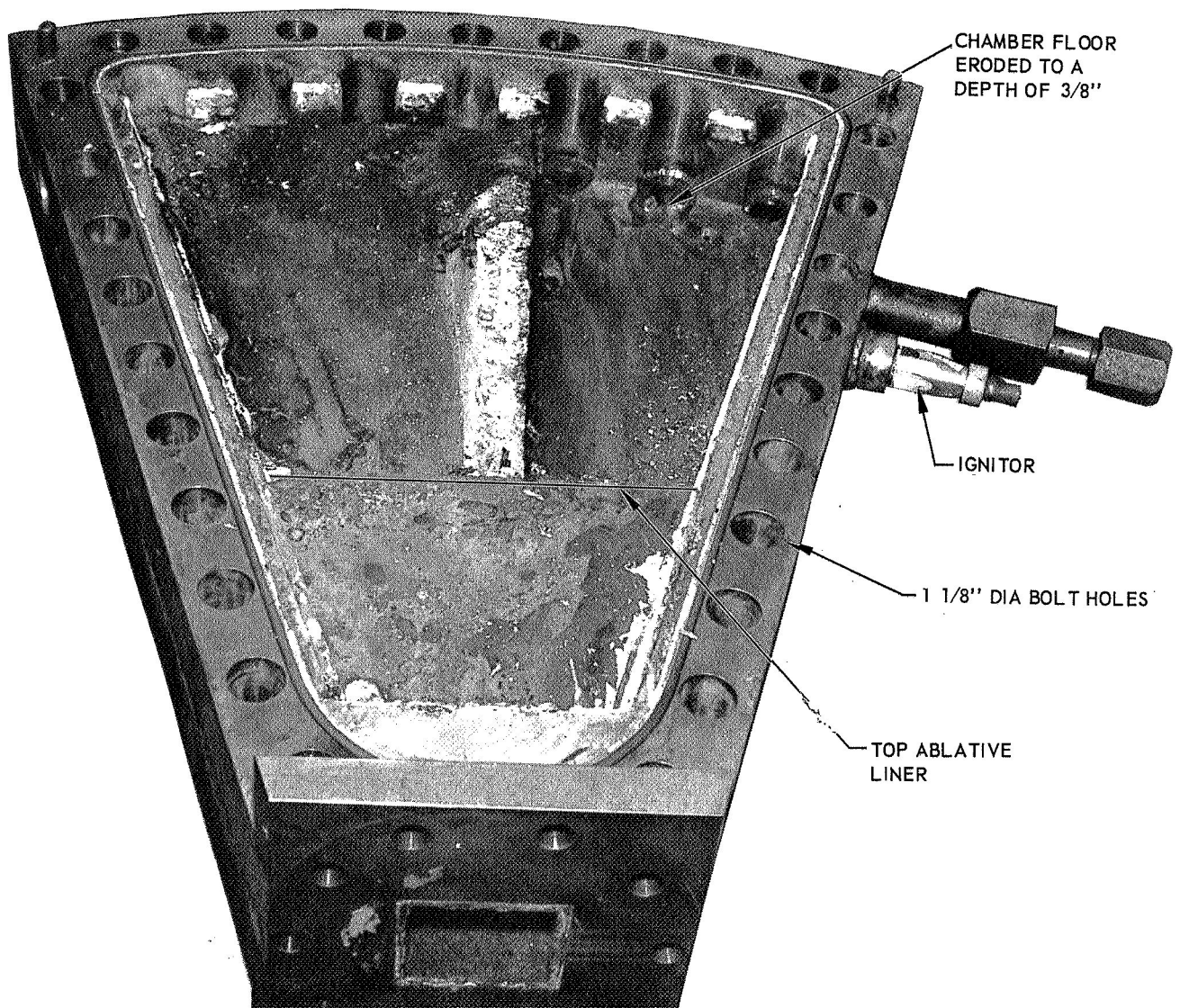
Figure 13

Concentric Sheet Injector for Annular Thrust Chamber Assembly



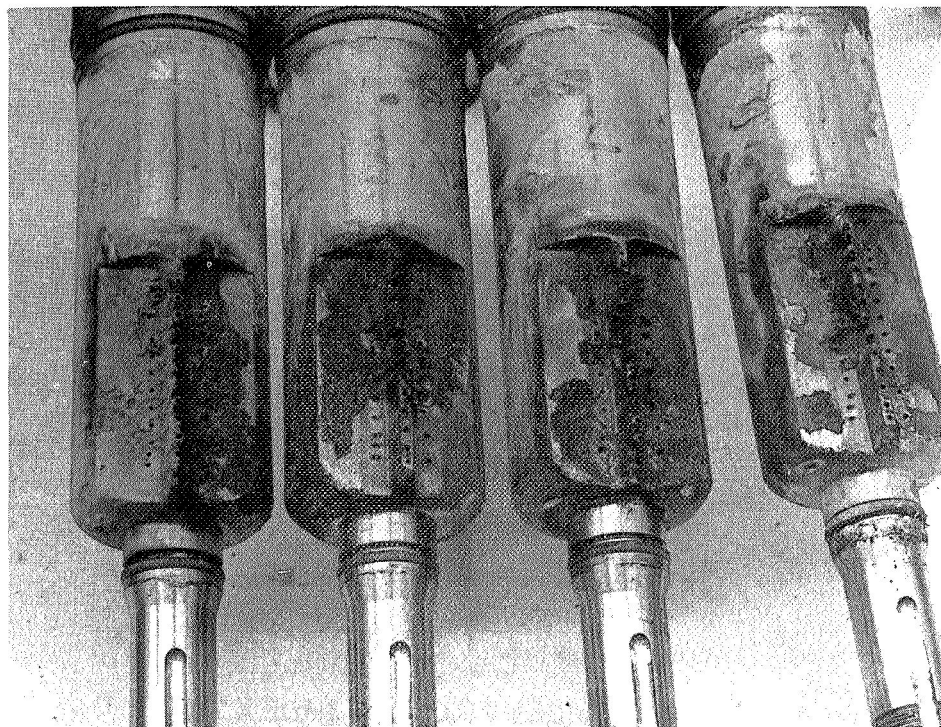
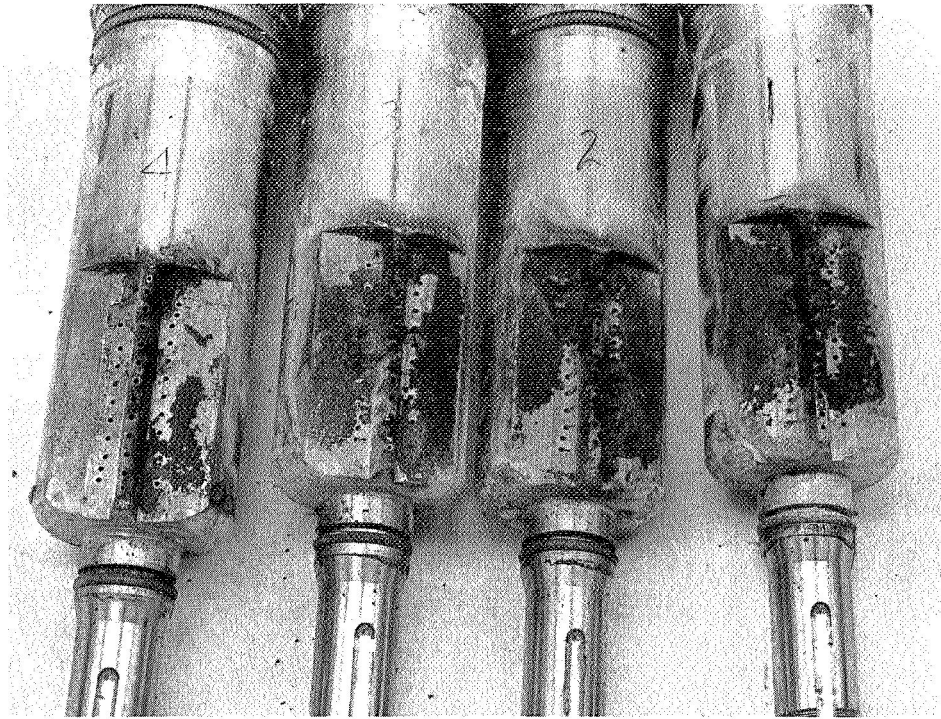
Damaged Injector Inserts from Test 002

Figure 14



Damaged Excitation Chamber

Figure 15



Damaged Injector Inserts from Tests 005 and 006

Figure 16

APPENDIX B

ANALYTICAL MODEL

TABLE OF CONTENTS

	<u>Page</u>
I. Theory	1
A. General Approach	1
B. Governing Equations	2
C. Combustion Response	12
D. Nozzle Admittance Coefficients	29
E. Characteristic Equation	43
F. Discussion of Restrictions	61
II. Program Listing	65
III. References	124

FIGURE LIST

	<u>Figure</u>
The General Interaction Index for Two Types of Combustion Sensitivities	1
The Variation of the Feedback Factors R_{η} and I_{η} with Frequency	2
Sprays Produced by Various Orientations of the Injector Spud	3
Examples of Nonlinear Response Functions	4
Exhaust Nozzle Coordinate System	5
Nozzle Geometry and Comparison of Entrance Portions of Approximate and Actual Nozzle Geometries	6
Real Part of ξ Versus Axial Distance	
Real Part of $\xi^{(2)}$ Versus Axial Distance	8
Real Part of Pressure Admittance Coefficient Versus Axial Distance	9
Imaginary Part of Radial Velocity Admittance Coefficient Versus Axial Distance	10
Typical Solutions of (ω) and $\tau(\omega)$	11
Stable and Unstable Regions on the η , τ -Plane	12
Relationship of Various Transverse Modes on the η , τ -Plane	13
The Shift of the Stability Zone Due to Nonlinear and Velocity Effects	14
Applicable Frequency Ranges of Linear, Transverse Mode Sensitive Time Lag Model	15

LIST OF ABBREVIATIONS AND SYMBOLS

(Refer to Appendix B for Equations Listed)

A	Nozzle admittance coefficient defined by equation (35)
A_R, A_i	Real and imaginary part of A
$A_{v\eta}$	Injector non-uniformity coefficient for pressure effects
B	Nozzle admittance coefficient defined by equation (35)
B_r, B_i	Real and imaginary parts of B
$B_{v\eta}$	Injector non-uniformity coefficient for radial velocity effects
C	Nozzle admittance coefficient defined by equation (35)
C_r, C_i	Real and imaginary parts of C
$C_{v\eta}$	Injector non-uniformity coefficient for tangential velocity effects
c_e	Effective speed of sound
c_o^*	Speed of sound, ft/sec
d_f	Fuel orifice diameter, in.
d_i	Central orifice diameter of a coaxial injector element, in.
d_o	Oxidizer orifice diameter, in.
E	Transverse nozzle admittance coefficient
E_R, E_i	Real and imaginary parts of E
f^*	Frequency, HERTZ (hz)
f	Describing function
h	Chamber damping effects
h_r, h_i	Real and imaginary parts of h
h_s	Total enthalpy, Btu/lb
I	Imaginary part of P
I	Sinusoidal input to nonlinear element

Report 20672-PIF, Appendix B

LIST OF ABBREVIATIONS AND SYMBOLS (cont.)

TF	Equivalent linear transfer function
TF _{um}	Limiting linear transfer function
t	Time, sec
t ₁	Burning time, sec
u	Axial dependency of the axial velocity perturbation
μ	Axial component of the velocity vector
μ _e	Mach number at the exit of the combustion chamber
VR	Velocity ratio of injected propellant fuel velocity to oxidizer velocity
V	Axial dependency of the radial perturbation
v	Radial component of the velocity vector
v _F	Fuel injection velocity, ft/sec
v _x	Oxidizer injection velocity, ft/sec
w	Tangential component of the velocity vector
\dot{w}_F	Fuel flowrate, lb/sec
\dot{w}_x	Oxidizer flowrate, lb/sec
Y _x	Mass fraction concentration
z	Axial component of cylindrical coordinate system
z _e	Axial location of chamber exit, in.
Γ	Auxiliary function defined by equation (15)
γ	Ratio of the specific heats
δ _r	Radial displacement parameter defined by equation (21)
δ _θ	Tangential displacement parameter defined by equation (21)
ζ	Dummy variable of integration

LIST OF ABBREVIATIONS AND SYMBOLS (cont.)

θ	Angular component of cylindrical coordinate system
θ	Elapsed fractional portion of total time lag
θ_F	Fuel orifice impingement angle
θ_X	Oxidizer orifice impingement angle
λ	Real part of complex frequency
ρ	Density, $\frac{th}{ft^3}$
σ	Complex frequency ($\sigma = \lambda + i\omega$)
τ	Sensitive time lag
τ_T	Total time lag
ϕ	Velocity potential
ψ	Stream function
Ω	Auxiliary function defined by equation (15)
ω	Imaginary component of complex frequency
ω_C	Chamber frequency, hz
ω_N	Nozzle frequency, hz

SUBSCRIPT: e Chamber exit

L Liquid

\rightarrow Vector

SUPERSCRIPTS: $\bar{}$ Steady state parameter

* Complex conjugate

* Dimensioned variable

$\hat{}$ Perturbation value

Report 20672-PIF Appendix B

LIST OF ABBREVIATIONS AND SYMBOLS (cont.)

k	Gas/liquid momentum interchange coefficient
L_c^*	Cylindrical chamber length, in.
ℓ_r	Radial velocity interaction index defined by equation (18)
ℓ_θ	Tangential velocity interaction index defined by equation (18)
M_c	Chamber Mach number
MR	Ratio of oxidizer flow rate to fuel flow rate
\dot{M}_b	Burning rate
\dot{M}_i	Injection rate lb/sec
M_r	radial displacement index defined in (21)
M_θ	Tangential displacement index defined in (21)
N	Generalized interaction index
N_L	Longitudinal mode number
N_η	Normalized counterpart of N
N_ω	Number of chamber frequencies to be used
η	Directional normal to streamline
η	Pressure interaction index defined by equation (18)
η_{\min}	Minimum value of pressure interaction index
O	Nonlinear output of a nonlinear element
P	Pressure feedback parameter defined by equation (23)
P	Axial dependency of the pressure perturbation
p_c	Chamber pressure, psia
p_{cr}	Critical pressure, psia
p	Chamber pressure, psia

Report 20672--PIF Appendix B

LIST OF ABBREVIATIONS AND SYMBOLS (cont.)

p_r	Ratio of chamber pressure to critical pressure of controlling propellant
Q	Burning rate per unit volume
\vec{q}	Velocity vector
R	Radial velocity feedback parameter defined by equation (23)
R_r	Same as R
R_δ	Displacement counterpart of R
R	Real part of P
R_η	Defined by equation (26)
r	Radial component of cylindrical coordinate system
r_c^*	Chamber radius, in.
S	Axial dependency of the entropy pertrubation
$s_{v\eta}$	Transverse acoustic mode number defined by equation (15)
$s_{v\eta}$	Same as $S_{v,\eta}$ defined by equation (69)
s	Streamline direction
T	Tangential velocity feedback parameter defined by equation (23)
T_v	Same as T
T_δ	Displacement counterpart of T
T	Temperature, °R

I. THEORY

A. GENERAL APPROACH

The simplifying assumptions on which the mathematical treatment of combustion instability are based are the following:

(a) The substance contained in the combustion chamber is either in the form of liquid propellants, of practically zero volume, or in the form of complete combustion gases.

(b) The combustion gases are of constant composition; they obey the perfect gas law and have constant specific heats.

(c) Frictional effects on the walls are neglected, and only those are taken into account which result in the liquid droplet drag.

(d) The flow of injected propellants is unaffected by pressure oscillations in the chamber, and hence the injection flux and velocity are the same as steady conditions.

(e) The steady-state gas flow is uniform across any chamber section.

(f) In steady-state, the total energy (internal and kinetic) of the droplets remains constant.

(g) The steady-state flow in the nozzle is one-dimensional.

(h) The unsteady, oscillatory quantities in the chamber and in the nozzle can be obtained by superposing small perturbations to the steady-state quantities.

I, A, General Approach (cont.)

(i) The gas flow Mach number is always sufficiently small so that the cube can be neglected compared to unity.

(j) The time dependence of the perturbations can be expressed in complex form as $\exp(\sigma t)$ where $\sigma = \lambda + i\omega$ is the same complex quantity for all perturbations. Here, ω is the angular frequency and λ the amplification coefficient.

B. GOVERNING EQUATIONS

1. General Equations

The equations governing the unsteady, two-phase flow in the combustion chamber are derived from the principles of conservation of mass, momentum, and energy, and the equation of state, according to the assumptions discussed in the previous section. It is convenient to work with the equations in nondimensional form. The reference quantities for the nondimensionalization are taken as the stagnation gas properties at the injector face (pressure, temperature, density, and speed of sound) together with a reference length, which is the chamber radius for transverse modes (the chamber length is generally used for longitudinal modes). The governing equations take the following forms:

Conservation of mass,

$$\frac{\partial \rho}{\partial t} + \nabla \cdot (\rho \vec{q}) = Q = - \frac{\partial \rho_L}{\partial t} - \nabla \cdot (\rho_L \vec{q}_L) \quad (1)$$

Conservation of momentum,

$$\rho \frac{\partial \vec{q}}{\partial t} + \rho \vec{q} \cdot \nabla \vec{q} + \frac{1}{\gamma} \nabla p = (Q + k \rho_L) (\vec{q}_L - \vec{q}) \quad (2)$$

I, B, Governing Equations (cont.)

Conservation of energy,

$$\rho \frac{\partial h_s}{\partial t} + \rho \vec{q} \cdot \nabla h_s - \frac{\gamma-1}{\gamma} \frac{\partial p}{\partial t} = Q (h_{Ls} - h_s) \quad (3)$$

Equation of state for the gas,

$$P = \rho T \quad (4)$$

Droplet drag (gas/liquid momentum interchange),

$$\frac{\partial \vec{q}_L}{\partial t} + \vec{q}_L \cdot \nabla \vec{q}_L = k (\vec{q} - \vec{q}_L) \quad (5)$$

and droplet energy,

$$\frac{\partial h_{Ls}}{\partial t} + \vec{q}_L \cdot \nabla_{Ls} = 0 \quad (6)$$

It is necessary to express the governing equations, (1) to (6), in steady-state form and perturbed form. The separation is accomplished by writing all the unsteady relationships as the sum of a steady-state solution and an unsteady solution. For example,

$$p = \bar{p} + p' e^{\sigma t} \quad (7)$$

$$u = \bar{u} + u' e^{\sigma t}$$

I, B, Governing Equations (cont.)

It is noted that the perturbed portion of each parameter is harmonic with respect to time.

2. Steady-State Equations

The steady-state solution is assumed to be one dimensional although the perturbations are considered in three dimensions. Therefore, the steady-state vectorial components of gas velocity, \vec{q} , and liquid velocity, \vec{q}_L , are given by the following relationships:

$$\vec{q} = \vec{u}, \quad \vec{q}_L = \vec{u}_L \quad (8)$$

$$\vec{v} = \vec{w} = \vec{v}_L = \vec{w}_L = 0$$

where u, u_L are the axial components, v, v_L are the radial components, and w, w_L are the tangential components of \vec{q}, \vec{q}_L . Substituting the relationships given by (7) and (8) into (1) to (6) and neglecting the time dependence, yields the following system of steady-state equations:

Conservation of mass,

$$\frac{d}{dz} (\bar{\rho} \bar{u}) = \bar{Q} = - \frac{d}{dz} (\bar{\rho}_L \bar{u}_L) \quad (9a)$$

Conservation of momentum,

$$\frac{d}{dz} (\bar{\rho} \bar{u}^2) + \frac{d}{dz} (\bar{\rho}_L \bar{u}_L^2) = - \frac{1}{\gamma} \frac{d\bar{p}}{dz} \quad (9b)$$

I, B, Governing Equations (cont.)

Conservation of energy,

$$\bar{\rho} \bar{u} \frac{dh_s}{dZ} = -\bar{Q} (h_s - \bar{h}_{Ls}) \quad (9c)$$

Equation of state (gas),

$$\bar{p} = \bar{\rho} \bar{T} \quad (9d)$$

Droplet drag,

$$\bar{u}_L \frac{d\bar{u}_L}{dZ} = k (\bar{u} - \bar{u}_L) \quad (9e)$$

Droplet energy,

$$\frac{dh_{Ls}}{dZ} = 0 \quad (9f)$$

These equations are easily integrated to give the following relations:

$$\bar{\rho} \bar{u} = \int_0^Z \bar{Q}(\zeta) d\zeta = \bar{\rho}_{L0} \bar{u}_{L0} - \bar{\rho}_L \bar{u}_L \quad (10a)$$

$$\bar{p} = \bar{\rho} = \frac{1 - \gamma (\bar{\rho}_L \bar{u}_L^2 - \bar{\rho}_{L0} \bar{u}_{L0}^2)}{(1 + \gamma \bar{u}^2)} \quad (10b)$$

$$\bar{h}_{Ls} = \bar{h}_{Ls0} = \bar{h}_{s0} = \bar{h}_s \quad (10c)$$

I, B, Governing Equations (cont.)

$$(\bar{u}_L)_{j+1} = (\bar{u}_L)_j + k \left[\frac{\bar{u} - \bar{u}_L}{\bar{u}_L} \right]_j \Delta Z \quad (10d)$$

$$j = 0, 1, 2, \dots$$

$$\bar{Q}(Z) = \frac{\bar{\rho}(1-\gamma\bar{u}^2) \frac{d\bar{u}}{dZ} - \gamma k \rho_L (\bar{u} - \bar{u}_L) \bar{u}}{1+\gamma (\bar{u} - \bar{u}_L) \bar{u}} \quad (10e)$$

$$\bar{\rho}_L = \frac{\bar{\rho}_{LO} \bar{u}_{LO} - \bar{\rho} \bar{u}}{\bar{u}_L} \quad (10f)$$

It should be noted that, at $Z = 0$, $\bar{u} = 0$ and $\bar{p} = \bar{\rho} = 1$ because of the nondimensionalizing scheme. At $Z = Z_E$, combustion is assumed to be complete so that $\bar{\rho}_L = 0$ and $\bar{Q} = 0$. The droplet drag equation is most conveniently integrated numerically for \bar{u}_L (Equation (10d)).

3. The Perturbation Equations: Wave Equations

The perturbed equations are considered in three dimensional form and the resulting system of equations is linearized. That is, the perturbed quantities are considered to be small and, therefore, all products of two or more perturbed terms are considered to be zero. Substituting Equations (7) and (8) into Equations (1) to (6) yields the following system of equations:

$$\begin{aligned} (\sigma + \frac{d\bar{u}}{dZ}) \rho' + u \frac{\partial \rho'}{\partial Z} + \frac{d\bar{\rho}}{dZ} u' + \rho \left(\frac{\partial v'}{\partial r} + \frac{v'}{r} \right. \\ \left. + \frac{1}{r} \frac{\partial w'}{\partial \theta} + \frac{\partial u'}{\partial Z} \right) = \bar{Q} (P_p' + Rv' + Tw') \end{aligned} \quad (11a)$$

I, B, Governing Equations (cont.)

where $P = n(1 - e^{-i\omega\tau})$,

$$R = \ell_r (1 - e^{-i\omega\tau}) = \frac{1}{n} r P, \text{ and}$$

$$T = l_\theta (1 - e^{-i\omega\tau}) = \frac{1}{n} \theta P$$

Conservation of axial momentum,

$$\begin{aligned} & (\sigma \bar{u} + 2\bar{u} \frac{d\bar{u}}{dZ}) \rho' + (\sigma \bar{u}_L + 2\bar{u}_L \frac{d\bar{u}_L}{dZ}) \rho'_L + \bar{u}^2 \frac{\partial \rho'}{\partial Z} + \bar{u}_L^2 \frac{\partial \rho'_L}{\partial Z} \\ & + (\sigma \bar{\rho} + 2\bar{\rho} \frac{d\bar{u}}{dZ} + 2\bar{u} \frac{\partial \bar{\rho}}{\partial Z}) u' + (\sigma \bar{\rho}_L + 2\rho_L \frac{d\bar{u}_L}{dZ} + 2\bar{u}_L \frac{d\bar{\rho}_L}{dZ}) u'_L \\ & + 2\bar{\rho} \bar{u} \frac{\partial u'}{\partial Z} + 2\bar{\rho}_L \bar{u}_L \frac{\partial u'_L}{\partial Z} + \bar{\rho} \bar{u} (\frac{\partial v'}{\partial r} + \frac{v'}{r} + \frac{1}{r} \frac{\partial w'}{\partial \theta}) \\ & + \bar{\rho}_L \bar{u}_L (\frac{\partial v'_L}{\partial r} + \frac{v'_L}{r} + \frac{1}{r} \frac{\partial w'_L}{\partial \theta}) = - \frac{1}{\gamma} \frac{\partial p'}{\partial Z} \end{aligned} \quad (11b)$$

Conservation of radial momentum,

$$\begin{aligned} & (\sigma \bar{\rho} + \bar{\rho} \frac{d\bar{u}}{dZ} + \bar{u} \frac{d\bar{\rho}}{dZ}) v' + (\sigma \bar{\rho}_L + \bar{\rho}_L \frac{d\bar{u}_L}{dZ} + \bar{u}_L \frac{d\bar{\rho}_L}{dZ}) v'_L \\ & + \bar{\rho} \bar{u} \frac{\partial v'}{\partial Z} + \bar{\rho}_L \bar{u}_L \frac{\partial v'_L}{\partial Z} = - \frac{1}{\gamma} \frac{\partial p'}{\partial r} \end{aligned} \quad (11c)$$

I, B, Governing Equations (cont.)

Conservation of tangential momentum,

$$\begin{aligned}
 & (\sigma \bar{\rho} + \bar{\rho} \frac{d\bar{u}}{dZ} + \bar{u} \frac{d\bar{\rho}}{dZ}) w' + (\sigma \bar{\rho}_L + \bar{\rho}_L \frac{d\bar{u}_L}{dZ} + \bar{u}_L \frac{d\bar{\rho}_L}{dZ}) w'_L \\
 & + \bar{\rho} \bar{u} \frac{\partial w'}{\partial Z} + \bar{\rho}_L \bar{u}_L \frac{\partial w'_L}{\partial Z} = - \frac{1}{\gamma r} \frac{\partial p'}{\partial \theta}
 \end{aligned} \tag{11d}$$

Conservation of energy and equation of state, combined,

$$\begin{aligned}
 & (\sigma \bar{\rho} + \bar{Q} - \bar{u} \frac{d\bar{\rho}}{dZ}) \rho' + \bar{\rho} \bar{u} \frac{\partial \rho'}{\partial Z} - (\gamma - 1) \bar{\rho} \bar{u} (\sigma \bar{\rho} + \bar{Q} + \bar{u} \frac{d\bar{u}}{dZ}) u' \\
 & - (\gamma - 1) (\bar{\rho} \bar{u}^2 \frac{\partial u'}{\partial Z}) = (\sigma \frac{\bar{\rho}}{\gamma} + \bar{Q} - \bar{u} \frac{d\bar{\rho}}{dZ}) p' + \bar{\rho} \bar{u} \frac{\partial p'}{\partial Z}
 \end{aligned} \tag{11e}$$

Droplet dynamics,

Defining $K = \frac{k}{k+\sigma}$

And $\xi = (k+\sigma) \frac{dZ}{\bar{u}_L}$

Then

$$u'_L = K u' - \frac{K}{\bar{u}_L} e^{-\xi} \left\{ \int_0^Z \frac{d\bar{u}_L}{dZ} e^{\xi} u' dZ + \int_0^Z \bar{u}_L e^{\xi} \frac{\partial u'}{\partial Z} dZ \right\} \tag{11f}$$

$$v'_L = K(1 - e^{-\xi}) v' - K e^{-\xi} \int_0^Z e^{\xi} \frac{\partial v'}{\partial Z} dZ \tag{11g}$$

$$w'_L = K(1 - e^{-\xi}) w' - K e^{-\xi} \int_0^Z e^{\xi} \frac{\partial w'}{\partial Z} dZ \tag{11h}$$

I, B, Governing Equations (cont.)

$$\begin{aligned}
& (\sigma + \frac{d\bar{u}}{dZ})\rho' + (\alpha + \frac{d\bar{u}_L}{dZ})\rho'_L + \bar{u} \frac{\partial \rho'}{\partial Z} + \bar{u}_L \frac{\partial \rho'_L}{\partial Z} \\
& + \bar{\rho} (\frac{\partial v'}{\partial r} + \frac{v'}{r} + \frac{1}{r} \frac{\partial w'}{\partial \theta} + \frac{\partial u'}{\partial Z}) + \bar{\rho}_L (\frac{\partial v'_L}{\partial r} + \frac{v'_L}{r} \\
& + \frac{1}{r} \frac{\partial w'_L}{\partial \theta} + \frac{\partial v'_L}{\partial Z}) + \frac{d\bar{\rho}}{dZ} u' + \frac{d\bar{\rho}_L}{dZ} u'_L = 0
\end{aligned} \tag{11i}$$

In general, separation of variables is not possible with these equations. A solution can be obtained by writing each quantity in a series such that each successive term in the series is less than its predecessor. Therefore, the pressure perturbation is written in the form

$$p' = p_0 + p_1 + p_2 + p_3 + \dots + p_n + \dots \tag{12}$$

where p_0 can assume any magnitude within the restrictions of the analysis. Then $p_1 = 0$ ($\bar{u}_e \cdot p_0$)*, $p_2 = 0$ ($\bar{u}_e^2 \cdot p_0$) and $p_n = 0$ ($\bar{u}_e^n \cdot p_0$) where \bar{u}_e is the chamber Mach number. Applying this approach to Equations (11a) through (11b), collecting terms of like order, and solving for the pressure results in wave equations for p_0 , p_1 , and p_2 :

$$\sigma^2 p_0 - \bar{\rho} p_0 = 0 \tag{13a}$$

$$\begin{aligned}
\sigma^2 p_1 - \bar{\rho} p_1 &= \sigma \bar{\gamma} \bar{Q} (p_1 p_0 - R_1 \frac{1}{\sigma \bar{\gamma} \bar{\rho}} \frac{\partial p_0}{\partial r} \\
&- T_1 \frac{1}{\sigma \bar{\gamma} \bar{\rho} r} \frac{\partial p_0}{\partial \theta}) - \sigma^2 \frac{d\bar{u}}{dZ} + (\gamma-1) \frac{\bar{Q}}{\bar{\rho}} + \frac{k}{k+\sigma} \frac{\bar{\rho}_L}{\bar{\rho}} p_0
\end{aligned} \tag{13b}$$

*This notation is used to indicate the order of magnitude of a given parameter.

I, B, Governing Equations (cont.)

$$\sigma^2 P_2 - \nabla^2 P_2 = \lambda_1 P_2 + \lambda_2 R_2 + \lambda_3 T_2 + \lambda_4 \quad (13c)$$

$$\text{where} \quad \nabla^2 = \frac{\partial^2}{\partial r^2} + \frac{\partial}{\partial r} + \frac{1}{r} \frac{\partial^2}{\partial \theta^2} + \frac{\partial^2}{\partial Z^2}$$

and $\lambda_1, \lambda_2, \lambda_3$, and λ_4 are complicated functions of the lower-order solutions, p_0 and p_1 . P_1, R_1 , and T_1 are the first-order approximations to the burning rate functions defined in Equation (11a); and P_2, R_2 , and T_2 are the corrected values resulting from the second-order solutions.

The solutions of (13a) to (13c) are given by

$$p_0(Z, r, \theta) = P_{00} \cos h \Omega(Z) \psi(r) \theta(\theta) \quad (15a)$$

$$P_0(Z, r, \theta) = P_{00} (\Gamma_{11} P_1 + \Gamma_{10}) \psi(r) \theta(\theta) \quad (15b)$$

$$p_0(Z, r, \theta) = P_{00} (\Gamma_{21} P_2 + \Gamma_{20}) \psi(r) \theta(\theta) \quad (15c)$$

$$\text{where} \quad \psi(r) = J_\nu(s_{\nu\eta} \cdot r)$$

$$\begin{array}{ll} \cos \nu\theta & \text{STANDING MODE} \\ \theta(\theta) & \\ e^{-\nu\theta} & \text{SPINNING MODE} \end{array} \quad (15d)$$

and J_ν represents the Bessel function for the first kind of order ν

$$\Gamma_{11} = \frac{1}{\Omega} (-\sigma \gamma A_{\nu\eta} + \frac{\ell_r}{n} B_{\nu\eta} + \frac{\ell_\theta}{n} C_{\nu\eta}) \int_0^Z \bar{Q}(\zeta) \sin h [\Omega(Z-\zeta)] d\zeta \quad (15e)$$

$$\text{where} \quad \Omega^2 = \sigma^2 + s_{\nu\eta}^2$$

I, B, Governing Equations (cont.)

$$\begin{aligned}
 \Gamma_{10} &= \frac{\sigma}{\Omega} (\gamma-1) \int_0^Z \bar{Q}(\zeta) \sin h [\Omega(Z-\zeta)] d\zeta \\
 &+ 2 \int_0^Z \frac{d\bar{u}}{dZ}(\zeta) \sin h [\Omega(Z-\zeta)] d\zeta \\
 &+ \frac{k\sigma}{k+\sigma} \int_0^Z \frac{\bar{\rho}_L}{\bar{\rho}}(\zeta) \sin h [\Omega(Z-\zeta)] d\zeta
 \end{aligned} \tag{15f}$$

$$\begin{aligned}
 \Gamma_{21} &= \frac{1}{\Omega} A_{v\eta} \int_0^Z \lambda_1(\zeta) \sin h [\Omega(Z-\zeta)] d\zeta \\
 &+ \left(\frac{\ell_r}{n} B_{v\eta} + \frac{\ell_\theta}{n} C_{v\eta} \right) \int_0^Z \lambda_2(\zeta) \sin h [\Omega(Z-\zeta)] d\zeta
 \end{aligned} \tag{15g}$$

$$\Gamma_{20} = \frac{1}{\Omega} \int_0^Z \lambda_4(\zeta) \sin h [\Omega(Z-\zeta)] d\zeta \tag{15h}$$

These solutions depend on the following boundary conditions:

$$\begin{aligned}
 Z = 0, \quad u' &= 0 \\
 r = 1, \quad v' &= 0 \\
 r = 0, \quad v' &< \infty
 \end{aligned}$$

To complete the analysis, the combustion terms must be considered in detail and the boundary condition at the nozzle entrance (viz., the nozzle admittance condition) must be specified.

I, Theory (cont.)

C. COMBUSTION RESPONSE

1. General Formulation

It is necessary now to provide a mathematical formulation for the combustion terms in the flow equations in terms of the chamber conditions. Our quantitative understanding of the actual combustion processes is not sufficient to provide a mathematical model. Fortunately, the heuristic formulation based on the sensitive time lag concept seems to provide a good representation of the actual combustion response. The relation between time lag and burning rate is immediately found by considering that the fraction of propellant burning at a certain station in a time interval dt must have been injected during the interval $d(t-\tau_t)$. If, then, \dot{M}_b and \dot{M}_i are the corresponding burning and injection rates, we must have

$$\dot{M}_b dt = \dot{M}_i d(t-\tau_t)$$

In steady-state τ_t does not vary with time, and hence, if the injection rate is unaffected by the oscillations

$$\bar{\dot{M}}_b = \bar{\dot{M}}_i$$

From these two relations we obtain the fractional perturbation of the burning rate in the form

$$\frac{\dot{M}_b}{\bar{\dot{M}}_b} = \frac{\dot{M}_b - \bar{\dot{M}}_b}{\bar{\dot{M}}_b} = - \frac{\partial \tau_t}{\partial t} = \frac{-d\tau}{dt} \quad (16)$$

where, in accordance with the definition of sensitive time lag, the variation of τ with time is entirely due to the variation of τ_t , and where τ has been assumed to be the same for all propellant elements, and hence independent of the space coordinates.

I, C, Combustion Response (cont.)

Turning to the evaluation of $d\tau/dt$, a satisfactory mathematical description is obtained if one imagines that during the sensitive time lag certain preparatory processes, which need not be more precisely defined, take place at a rate depending on the local, instantaneous values of quantities representing the state and the motion of the gas and droplets. When these preparatory processes, integrated over the duration of the sensitive time lag, reach a certain fixed level, the conversion into hot gases takes place abruptly. It is clear, then, that when the state and the motion conditions vary, also the duration of the sensitive (and hence, the total) time lag will vary, resulting in a variable rate of gas production.

The quantitative formulation follows at once. If the rate of the preparatory processes is given by a function $f(p, T, v, \dots)$ of the pertinent values of the pressure, temperature, any representative velocity (for instance the radial gas velocity) and possibly other quantities representing the conditions in the chamber, the sensitive time lag τ for an element burning at the time t will be given by the equation

$$\int_{t-\tau}^t f(p, T, v, \dots) dt, = \text{Const.}$$

where t_1 represents the burning time. Here the values of p, T, v, \dots must be evaluated not only at time t_1 , but also at the position where the particular propellant element finds itself at that time. Since the above relation must be satisfied also in steady operation, indicating the steady-state quantities with a superimposed bar we must have

$$\int_{t-\tau}^t f(p, T, v, \dots) dt, = \int_{t-\tau}^t f(\bar{p}, \bar{T}, \bar{v}, \dots) dt_1 \quad (17)$$

I, C, Combustion Response (cont.)

Now we introduce the perturbations, such that

$$p = \bar{p} + p'; \quad T = \bar{T} + T'; \quad v = \bar{v} + v'; \quad$$

and expand the rate function in a Taylor series

$$f(p, T, v,) = \bar{f} + \bar{f}_p p' + \bar{f}_T T' + \bar{f}_v v' +$$

where $\bar{f} = f(\bar{p}, \bar{T}, \bar{v},)$ and similarly for the partial derivatives $\bar{f}_p, \bar{f}_T, \bar{f}_v$ of f with respect to the subscripts. Observe that, under the small perturbations assumption, the Taylor series must be stopped after the first order terms.

If it is assumed that the temperature is a function only of the pressure (for instance, through the isentropic defining relation)

$T' = p'(dT/dp)$. Then, defining the nondimensional interaction indices

$\eta, \ell,$ as

$$\eta = \frac{\bar{f}_p}{\bar{f}} + \bar{f}_T (dT/dp), \quad \ell = \frac{\bar{f}_v}{\bar{f}}, \quad \quad (18)$$

$$f(p, T, v,) = \bar{f} \left(1 + \eta \frac{p'}{\bar{p}} + \ell v' + \right)$$

and Equation (17) can be written in the form

$$\begin{aligned} & \int_{t-\tau}^{t-\bar{\tau}} \bar{f} \left(1 + \eta \frac{p'}{\bar{p}} + \ell v' + \right) dt_1 + \int_{t-\bar{\tau}}^t \bar{f} \left(1 + \eta \frac{p'}{\bar{p}} + \ell v' + \right) dt_1 \\ & = \int_{t-\tau}^t \bar{f} dt_1 \end{aligned}$$

I, C, Combustion Response (cont.)

Here the integration interval at the L.H.S. of Equation (17) has been split in two parts. The first interval, from $t - \tau$ to $t - \tau$ is of duration $\tau - \tau$ and hence of the order of the perturbation of the time lag. Hence, compared with the other two integrals, the first integral is of the order of a perturbation. As a result in its evaluation one can disregard in the integrand the terms containing the perturbations which, in view of the small perturbation assumption, would result in a negligible second order contribution. Then, simplifying, the above equation becomes

$$\int_{t-\tau}^t \bar{f} dt_1 = \int_{t-\tau}^t \bar{f}(\eta \frac{p'}{\bar{p}} + \ell v' + \dots) dt_1$$

In the combustion \bar{p} is approximately constant, and if v is the radial gas velocity, so that $\bar{v} = 0$ then $\bar{f}(\bar{p}, \bar{v})$ is a constant, and so are η and ℓ .

Then we obtain simply

$$\tau - \tau = \eta \int_{t-\tau}^t \frac{p'}{\bar{p}} dt_1 + \ell \int_{t-\tau}^t v' dt_1 + \dots$$

or, differentiating with respect to t

$$-\frac{d\tau}{dt} = \eta \left[\frac{p'}{\bar{p}}(t) - \frac{p'}{\bar{p}}(t-\tau) \right] + \ell \left[v'(t) - v'(t-\tau) \right] + \dots \quad (19)$$

Again, it must be specified that while $p'(t)$ is evaluated at the conversion instant t at the location where the conversion takes place, $p'(t - \tau)$ must be evaluated not only at time $t - \tau$, but also at the location where the propellant was at that time. However, the displacement of the propellant during the time τ produces an effect of second order in the expression (19). As a reasonable approximation, therefore, both $p'(t)$ and $p'(t - \tau)$ can be evaluated at the station when the conversion into burned gases takes place. And, of course, the same applies to the velocity effect of Equation (19), and to other possible effects.

I, C, Combustion Response (cont.)

In Equation (19) only the pressure sensitivity and the radial velocity sensitivity are explicitly considered. Concerning the last it must be added that other components of the gas velocity can be treated in exactly the same fashion. If one is interested, for instance, in the effect of the transversal nonuniformity of the gas composition, then also the tangential velocity component is relevant, and correspondingly another velocity sensitive term must appear in Equation (19), which becomes, in the absence of other interactions

$$-\frac{d\tau}{dt} = \eta [p'(t) - p'(t-\bar{\tau})] + \lambda_r [v'(t) - v'(t-\bar{\tau})] + \lambda_\theta [w'(t) - w'(t-\bar{\tau})] \quad (20)$$

It must be observed that, actually, when only the effects of the nonuniform gas composition on the burning rate are sought, what counts is the displacement of the gases with respect to the droplets, rather than the relative velocity. This can be formalized by writing, for instance, instead of (20),

$$-\frac{d\tau}{dt} = \eta \left[\frac{p'}{\bar{p}}(t) - \frac{p'}{\bar{p}}(t - \bar{\tau}) \right] + M_r \left[\delta'_r(t) - \delta'_r(t - \bar{\tau}) \right] + M_\theta \left[\delta'_\theta(t) - \delta'_\theta(t - \bar{\tau}) \right] \quad (21)$$

where M_r and M_θ are two displacement indices relative to the radial and tangential displacements δ_r , δ_θ respectively. The two formulations (20) and (21) are closely correlated, because of the relations existing between velocities and displacements.

If the time dependence of the perturbations in Equations (20) and (21) is taken to be $\exp(st)$, the result is

$$-\frac{d\tau}{dt} = -(Pp' + R_v v' + T_w w') - (Pp' + R_\delta \delta'_r + T_\delta \delta'_\theta) \quad (22)$$

I, C, Combustion Response (cont.)

where the quantities defined by

$$\frac{P}{n} = \frac{P_v}{\ell_r} = \frac{T_v}{\ell_\theta} = \frac{R_\delta}{M_r} = \frac{T_\delta}{M_\theta} = 1 - e^{-\sigma \bar{\tau}}, \quad (\sigma = \lambda + iw) \quad (23)$$

are, in view of (16), to be interpreted as feedback factors. In this case the relation between velocities and displacements is simply $v' = \sigma \delta' r$, $w' = \sigma \delta'_\theta$ so that

$$R_\delta = \sigma R_v, \quad T_\delta = \sigma T_v$$

2. Relevance of the Time Lag Formulation

The implications of these equations are immediately seen, by discussing for instance the pressure feedback factor P . From (23) it can be seen that $P = R + iI$ is a complex quantity, having a component R in phase with the pressure oscillations and one I in quadrature. The component in Phase is actually only one responsible for the magnitude of the energy feedback. For neutral oscillations ($\lambda=0$), its magnitude is immediately found to be $\eta(1 - \cos \omega \bar{\tau})$. Thus, for given η and for ω determined by one of the proper frequencies of the chamber, the energy feedback is zero if $\omega \bar{\tau}$ is a multiple of 2π , and has its maximum value when $\omega \bar{\tau}$ is $\pi, 3\pi, 5\pi, \dots$. When $\bar{\tau}$ is around the latter values, instability is most likely to appear. Hence, if $\bar{\tau}$ has an assigned value (characteristic of the combustion system considered) there would be according to the present formulation, not one but a series of preferred frequency ranges. This conclusion does not agree with the experimental observations, and would seem to cast a doubt on the validity of the heuristic combustion model derived from the sensitive time lag concept.

However, a closer examination shows where the reason of the disagreement resides. In Equation (17) the rate function $f(p, T, v, \dots)$ has been assumed to depend on the chamber conditions, but not on the progress of the preparatory process themselves, and hence on the time elapsed since the

I, C, Combustion Response (cont.)

entrance of the propellant in the sensitive portion of the time lag. In other words, the effect of given perturbations of the chamber conditions on the value of the integral at the L.H.S. of Equation (17) is the same no matter where during the sensitive time lag, the perturbations take place. This is, indeed, in line with the step function assumption concerning the sensitivity, which has been assumed to be zero during the insensitive portion, and at a constant level during the sensitive portion of the total time lag τ_t .

In a more realistic model, the step function sensitivity should be replaced by an appropriate smooth distribution of some kind during the whole τ_t , with a maximum toward its end. Without entering into the details of the analysis (which can be found in Ref. 8), the equation replacing Equation (19) for the case of pure pressure sensitivity can be given as

$$-\frac{\partial \tau_t}{\partial t} = \bar{\tau}_t \int_0^1 \frac{N(\theta)}{\bar{p}} \frac{\partial}{\partial t} [p(t - \bar{\tau}_t \theta)] d\theta \quad (24)$$

where θ represents the fraction of the total time lag already elapsed (starting from the injection instant), and $N(\theta)$ is a generalized interaction index, which is now a general function of the instant considered during the time lag. It can easily be checked that for $N(\theta) = \text{const}$ Equation (19) will be obtained.

If the exponential time dependence of p (with $\lambda = 0$) is introduced, the feedback factor is

$$p = R + iI = \frac{\bar{M}_b}{\bar{M}_b} \bigg/ \frac{p'}{\bar{p}} = i\omega \bar{\tau}_t \int_0^1 N(\theta) e^{i\omega \bar{\tau}_t \theta} d\theta \quad (25)$$

I, C, Combustion Response (cont.)

the real part of which, responsible for the energy feedback, reduces to $\eta(1 - \cos \omega\tau)$ if N is assumed to take the values zero for $0 \leq \bar{\tau}_t - \theta \leq \bar{\tau}_t - \bar{\tau}$ and η for $\bar{\tau}_t - \bar{\tau} \leq \bar{\tau}_t - \theta \leq \bar{\tau}_t$, in accordance to the step function assumption about the sensitivity. This is indeed the expression which leads to the incorrect prediction of more than one preferred frequency range for a given τ .

If, however, N is given a smooth variation this erroneous prediction disappears. Take, for instance, $N(\theta) \sim (1 - \cos 2\pi\theta) \exp(-a\theta)$. This sensitivity distribution vanishes at the two ends of the total time lag, and, for sufficiently large values of α , is strongly skewed towards its end, as Figure 1, corresponding to $\alpha = 30$ shows. Here we have plotted the "normalized" sensitivity $N_\eta = N/(N)$, where $(N) = \int_0^1 N d\theta$ has been plotted. Defining also $R_\eta = R/(N)$ and $I_\eta = I/(N)$ the real part of the feedback factor, for large a is given by

$$R_\eta = 2\pi \frac{\alpha\beta^2 (\alpha^2 + 1) (3\alpha^2 + 1 - \beta^2)}{(\alpha^2 + \beta^2) [(\alpha^2 + 1 - \beta^2)^2 + 4\alpha^2\beta^2]} \quad (26)$$

where $\alpha = a/2\pi$ and $\beta = \omega\bar{\tau}_t/2\pi$. It is clear that, contrary to the value of R corresponding to the step-function distribution of N , this value of R_η is positive only for $\omega\bar{\tau}$ smaller than a well defined value, above which it becomes and stays negative. In the region of positive R_η there is only one peak. Figure 2 shows the distribution of R_η and I_η up to the peak, and shows for comparison curves obtained from the equations

$$R_{*\eta} = \eta_\eta (1 - \cos \omega\tau), \quad I_{*\eta} = \eta_\eta \sin \omega\tau$$

for three different choices of η_η and τ , corresponding to the step-function distributions shown on the previous Figure 1. It appears that, despite the great difference in the analytic form, equations of this type, based on the

I, C, Combustion Response (cont.)

sensitive time lag concept, are apt to represent quite well the actual behavior around the maximum of R_η . This is particularly true if one concentrates on reproducing well only one of the two curves, for instance R_η , on which the energy feedback depends.

The conclusion to be drawn from these considerations is that the sensitive time lag formulation, in its simplicity, can represent quite well more realistic cases, provided one disregards all higher frequency ranges of instability and keeps only the one corresponding to the lowest frequency. This conclusion, derived from the heuristic formulation presented above, seems to apply also to combustion models based on more physical grounds. It applies, for instance, to the feedback factor calculated numerically by Heidmann on the grounds of the droplet evaporation model. This is shown by Figure 2, where the feedback factors based on Heidmann's calculations for two different pressure oscillation amplitudes are plotted as a function of the frequency (dashed curves), and correspond quite well with the curves obtained with appropriate values of n and τ , provided the comparison is limited to a range of frequency around the peak of feedback. All of these considerations help to give a certain amount of confidence in the sensitive time lag combustion model, and its capability to represent quite well the energy feedback in the region where this assumes dangerous values. However, in general, it is meaningless to look for an immediate correspondence between the values of n and τ and the fundamental combustion processes.

I, C, Combustion Response (cont.)

3. Velocity Sensitive Combustion

It is desirable to take a closer look at the dynamic aspects of velocity sensitive combustion. The most significant velocity effects are those resulting from the radial and tangential components of the gas velocity perturbation. In the case of purely transverse modes, the longitudinal velocity perturbation component is always much smaller than the transverse components. In addition, the longitudinal component vanishes at the injector face and has its smallest magnitude in the early combustion zone, the region which appears to have the greatest significance for transverse modes. It is possible that in certain combustion chambers the axial spreading of the combustion will result in sizable longitudinal velocity oscillations for higher order longitudinal or combined transverse-longitudinal modes. However, in such cases the pressure perturbation will become correspondingly small in that region, thus, the decreased pressure effect will cancel the increased velocity effect. In the present analysis, therefore only the effects of the transverse velocity oscillations will be considered in the combustion response.

Of the various intermediate processes occurring during the combustion of liquid bipropellants, those most sensitive to velocity are the vaporization of the liquid droplets and the mixing of the vaporized propellants that must precede chemical reaction. The theoretical study of unsteady vaporization by Wieber and Mickelsen (Ref. 1) indicates that the evaporation rate is dependent on the absolute magnitude of the relative velocity between droplet and gas, therefore, the vaporization velocity effect is seen to be essentially nonlinear, and cannot be treated within the framework of a linearized theory. On the other hand, the mixing of the propellants by the oscillating velocities may be linearized, and gives rise to important modifications of the stability behavior of a combustor. Although no detailed description of such a complex phenomenon is now

I, C, Combustion Response (cont.)

possible, the following discussion illustrates one process by which the burning rate may be caused to oscillate by an oscillating transverse gas velocity.

Consider first the mixture of gaseous combustion products, vaporized propellants (oxidizer and fuel), and liquid propellant droplets at some axial station downstream from a fuel-on-oxidizer impinging doublet injector element. Since liquid mixing is imperfect, some stratification will exist in the mixture. For concreteness, assume that the line of centers of the doublet is aligned tangentially (i.e., normal to a radius). Then the stratification is almost entirely in the tangential direction, as shown schematically in Figure 3 by the lines of constant mass fraction of vaporized oxidizer in the mixture γ_x . The exact shape of the constant γ_x contours will be dependent on the injector design, operating conditions, and propellant characteristics. Because of the turbulence in the combustion chamber, the stratification pattern shown represents only a mean condition.

As a droplet evaporates, the vapor diffuses away and must mix with the other vaporized propellant in the propellant proportions for chemical reaction. In a rocket combustor, the transport and mixing are most likely to be carried out by turbulence rather than by molecular diffusion. The overall burning rate of a fuel-rich droplet will, therefore, be a function of the amount of oxidizer vapor near the droplet. In the presence of small, periodic tangential gas velocity oscillations ($w'e^{i\omega t}$), the gaseous mixture will be displaced relative to the droplets, causing oscillations of the local mass fractions of both oxidizer and fuel. Since a fuel droplet is in an oxidant-deficient region, a velocity perturbation which increases the oxidizer fraction in the vicinity of the droplet will increase the contribution of that droplet to the overall burning rate. The opposite is true for an oxidizer-rich droplet subject to the same perturbation,

I, C, Combustion Response (cont.)

since an oxidizer fraction increase corresponds to a fuel fraction decrease. Thus, the effects of the same velocity perturbation on the two droplets will tend to cancel, unless the propellants have significantly different vaporization rates. In the latter case, at any axial station, there will be a greater number of droplets of the less-volatile propellant, and summation of the velocity effect over all of the droplets in the spray will result in a net contribution to the burning rate. This contribution will clearly depend on the amplitude of the velocity as well as its direction. For small perturbations, and for the doublet spray shown in Figure 3a, the burning rate contribution can be written in the form

$$f' = \ell w' e^{i\omega t}$$

where ℓ is a velocity interaction index analogous to the pressure interaction index defined by Crocco. In the case of an arbitrarily oriented spray, such as shown in Figure 3b, the burning rate perturbation due to velocity effects becomes

$$f' = (\ell_r v' + \ell_t w') e^{i\omega t} \quad (27)$$

so that, in general, two velocity indices are necessary.

It is clear that this linearized expression will not be valid for all types of injection patterns. For example, approximately linear effects can be expected with a fuel-on-oxidizer doublet and for a like-on-like pattern if the spacing between unlike fans is sufficiently small. However, for large spacings, nonlinear velocity effects must be taken into consideration.

At present, the magnitudes of the velocity indices cannot be calculated because of the lack of quantitative knowledge of the processes involved in liquid propellant combustion under turbulent conditions.

I, C, Combustion Response (cont.)

It is also possible to formulate the above discussion in terms of displacement interaction indices. Letting the radial and transverse components of the displacements be $\delta_r e^{i\omega t}$ and $\delta_{\theta} e^{i\omega t}$, the net combustion process rate perturbation can be written

$$f' = (m_r \delta_r + m_{\theta} \delta_{\theta}') e^{i\omega t} \quad (28)$$

It is clear that $m_r = i\omega l_r$ and $m_{\theta} = i\omega l_{\theta}$. Thus, the displacement indices present at 90° phase shift with respect to the velocity indices.

The analysis of the effects of velocity (or displacement) sensitivity on the stability of a combustor is considerably simplified by assuming that the velocity effects occur during the same interval (the sensitive time lag) as the pressure effects. In this case, the burning rate perturbation becomes

$$Q' = \bar{Q} P p'[X_i(t)] + R v'[X_i(t)] + T w'[X_i(t)] \quad (29)$$

where

$$\begin{aligned} P &= n(1 - e^{-\sigma \tau}) \\ R &= l_r(1 - e^{-\sigma \tau}) \\ T &= l_{\theta}(1 - e^{-\sigma \tau}) \end{aligned}$$

In equation (29), additional simplifications have been introduced by assuming that all propellant elements have equal mean sensitive time lags, and that the space lag associated with the sensitive time lag is

I, C, Combustion Response (cont.)

a negligible fraction of the wave length. In general, of course, the mean sensitive time lag varies from one propellant element to another. Crocco and Cheng have shown that this nonuniformity of the sensitivity time lag leads to increased stability of the combustor. Therefore, the assumption of a uniform time lag produces a conservative stability prediction.

It would be possible to generalize the burning rate expression to allow for different time lags for pressure and velocity effects. However, both mathematical and physical considerations indicate the desirability of the simpler formulation.

4. Approximate Treatment of Nonlinear Combustion Response

Nonlinearities associated with oscillatory combustion chamber operation can derive from two sources: (1) the fluid mechanical behavior of the gases in the chamber, and (2) the dynamics of the combustion process. It is clear that significant interactions between the two kinds can also occur. The general nature of nonlinear effects, with particular emphasis on the fluid mechanical aspects, is discussed in Section IE. The studies of Priem and Guentert have shown that combustion process nonlinearities can be important even for oscillation amplitudes less than 20% of the mean chamber pressure. Thus, it is worthwhile to consider nonlinearity of the combustion response while retaining the linearized fluid mechanical analysis with its attendant simplification.

To insert nonlinear combustion dynamics into the framework of the linear theory, some method of equivalent linearization must be used. The method selected in this analysis is the "describing function" method.

I, C, Combustion Response (cont.)

When a sinusoidal signal is input to a nonlinear element, the output will not, in general, be sinusoidal. Fourier analysis of the output will reveal many frequency components, among which is one (the fundamental) that corresponds to the frequency of the input signal. For the analysis of stability, only the fundamental frequency component is required, as shown by Reardon (Ref 2). An equivalent linear transfer function for the nonlinear element can be defined as the ratio of the fundamental component of the output to the input. Thus, if

$$I(t) = I_e e^{i\omega_f t}$$

is the input, and

$$O(t) = O_f(\omega_f) e^{i\omega_f t} + \sum_{j \neq f} O_j e^{i\omega_j t} \quad (30)$$

is the output, the equivalent linear transfer function is

$$TF = \frac{O_f(\omega_f)}{I_e}$$

For nonlinearities that can be treated by this method, linear behavior is obtained for limiting values of the input (e.g., $I \rightarrow 0$ or $I \rightarrow \infty$). It is convenient to define a "describing function" f as

$$f(\omega) = TF / (TF)_{LIN} \quad (31)$$

where $(TF)_{LIN}$ is the limiting linear transfer function. Thus, a linear analysis can be extended to include isolated nonlinear effects by replacing the linear transfer function of the nonlinear element by $f(\omega) \cdot (TF)_{LIN}$.

I, C, Combustion Response (cont.)

In applying this approach to the combustion instability problem, it is assumed that the only significant nonlinearities are those associated with the response of the combustion process to pressure and velocity perturbations. Three describing functions are required, corresponding to the combustion response to pressure, radial velocity, and tangential velocity perturbations. Thus, the combustion rate perturbation becomes

$$Q' = \bar{Q}[f_p(p')Pp' + f_R(v')Rv' + f_T(W')TW'] \quad (32)$$

In the above expression, the dependence of the describing functions on the perturbation (input) amplitude is shown explicitly. This dependence on amplitude introduces complications into the solution of the perturbation equations. In general, the input amplitude is a function of the axial, as well as the transverse, space coordinate. To obtain a solution, it is necessary to introduce the additional simplification of neglecting the axial variation of perturbation amplitude in the evaluation of the describing function. For purely transverse modes, this is not an unreasonable approximation, and it breaks down significantly only for higher-order longitudinal modes. The error made by using the perturbation amplitudes at the injector face will be small.

To calculate the describing functions, it is necessary to know the shape of the combustion response to each perturbation. Since it is assumed that the effects are independent of each other, the burning rate perturbation can be written

$$\frac{Q'}{\bar{Q}} = \phi_P(p') + \phi_R(v') + \phi_T(w')$$

I, C, Combustion Response (cont.)

The procedure for calculating each describing function is the same; therefore, it is necessary only to discuss one, say, the pressure-effect describing function.

The input perturbation is $\theta_{Pf} = P \cos \psi$ where $\psi = \omega t$ and, from Fourier analysis the fundamental term of the output series is

$$\theta_{Pf}(P) = \frac{1}{\pi} \int_{C-\pi}^{C+\pi} \phi_P(P \cos \psi) e^{-i\psi} d\psi$$

Thus, the describing function is given by

$$f_P = \frac{1}{\pi P (TF)_{LIN}} \int_{C-\pi}^{C+\pi} \phi_P(P \cos \psi) e^{-i\psi} d\psi \quad (33)$$

In the expressions above, C is an arbitrary constant, and $(TF)_{LIN}$ is a suitable normalizing factor, such that $f_P \rightarrow 1$ for equivalent linear operation. The choice of $(TF)_{LIN}$ depends on the characteristics of each nonlinear response function, and a general rule does not appear feasible.

The describing function method applies well to nonlinearities with odd symmetry (Figure 4a). It is not applicable to response functions with even symmetry, such as the velocity effect on vaporization, since there is no contribution to the fundamental term of the Fourier series. An intermediate case is that of asymmetric response function (Figure 4b). In this case, there will be a significant contribution to the fundamental oscillation, but a change in the mean burning rate as well. This change in the mean burning rate occurs only during the sensitive portion of the total time lag and so will have a negligible influence on the steady-state solution.

I, C, Combustion Response (cont.)

In general, the describing function is complex; that is, the nonlinear combustion response introduces a phase shift as well as an amplitude change. However, for response functions with odd symmetry, the fundamental component of the output is in phase with the input, so that the describing function is real.

D. NOZZLE ADMITTANCE COEFFICIENTS

In any rocket combustion instability analysis, it is desirable to apply a boundary condition at the nozzle entrance to describe the effect of the nozzle upon wave motion in the combustion chamber. In a linearized analysis, this boundary condition is written in the form of an admittance relation; that is, a linear relation between the perturbations of two thermodynamic properties and of the velocity components. The coefficients in this relation are termed admittance coefficients and are calculated by means of an analysis of the oscillatory flow in the nozzle. In this section, the analysis and numerical integration which lead to the determination of these coefficients are discussed.

The divergent portion of the supercritical nozzle need not be analyzed; all that is pertinent is the subsonic flow in the convergent portion since any disturbances to the supersonic flow cannot propagate upstream through the throat. Therefore, disturbances in the subsonic portion of the nozzle and in the chamber are neither affected nor caused by disturbances in the supersonic region. (The opposite, however, is not true.)

To date, two types of nozzles have been analyzed: axisymmetric designs and two-dimensional designs. The axisymmetric case is presently the one of the most practical significance and is the one to be discussed here. The two-dimensional case applies to thin annular chambers and to certain experimental configurations. The analyses of the two cases are similar; details of both are given in Reference 3.

I, D, Nozzle Admittance Coefficients (cont.)

The unperturbed, or steady-state, flow is considered to be one-dimensional in order to simplify the analysis. The perturbed flow, however, may be three-dimensional. The combustion process is assumed to be completed before the flow enters the nozzle so that there are no source terms in the differential equations of motion. The equations do allow for the occurrence of entropy waves and vorticity waves in the nozzle due to the combustion chamber.

The three-dimensional coordinate system (Figure 5) employs the values of the velocity potential ϕ and the stream function ψ of the unperturbed flow in addition to the azimuthal angle, with

$$\bar{q} = \frac{\partial \phi}{\partial s}$$

$$r\rho\bar{q} = \frac{\partial \psi}{\partial n}$$

where s is the streamline direction and n is the direction normal to the streamline. Since the value of the stream function is a constant at the nozzle walls where the boundary conditions are applied, separation of variables is allowed. Culick (Ref 4) did not use this coordinate transformation and was forced to a more cumbersome analysis.

Under the usual assumption of small-amplitude oscillations, linear partial differential equations are obtained that govern the perturbations. These equations are separated under the assumption that the nozzle is sufficiently long that the cosine of the semi-angle of convergence may be approximated by unity. The time and azimuthal dependencies are given by sinusoidal functions. The radial dependencies are given in terms of Bessel functions of the first kind and their derivatives. The axial dependencies are related to

I, D, Nozzle Admittance Coefficients (cont.)

the solution to a certain second-order linear ordinary differential equation with complex-variable coefficients which can only be obtained in exact form by numerical integration.

This second order differential equation is singular at the throat; one of the homogeneous solutions will be regular there and the other one will be singular. The singular solution is cast away. This procedure has been demonstrated to be equivalent to disallowing perturbations to propagate upstream from the supersonic portion of the nozzle (Ref 5).

It has been shown that the admittance coefficients are functions of the solutions to certain first order equations that are obtained by reduction of the original second order equation. So, while it would be necessary to integrate the second order equation in order to determine the variation of the flow properties, it is not necessary for the purpose of determining the admittance coefficients. Since the interest lies in the prediction of global stability characteristics and not in the details of the flow itself, only the equations immediately needed to determine the admittance coefficient will be presented. The derivations and additional analyses may be found in Reference 3.

The admittance coefficients for a given geometry are determined as functions of the axial coordinate or, equivalently, of the local mean-flow Mach number. This implies that, when the admittance coefficient at the nozzle entrance is desired, the axial coordinate at the entrance or the entrance Mach number must be known before the admittance coefficients can be determined.

I, D, Nozzle Admittance Coefficients (cont.)

The linear admittance condition is given by

$$\gamma U + A P + \gamma B S_{v_n} V + \gamma C S = 0 \quad (34)$$

where U, P, B, and S are the axial dependencies of the nondimensional perturbations of axial velocity, pressure, radial velocity, and entropy, respectively. The admittance coefficients A, B, and C are given by

$$\begin{aligned} A &= \left(\frac{\gamma+1}{2}\right) \frac{\frac{\gamma+1}{2(\gamma-1)} \frac{\bar{q}}{\bar{c}}}{\left(\frac{2}{\gamma-1}\right) \frac{\bar{q}}{\bar{c}}} \frac{c^{2\hat{\xi}} (1) \hat{\xi}}{\bar{q}^2 (\bar{c}^{2\hat{\xi}} (1) - \hat{\xi}) - (1/2) i\hat{\omega}} \\ B &= i S_{v_n} \frac{\frac{\hat{w} \bar{q}}{\bar{c}} \frac{1}{(\gamma-1)}}{\bar{c} \left(\frac{1}{\gamma-1}\right)} \frac{c^{-2\hat{\xi}} (1)}{\bar{q}^2 (\bar{c}^{2\hat{\xi}} (1) - \hat{\xi}) - (1/2) i\hat{\omega}} \\ C &= \left(\frac{2}{\gamma+1}\right)^{1/2} \frac{\bar{q}^{-2}}{\bar{q} \bar{c}} \frac{(1/2) (1 - \bar{q}^2) \hat{\xi} (1) - (1/2) i\hat{\omega} (2) + f_3 \hat{\xi}}{\bar{q}^2 (\bar{c}^{2\hat{\xi}} (1) - \hat{\xi}) - (1/2) i\hat{\omega}} \end{aligned} \quad (35)$$

in which \bar{q} and \bar{c} are the local gas velocity and speed of sound nondimensionalized with respect to the steady-state speed of sound at the throat. The admittance coefficients are complex because $\hat{\xi}$, $\hat{\xi}(1)$, $\hat{\xi}(2)$, f_3 and $i\hat{\omega}$ are complex. The auxiliary functions $\hat{\xi}$, $\hat{\xi}(1)$, $\hat{\xi}(2)$ are given by first order differential equations in the axial coordinate ϕ :

I, D, Nozzle Admittance Coefficients (cont.)

$$\left(\frac{d\hat{\zeta}}{d\hat{\phi}} + \hat{\zeta}^2 \right) = (g + ih) \hat{\zeta} - (j - ik) \quad (36)$$

$$\begin{aligned} \frac{d}{d\hat{\phi}} [(1-\bar{q}^{-2}) \hat{\xi}^{(1)}] = & - \left\{ \hat{\zeta} - i\hat{\omega} \left(\frac{1}{2\bar{q}^{-2}} + \frac{2}{(\gamma+1)(1-\bar{q}^{-2})} \right) \right\} [(1-\bar{q}^{-2}) \hat{\xi}^{(1)}] \\ & + \frac{2}{\gamma+1} \frac{\hat{S}_{v\eta}^2}{4} \frac{\bar{c}^{\frac{2}{\gamma-1}}}{\bar{q}} \end{aligned} \quad (37)$$

$$\begin{aligned} \frac{d}{d\hat{\phi}} [(1-\bar{q}^{-2}) \xi^{(2)}] = & - \left\{ \hat{\zeta} - i\hat{\omega} \left(\frac{1}{2\bar{q}^{-2}} + \frac{2}{(\gamma+1)(1-\bar{q}^{-2})} \right) \right\} [(1-\bar{q}^{-2}) \xi^{(2)}] \\ & + \frac{2}{\gamma+1} \frac{d_{f3}}{d\hat{\phi}} + \frac{S_{v\eta}^2 \bar{c}^{\frac{2}{\gamma-1}}}{2 i\hat{\omega} \bar{q}} \left(\frac{1-\bar{q}^{-2}}{2\bar{q}^{-2}} + \frac{\bar{c}^{-2}}{\bar{q}^{-2}} + \frac{\bar{c}^{-2}}{\bar{q}^{-2}} f_3 \right) \end{aligned} \quad (38)$$

where the following definitions apply:

$$b = \bar{q}^{-2} (\bar{c}^{-2} - \bar{q}^{-2})$$

$$g = \frac{\gamma+1}{2} \frac{\bar{q}^{-2}}{\bar{c}^{-2}} \frac{d\bar{q}^{-2}}{d\hat{\phi}}$$

$$h = \hat{\omega} \bar{q}^{-2}$$

$$j = \frac{\hat{\omega}^2}{4} \frac{\bar{q} \bar{c}^{\frac{2}{\gamma-1}}}{4} S_{v\eta}^2$$

$$k = \frac{\gamma-1}{4} \frac{\bar{q}^{-2}}{\bar{c}^{-2}} \frac{d\bar{q}^{-2}}{d\hat{\phi}} \hat{\omega}$$

I, D, Nozzle Admittance Coefficients (cont.)

$$\hat{\phi} = 2\kappa (\phi - \phi_{th})$$

$$\hat{\omega} = \omega/\kappa$$

$$\hat{S}_{v\eta} = S_{v\eta}/\kappa$$

$$\kappa = \frac{dq}{dz_{th}} = \kappa$$

where the angular frequency ω is nondimensionalized with respect to the throat speed of sound divided by the throat radius, $s_{v\eta}$ is the eigenvalue for the particular mode of oscillation, and the subscript th denotes conditions at the throat.

The nonlinear, first order equation for $\hat{\zeta}$ is a complex Riccati equation and may only be solved by numerical integration. Once this is done, the linear, first order equations for $\hat{\xi}(1)$ and $\xi(2)$ may be solved obtaining the standard integral forms. However, rather than numerically evaluating the integral solutions, it is more convenient to solve all three complex (or six real) equations simultaneously by numerical integration.

The numerical integration requires statements of the initial conditions. These are provided by the condition of regularity at the throat ($\hat{\phi} = 0$). After assuming a Taylor series expansion about the throat and evaluating the coefficients in the series, we find the following

$$\hat{\zeta}(0) = \alpha_0 + i\beta_0$$

$$\hat{\xi}(1)_{(0)} = 0$$

$$\xi(2)_{(0)} = 0$$

I, D, Nozzle Admittance Coefficients (cont.)

where

$$\alpha_0 = \frac{\frac{\gamma+1}{2} \frac{\hat{\omega}^2 - s_{v\eta}^2}{4} - \frac{\gamma-1}{4} \hat{\omega}^2}{\hat{\omega}^2 + \left(\frac{\gamma+1}{2}\right)^2}$$

$$\beta_0 = - \frac{\frac{\gamma^2-1}{8} + \frac{\hat{\omega}^2 - s_{v\eta}^2}{4}}{\hat{\omega}^2 + \left(\frac{\gamma+1}{2}\right)^2}$$

Since the Riccati equation is singular at the throat ($\bar{c}^2 - \bar{q}^2 = 0$), the numerical integration cannot begin exactly there. So, in addition to the above conditions, the first derivative of $\hat{\xi}$ at the initial point must be obtained from the regular expansion and supplied to the numerical integration scheme. This initial condition is:

$$\left(\frac{d\hat{\xi}}{d\hat{\phi}}\right)_{th} = \alpha_1 + i\beta_1$$

where

$$\alpha_1 = \frac{1}{\hat{\omega}^2 + (\gamma+1)^2} \left\{ \frac{(\gamma+1)^2}{2} (\alpha_0^2 - \beta_0^2) + (\gamma+1)\hat{\omega} \alpha_0 \beta_0 \right.$$

$$+ \left[\hat{\omega}^2 + \frac{(\gamma+1)^3}{4} + (\gamma+1)^2 \hat{b} \right] \alpha_0 + \frac{(\gamma+1)(\gamma-3)}{4} \hat{\omega} \beta_0$$

$$\left. + \frac{\gamma^2-1}{8} (\hat{\omega}^2 - s_{v\eta}) + \frac{\gamma-1}{2} \hat{\omega}^2 \hat{b} \right\}$$

I, D, Nozzle Admittance Coefficients (cont.)

$$\beta_1 = \frac{1}{\hat{\omega}^2 + (\gamma+1)^2} \left\{ (\gamma+1)^2 \alpha_0 \beta_0 - \frac{\gamma+1}{2} \hat{\omega} (\alpha_0^2 - \beta_0^2) \right. \\ \left. + (\gamma+1) \frac{1-\gamma}{2} \hat{\omega} \alpha_0 - (\gamma+1) \hat{\omega} \alpha_0 \hat{b} + [\hat{\omega}^2 + \frac{(\gamma+1)^3}{4}] \beta_0 \right. \\ \left. + \frac{\gamma-1}{8} \hat{\omega} [S_{v\eta}^2 + (\gamma+1)^2] + \frac{\gamma^2-1}{2} \hat{\omega} \hat{b} \right\}$$

Note that \hat{b} is a coefficient in the power series expansion for \bar{q}^2 . That is, $\bar{q}^2 = 1 + \hat{\phi} + \hat{b} \hat{\phi}^2 + \dots$, the value of \hat{b} being determined by the nozzle geometry in the throat vicinity. The above-mentioned power series shows the convenience of the transformation of the independent variable from ϕ to $\hat{\phi}$; the coefficient of the first order term in the power series is unity.

The function f_3 is given by an integral expression involving known quantities. However, it is more convenient to solve a first order differential equation for f_3 simultaneously with the equations for $\hat{\zeta}$, $\hat{\xi}^{(1)}$, and $\hat{\xi}^{(2)}$. The proper equation is follows:

$$\frac{d}{d\hat{\phi}} (\bar{c}^{-2} f_3) - \frac{i\omega}{2\hat{q}} (\bar{c}^{-2} f_3) = \frac{1}{2} \frac{d\bar{q}^{-2}}{d\hat{\phi}} \quad (39)$$

Subject to the initial condition that $f_3(0) = 0$.

In addition to the admittance coefficients A, B, and C, two other complex admittance coefficients are useful and have been calculated. They are

I, D, Nozzle Coefficients (cont.)

$$\alpha = - \left(\frac{\gamma+1}{2} \right)^{\frac{\gamma+1}{2(\gamma-1)}} \frac{\bar{q}}{\bar{c}^{-2/\gamma-1}} \frac{\hat{\xi}}{\bar{q}^{-2} + i \frac{\hat{\omega}}{2}} \quad (40)$$

$$E = A - \frac{s_{v\eta} B}{i \omega_c}$$

where ω_c is the frequency nondimensionalized by the ratio of the steady-state stagnation speed of sound to the nozzle entrance radius.

α is the admittance coefficient to be used in the relation $U = (\alpha/\gamma)P$ at the nozzle entrance in the absence of vorticity and entropy perturbations. Of course, when $s_{v\eta} = 0$, α is also the admittance coefficient for isentropic longitudinal oscillations.

E is a combination of A and B which becomes important in transverse-mode combustion instability applications. It can be shown that for low Mach numbers, α and $-E$ are approximately equal. This means that at low mean-flow Mach numbers E becomes approximately independent of $\hat{\xi}^{(1)}$ even though A and B are dependent upon it.

The steady-state velocity profile $\bar{q}(\hat{\phi})$ must be determined for the given geometry of the convergent portion of the nozzle. This cannot be found in closed form but must be determined either approximately or indirectly. It is difficult to find an approximate form of $\bar{q}(\hat{\phi})$ which is very accurate over a wide class of nozzle geometries. Therefore, an indirect approach is used, in which the exact form of $\bar{q}(\hat{\phi})$ is determined and a table constructed. This method proceeds as follows: The shape of the nozzle is prescribed as a portion of a cone with circular-arc sections at the throat and at the transition section at the nozzle entrance (Figure 6). With the cone angle

I, D, Nozzle Coefficients (cont.)

and the radii given, the cross-sectional area at any axial station can be calculated. A table is constructed that relates the local Mach number to the area, according to the equation

$$\frac{A(Z)}{A_{th}} = \frac{1}{M(z)} \left[\left(\frac{2}{\gamma+1} \right) \left(1 + \frac{\gamma-1}{2} M^2(z) \right) \right]^{\frac{\gamma+1}{2(\gamma-1)}} \quad (41)$$

The Mach number at each station in the nozzle is then obtained by interpolation in this table. The velocity \bar{q} is related to the Mach number by

$$\bar{q}^2 = \frac{\frac{\gamma+1}{2} M^2}{1 + \frac{\gamma-1}{2} M^2} \quad (42)$$

Finally, the velocity potential is obtained by integration along the nozzle, starting from the throat $Z = 0$, where $\hat{\phi}$ is assigned the value zero:

$$\hat{\phi} = 2 \kappa \int_0^Z \bar{q} dZ' \quad (43)$$

To illustrate the nature of the solution for the nozzle admittance coefficients, calculations have been performed for a conical nozzle with no transition section at the nozzle entrance. The advantage of using such an approximation to the usual smooth transition is that the variation of the admittance coefficients with chamber Mach number can be seen from the results of a single integration. Results for $\gamma = 1.2$, $\hat{\omega} = 0.5$ and $S_{v\eta} = 1.0$ are shown in Figures 7 to 9.

One of the most interesting results is that the nozzle may have a destabilizing effect upon the transverse modes of oscillation. This is indicated by negative values of the real part of α and positive values of the real

I, D, Nozzle Admittance Coefficients (cont.)

part of E. (The importance of the signs of these quantities will be discussed in Section I E.) Negative α_r and positive E_r generally seem to occur in the range of "purely" transverse modes where ω_c is close to $S_{v\eta}$. So here the nozzle would have a destabilizing effect. For longitudinal modes and those mixed modes where the longitudinal dimensions are most significant in determining the frequency ($\omega_c \gg S_{v\eta}$), α_r is positive and E_r is negative so that the nozzle has a damping effect upon the oscillations.

Numerical calculations indicate that the value of the admittance coefficient C are generally quite small compared to the coefficients A and B. This and the fact that the amplitude of the entropy oscillation is small compared to the amplitude of the pressure and velocity oscillations in most situations of physical interest mean that usually (34) may be simplified to the following form

$$U + AP + S_{v\eta} BV = 0 \quad (44)$$

In Figure 7, $\hat{\xi}_r$ is plotted versus axial distance showing a gradual change in $\hat{\xi}_r$ due to the relatively large pressure wavelength. Figure 8 shows $\hat{\xi}_r$ (2) to be undulating* rapidly due to the relatively small entropy and vorticity wavelengths. Note, of course, that pressure waves propagate with the speed of sound while entropy and vorticity waves propagate with the subsonic gas velocity. Figures 9 and 10 show the admittance coefficients A_r and B_i (which are the most pertinent from a stability point of view) plotted versus axial distance. Superimposed upon a gradual change due to the pressure waves, there is a rapid undulation due to the entropy and vorticity waves.

At higher frequencies the oscillations become more severe since undulations in the admittance coefficients occur due to pressure waves in that case. The undulations due to entropy and vorticity waves become still more rapid.

*"Undulation" pertains to space-wise variations while "oscillation" pertains to time-wise variations.

I, D, Nozzle Admittance Coefficients (cont.)

A limited number of calculations have been performed wherein the throat wall curvature, the cone angle, and the ratio of specific heats have been changed. It was found that changing the last parameter from the standard value of $\gamma = 1.2$ to $\gamma = 1.4$ generally produced a change in the admittance coefficients of only a few percent. The other two parameters affected the results more significantly.

Calculations were made with $R = 3.0$ (versus $R = 2.0$ in the standard cases) and $\theta_1 = 30^\circ$ and also with $R = 2.0$ and $\theta_1 = 15^\circ$ (versus $\theta_1 = 30^\circ$ in the standard cases). When R was changed and θ_1 left constant, the results changed most significantly in the high Mach number range near the throat. Further upstream in the low Mach number range, the difference between the $R = 2.0$ and $R = 3.0$ cases is smaller. On the basis of this small amount of evidence, it seems that far away from the throat the results do not depend very strongly on the particulars of the nozzle shape near the throat. When θ_1 was changed and R left constant, the solution near the throat did not change, of course. Only in the conical portion of the nozzle was a change produced.

It should be noted that the results of the calculations for the standard three-dimensional axisymmetric nozzle may be scaled for use with certain annular nozzles. The major restriction is that the inner wall of the annular nozzle must have the same shape as a stream tube contour in the three-dimensional nozzle. This implies that the two nozzle flows are identical in the steady-state (that is, of course, only in the common region where both flows exist). Also, under the long-nozzle, one dimensional steady-state flow assumption this means that the ratio of the outer wall radius to the inner wall radius is constant along the convergent section of the nozzle.

The equations for the annular nozzle may be separated in the same manner and the same differential equations remain to be integrated as in the

I, D, Nozzle Admittance Coefficients (cont.)

three dimensional case. However, now $S_{v\eta}$ is no longer the h^{th} root of $j'_v(x) = 0$ but rather it is the h^{th} root of $J'_v(x) Y'_v(\beta x) - J'_v(\beta x) Y'_v(x) = 0$. Here J_v and Y_v are Bessel functions of the first and second kind, respectively, and β is the ratio of the inner to outer wall diameter. (v is an integer, here.) So using the proper value of $S_{v\eta}$, the results of the three dimensional nozzle calculations for both admittances and flow properties may be used for the annular nozzle. The values of $S_{v\eta}$ for various annuli may be found in Reference 29.

The admittance coefficients for a whole family of nozzles may be obtained by scaling the results calculated for a particular reference nozzle. If k is the scale factor and if a nozzle has a velocity distribution

$$\bar{q}(Z) = \bar{q}_{\text{ref}}(kZ)$$

then the admittance coefficients for this nozzle are given by the following formulas

$$A(\bar{q}, \omega, s) = A_{\text{ref}}\left(\bar{q}, \frac{\omega}{k}, \frac{s_{v\eta}}{k}\right)$$

$$B(\bar{q}, \omega, s) = k B_{\text{ref}}\left(\bar{q}, \frac{\omega}{k}, \frac{s_{v\eta}}{k}\right)$$

$$C(\bar{q}, \omega, s) = C_{\text{ref}}\left(\bar{q}, \frac{\omega}{k}, \frac{s_{v\eta}}{k}\right)$$

$$E(\bar{q}, \omega, s) = E_{\text{ref}}\left(\bar{q}, \frac{\omega}{k}, \frac{s_{v\eta}}{k}\right)$$

$$\alpha(\bar{q}, \omega, s) = \alpha_{\text{ref}}\left(\bar{q}, \frac{\omega}{k}, \frac{s_{v\eta}}{k}\right)$$

I, D, Nozzle Admittance Coefficients (cont.)

A scale transformation of this type is merely a linear deformation of the nozzle walls in the axial direction. Scaling in the radial direction is trivial since all lengths have been nondimensionalized with respect to the throat radius.

The extension of the theory to the nonlinear case is discussed in References 3 and 6.

I, Theory (cont.)

E. CHARACTERISTIC EQUATION

1. Formulation of the Stability Problem

Solution of the perturbation equations gives the pressure perturbation in the form of a Bessel-Fourier series:

$$p' = P_{oo} \left[p_{v\eta}(Z) \psi_{v\eta}(r) \gamma_v(\theta) + \sum_{p \neq v} \sum_{q \neq \eta} P_{pq}(Z) \psi_{pq}(r) \gamma_q(\theta) \right] \quad (45)$$

In this expression the indices v and η refer to the fundamental term, that is, to the oscillatory mode under consideration. The other terms in the series account for the distortion introduced by flow, injection distribution, velocity effects, and nonlinear combustion response. For values of the indices p, q different from v, η , each term in the series includes an integration constant. However, the integration constant for the fundamental term can be shown to be of order M^3 , and so can be neglected in the present analysis. The constant P_{oo} represents the perturbation amplitude level; in this linearized analysis, the amplitude has no effect on the stability solution.

Since the perturbation solution is obtained in the form of a series, the nozzle admittance boundary condition must be applied term by term. For each $p, q \neq v, \eta$, the nozzle boundary condition can be used to determine the integration constant. Application of the remaining condition,

$$\gamma U_{v\eta}(Z_E) + A P_{v\eta}(Z_E) + B s_{v\eta} \gamma V_{v\eta}(Z_E) + C \gamma S_{v\eta}(Z_E) = 0 \quad (46)$$

results in an eigenvalue problem. That is, this equation is the characteristic equation for the eigenvalues $\sigma = \lambda + i\omega$. For a given combustor geometry and for a given value of the combustion parameters, n, τ, ℓ_r , and ℓ_θ , the

I, E, Characteristic Equation (cont.)

characteristic equation can, in principle, be used to determine the frequency of oscillation ω and the growth rate λ of the perturbation amplitude.

However, since the coefficients of the characteristic equation are functions of the variable σ , it is more convenient to regard σ as one of the independent variables. Considerable simplification results if $\lambda = 0$, that is, $\sigma = i\omega$, which is interpreted physically as an oscillation, the amplitude of which neither grows nor decays with time. The neutral condition is clearly the boundary between stable and unstable operation, and is sometimes referred to as the stability limit.

For neutral oscillations, regarding the frequency as an independent variable, the characteristic equation becomes a relation between the combustion parameters. Since the equation is complex, two of the combustion parameters can be determined in terms of the other two. It is natural to select the sensitive time lag τ and the pressure interaction index n as the dependent variables, because these parameters are significant to all modes of oscillation. Following this procedure, the characteristic equation can be written in the form:

$$n (1 - e^{-i\omega\tau}) = \frac{h(\omega)}{A + B \left(\frac{\ell_r}{n}\right) + C \left(\frac{\ell_\theta}{n}\right)} = \tilde{h}_r + i \tilde{h}_i \quad (47)$$

The solution is

$$n \left(\omega, \frac{\ell_r}{n}, \frac{\ell_\theta}{n} \right) = \frac{\tilde{h}_r^2 + \tilde{h}_i^2}{2 \tilde{h}_r} \quad (48)$$

I, E, Characteristic Equation (cont.)

$$\tau(\omega, \frac{l_r}{n}, \frac{l_\theta}{n}) = \frac{1}{\omega} \sin^{-1} \left(\frac{h_1}{n} \right) = \frac{1}{\omega} \cos^{-1} \left(1 - \frac{h_r}{n} \right) \quad (49)$$

where τ is determined to within an additive constant $\frac{2\pi}{\omega}$.

A typical solution for $n(\omega)$ and $\tau(\omega)$ for assumed values of the velocity indexes is shown in Figure 11. This solution applies at the stability limits, where $\lambda = 0$. It can be seen that for any value of τ only one value of n is consistent with neutral oscillations. For the same τ , a larger n corresponds to instability ($\lambda > 0$) and a smaller n to stability ($\lambda < 0$). In the case of transverse modes, for values of n in the range of interest (≤ 2), the frequency varies over a very narrow range, and is very nearly equal to the corresponding acoustic frequency. For longitudinal modes, both the frequency range and the departure from the acoustic-mode frequency are somewhat larger. The narrow frequency range result is related directly to the fact that high frequency instability involves the interaction of the combustion chamber. The chamber acoustics are somewhat modified by the presence of the exhaust nozzle and the mean gas flow, but a good approximation of the resonant frequencies can be made without reference to the combustion effects.

2. Graphical Representation: The n, τ -Plane

In view of the narrow frequency range, a more convenient graphical representation is obtained by plotting the stability limit curves on the plane defined by the interaction index n as ordinate and the sensitive time lag τ as abscissa. This plot will be referred to as the n, τ -plane. A typical example is shown in Figure 12, in which the stability limit curves for a single mode are seen to divide the n, τ -plane into stable and unstable regions.

I, E, Characteristic Equation (cont.)

According to the sensitive time lag model, the dynamic behavior of the combustion process can be described by the parameters n and τ , which are empirical coefficients measuring the pressure sensitivity and characteristic time, respectively, of the combustion process. It is clear that, in general, these parameters are functions of the propellant combination, the injector pattern, and the operating conditions. A given combination of these factors, that is, a given combustion process, is represented on the n, τ -plane as a point. For a given engine configuration, stability limits can be determined for each oscillatory mode of interest, and the n, τ -plane divided into stable and unstable regions. The stability of the given engine is determined by the relation between the point representing the combustion and the regions defined by the stability limits. If the combustion point lies within the stable region (e.g., point A in Figure 13), stable combustion is expected. On the other hand, if the combustion point lies within an unstable region, oscillations would be expected, with the mode of oscillation corresponding to that of the unstable region. For example, in Figure 13, point B would be unstable in the first tangential mode, whereas point C would oscillate in the third tangential mode.

The basic theory considers only very small perturbations and pressure-sensitive combustion. Therefore, the stability predictions are applicable only to injector patterns or modes which exhibit no velocity effects and to combustion chamber oscillations that grow from the normal, low-level combustion noise. As discussed above, velocity and nonlinear effects can be treated within the framework of the theory, and appear in the characteristic equation in the coefficients A, B, and C, and the indices $\frac{\ell_r}{n}$ and $\frac{\ell_\theta}{n}$. The effect of introducing these effects is to shift the stability limit curves, thereby moving the zones of unstable operation.

I, E, Characteristic Equation (cont.)

To illustrate, consider the stability of a single mode, say, the first tangential. Assuming that the pressure sensitivity is not coupled to the velocity sensitivity, the combustion point on the n, τ -plane remains fixed. Several possible cases can be examined:

a. The injector is insensitive to velocity effects ($\ell_r = \ell_\theta = 0$) or a standing mode is considered ($A = C = 0$). The resulting stability limit is shown in Figure 14 as curve 1. Since the combustion point lies below the limit curve, it is in a stable region, and the combustion noise will not grow into first tangential instability.

b. The injector is sensitive to tangential velocity effects only, with a certain value of $\frac{\ell_\theta}{n}$. In this case, the stability limit curve is shifted downward, for a spinning mode, to curve 2. First tangential mode oscillations growing spontaneously out of the combustion noise are expected.

c. The injector is sensitive to radial velocity effects only, with the same value of the velocity index as in case b. The stability limit curve is curve 3, and stable operation is expected.

d. Nonlinear tangential velocity effects are present, with a deadband type or nonlinearity. Using the describing function method, the following results are obtained:

(1) For pressure amplitudes less than 10% of mean chamber pressure, the stability limit curve is curve 1.

(2) For an amplitude of 20% the limit curve is curve 4.

(3) For an amplitude of 40%, the limit curve is curve 2.

I, E, Characteristic Equation (cont.)

For this situation, it would be predicted that a bomb or pulse producing an amplitude of greater than 20% of mean chamber pressure would be required to initiate oscillatory combustion.

3. Interpretation of Terms in the Characteristic Equation

In order to interpret the terms in the characteristic equation, it is convenient to rederive that equation in a different manner which shows the origins of each term. The same assumptions as before apply. In nondimensional form the equations of motion are written as follows:

Continuity:

$$\frac{\partial \rho}{\partial \tau} + \nabla \cdot \rho \vec{q} = Q \quad (50)$$

Momentum:

$$\rho \frac{D\vec{q}}{Dt} + \frac{1}{\gamma} \nabla p = (Q + k \rho_\ell) (\vec{q}_\ell - \vec{q}) \equiv \vec{F} \quad (51)$$

Energy:

$$\rho \frac{D}{Dt} \left(\frac{1}{\gamma-1} \frac{p}{\rho} + \frac{q^2}{2} \right) - \frac{1}{\gamma} \frac{\partial p}{\partial \tau} = Q (h_{\ell s} - h_s) \equiv G \quad (52)$$

where:

$$\frac{D}{Dt} = \frac{\partial}{\partial \tau} + \vec{q} \cdot \nabla$$

The right-hand sides of (50), (51), and (52) are in the order of the mean flow Mach number.

I, E, Characteristic Equation (cont.)

If the dot product of \vec{q} and (51) is subtracted from (52),
one obtains

$$\frac{1}{\gamma} \frac{Dp}{Dt} - a^2 \frac{D\rho}{Dt} = (\gamma-1) (G - \vec{q} \cdot \vec{F}) \quad (53)$$

The right-hand side of (53) may be shown to be $p Ds/Dt$. Consider (53) as a replacement for (52).

Now, the time derivative of (53) and the divergence of (51) are subtracted, the time derivative of (50) is employed to eliminate the derivatives of ρ , and other minor rearrangements are made to obtain the following:

$$\begin{aligned} \frac{1}{\gamma} \frac{\partial^2 p}{\partial t^2} - \frac{a^2}{\gamma} \nabla^2 p &= a^2 \frac{\partial Q}{\partial t} - a^2 \nabla \cdot (\vec{F} + Q \vec{q}) - (\nabla \cdot \rho \vec{q} \vec{q}) \\ &+ (\gamma-1) \frac{\partial}{\partial t} (G - \vec{q} \cdot \vec{F}) - \frac{\partial}{\partial t} (p \vec{q} \cdot \nabla s) \\ &+ \frac{\partial \rho}{\partial t} \frac{\partial a^2}{\partial t} \end{aligned} \quad (54)$$

Equation (54) is the wave equation governing the pressure oscillations in the chamber. It may be perturbed and the equation which governs the first order perturbations (denoted by primes) becomes

$$\begin{aligned} \frac{1}{\gamma} \frac{\partial^2 p'}{\partial t^2} - \frac{1}{\gamma} \nabla^2 p' &= \frac{\partial Q'}{\partial t} - \nabla \cdot (\vec{F} + Q \vec{q}) - (\nabla \cdot \rho \vec{q} \vec{q}) \\ &+ (\gamma-1) \frac{\partial}{\partial t} (G - \vec{q} \cdot \vec{F})' - \bar{q} \frac{\partial}{\partial z} \frac{\partial s'}{\partial t} \end{aligned} \quad (55)$$

I, E, Characteristic Equation (cont.)

Again, the mean flow has been considered one-dimensional. Neglecting terms of order Mach number squared, we obtain

$$(\vec{F} + \vec{Q} \cdot \vec{q})' \approx -k \bar{\rho} \ell \vec{q}' \quad (56)$$

$$(\vec{G} - \vec{q} \cdot \vec{F})' \approx -\bar{Q} h'_s - \frac{\bar{Q}}{\gamma} p' \quad (57)$$

$$\begin{aligned} \nabla \cdot (\nabla \cdot \rho \vec{q} \vec{q})' &\approx \bar{q} \frac{d}{dz} (\nabla \cdot \vec{q}') + \frac{d}{dz} (\bar{q} \nabla \cdot \vec{q}') \\ &+ \frac{d}{dz} (\vec{q}' \cdot \vec{e}_z \frac{d\bar{q}}{dz}) + \nabla \cdot (\vec{q}' \frac{d\bar{q}}{dz}) \end{aligned} \quad (58)$$

where \vec{e}_z is a unit vector in the axial direction. Note that the last term on the right-hand-side of (55) is not considered of higher order in Mach number since entropy gradients may be large due to entropy waves.

Note that

$$\vec{q} = u\vec{e}_z + v\vec{e}_r + w\vec{e}_\theta$$

The perturbations can be written as the product of a space dependent function and a time dependent function. That is

$$\begin{aligned} p' &= \tilde{p} e^{\sigma t} \\ \vec{q}' &= \tilde{\vec{q}} e^{\sigma t} \end{aligned} \quad (59)$$

I, E, Characteristic Equation (cont.)

$$s' = \tilde{s} e^{\sigma t}$$

$$Q' = Q e^{\sigma t}$$

Substituting (56) through (59) into (55) yields

$$\begin{aligned} \frac{\sigma^2}{\gamma} \tilde{p} - \frac{1}{\gamma} \nabla^2 \tilde{p} &= \sigma \tilde{Q} + k \bar{\rho}_\ell \nabla \cdot \tilde{q} + \bar{q} \frac{\partial}{\partial Z} (\nabla \cdot \tilde{q}) \\ &+ \frac{\partial}{\partial Z} (\bar{q} \nabla \cdot \tilde{q}) + \frac{\partial}{\partial Z} \left(\tilde{u} \frac{d\bar{q}}{dZ} \right) \\ &+ \nabla \cdot \left(\tilde{q} \frac{d\bar{q}}{dZ} \right) - \frac{\gamma-1}{\gamma} \sigma \bar{Q} \tilde{p} - \sigma \bar{q} \frac{\partial s}{\partial Z} \equiv I \end{aligned} \quad (60)$$

Here the right-hand-side is of order Mach number so that neglecting it the result to lowest order

$$\nabla^2 \tilde{p} = \sigma^2 \tilde{p} \quad (61)$$

To this same order the perturbation of (51) yields

$$\tilde{q} = - \frac{\nabla p}{\gamma \sigma} \quad (62)$$

so that together with (61) we find to lowest order

$$\nabla \cdot \tilde{q} = - \frac{\nabla^2 p}{\gamma \sigma} = - \frac{\sigma}{\gamma} \tilde{p} \quad (63)$$

I, E, Characteristic Equation (cont.)

This may be substituted in I in (60). The result is that with error of the order of Mach number squared we may write

$$\begin{aligned}
 \tilde{I} = & \sigma \tilde{Q} - \frac{k \bar{\rho}_\ell^\sigma}{\gamma} \tilde{p} - \frac{\sigma}{\gamma} \bar{q} \frac{\partial p}{\partial Z} - \frac{\sigma}{\gamma} \frac{\partial}{\partial Z} (\bar{q} \tilde{p}) \\
 & + \frac{\partial}{\partial Z} (\tilde{u} \frac{d\bar{q}}{dZ}) - \frac{\sigma}{\gamma} \tilde{p} \frac{d\bar{q}}{dZ} + \tilde{u} \frac{d^2 \bar{q}}{dZ^2} \\
 & - \frac{\gamma-1}{\gamma} \sigma \bar{Q} \tilde{p} - \sigma \bar{q} \frac{\partial s}{\partial Z}
 \end{aligned} \tag{64}$$

Now the space variables will be separated by means of an eigenfunction expansion. Actually, this expansion is doubly infinite, but only the primary component (assuming there is only one which predominates) will be considered. Letting v and h indicate the primary component,

$$\begin{aligned}
 \tilde{p} &= P_{vh} (Z) J_v (s_{vh} r) e^{iv\theta} + - - \\
 \tilde{u} &= U_{vh} (Z) J_v (s_{vh} r) e^{iv\theta} + - - \\
 \tilde{v} &= V_{vh} (Z) \frac{dJ_v}{dr} (s_{vh} r) e^{iv\theta} + - - \\
 \tilde{w} &= W_{vh} (Z) \frac{J_v (s_{vh} r)}{r} e^{iv\theta} + - - \\
 \tilde{s} &= S_{vh} (Z) J_v (s_{vh} r) e^{iv\theta} + - - \\
 \tilde{Q} &= Q_{vh} (Z) J_v (s_{vh} r) e^{iv\theta} + - - \\
 \tilde{I} &= I_{vh} (Z) J_v (s_{vh} r) e^{iv\theta} + - -
 \end{aligned} \tag{65}$$

I, E, Characteristic Equation (cont.)

(65) and (64) yield

$$\begin{aligned}
 I_{vh} = & \sigma Q_{vh} - \frac{k\rho_\ell \sigma}{\gamma} P_{vh} \frac{\sigma}{\gamma} \frac{dP_{vh}}{dZ} - \frac{\sigma}{\gamma} \frac{d}{dZ} (\bar{q} P_{vh}) \\
 & + \frac{d}{dZ} (U_{vh} \frac{d\bar{q}}{dZ}) - \frac{\rho}{\gamma} P_{vh} \frac{d\bar{q}}{dZ} + U_{vh} \frac{d^2 \bar{q}}{dZ^2} \\
 & - \frac{\gamma-1}{\gamma} \sigma \bar{Q} P_{vh} \frac{dS_{vh}}{dZ} - \sigma \bar{q} \frac{dS_{vh}}{dZ}
 \end{aligned} \tag{66}$$

and (60) and (66) yield

$$\frac{1}{\gamma} \frac{d^2 P_{vh}}{dZ^2} - \left[\frac{(\sigma^2 + s_{vh}^2)}{\gamma} \right] P_{vh} = -I_{vh} \tag{67}$$

s_{vh} is the eigenvalue of the solution

$$J_v'(s_{vh}) = 0 \tag{68}$$

It is convenient to write the variables as the sum of two terms: one of order unity (zero superscript) and the other of the order of the Mach number (one superscript). Omitting the vh subscript,

$$\begin{aligned}
 P_{vh} &= P^{(0)} + P^{(1)} \\
 U_{vh} &= U^{(0)} + U^{(1)} \\
 Q_{vh} &= Q^{(1)} \\
 S_{vh} &= S^{(1)} \\
 \sigma &= \sigma^{(0)} + \sigma^{(1)}
 \end{aligned} \tag{70}$$

I, E, Characteristic Equation (cont.)

Now (66), (67), (69), and (70) yield after separation according to order in Mach number

$$\frac{1}{\gamma} \frac{d^2 P^{(0)}}{dZ^2} - \left[\frac{(\sigma^{(0)})^2 + (s_{vh})^2}{\gamma} \right] P^{(0)} = 0 \quad (71)$$

$$\begin{aligned} \frac{1}{\gamma} \frac{d^2 P^{(1)}}{dZ^2} - \left[\frac{(\sigma^{(0)})^2 + s_{vh}}{\gamma} \right] P^{(1)} &= \frac{2\sigma^{(0)}\sigma^{(1)}}{\gamma} P^{(0)} \\ &- \sigma^{(0)} Q^{(0)} + \frac{k\rho_\ell \sigma^{(0)}}{\gamma} P^{(0)} + \frac{\sigma^{(0)}}{\gamma} \frac{d}{dx} (\bar{q} P^{(0)}) + \frac{\sigma^{(0)}}{\gamma} \bar{q} \frac{d}{dx} P^{(0)} \\ &+ \frac{d}{dx} (U^{(0)} \frac{d\bar{q}}{dx}) + \frac{\sigma^{(0)}}{\gamma} P^{(0)} \frac{d\bar{q}}{dx} - U^{(0)} \frac{d^2 \bar{q}}{dx^2} \\ &+ \frac{\gamma-1}{\gamma} \sigma^{(0)} \bar{Q} P^{(0)} + \sigma^{(0)} \bar{q} \frac{dS^{(1)}}{dx} \equiv f(x) \end{aligned} \quad (72)$$

One can show from (51) that if the axial velocity disappears at the injector face the boundary conditions give

$$\frac{dP^{(0)}}{dZ} = 0 \text{ at } Z = 0 \quad (73)$$

and

$$\frac{dP^{(1)}}{dZ} = 0 \text{ at } Z = 0 \quad (74)$$

I, E, Characteristic Equation (cont.)

Similarly, assuming the nozzle admittance coefficients to be of the order of the Mach number, at the nozzle entrance Z_e , corresponding relations are

$$\frac{dP^{(0)}}{dZ} = 0 \text{ at } Z = Z_e \quad (75)$$

and

$$\frac{dP^{(1)}}{dZ} = \sigma^{(0)} E P^{(0)} \text{ at } Z = Z_e \quad (76)$$

The solution of (71) subject to (73) and (75) is

$$P^{(0)} = \cos [(\omega^{(0)})^2 - (s_{vh})^2]^{1/2} Z \quad (77)$$

where $\omega^{(0)} = i\sigma^{(0)}$. It follows from (13) and (15) that

$$U^{(0)} = \frac{(\omega^{(0)})^2 - (s_{vh})^2}{\gamma \sigma^{(0)}} \sin \sqrt{(\omega^{(0)})^2 - (s_{vh})^2} Z \quad (78)$$

In (27) and (28), $\omega^{(0)}$ is given by

$$(\omega^{(0)})^2 = (s_{vh})^2 + \frac{\pi^2 m^2}{Z_e^2}, \quad m = 0, 1, 2, \dots$$

Now with (77) and (78) substituted into the right-hand side of (72), that equation may be solved subject to (74) and (76). The solution is straightforward but generally cumbersome except in the "pure" transverse case where $\omega^{(0)} = s_{vh}$. Then (72) simplifies since $U^{(0)} = 0$ and $P^{(0)} = 1$ and

I, E, Characteristic Equation (cont.)

$$\begin{aligned} \frac{1}{\gamma} \frac{d^2 p^{(1)}}{dz^2} &= \frac{2i s_{vh} \sigma^{(1)}}{\gamma} - i s_{vh} Q^{(0)} + \frac{i s_{vh} k \bar{\rho}_\ell}{\gamma} \\ &+ \frac{2i s_{vh}}{\gamma} \frac{d\bar{q}}{dz} + (\gamma-1) \frac{i s_{vh}}{\gamma} \frac{d\bar{q}}{dz} + i s_{vh} \bar{q} \frac{dS^{(1)}}{dz} \end{aligned} \quad (72a)$$

Integration of (72a) subject to (74) and (76) yields

$$\begin{aligned} \frac{-E}{\gamma} + \frac{2\sigma^{(1)}}{\gamma} z_e + - \int_0^{z_e} Q^{(0)} dz + \frac{k}{\gamma} \int_0^{z_e} \bar{\rho}_\ell dz \\ + \frac{2q_e}{\gamma} + (\gamma-1) \frac{q_e}{\gamma} + q_e S^{(1)}(z_e) - \int_0^{z_e} S^{(1)} \frac{d\bar{q}}{dz} dz = 0 \end{aligned} \quad (79)$$

Since $S^{(1)}$ and $\frac{d\bar{q}}{dz}$ are of order Mach number, the last two terms are of the order of the Mach number squared and may be neglected.

Noting that $\sigma^{(1)} = \lambda^{(1)} + i\omega^{(1)}$, Equation (79) can be separated into its real and imaginary parts to obtain

$$\begin{aligned} 2\lambda^{(1)} z_e = E_r + \gamma \int_0^{z_e} Q_r^{(0)} dz - k \int_0^{z_e} \bar{\rho}_\ell dz \\ - [2 + (\gamma-1)] \bar{q}_e \end{aligned} \quad (80)$$

$$2\omega^{(1)} z_e = E_i + \int_0^{z_e} Q_i^{(0)} dz \quad (81)$$

I, E, Characteristic Equation (cont.)

According to the sensitive time lag theory, we have

$$Q_r^{(0)} = \frac{d\bar{q}}{dZ} n (1 - \cos \omega\tau)$$

$$Q_i^{(0)} = \frac{d\bar{q}}{dZ} n \sin \omega\tau$$

p

so that (80) and (81) become

$$\frac{2\lambda^{(1)} Z_e}{\bar{q}_e} = \frac{E_r}{\bar{q}_e} + n (1 - \cos \omega\tau)$$

$$\frac{-k}{\bar{q}_e} \int_0^{Z_e} \bar{\rho}_\ell dZ - 2 + (\gamma-1) \quad (80a)$$

$$\frac{2\omega^{(1)} Z_e}{\bar{q}_e} = \frac{E_i}{\bar{q}_e} + n \sin \omega\tau \quad (81a)$$

Since $\lambda^{(1)}$ is the real part of the coefficient of time in the exponential, positive $\lambda^{(1)}$ in (80) implies linear instability while negative $\lambda^{(1)}$ implies linear stability. Zero $\lambda^{(1)}$, of course, indicates neutral stability. Any term on the right-hand side of (80) which is positive must be considered as destabilizing while any term which is negative is stabilizing.

The first term on the right-hand side of (80) contains the real part of the nozzle admittance coefficient. Often, it surprisingly is positive for first tangential mode oscillations, indicating that the nozzle has a destabilizing effect for that mode. Calculations indicate that E_r/\bar{q}_e

I, E, Characteristic Equation (cont.)

can be of order unity in certain cases. In those cases, the effect of the nozzle is important compared to other effects to be discussed. In other cases, calculations show that this term is negligible compared to unity and has, therefore, negligible effect upon the instability (except perhaps in marginal cases). One cannot neglect the significant changes in the stability characteristics of an engine which can be achieved through modifications of the nozzle design.

The second term represents the driving mechanism provided by the combustion process (according to the sensitive time lag theory in (80) or more generally in (80)) and is, of course, destabilizing. This term has been thoroughly discussed in Section I,C and requires no further discussion here.

The third term describes the damping effect due to droplet drag. Here k is considered a constant although it actually may vary with axial position. Presently, there is no accurate way of determining k , but intuitively k/\bar{q}_e is expected to be of order unity. This means that the stabilizing term due to droplet drag could be of order unity and therefore significant if a substantial amount of liquid mass exists in the chamber, i.e.,

$$\int_0^Z \bar{\rho}_\ell dZ \text{ is order of unity.}$$

The final term in (80) equals $(\gamma+1)$ but has been written as the sum of "two" and $(\gamma-1)$. The quantity "two" is traced back to the term $\nabla \cdot (\nabla \cdot \rho q q)'$ in Equation (55). That term is the divergence of the perturbation of the momentum flux and is nonzero only in the distributed combustion case. It is a most important stabilizing factor; only the liner can sometimes provide a larger stabilizing effect. The quantity $(\gamma-1)$ is considerably smaller and is traced back to the term $(\gamma-1) \frac{\partial}{\partial t} (G-q \cdot F)'$ in (55). As mentioned after Equation (53), this can be shown to be related to the change of entropy of the gas.

I, E, Characteristic Equation (cont.)

Equation (81) gives the frequency correction due to the nozzle and combustion process. This equation is weakly coupled to (80) since frequency appears implicitly in the arguments of the nozzle admittance coefficient and explicitly in the combustion response term.

The question arises as to whether (80) and (81) apply in the limiting case of concentrated combustion. Zinn (Ref 6) considered transverse oscillations with combustion concentrated at the injector and obtained a different result. One must look carefully, however, at what was done there. When the combustion is not distributed $d\bar{q}/dZ = 0$ and from (58) one can show that, neglecting terms of the order of Mach number squared, $\nabla \cdot (\nabla \cdot \rho q q)'$ becomes zero for the transverse modes. This implies that the "two" in (80) is replaced by zero. However, the boundary condition at the injector is no longer given by (74). Through the proper boundary condition, two terms are introduced to the stability relation: one is a combustion response term equivalent to the one in (80) and the other, originating through the density variation at the injector, appears as a "unity" in the equation equivalent to (80). There is now a "unity" instead of a "two" so that according to Zinn the concentrated combustion case is considerably more unstable than the distributed case. Zinn also assumed isentropic oscillations so that the $(\gamma-1)$ term did not appear but that is beside the point to be made here.

The discrepancy lies in the fact that Zinn did not account for the change in velocity which a particle undergoes as it changes pulse. This change of velocity provides an important damping effect. Suppose in the distributed case $q_\lambda = q$ so that $F = 0$. Then (56) is replaced by

$$\underset{\rightarrow}{(F + Q q)}' \approx \bar{Q} \underset{\rightarrow}{q}' \quad (56a)$$

I, E, Characteristic Equation (cont.)

The $\bar{Q} q' = \frac{d\bar{q}}{dZ} q'$ now appears where it did not before. This leads to a "minus unity" appearing in the stability relation so that when combined with the "two" from the momentum flux term the result is "unity" as obtained by Zinn.

Therefore, the implication is that (80) and (81) should be used even in the concentrated case and those relations were not obtained by Zinn only because he neglected certain physical effects.

Similar interpretations could be given to the terms appearing in the stability relations for longitudinal and mixed mode oscillations which would result from the integration of (72).

I, Theory (cont.)

F. DISCUSSION OF RESTRICTIONS

This section will be concerned with the restrictions imposed by the chamber Mach number, chamber length-to-diameter ratio, and frequency of oscillation. These restrictions have been selected because they effect the region over which the analysis is applicable.

In order to obtain a solution to equations (11a) through (11i), it was necessary to express the pressure perturbation, p , in the form of a series as shown by equation (12). The restriction considered herein occurs at the outset of the analysis; therefore, it is instructive to interpret each term in the p series.

If the series is expressed in terms of the acoustic solution, i.e.,

$$p' = p_0$$

then the following restrictions are imposed: (1) the exhaust nozzle is replaced by a flat plate at the chamber exit, (2) there is no flow - no combustion - within the chamber, and (3) the injector is replaced by a flat plate. The solution of this problem results in the three-dimensional acoustic solution for a cylinder closed at both ends.

When the next term in the pressure perturbation series is included, i.e.,

$$p' = p_0 + p_1$$

the result is that p_1 modified the acoustic solution by incorporating the primary effects of the injector, combustion process, and the exhaust nozzle. However, the contribution of the gas flow between the axial position where

I, F, Discussion of Restrictions (cont.)

combustion is completed, Z_c , and the exhaust nozzle inlet, Z_e , is not considered. Equation (13b) shows that all the p_1 - effects (with the exception of the exhaust nozzle) exist only in the interval, $0 < Z < Z_c$, and only the acoustic solution exists in the interval, $Z_c < Z < Z_e$.

The work by Scala and Reardon (Refs. 7 and 2) was restricted to small combustion chamber Mach numbers. This restriction simplified the mathematics of the analysis and confined their analysis to the partial sum of the perturbation series

$$p' = p_0 + p_1$$

The acoustic solution is assumed to be of the form

$$p_0(A, r, \theta) = P_0(Z) \Psi_{v\eta}(r) (H_v(\theta))$$

where the variables on the right side of the equation were given by

$$P_0(Z) = \cosh \Omega Z$$

$$\Psi_{v\eta}(r) = J_v(S_{v\eta} r)$$

$\cos v\theta$, standing mode

$$H_v(\theta) =$$

$e^{-v\theta}$, spinning mode

where

$$\Omega^2 = s_{v\eta}^2 - \omega^2$$

I, F, Discussion of Restrictions (cont.)

The subject restriction is concerned with the treatment of $P_o(Z)$; consequently, in the discussion hereafter, $\Psi_{v\eta}(r)$ and $H_v(\theta)$ will not be mentioned.

The restriction is made in the analysis that

$$\frac{\partial P_o}{\partial Z} = \Omega \sinh \Omega Z \leq 0 \quad (\bar{u}_e)$$

from observations based on the nozzle admittance relationship (see Reference 2). Note that this restriction imposes the Mach number on an expression that involves only the nondimensional frequency, ω , the acoustic mode number, $s_{v\eta}$, and the chamber length, Z , even though the acoustic solution for $P_o(Z)$ and $\partial P_o/\partial Z$ are explicitly independent of the chamber Mach number.

Rocket engine designers generally relate the size of an engine by the ratio of the chamber length to chamber diameter (L/D). The nondimensional length Z , is related to L/D as follows

$$Z = \frac{L_c^*}{r_c^*} = 2 \frac{L_c^*}{D_c^*} = 2 \frac{L}{D}$$

In practice, the frequency range of interest has been taken in the range of $\pm 10.0\%$ of the acoustic mode number, i.e.,

$$\omega = \tilde{\eta} s_{v\eta}$$

where $0.90 \leq \tilde{\eta} \leq 1.10$. The reason for using a range of frequencies rather than the acoustic resonant frequency is twofold. First, the acoustic resonant frequency exists only for a closed-closed cylinder and the presence

I, F, Discussion of Restrictions (cont.)

of flow, combustion, and exhaust nozzle (i.e., system losses) shift the actual resonant frequency away from the acoustic resonant frequency. Second, the correlation of empirical instability data requires knowledge of the intersection points of adjacent modes on the instability plane.

The effect of this restriction is shown in Figure 15 which indicates the applicable frequency ranges for the first and second tangential as a function of L/D. The frequency range for which the current analysis is applicable exists between similarly coded lines. It can be seen that the region of applicability decreases significantly as the L/D ratio increases. Furthermore, the region of applicability decreases - for a given L/D - as the mode of instability is increased.

II. PROGRAM LISTING

The following pages give a listing of the computer program. The input requirements as well as the logic flow charts for this program can be found in Section V,B, Case II, Application of Results.

Report 20672-PIF, Appendix B

SEXECUTE	ISJOB	BLOCK
SIBJOB	MAP,ALTIO	BLOCK 10
SIBFTC BLOCK	LIST,M94	BLOCK 20
	BLOCK DATA	BLOCK 30
C	COMMON /PROLOG/ LOGIK(50), SL1, SL2, EORJ	BLOCK 40
	LOGICAL LOGIK, SL1, SL2, EORJ	BLOCK 50
C	DATA SL1, SL2 / .FALSE., .FALSE. /	BLOCK 60
	END	BLOCK 70
		BLOCK 80
		BLOCK 90
SIBFTC V8050	LIST,M94 0
	COMMON /PROLOG/ LOGIK(50), SL1, SL2, EORJ 10
	LOGICAL LOGIK, SL1, SL2, EORJ 20
C	10 CALL CHAMBR 30
C	 40
C	RETURNS FROM MAJOR PROGRAM IF AND ONLY IF AN INJECTOR PROGRAM 50
C	IS TO BE CALLED... INJCTR DETERMINES WHICH, WRITES SCRATCH 60
C	TAPE, AND CALLS PROPER ROUTINE. 70
C	 80
C	CALL INJCTR 90
C	 100
	GO TO 10 110
	END 120
	 130
SIBFTC OUT	LIST,M94	OUT
	SUBROUTINE OUTAS(A,K)	OUT 10
	DIMENSION A(12)	OUT 20
	WRITE(6,10)(A(I),I=1,K)	OUT 30
10	FORMAT(1X,12A6)	OUT 40
	RETURN	OUT 50
	END	OUT 60
SIBFTC IN	LIST,M94	IN
	SUBROUTINE INASS(A)	IN 10
	DIMENSION A(12)	IN 20
	READ(5,10)A	IN 30
10	FORMAT(12A6)	IN 40
	RETURN	IN 50
	END	IN 60
SIBMAP *KTRAN	50,LIST,REF,DECK,M/94,RELMOD	*KTR
*		*KTR 10
*	KISMET TRANSFER VECTOR AS APPLIED TO IBM 7094 IBSYS S/ /64	*KTR 20
		*KTR 30
ENTRY	KOVFLO	*KTR 40
ENTRY	KUNFLO	*KTR 50
ENTRY	KDATEA	*KTR 60
ENTRY	KERROR	*KTR 70
ENTRY	KFINIS	*KTR 80
ENTRY	KINDX4	*KTR 90
ENTRY	KINDX1	*KTR 100
ENTRY	KINDX2	*KTR 110
ENTRY	KOPIMP	*KTR 120
ENTRY	KISORG	*KTR 130
ENTRY	KDATEZ	*KTR 140
KSTCHA EGU	29	*KTR 150
KPRINT EGU	10	*KTR 160
KPUNCH EGU	15	*KTR 170
SYSDAT EGU	65	*KTR 180
KOPIMP TRA	1,4	*KTR 190
KFINAL TSK	KFINIS,4	*KTR 200
TTR		*KTR 210
KOVFLO TTR	KERROR	*KTR 220
KUNFLO TTR	KERROR	*KTR 230
KINDX1 PZE		*KTR 240
KINDX2 PZE		*KTR 250
KINDX4 PZE		*KTR 260
KDATEA BCI	2,	*KTR 270
KISORG PZE	1486,1486	*KTR 280
KERROR TSK	KFINIS,4	*KTR 290
KFINIS CALL	EXIT	*KTR 300
*		*KTR 310
*	KDATEZ, TODAY-S DATE FOR KISMET-MAP OR FORTRAN IV PROGRAMS	*KTR 320
KDATEZ TRA	1,4	*KTR 330
	END	*KTR 340
		*KTR 350

SIBMAP	*AAS58			*AAS0010
*	AS58K9			*AAS0020
*				*AAS0030
	ENTRY	AS58		*AAS0040
	ENTRY	AS138		*AAS0050
KISORG	EQU	1486		*AAS0060
AS138	SAVE			*AAS0070
	CAL	4,4		*AAS0080
	ALS	18		*AAS0090
	ORA	3,4		*AAS0100
	SLW	BOGUS		*AAS0110
	CAL	5,4		*AAS0120
	LXA	GETOUT-2,4		*AAS0130
	TXH	BADGUY,4,0	CHECK FOR PREVIOUS EOF	*AAS0140
	STA	GETOUT		*AAS0150
	TSX	AS58,4		*AAS0160
BOGUS	EQU	*		*AAS0170
	PZE	***,***	DATA,TCARD	*AAS0180
	TTR	GETOUT-2		*AAS0190
	TTR	GETOUT-2		*AAS0200
	PXA	***,0	EOF ENCOUNTERED FLAG IF ADDR UNZERO	*AAS0210
	ADD	SBONE		*AAS0220
GETOUT	STO	**		*AAS0230
	RETURN	AS138		*AAS0240
BADGUY	EQU	*		*AAS0250
	SXA	GETOUT-2,0	RESET EOF FLAG	*AAS0260
	TTR	KFINIS	WRITE A NOTE....THEN FLUSH HIM	*AAS0270
EOFMES	BCI	9,1	READING PAST END-OF-FILE ON INPUT TAPE...JOB FLUSHED	*AAS0280
AS58	CLS	1,4		*AAS0290
	SXA	58IR1,1		*AAS0300
	SXA	58IR2,2		*AAS0310
	SXD	58IR4,4		*AAS0320
AS58X4	LXD	58IR4,4		*AAS0330
	CAL	1,4		*AAS0340
	STA	**5		*AAS0350
	STT	**4		*AAS0360
	ARS	18		*AAS0370
	STA	**6		*AAS0380
	STT	**5		*AAS0390
	PXA	***,***		*AAS0400
	SBM	*-1		*AAS0410
	STA	AS58D	SETD,T FOR DATA	*AAS0420
	STA	AS58X		*AAS0430
	PXA	***,***		*AAS0440
	SBM	*-1		*AAS0450
	STA	AS58B2	SET B,T FOR	*AAS0460
	STA	AS58B	SET B,TAG FOR BCD HEADER	*AAS0470
	STO	AS58C2-3	SET TAPE ERROR FLAG NEG.	*AAS0480
	SBM	AS58E+3	L(12) HEAD+12	*AAS0490
	STA	AS58C1		*AAS0500
	LXA	KOVFLO,2		*AAS0510
	SXA	AS58C+3,2		*AAS0520
	AXT	AS58G,2		*AAS0530
	SXA	KOVFLO,2		*AAS0540
	STZ	58YYAS+2	0 TO CARD ERROR IND.	*AAS0550
	LXA	GETOUT-2,4	EOF CHECK	*AAS0560
	TXH	BADGUY,4,0	READING PAST EOF	*AAS0570
	LXA	AS58R,4		*AAS0580
	TXH	AS58A,4,KISORG	STORAGE INTO MONITOR	*AAS0590
	CALL	OUTAS8(58BCD,7)		*AAS0600
	TRA	KERROR		*AAS0610
58BCD	BCI	7, B,TAG TOO LOW IN MEMORY USING AS58 INPUT		*AAS0620
	BCI	2, DATA D,T		*AAS0630
AS58Z	TXH	AS58A,4,0		*AAS0640
	TSX	OUTAS8,4		*AAS0650
	TRA	AS58A		*AAS0660
	TTR	115		*AAS0670
AS58B	PZE	**		*AAS0680
	CLA	*12		*AAS0690
AS58A	TSX	INAS58,4		*AAS0700
	TRA	58IR4		*AAS0710
	TTR	115		*AAS0720
AS58B2	PZE	**		*AAS0730
58IR4	TXL	**3,***	NORMAL RETURN	*AAS0740
58ERR	CLS	AS58C2-1		*AAS0750
	STO	AS58C2-3	ERROR FLAG	*AAS0760
	CAL*	AS58B		*AAS0770
	LRS	30		*AAS0780
	SUB	AS58J		*AAS0790
	THZ	AS58C2		*AAS0800
	CLA	AS58C2-2		*AAS0810
	LRS	30		*AAS0820
AS58C	SLW*	AS58B		*AAS0830
	LXD	58IR4,4		*AAS0840
	LDO	AS58C2-3		*AAS0850
	CAL	58YYAS+2		*AAS0860
58IR2	AXT	**2		*AAS0870
	AXT	**0,1	RESTORE TRA VECTOR	*AAS0880
	SXA	KOVFLO,1		*AAS0890
58IR1	AXT	**1		*AAS0900
	TGP	**2		*AAS0910
	TZE	4,4	NORMAL OR EOF EXIT	*AAS0920
	LXD	58IR4,4		*AAS0930
	TRA	2,4	ERROR EXIT FROM AS58	*AAS0940
58EOF	LXD	58IR4,4		*AAS0950
	SXA	GETOUT-2,4	EOF IND	*AAS0960
	TXI	AS58C+2,4,1		*AAS0970
	THX	AS58C9,2,1	SKIP IF END OF CARD	*AAS0980
AS58C1	LDO	**0,2		*AAS0990
	TXI	AS58E+1,2,500	RETURN WITH NEXT BCD WORD IN HQ	*AAS1000
AS58P	CALL	OUTAS8(58BCD+9,1)		*AAS1010
	CALL	OUTAS8(58BCD+1,6)		*AAS1020
AS58Q	AXT	0,4	TRA HERE IF ERROR	*AAS1030
	CLA	58YYAS+2		*AAS1040
	ALS	1		*AAS1050
	TXH	**2,4,0		*AAS1060
	ORA	SBONE	PX1	*AAS1070
	STO	58YYAS+2		*AAS1080
	ORS	58YYAS+2		*AAS1090
	TXL	AS58Z,0,32	TO READ NEXT CARD	*AAS1100
AS58C3	TXL	AS58Q+1,2,0		*AAS1110
	LXD	*-2,1		*AAS1120
	TXI	AS58Q,2,-1		*AAS1130
AS58J	OCT	43,21		*AAS1140
	OCT	3008003,53,21		*AAS1150
	DEC	9008000,9008000,90000,9000,900,90,9,294		*AAS1160
	DEC	8000000,8000000,80000,8000,800,80,8,128		*AAS1170
	DEC	7000000,7000000,70000,7000,700,70,7,216		*AAS1180
	DEC	6000000,6000000,60000,6000,600,60,6,168		*AAS1190
	DEC	5000000,5000000,50000,5000,500,50,5,280		*AAS1200
	DEC	4000000,4000000,40000,4000,400,40,4,196		*AAS1210

Report 20672-PIF, Appendix B

```

DEC 3000000.300000.30000.3000.300.30.3.304
DEC 2000000.200000.20000.2000.200.20.2.19988
DEC 1000000.100000.10000
38MIL DEC 1000 FX1000
38CENT DEC 100 FX100
38TEN DEC 10 FX10
38ONE DEC 1 FX1
DEC 1E9.1E8.1E7.1E6.1E5.1E4.1E3.1E2.1E1
DEC 0.48
AS58C2 SVN 0-1.7-1
          AXT 0.1
          ART 0.2
          STP AS58G+3
          STZ AS58V1
          TXI AS58D1+1.2.13 ZERO FIRST NUMBER FLAG
          LXA 0+3.2
          TXL AS58P+2-KISORG STORAGE INTO MONITOR
          TXI 0+1.2.1 BUMP STORAGE ADDR.
AS58D STO 000
          SKA 0-1.2
          SKA AS58V1.2
          PXD 1.0
          TXL 0+2.1.56
          SSM
          STO 58VYAS+1
          LXD AS58F1+5.2 RELOAD
AS58D1 LDQ 58VYAS+3
          SXD AS58F+0
          SKD AS58V+1 SAVE IR1
          STZ 58VYAS
          LXD AS58F+1.4 7 TO IR4
          SKD AS58K+4
          PXD 0.0
AS58E TNX AS58C1-1.2.100 TRA IF NO EXHAUSTED
          LGL 6
          ALS 3
          PAX 12.1
          TXM AS58F1+1.72
          CAL 58VYAS
          TXL AS58F2+1.0
AS58K TXI 0+1.1.00
          ADD AS58C2-4.1
          SLW 58VYAS
          TIX AS58E-2+4.1
          STQ 58VYAS+9
          ORA 58MIL-4
          FAD 58MIL-4
          LDQ 58VYAS+1
          LLS 0
          LXD 0+2.4 7 TO IR4
AS58F TXI 0+1.4.000
          TXL 0+4.4.7
          STO 58VYAS
          FMP AS58C2-10 1E7
          FAD 58VYAS
          STO 58VYAS+1
          LDQ 58VYAS+3
          SKD AS58F+4
          TXL AS58E-4.0.64
AS58F1 LXD 0-1.1
          CAS 58ONE+1.1
          TIX 0-1.1.8
          TXM AS58G-2.1.8
          TIX 0-3.1.8
          TXL AS58Q.0.000 BCD POSITION
AS58F2 ZET AS58V1
          TRA AS58E+10
          AXT 56.1
          SKA AS58V1+1
          TXL AS58E-2.1.16
AS58G STQ 58VYAS+3
          SKD AS58F1+5.2
          LXD AS58F+2
          NOP AS58X-1
          TXM AS58H+4.6
          CLA 58VYAS
          ORA 58MIL-4
          FAD 58MIL-4
          FDP AS58C2-3.4
          CLA 58VYAS+1
          LRS 0
          STQ 58VYAS
          SKD 0+2.4
          LXD AS58F+1.4 7
          TXM AS58H+1.4.000
          SKD 0+4.4
          TXL 0+3.2.0
          LDQ 58VYAS+1
          FMP AS58C2-3.4
          TXI 0+2.2.000
AS58H CLA 58VYAS+1
          FAD 58VYAS
          STO 58VYAS+1
          LXD AS58V+4
          TXM 0+4.4.48
          TXM AS58V+1.4.40
          TXL 0+3.1.48
          TXL AS58D+3.2.0
          TXM AS58D-3.1.48 TO STORE RESULT
          TXL AS58W+1.40
          SKD AS58F+2
          SKD 0+4.2
          LXD AS58F1+5.2
          LDQ 58VYAS+3
AS58V TXL AS58D1+2.0.000 CODE
          TXM AS58W-1.2.000
          CLA 58VYAS+1
          TXL 0+4.2.9
          FDP AS58C2-12 1E9
          STQ 58VYAS+1
          TXI 0-4.2.0-9
          TXL 0+4.2.0
          FDP AS58C2-3.2
          STQ 58VYAS+1
          CLA 58VYAS+1
          SKD AS58V+1.0
          TXM AS58D-3.1.40 STORE IF 0 OR - OR +
AS58W LDQ 0+7 NEXT IS E.L.A
          SLQ AS58G+3 SET FIXED
          SLQ AS58V SET POSITIVE
          TXM AS58D1-1.3.32 NEXT CODE E

```

```

*AA51220
*AA51230
*AA51240
*AA51250
*AA51260
*AA51270
*AA51280
*AA51290
*AA51300
*AA51310
*AA51320
*AA51330
*AA51340
*AA51350
*AA51360
*AA51370
*AA51380
*AA51390
*AA51400
*AA51410
*AA51420
*AA51430
*AA51440
*AA51450
*AA51460
*AA51470
*AA51480
*AA51490
*AA51500
*AA51510
*AA51520
*AA51530
*AA51540
*AA51550
*AA51560
*AA51570
*AA51580
*AA51590
*AA51600
*AA51610
*AA51620
*AA51630
*AA51640
*AA51650
*AA51660
*AA51670
*AA51680
*AA51690
*AA51700
*AA51710
*AA51720
*AA51730
*AA51740
*AA51750
*AA51760
*AA51770
*AA51780
*AA51790
*AA51800
*AA51810
*AA51820
*AA51830
*AA51840
*AA51850
*AA51860
*AA51870
*AA51880
*AA51890
*AA51900
*AA51910
*AA51920
*AA51930
*AA51940
*AA51950
*AA51960
*AA51970
*AA51980
*AA51990
*AA52000
*AA52010
*AA52020
*AA52030
*AA52040
*AA52050
*AA52060
*AA52070
*AA52080
*AA52090
*AA52100
*AA52110
*AA52120
*AA52130
*AA52140
*AA52150
*AA52160
*AA52170
*AA52180
*AA52190
*AA52200
*AA52210
*AA52220
*AA52230
*AA52240
*AA52250
*AA52260
*AA52270
*AA52280
*AA52290
*AA52300
*AA52310
*AA52320
*AA52330
*AA52340
*AA52350
*AA52360
*AA52370
*AA52380
*AA52390
*AA52400
*AA52410
*AA52420

```

Report 20672-PIF, Appendix B

	TXM	AS58D-3,4,32	TO STORE IF PREV. CODE WAS	*AAS2430
	TXL	AS58D1-1,2,0	+, -, 0, OR E	*AAS2440
	TXL	AS58D-3,4,0	TO STORE IF DIGITS HAVE BEEN	*AAS2490
	TXL	AS58D1-1,0,497464	READ WITH NO CODE	*AAS2460
	TXM	AS58D,2,0	ERROR	*AAS2470
AS58X	PXD	*0,0		*AAS2480
	TXL	*+5,4,6		*AAS2490
	TXL	*+2,1,56	SET NEGATIVE	*AAS2500
	STP	*+4		*AAS2510
	LXD	AS58F1+5,2		*AAS2520
	TXM	AS58D1+3,1,48		*AAS2530
	STP	AS58G+3	SET FIXED	*AAS2540
AS58Y	NOP	*+2		*AAS2550
	SSM			*AAS2560
	LQG	58YYAS		*AAS2570
	DVP	58ONE,4		*AAS2580
	STG	58YYAS		*AAS2590
	LXD	AS58V,4		*AAS2600
	TXL	*+13,4,32		*AAS2610
	LXA	58YYAS,2		*AAS2620
	TXM	AS58G,2,38	ERROR	*AAS2630
	TXI	AS58V+2		*AAS2640
	LQG	58YYAS+1		*AAS2650
	TXL	*+4,2,9		*AAS2660
	FMP	58ONE+1		*AAS2670
	STG	58YYAS+1		*AAS2680
	TXI	*-4,2,-9		*AAS2690
	TXL	AS58W-5,2,0		*AAS2700
	FMP	AS58C2-3,2		*AAS2710
	STG	58YYAS+1		*AAS2720
	TXL	AS58W-2,0,0		*AAS2730
	CLA	58YYAS	L OR A	*AAS2740
	ADM	AS58E-1		*AAS2750
	TXL	*+2,4,24		*AAS2760
	ADM	AS58X		*AAS2770
	STA	AS58D	SET NEW STORAGE LOCATION	*AAS2780
	TXL	AS58W,1,32		*AAS2790
	TXL	AS58G,1,40	ERROR	*AAS2800
	TRA	AS58D+3		*AAS2810
AS58YI	PZE	0		*AAS2820
58YYAS	EGU	COMMON		*AAS2830
COMMON	BSS	50		*AAS2840
ZZZZZZ	PZE			*AAS2850
COMMON	COMTRL	COMMON,ZZZZZZ		*AAS2860
	END			*AAS2870

Report 20672-PIF, Appendix B

SIBMAP	*INTG	LIST,REP,DECK	INTG0010
*	GLAUZ -	BOOGLES INTEGRATION - SIMPSON'S ERROR CONTROL (F,I,X,M)	INTG0020
	ENTRY	INTGR	INTG0030
	ENTRY	INTGS	INTG0040
INTGR	SAVE	1,2,4	INTG0050
	CLA*	4,4	INTG0060
	SXA	IR4,4	INTG0070
	STO	B	INTG0080
	LDQ*	3,4	INTG0090
	STQ	A	INTG0100
	PSB	A	INTG0110
	STO	IVAL	INTG0120
	CLA*	6,4	INTG0130
	LDQ	ZERO	INTG0140
	ALS	18	INTG0150
	STA	INT	INTG0160
	ANA	MASK	INTG0170
	TRZ	*+2	INTG0180
	CLA	FR	INTG0190
DBL	STO	DECA	INTG0200
	STZ	DECB	INTG0210
	STZ	INT	INTG0220
	STZ	ERR	INTG0230
	AXT	4,4	INTG0240
	SXA	1,4	INTG0250
	PDX	0,4	INTG0260
	TXI	*+1,4,1	INTG0270
	SXA	12,4	INTG0280
	ANA	MASK	INTG0290
	ARS	18	INTG0300
	ADD	MAS	INTG0310
	FAD	MAS	INTG0320
	STO	XN	INTG0330
	CLA	B	INTG0340
IR4	AXT	*+4	INTG0350
	STO*	5,4	INTG0360
	RETURN	INTGR	INTG0370
INTGS	SAVE	1,2,4	INTG0380
	SXA	IR1,1	INTG0390
	SXA	IR2,2	INTG0400
I1	AXT	*+1	INTG0410
I2	AXT	*+2	INTG0420
	LDQ	FRE	INTG0430
	TXL	*+3,2,1	INTG0440
DECA	TXH	*+2,2,*+*	INTG0450
	LDQ	TAB1+4,1	INTG0460
	FMP*	3,4	INTG0470
	FAD	INT	INTG0480
	STO	INT	INTG0490
	LDQ	ONE	INTG0500
	TXL	*+3,2,1	INTG0510
DECB	TXH	*+2,2,*+*	INTG0520
	LDQ	TAB2+4,1	INTG0530
	FMP*	3,4	INTG0540
	FAD	ERR	INTG0550
	STO	ERR	INTG0560
	TXI	*+2,1,1	INTG0570
	AXT	4,1	INTG0580
	SXA	11,1	INTG0590
IR1	AXT	*+1	INTG0600
	TXI	INC,2,1	INTG0610
	PDP	INT	INTG0620
	STO	TEMPA	INTG0630
	STO	TEMPO	INTG0640
	LDQ	TEMPA	INTG0650
	CLA	TEMPO	INTG0660
	SSP		INTG0670
	SXD*	5,4	INTG0680
	TXI	FIN	INTG0690
IRT	AXT	*+2	INTG0700
	TXI	*+1,2,1	INTG0710
	TXH	FIN,2,7	INTG0720
	SXA	IRT,2	INTG0730
	LXA	IR2,2	INTG0740
	CLA	DECA	INTG0750
	ALS	1	INTG0760
	TRA	DBL	INTG0770
INC	SXA	12,2	INTG0780
	TXI	*+1,2,-1	INTG0790
	PXA	0,2	INTG0800
	ADD	MAS	INTG0810
	FAD	MAS	INTG0820
	FDP	XN	INTG0830
	FMP	IVAL	INTG0840
	FAD	A	INTG0850
IR2	AXT	*+2	INTG0860
	TRA	IR4	INTG0870
FIN	CLA	INT	INTG0880
	FDP	XN	INTG0890
	FMP	IVAL	INTG0900
	FDP	PRF	INTG0910
	STO*	4,4	INTG0920
	STZ*	6,4	INTG0930
	CLA	DECA	INTG0940
	ARS	18	INTG0950
	STA*	6,4	INTG0960
	LXA	IR2,2	INTG0970
	RETURN	INTGS	INTG0980
MASK	OCT	077774000000	INTG0990
FR	OCT	000004000000	INTG1000
MAS	OCT	233000000000	INTG1010
FRE	DEC	14,	INTG1020
TAB1	DEC	28,,64,,24,,64,,	INTG1030
ONE	DEC	1,	INTG1040
TAB2	DEC	2,,4,,6,,8,,4,,	INTG1050
PRF	DEC	49,	INTG1060
A	BSS	1	INTG1070
B	BSS	1	INTG1080
ERR	BSS	1	INTG1090
INT	BSS	1	INTG1100
IVAL	BSS	1	INTG1110
XN	BSS	1	INTG1120
TEMPA	BSS	1	INTG1130
TEMPO	BSS	1	INTG1140
ZERO	DEC	0	INTG1150
	END		INTG1160

Report 20672-PIF, Appendix B

```

SIBMAP *KDATE 50,LIST,REF,DECK,M/94,RELMOO          *KDA
*          DATE -- TODAY-S DATE IN THE FORM DD MMMM YYYY          *KDA 10
*          CALL DATE (BCDATE), WHERE BCDATE IS 2 CELLS WHICH WILL CONTAIN          *KDA 20
*          THE BCD FORM OF TODAY-S DATE          *KDA 30
*          *KDA 40
*          *KDA 50
*          *KDA 60
*          *KDA 70
*          *KDA 80
*          *KDA 90
*          *KDA 100
*          *KDA 110
*          *KDA 120
*          *KDA 130
*          *KDA 140
*          *KDA 150
*          *KDA 160
*          *KDA 170
*          *KDA 180
*          *KDA 190
*          *KDA 200
*          *KDA 210
*          *KDA 220
*          *KDA 230
*          *KDA 240
*          *KDA 250
*          *KDA 260
*          *KDA 270
*          *KDA 280
*          *KDA 290
*          *KDA 300
*          *KDA 310
*          *KDA 320
*          *KDA 330
*          *KDA 340
*          *KDA 350
*          *KDA 360
*          *KDA 370
*          *KDA 380
*          *KDA 390
*          *KDA 400
*          *KDA 410
*          *KDA 420
*          *KDA 430
*          *KDA 440
*          *KDA 450
*          *KDA 460
*          *KDA 470
*          *KDA 480
*          *KDA 490
*          *KDA 500

```

```

SIBFTC *NT4 LIST,M94          INT4
SUBROUTINE INT4(X,Y,XI,YO)          INT4 10
DIMENSION X(9),Y(9),XC(4),YC(4)          INT4 20
EQUIVALENCE (XC(1),X1),(XC(2),X2),(XC(3),X3),(XC(4),X4),(YC(1),Y1)          INT4 30
1,(YC(2),Y2),(YC(3),Y3),(YC(4),Y4)          INT4 40
10 ASSIGN 90 TO NA          INT4 50
J=2          INT4 60
B=XI          INT4 70
20 IF(X(J)130,40,30          INT4 80
30 GO TO NA,(90,160)          INT4 90
40 IF(Y(J)130,50,30          INT4 100
50 IF(J-2)160,60,70          INT4 110
60 YE=0.0          INT4 120
GO TO 180          INT4 130
70 ASSIGN 150 TO NB          INT4 140
J=J-1          INT4 150
80 X1=X(J)          INT4 160
X2=X(J-1)          INT4 170
X3=X(J-2)          INT4 180
Y1=Y(J)          INT4 190
Y2=Y(J-1)          INT4 200
Y3=Y(J-2)          INT4 210
GO TO NB,(150,170)          INT4 220
90 IF(X(J)-B)120,100,100          INT4 230
100 IF(J-2)130,130,110          INT4 240
110 ASSIGN 160 TO NA          INT4 250
120 J=J+1          INT4 260
GO TO 20          INT4 270
130 DO 140 J=1,3          INT4 280
XC(J)=X(J)          INT4 290
YC(J)=Y(J)          INT4 300
140 D=X2-X1          INT4 310
A1=B-X1          INT4 320
A2=B-X2          INT4 330
YE=A1*A2/2.0/D*((Y3-Y2)/(X3-X2)-(Y2-Y1)/D)-A2/D*Y1+A1/D*Y2          INT4 340
GO TO 180          INT4 350
160 ASSIGN 170 TO NB          INT4 360
GO TO 80          INT4 370
170 X4=X(J-3)          INT4 380
Y4=Y(J-3)          INT4 390
D=X3-X2          INT4 400
A1=B-X2          INT4 410
A2=B-X3          INT4 420
XM12=(Y2-Y1)/(X2-X1)          INT4 430
XM23=(Y3-Y2)/D          INT4 440
XM34=(Y4-Y3)/(X4-X3)          INT4 450
YE=A1*A2**2/2.0/D**2*(XM12-XM23)+A2*A1**2/2.0/D**2*(XM34-XM23)-A2*          INT4 460
1Y2/D+A1*Y3/D          INT4 470
180 YO=YE          INT4 480
RETURN          INT4 490
END          INT4 500

```

```

SIBFTC *NT4D LIST,M94          INT4D
SUBROUTINE INT4D(X,Y,XI,YO,DY)          INT4D 10
DIMENSION X(9),Y(9),XC(4),YC(4)          INT4D 20
EQUIVALENCE (XC(1),X1),(XC(2),X2),(XC(3),X3),(XC(4),X4),(YC(1),Y1)          INT4D 30
1,(YC(2),Y2),(YC(3),Y3),(YC(4),Y4)          INT4D 40
10 ASSIGN 90 TO NA          INT4D 50
J=2          INT4D 60
B=XI          INT4D 70
20 IF(X(J)130,40,30          INT4D 80
30 GO TO NA,(90,160)          INT4D 90
40 IF(Y(J)130,50,30          INT4D 100

```

Report 20672-PIF, Appendix B

50 IF(J-2)60,60,70	INT40110
60 YE=0.0	INT40120
GO TO 180	INT40130
70 ASSIGN 150 TO NB	INT40140
J=J-1	INT40150
80 X1=X(J)	INT40160
X2=X(J-1)	INT40170
X3=X(J-2)	INT40180
Y1=Y(J)	INT40190
Y2=Y(J-1)	INT40200
Y3=Y(J-2)	INT40210
GO TO NB,(150,170)	INT40220
90 IF(X(J)-B)120,100,100	INT40230
100 IF(J-2)130,130,110	INT40240
110 ASSIGN 160 TO NA	INT40250
120 J=J+1	INT40260
GO TO 20	INT40270
130 DO 140 J=1,3	INT40280
XC(J)=X(J)	INT40290
140 YC(J)=Y(J)	INT40300
150 D=X2-X1	INT40310
A1=B-X1	INT40320
A2=B-X2	INT40330
XM23=(Y3-Y2)/(X3-X2)	INT40340
XM12=(Y2-Y1)/(X2-X1)	INT40350
XM2B=(XM23-XM12)/2.0/D	INT40360
YO=A1*A2*XM2B-A2*Y1/D+A1*Y2/D	INT40370
DY=XM2B*(A1+A2)+XM12	INT40380
GO TO 180	INT40390
160 ASSIGN 170 TO NB	INT40400
GO TO 80	INT40410
170 X4=X(J-3)	INT40420
Y4=Y(J-3)	INT40430
D=X3-X2	INT40440
A1=B-X2	INT40450
A2=B-X3	INT40460
XM12=(Y2-Y1)/(X2-X1)	INT40470
XM23=(Y3-Y2)/D	INT40480
XM34=(Y4-Y3)/(X4-X3)	INT40490
AM2=A2*(XM12-XM23)	INT40500
AM1=A1*(XM34-XM23)	INT40510
YO=(A1*A2/2.0/D*(AM2+AM1)-A2*Y2+A1*Y3)/D	INT40520
DY=(AM2*(2.0*A1+A2)+AM1*(2.0*A2+A1))/2.0/D**2+XM23	INT40530
180 RETURN	INT40540
END	INT40550

SIBFTC	PAGER	LIST	M94	PAGE
			SUBROUTINE PAGE(LINES)	PAGE 10
C				PAGE 20
C			HEAD MOVED TO /PROLOG/ AND PAGE MODIFIED TO PRINT HEAD 25JUL 67	PAGE 30
C				PAGE 40
			COMMON /PROLOG/ LOGIK(38), HEAD(12), SL1, SL2, EORJ	PAGE 50
			DIMENSION TODAY (2)	PAGE 60
			DATA KPG / 0 /	PAGE 70
C				PAGE 80
			IF(LINES-60)20,10,10	PAGE 90
10			L=2	PAGE 100
			GO TO 60	PAGE 110
20			K=L+LINES	PAGE 120
			IF(K-60)30,30,30	PAGE 130
30			L=K	PAGE 140
40			RETURN	PAGE 150
C				PAGE 160
			50 L=LINES+2	PAGE 170
			60 IF (KPG .EQ. 0) CALL DATE (TODAY)	PAGE 180
			70 KPG = KPG + 1	PAGE 190
			WRITE (6,80) TODAY, HEAD, KPG	PAGE 200
80			FORMAT (1H1 3X 6HDATE 2A6, 12X 12A6, 11X 5HPAGE 15)	PAGE 210
			GO TO 40	PAGE 220
			END	PAGE 230

Report 20672-PIF, Appendix B

```

SORIGIN      ALODE
$INCLUDE     ABCDF
$IBFTC CHAMB LIST,M94
SUBROUTINE   CHAMBR
C
C          20 SEP 67 MODIFIED FOR TABULAR INJECTOR COEFFICIENTS
C
LOGICAL LOGIK, ARUN,BRUN,CRUN,DRUN,ERUN,FRUN,GRUN,HRUN,IRUN,JRUN
LOGICAL SL1, SL2, EORJ
REAL MACH
COMMON / /
1 GAM, NW1, WIT(30), AVH(30), BVH(30), CVNR(30), CVHI(30), EE,DSC
COMMON /PROLOG/ LOGIK(18), HEAD(12), SL1, SL2, EORJ
COMMON/ABCD/ DIMP,STOW
DIMENSION EXTRA(100), WC(75)
DIMENSION DIMP(4300),A(1),B(1),C(1),D(1)
DIMENSION X(135),Y(135),Q(134),STOW(222),STODAT(4607)
DIMENSION ZZ(205)
DIMENSION G(1),DISTL(20),DISTM(20)
DIMENSION AMIT(90)
EQUIVALENCE ( EXTRA, DIMP, STODAT )
EQUIVALENCE
1 (LOGIK(1), ARUN), (LOGIK(2), BRUN), (LOGIK(3), CRUN),
2 (LOGIK(4), DRUN), (LOGIK(5), ERUN), (LOGIK(6), FRUN),
3 (LOGIK(7), GRUN), (LOGIK(8), HRUN), (LOGIK(9), IRUN),
4 (LOGIK(10), JRUN)
EQUIVALENCE (EXTRA(1),CA), (EXTRA(2),CB), (EXTRA(3),CC), (EXTRA(4),
1CD), (EXTRA(5),CE), (EXTRA(6),CF), (EXTRA(7),CG), (EXTRA(8),CH)
EQUIVALENCE (EXTRA(9),CI)
EQUIVALENCE (DIMP(1),A), (DIMP(3001),B), (DIMP(3401),D),
1(DIMP(3901),G), (DIMP(3801),C), (EXTRA(21),WC), (B(4),UE)
EQUIVALENCE (DIMP(601),AMIT), (DIMP(2815),Q), (DIMP(3901),X),
1 (DIMP(3651),Y)
EQUIVALENCE
1 (STOW(1),ZZ), (STOW(213),YH)
2 (STOW(214),J), (STOW(215),NE), (STOW(216),YL), (STOW(217),KI)
3 (STOW(218),N), (STOW(219),KER), (STOW(220),XH)
4 (STOW(221),KQUAD), (STOW(222),XL)
5 (EXTRA(51),DISTL), (EXTRA(71),DISTM)
6 (EXTRA(101),CJ), (EXTRA(21),SNH), (EXTRA(12),MACH)
7 (DIMP(107),UIBAR)
C
C*****
10 FORMAT(100,60H A B C D E F G H
1 I J // 3X,(10F6.0))
20 FORMAT(//,9X,108H***** THE FOLLOWING MAIN CONT
1ROL DATA WILL BE USED IN THIS CASE ***** //,
245X,33H RATIO OF SPECIFIC HEAT (GAMMA) = ,F7.4, //,45X,22H DESIRED MACH
3CH NUMBER = ,E12.5,24H (=0 IF BEING CALCULATED) //,45X
5AMBER RADIUS = ,F7.3, 9H (INCHES) //,45X,17H CHAMBER LENGTH = ,F7.3CHAM
6, 9H (INCHES) //,45X,17H SPEED OF SOUND = ,F10.3, 9H (FT/SEC) //,
745X, 27H CHAMBER MODE DESCRIPTION = ,F8.5, 28H (=0 FOR LONGITUDINAL
8 MODES) //,
30 FORMAT(//,33X,48H***** CHAMBER FREQUENCIES (WC) *****
1 ,//)
40 FORMAT(5F20.5, / )
50 FORMAT(30X, 64H***** MACH DISTRIBUTION IN CHAMBER AS A FUNCTION OF
1 LENGTH ***** //,11X,7H CHAMBER,15X,4HMACH,14X,7H CHAMBER,15X,4HMACH
2,14X,7H CHAMBER,15X,4HMACH, //,12X,6H LENGTH,11X,12H DISTRIBUTION,11X,
36H LENGTH,11X,12H DISTRIBUTION,11X,6H LENGTH,11X,12H DISTRIBUTION,/,
60 FORMAT(6I10X,F10.5))
C*****
C*****
C IF ( SL2 ) GO TO 170
C
SL2 = .TRUE.
DO 70 I = 1, 4300
70 DIMP (I) = 0.0
GO TO 110
C*****
C*****
80 WRITE (6,100) NE
90 CALL EXIT
100 FORMAT (1H01X17H INPUT ERROR, NE = 15, 19H, HENCE TERMINATION )
C*****
C*****
110 KER = 0
CALL DVCHK (KCHK)
C
DO 120 I = 1, 10
120 DIMP(I) = 0.0
CALL AS138 ( DIMP(1), HEAD(1), NE )
IF ( NE .NE. 1 ) GO TO 80
ARUN = CA .NE. 0.0
BRUN = CB .NE. 0.0
CRUN = CC .NE. 0.0
DRUN = CD .NE. 0.0
ERUN = CE .NE. 0.0
FRUN = CF .NE. 0.0
IRUN = CI .NE. 0.0
JRUN = CJ .NE. 0.0
OGRUN = DIMP(22) .LE. 0.0
1 .AND. ( ARUN .OR. BRUN .OR. CRUN .OR. IRUN )
C
PRINT NEW MAIN CONTROL DATA
C*****
CALL PAGE ( 60 )
WRITE (6,10) (DIMP(I), I=1,10)
WRITE (6,20) DIMP(11), MACH, DIMP(14), DIMP(15), DIMP(16), SNH
C*****
C ARE FREQUENCIES TO BE CALCULATED... IF SO, CALCULATE AND PRINT.
C*****
IF ( .NOT. GRUN ) GO TO 130
CALL 'GENNEG' ( WC(1) )
IF ( BRUN .OR. ARUN ) CRUN = .TRUE.
IF ( CRUN ) CC = CC + 11.0
130 JOMEGA=ABS(EXTRA(22))+22.0001
WRITE (6,30)
WRITE (6,40) (EXTRA(I), I=23,JOMEGA)
WRITE (6,50)
WRITE (6,60) (DISTL(I), DISTM(I), DISTL(I+7), DISTM(I+7)
1, DISTL(I+14), DISTM(I+14), I=1,6 ), DISTL(7), DISTM(7),
2DISTL(14), DISTM(14)
C*****
C*****
EORJ = ERUN .OR. JRUN .OR. IRUN

```

Report 20672-PIF, Appendix B

```

IF ( CRUN .OR. EORJ ) CALL PAGE ( 60 )
140 IF ( .NOT. EORJ ) GO TO 200
WRITE (14) STODAT
BACKSPACE 14
EE = CE
DSC = CI
QAM = DIMP(11)
IF ( .NOT. IRUN ) GO TO 160
NWI = (. JOMEGA-22 1/2 +1
DO 150 I = 1, NWI
150 WIT(I) = DIMP( 2*I+21 )
WIT(NWI) = DIMP( JOMEGA )
C
160 RETURN
*****
PROGRAM RETURNS IF AND ONLY IF INJECTOR PROGRAM IS TO BE RUN
C=====
C=====
C=====
C=====
170 READ (14) STODAT
BACKSPACE 14
IF ( .NOT. ERUN ) GO TO 200
C
DIMP(3408) = NWI
DO 180 I = 1, NWI
DIMP(I+4522) = WIT(I)
DIMP(I+4599) = AVN (I)
DIMP(I+4556) = BVN (I)
DIMP(I+4579) = CVNR(I)
180 DIMP(I+4590) = CVNI(I)
DO 190 I = NWI, 84, 17
190 DIMP(I+4523) = 0.0
C=====
C=====
200 WC(2) = ABS( WC(2) )
C=====
C=====
FIX NUMBER OF FREQUENCIES AND TEST DESIRE FOR INTERNAL C FLAG
C=====
210 NOMEG=WC(2)+.0001
IF(EXTRA(12))230+220+230
220 DIMP(3802)=5.0
GO TO 240
230 UBAR = MACH
UE = MACH
240 IF ( .NOT. CRUN ) GO TO 390
C=====
C=====
SET UP DATA FOR PROGRAM C.
C=====
C=====
250 DIMP(3801)=EXTRA(11)
NNHAF = NOMEG/2 + 1
ZZ(1)=EXTRA(14)
ZZ(2)=EXTRA(15)
ZZ(3)=EXTRA(16)
DIMP(3805) = EXTRA(14)
DIMP(3803)=NNHAF
IF ( DIMP(3809) .EQ. 0.0 ) DIMP(3809) = 101.0
K = 0
ZAVE=((EXTRA(11)+1.0)/2.0)*SORT(DIMP(3806)*DIMP(3807))
IF(EXTRA(21))270+260+270
260 SNOZ = 0.0
C=====
C=====
USING HALF OF CHAMBER FREQUENCIES, CALCULATE NOZZLE FREQUENCIES
FOR USE IN PROG C.
C=====
RORL = EXTRA(15)
GO TO 280
270 RORL = EXTRA(14)
GRAD = SORT((2.0/(EXTRA(11)+1.0))*((DIMP(3804)/DIMP(3807)))
SNOZ = SNH/GRAD
280 DO 290 I=1,NNHAF
KN=(2*I)-1
NN=4210+K
DIMP(NN) = ZAVE*WC(KN)/RORL
DIMP(NN+1) = SNOZ
DIMP(NN+2) = MACH
K=K+3
290 CONTINUE
DIMP(NN)=ZAVE*(WC(NOMEG+2)/EXTRA(14))
300 CALL CCC(C(1),ZZ(1),WC(1),CC,KER)
SET UP NOZZ ADM FOR A,B
IF(KER) 310,330+310
310 WRITE (6,320)
320 FORMAT (1M0 30X39H ERROR PROGRAM C, ALL CASES TERMINATED )
CALL CORE(C(1),420;CC)
GO TO 90
330 IF ( .NOT. ARUN ) GO TO 360
C=====
C=====
MOVE OUTPUT FROM C INTO INPUT BLOCK TO A
C=====
340 NP = C(3)
IWO = 0
DO 350 I = 1, NP
IWO = IWO + 2
AMIT(I) = ZZ(IWO)
AMIT(I+30) = ZZ(IWO+ 1)
AMIT(I+60) = ZZ(IWO+101)
350 CONTINUE
ZEROS TO END TABLES
AMIT(NP+ 1) = 0.0
AMIT(NP+31) = 0.0
AMIT(NP+61) = 0.0
IF ( MACH .LE. 0.0 ) UBAR = ZZ(205)
GO TO 410
C
360 IF ( .NOT. BRUN .AND. SHM .EQ. 0.0 ) GO TO 340
C=====
C=====
MOVE OUTPUT FROM PROG C INTO INPUT BLOCK FOR PROG B.
C=====
370 DO 380 I=18,200
380 B(I)=ZZ(I)
B(A)=ZZ(205)
C
390 CONTINUE
HRUN = (CH.GT. 0.0) .OR. BRUN .AND.(UE.GE.0.1) .AND.(CH.EQ.0.0)
NOZZLE ADMITTANCE IS INPUT TO PROGS A, B.
C=====
C=====
400 IF ( .NOT. ARUN ) GO TO 490

```


Report 20672-PIF, Appendix B

```

C 410 CALL LONGL
C IF(KER)420,440,420
420 WRITE (6,430)
430 FORMAT(1H0,40X,18H ERROR PROGRAM A )
CALL CORE ( A(1), 700, CA )
440 CONTINUE
GO TO 110
C *****
C SET UP MAIN CONTROL DATA FOR USE IN B
C *****
450 IF ( .NOT. BRUN ) GO TO 530
B(1)=WC(1)
B(2)=EXTRA(15)/EXTRA(14)
B(3)=EXTRA(11)
B(5)=EXTRA(16)
B(6) = DIMP(17)
B(7) = DIMP(18)
B(8) = DIMP(19)
B(19)=WC(2)
DO 460 I=1,NOMEG
B(I+169)=WC(I+2)
460 CONTINUE
B(200) = DISTL(1) / DIMP(14)
B(220) = DISTM(1)
B(17) = 1.0
DO 480 I = 2, 20
IF(DISTM(I))490,490,470
470 B(I+199)=DISTL(I)/EXTRA(14)
B(I+219)=DISTM(I)
B(17)=B(17)+1.0
480 CONTINUE
490 CONTINUE
CALL TRANS ( B, X, CB, KER )
DO 500 I = 9, 100
D(I) = X(I)
500 IF(KER)530,510,530
510 WRITE (6,520)
520 FORMAT (1H0,40X,18H ERROR PROGRAM B )
CALL CORE(B(1),400,CB)
GO TO 110
C *****
530 IF ( .NOT. DRUN ) GO TO 620
540 DO 550 I=1,8
X(1)=D(1)
550 CONTINUE
560 X(5)=EXTRA(11)
DO 570 I = 9, 100
570 X(11) = D(I)
CALL DDD ( X(1), Y(1), CD, KER, ERR )
IF ( ERR ) 110,580,580
IF ( KER ) 610,590,610
580 WRITE (6,600)
590 FORMAT (1H0,40X,18H ERROR PROGRAM D )
CALL CORE(X(11),100,CD)
GO TO 110
610 CONTINUE
620 IF ( .NOT. FRUN ) GO TO 670
C *****
C SET UP DATA FOR PROG F (N, TAU )
C *****
630 Y(1)=EXTRA(14)
Q(101) = EXTRA(16)/Y(1) * 12.0/6.2831853
640 Y(2)=EXTRA(16)
CALL FFF ( Y(1), Q(1), CF, KER, WC(1) )
IF ( KER ) 670,650,670
650 WRITE (6,660)
660 FORMAT (1H0,40X,18H ERROR PROGRAM F )
CALL CORE(Y(1),100,CF)
670 GO TO 110
C *****
C *****
C *****
END

```

```

135F C WGEN LISTM94 WGEN 10
      SUBROUTINE GENMEG(W) WGEN 20
C ***** WGEN 30
      DIMENSION W(1) WGEN 40
C ***** WGEN 50
      LONGITUDINAL WILL HAVE NEG SMH WHICH WILL BE SET TO ZERO BEFORE RETURN WGEN 60
      IF SMH 0 LONGITUDINAL AND GENERATE + OR - 10 PERCENT OF PIE WGEN 70
C ***** WGEN 80
      IF(W(1))40,50,10 WGEN 90
C ***** WGEN 100
      FOR TRANSVERSE GENERATE 10 VALUES AROUND SMH 9 PERCENT BELOW AND WGEN 110
      11 PERCENT ABOVE WGEN 120
C ***** WGEN 130
      10 SMH=W(1) WGEN 140
      20 DELMEG=.1*SMH WGEN 150
      W(3)=SMH-DELMEG WGEN 160
      DELMEG=DELMEG/5.0 WGEN 170
      W(3)=W(3)+DELMEG WGEN 180
      DO 30 I=4,12 WGEN 190
      W(I)=W(I-1)+DELMEG WGEN 200
      30 CONTINUE WGEN 210
C ***** WGEN 220
      NEGATIVE 10 INDICATES TO PROGRAM THAT FREQUENCES ARE GENERATED INTERM WGEN 230
C ***** WGEN 240
      W(2)=-10.0 WGEN 250
      RETURN WGEN 260
C ***** WGEN 270
      NEG GENERATE + OR - 10 PERCENT OF POSITIVE INITIAL GUESS WGEN 280
C ***** WGEN 290
      40 SMH=-W(1) WGEN 300
      W(1)=0.0 WGEN 310
      GO TO 20 WGEN 320
      50 SMH=3.141592 WGEN 330
      GO TO 20 WGEN 340
      END WGEN 350

```

Report 20672-PIF, Appendix B

```

SORIGIN      BLODE      HYMN
SIBFTC HYMN  LIST,M94      HYMN 10
SUBROUTINE TRANS ( BIN, XOUT, CB, KER )      HYMN 20
C      HYMN 30
C      CALCULATES COMBUSTION PARAMETERS MR, HT      HYMN 40
C      PROGRAM BY LW VERNON FROM 11MAY67 ANALYSIS OF AJ SMITH, JR      HYMN 50
C      INCORPORATES CORRECTIONS TO ANALYSIS THRU 1 JUN 67      HYMN 60
C      BOOLE INTEGRATION AS OF 12 JUNE 67      HYMN 70
C      RHO, RHOL CONVENTIONS CORRECTED 22JUN 67      HYMN 80
C      20 SEP 67 MODIFIED FOR TABULAR INJECTOR COEFFICIENTS      HYMN 90
C      HYMN 100
C      *****      HYMN 110
C      REAL IAR, IAI, IBR, IBI      HYMN 120
C      LOGICAL LOGIK, HRUN, CKOUT, SIMPL, KNOT, LIMIT, TABLR      HYMN 130
C      COMMON /PROLOG/ LOGIK(38), HEAD(12), SL1, SL2, EORJ      HYMN 140
C      COMMON /ABCD/ / DIN (4300)      HYMN 150
C      1  SPACE(222), WIT(17), AVN(17), BVN(17), CVNR(17), CVNI(17)      HYMN 160
C      DIMENSION      HYMN 170
C      1  ZZ ( 102 ) , STAB ( 102 ) , GL ( 12, 3 ) ,      HYMN 180
C      2  U ( 102 ) , CTAB ( 102 ) , SLAM ( 12 ) ,      HYMN 190
C      3  DU ( 102 ) , DZU ( 102 ) , ZAP ( 12 ) ,      HYMN 200
C      4  UL ( 102 ) , DUL ( 102 ) , G ( 12 ) ,      HYMN 210
C      5  RHO ( 102 ) , DRHO ( 102 ) , GLD ( 12 ) ,      HYMN 220
C      6  RHOL ( 102 ) , DROL ( 102 ) , ZING ( 6 ) ,      HYMN 230
C      7  QBAR ( 102 ) , DO ( 102 ) , SIMP ( 6 ) ,      HYMN 240
C      8  ZIP3 ( 102 ) , V1 ( 102 ) , ERRZ ( 6 ) ,      HYMN 250
C      9  ZIP5 ( 102 ) , V2 ( 102 ) , ZF ( 6 ) ,      HYMN 260
C      DIMENSION      HYMN 270
C      1  THR ( 30 ) , THI ( 30 ) , TMTR ( 30 ) , TMTI ( 30 )      HYMN 280
C      ODIMENSION      HYMN 290
C      1  BIN ( 240 ) , XOUT ( 100 ) , WC ( 28 ) ,      HYMN 300
C      2  WET ( 30 ) , ERT ( 30 ) , EIT ( 30 ) ,      HYMN 310
C      3  ZDIST ( 20 ) , CRT ( 30 ) , CIT ( 30 ) ,      HYMN 320
C      4  DISTH ( 20 ) ,      HYMN 330
C      EQUIVALENCE      HYMN 340
C      1 ( HRUN , LOGIK( 8 ) ) , ( CKOUT , LOGIK(13) ) , ( SIMPL , LOGIK(14) ) ,      HYMN 350
C      2 ( KNOT , LOGIK(15) ) , ( LIMIT , LOGIK(16) ) , ( TABLR , LOGIK(17) ) ,      HYMN 360
C      EQUIVALENCE      HYMN 370
C      1 ( B(1) , SNH ) , ( B(10) , ZINC ) , ( DIN(14) , RCH ) ,      HYMN 380
C      2 ( B(2) , ZE ) , ( B(18) , XNE ) , ( UL(1) , UL0 ) ,      HYMN 390
C      3 ( B(3) , GAM ) , ( B(19) , XNW ) , ( RHOL(1) , RHOLD ) ,      HYMN 400
C      4 ( B(4) , UE ) , ( B(170) , WC ) , ( B(20) , WET ) ,      HYMN 410
C      5 ( B(5) , SOUND ) , ( B(200) , ZDIST ) , ( B(50) , ERT ) ,      HYMN 420
C      6 ( B(6) , ULM ) , ( B(220) , DISTH ) , ( B(80) , EIT ) ,      HYMN 430
C      7 ( B(7) , XK ) , ( B(110) , CRT ) ,      HYMN 440
C      8 ( B(8) , XCMPL ) , ( B(140) , CIT ) ,      HYMN 450
C      EQUIVALENCE      HYMN 460
C      1 ( DIN(3406) , RLOH ) , ( DIN(3407) , TLOW ) ,      HYMN 470
C      EQUIVALENCE      HYMN 480
C      1 ( A1R , AL ( 1 ) ) , ( A2R , AL ( 3 ) ) , ( A4R , AL ( 5 ) ) ,      HYMN 490
C      2 ( A1I , AL ( 2 ) ) , ( A2I , AL ( 4 ) ) , ( A4I , AL ( 6 ) ) ,      HYMN 500
C      3 ( B20R , SLAM( 9 ) ) , ( B20I , SLAM(10) ) ,      HYMN 510
C      4 ( B20I , SLAM(11) ) , ( B20I , SLAM(12) ) ,      HYMN 520
C      *****      HYMN 530
C      10 FORMAT ( / 65H TRANSVERSE STABILITY PROGRAM... CALCULATES MR, HT      HYMN 540
C      1 OR NTR, HTI )      HYMN 550
C      20 FORMAT ( // 11H INPUT DATA// 9XSHSNH12X2MZE10XSHSAMNAPX2MUE9X      HYMN 560
C      1 14MSOUND (FT/SEC) 2X13H ULM (FT/SEC) 5X WAK (DRAQ14X11HXCOMPL      HYMN 570
C      2(IN) // F15.6, F14.8, F12.5, F14.8, F14.2, 2X 9F19.6 //      HYMN 580
C      3 5X10HINCREMENTS 8X4HLR/N 11X4MLT/N / 5XP8.1, 2F19.7 // )      HYMN 590
C      30 FORMAT ( // 25H NOZZLE ADMITTANCES INPUT// 19XSHOMEGA(CH) 12X      HYMN 600
C      1 3MERT 17X5MEIT 17X5MERT 17X5MCIT // )      HYMN 610
C      40 FORMAT ( ///22H CALCULATED RESULTS... 10X 20HFIRST-ORDER SOLN ( UN      HYMN 620
C      1NIP INJ ) 19X21HSECOND-ORDER SOLUTION // 17XSHOMEGA 12X6MH REAL      HYMN 630
C      2 14X6MH IMAG 13X7MHIT REAL 13X7MHIT IMAG )      HYMN 640
C      50 FORMAT ( 9XF19.7+ZE20.8 )      HYMN 650
C      60 FORMAT ( 9XF19.7+ZE20.8 )      HYMN 660
C      70 FORMAT ( // 31H INJECTOR COEFFICIENTS INPUT... // )      HYMN 670
C      80 FORMAT ( 11X3HANN 17X3HBNH 16X6HCNH RE 14X6HCNH IM / 4E20.8 )      HYMN 680
C      90 FORMAT ( 10XSHOMEGA16X3HANH17X3HBNH16X6HCNH RE14X6HCNH IM/(5E20.8) )      HYMN 690
C      100 FORMAT ( 12H0INTEGRALS 6E18.8 )      HYMN 700
C      110 FORMAT ( 6H ERROR 6X6E18.8 )      HYMN 710
C      120 FORMAT ( 29HODUMP OF TABULAR FUNCTIONS... // 6X2HZ212X1WJ11X2HOU      HYMN 720
C      1 11X2HJ11X3HMO9X4HMHOL9X4HGBAR9X4HZIP39X4ZIP5 // (1H 9E13.5) )      HYMN 730
C      130 FORMAT ( 18H0TABLES FOR HINACH//6X2HZ211X3H2U11X3HDUL9X4HDRHO9X      HYMN 740
C      1 4H0ROL10X2H2O11X2HW11X2MV2// )      HYMN 750
C      140 FORMAT ( 1H 9E13.5 )      HYMN 760
C      150 FORMAT ( /10X1HW14X3H1AR15X3H1A115X3H1BR15X3H1B114X5HERCON13X5HEICOW      HYMN 770
C      1N/8X4HG20R14X4HG21R14X5HDG20R13X5HDG21R14X3HM1R15X3HM2R15X2MCR      HYMN 780
C      2 /8X4HG20I14X4HG21I14X5HDG20I13X5HDG21I14X3HM1I15X3HM2I15X2MCI// )      HYMN 790
C      160 FORMAT ( 7E18.8 )      HYMN 800
C      *****      HYMN 810
C      *****      HYMN 820
C      *****      HYMN 830
C      *****      HYMN 840
C      *****      HYMN 850
C      *****      HYMN 860
C      *****      HYMN 870
C      *****      HYMN 880
C      *****      HYMN 890
C      *****      HYMN 900
C      *****      HYMN 910
C      *****      HYMN 920
C      *****      HYMN 930
C      *****      HYMN 940
C      *****      HYMN 950
C      *****      HYMN 960
C      *****      HYMN 970
C      *****      HYMN 980
C      *****      HYMN 990
C      *****      HYMN 1000
C      *****      HYMN 1010
C      *****      HYMN 1020
C      *****      HYMN 1030
C      *****      HYMN 1040
C      *****      HYMN 1050
C      *****      HYMN 1060
C      *****      HYMN 1070
C      *****      HYMN 1080
C      *****      HYMN 1090
C      *****      HYMN 1100
C      *****      HYMN 1110
C      *****      HYMN 1120
C      *****      HYMN 1130
C      *****      HYMN 1140
C      *****      HYMN 1150
C      *****      HYMN 1160
C      *****      HYMN 1170
C      *****      HYMN 1180
C      *****      HYMN 1190

```

```

      INT = 2
      IDZ = IDZ/4 * 4
      MUST BE POSITIVE MULTIPLE OF FOUR. LESS THAN 101
      GO TO 240
C
230 INT = 1
      IDZ = -IDZ/2 * 2
C
240 IF ( ( IDZ .EQ. 0 ) .OR. ( IDZ .GT. 100 ) ) IDZ = 80
C
      IDZ IS NUMBER OF Z-INCREMENTS.
C
      IDZP = IDZ + 1
      DZ = ZC / FLOAT(IDZ)
C
      ZZ(1) = 0.0
      U(1) = 1.0E-10
      DU(1) = 0.0
      RHO(1) = 1.0
      ULO = ULM/SOUND
      GF1 = -1.0 / (GAM-1.0)
      GF2 = (GAM-1.0) / 2.0
      RHOZE = ( 1.0 + GF2*UE*UE ) **GF1
      RHOLO = RHOZE * UE / ULO
      QBAR(1) = 0.0
      ZIP3(1) = 0.0
      ZIP5(1) = RHOLO
C
      ABOVE ARE FIRST TABULAR ENTRIES.
C
      Z = 0.0
C
      DO 250 IZ = 2, IDZP
      Z = Z + DZ
      CALL INT4D ( ZDIST, DISTM, Z, U(IZ), DU(IZ) )
      ZZ(IZ) = Z
      U(IZ) = U(IZ)*SCALE
      DU(IZ) = DU(IZ)*SCALE
      UL(IZ) = UL(IZ-1) + XK*DZ*( U(IZ-1)-UL(IZ-1) )/UL(IZ-1)
      TEMP = 1.0 + GAM*( U(IZ)-UL(IZ) )*(U(IZ)
      RHO(IZ) = ( 1.0 + GF2*U(IZ)*U(IZ) ) **GF1
      RHOL(IZ) = ( RHOZE*UE - RHO(IZ)*U(IZ) ) / UL(IZ)
      QBAR(IZ) = ( ( 1.0 - GAM*U(IZ)*U(IZ) )*(RHO(IZ)*DU(IZ)
      - GAM*U(IZ)*RHOL(IZ)*XK*( U(IZ)-UL(IZ) ) ) ) / TEMP
      ZIP3(IZ) = DU(IZ) + DU(IZ)
      ZIP5(IZ) = RHOL(IZ) / RHO(IZ)
250 CONTINUE
      ZZ(IDZP) = ZC
      U(IDZP) = UE
      DU(IDZP) = 0.0
      RHO(IDZP) = RHOZE
      RHOL(IDZP) = 0.0
      QBAR(IDZP) = 0.0
      ZIP3(IDZP) = 0.0
      ZIP5(IDZP) = 0.0
C
      QBAR, ZIP3, ZIP5 AS TABULATED ABOVE ARE FREQ-INDEPENDENT PARTS
      OF INTEGRANDS.
C
      IF ( .NOT. HRUN ) GO TO 270
C
      INITIAL VALUES FOR HI-ORDER TABLES
      HDZ = 0.5 * DZ
      D2U(1) = 0.0
      DRHO(1) = 0.0
      DROL(1) = 0.0
      DQ(1) = 0.0
      DUL(1) = -XK
      V1(1) = 0.0
      V2(1) = 1.0
C
      HDZR = 0.5/DZ
      A1 = HDZ/ULO
C
      HI-ORDER TABLES
      DO 260 IZ = 2, IDZP
      A2 = HDZ/UL(IZ)
      V1(IZ) = V1(IZ-1) + A1 + A2
      V2(IZ) = EXP( XK*V1(IZ) )
      A1 = A2
      DUL(IZ) = ( UL(IZ+1) - UL(IZ-1) )*(HDZR
      DRHO(IZ) = ( RHO(IZ+1) - RHO(IZ-1) )*(HDZR
      DROL(IZ) = ( RHOL(IZ+1) - RHOL(IZ-1) )*(HDZR
      DQ(IZ) = ( QBAR(IZ+1) - QBAR(IZ-1) )*(HDZR
      D2U(IZ) = ( DU(IZ+1) - DU(IZ-1) )*(HDZR
260 CONTINUE
C
      FINAL VALUES
      DUL(IDZP) = XK*(UE-UL(IDZP))/UL(IDZP)
      DROL(IDZP) = 0.0
      DRHO(IDZP) = 0.0
      DQ(IDZP) = 0.0
      D2U(IDZP) = 0.0
      D2U(2) = 0.5*D2U(3)
      DQ(2) = 0.5*DQ(3)
      D2U(IDZ) = 0.5*D2U(IDZ-1)
      DQ(IDZ) = 0.5*DQ(IDZ-1)
C
      KNOT = XK .EQ. 0.0
      XI2R = 0.0
      XI3R = 0.0
      XI4R = 0.0
      VK1 = 0.0
      VK2 = 0.0
      IF ( TABLR ) GO TO 270
      ANH = AVN(1)
      BNH = BVN(1) * RLON
      CNHR = CVNR(1) * TLON
      CNHI = CVNI(1) * TLON
C
270 CONTINUE
      NW = XNW
C
      CALCULATIONS FOR EACH FREQUENCY, W
C
      DO 820 IW = 1, NW
      W = WC(IW)
      OMEG2 = SNH*SNH - W*W
      OMEG = SORT(ABS(OMEG2))
      HYMN1200
      HYMN1210
      HYMN1220
      HYMN1230
      HYMN1240
      HYMN1250
      HYMN1260
      HYMN1270
      HYMN1280
      HYMN1290
      HYMN1300
      HYMN1310
      HYMN1320
      HYMN1330
      HYMN1340
      HYMN1350
      HYMN1360
      HYMN1370
      HYMN1380
      HYMN1390
      HYMN1400
      HYMN1410
      HYMN1420
      HYMN1430
      HYMN1440
      HYMN1450
      HYMN1460
      HYMN1470
      HYMN1480
      HYMN1490
      HYMN1500
      HYMN1510
      HYMN1520
      HYMN1530
      HYMN1540
      HYMN1550
      HYMN1560
      HYMN1570
      HYMN1580
      HYMN1590
      HYMN1600
      HYMN1610
      HYMN1620
      HYMN1630
      HYMN1640
      HYMN1650
      HYMN1660
      HYMN1670
      HYMN1680
      HYMN1690
      HYMN1700
      HYMN1710
      HYMN1720
      HYMN1730
      HYMN1740
      HYMN1750
      HYMN1760
      HYMN1770
      HYMN1780
      HYMN1790
      HYMN1800
      HYMN1810
      HYMN1820
      HYMN1830
      HYMN1840
      HYMN1850
      HYMN1860
      HYMN1870
      HYMN1880
      HYMN1890
      HYMN1900
      HYMN1910
      HYMN1920
      HYMN1930
      HYMN1940
      HYMN1950
      HYMN1960
      HYMN1970
      HYMN1980
      HYMN1990
      HYMN2000
      HYMN2010
      HYMN2020
      HYMN2030
      HYMN2040
      HYMN2050
      HYMN2060
      HYMN2070
      HYMN2080
      HYMN2090
      HYMN2100
      HYMN2110
      HYMN2120
      HYMN2130
      HYMN2140
      HYMN2150
      HYMN2160
      HYMN2170
      HYMN2180
      HYMN2190
      HYMN2200
      HYMN2210
      HYMN2220
      HYMN2230
      HYMN2240
      HYMN2250
      HYMN2260
      HYMN2270
      HYMN2280
      HYMN2290
      HYMN2300
      HYMN2310
      HYMN2320
      HYMN2330
      HYMN2340
      HYMN2350
      HYMN2360
      HYMN2370
      HYMN2380
      HYMN2390
      HYMN2400

```

```

C      LIMIT = .FALSE.
C      CALL INT4 ( WET, ERT, W, ER )
C      CALL INT4 ( WET, EIT, W, EI )
C      IF ( OMEG2 )      280,290,300
280    IM = 1
      GO TO 310
C
C      IM = 2
290    OMEG = 0.5E-10
      OMEG2 = 0.25E-20
C
C      IM = 3
300
C      EVALUATION OF SIX INTEGRALS BY BOOLE FORMULA ( OR SIMPSON )
C      BOOLE INTEGRATION IF ZINC INPUT POSITIVE, ELSE SIMPSON RULE
C      ( BOOLE IS SIMPSON RULE WITH ERROR FORMULA )
C
C      IM IS ( 1, 2, 3 ) AS OMEG2 IS ( -, 0, + ),
C      THEN USE ( CIRCULAR, LIMIT, HYPERBOLIC ) FUNCTIONS
C
310    DO 320 I = 1, 6
320      ZING(I) = 0.0
      NOD = 3
      DO 430 IZ = 1, IDZP, INT
        Z = ZZ(IZ)
        GO TO (350,340,330), NOD
C
C      330      WT = 1.0
        NOD = 1
        GO TO 360
C
C      340      WT = 2.0
        IF ( IZ .EQ. IDZP ) GO TO 330
        NOD = 1
        GO TO 360
C
C      350      WT = 4.0
        NOD = 2
C
C      360      PSI = OMEG * (ZE-Z)
        GO TO (390,370,380), IM
C
C      370      ZEZ = ZE - Z
        ZF(1) = QBAR(IZ) * ZEZ
        ZF(2) = QBAR(IZ)
        ZF(3) = ZIP3(IZ) * ZEZ
        ZF(4) = ZIP3(IZ)
        ZF(5) = ZIP5(IZ) * ZEZ
        ZF(6) = ZIP5(IZ)
        GO TO 410
C
C      380      CF = COSH(PSI)
        SF = SINH(PSI)
        GO TO 400
C
C      390      CF = COS (PSI)
        SF = SIN (PSI)
C
C      400      ZF(1) = QBAR(IZ) * SF
        ZF(2) = QBAR(IZ) * CF
        ZF(3) = ZIP3(IZ) * SF
        ZF(4) = ZIP3(IZ) * CF
        ZF(5) = ZIP5(IZ) * SF
        ZF(6) = ZIP5(IZ) * CF
C      ZF ARE COMPLETE INTEGRANDS
C
C      410      DO 420 I = 1, 6
        ZING(I) = ZING(I) + WT*ZF(I)
C      420      CONTINUE
C      430      CONTINUE
C
C      GO TO (460,440), INT
C
C      440      INT = 1
      DO 450 I = 1, 6
        SIMP(I) = ZING(I)*DZ/1.5
C      SIMP IS SIMPSON INTEGRAL FOR IDZ/2 INCREMENTS
C      GO TO 310
C
C      460      DO 470 I = 1, 6
        ZING(I) = ZING(I)*DZ/3.0
C      ZING IS SIMPSON INTEGRAL FOR IDZ INCREMENTS
C
C      IF ( SIMPL ) GO TO 490
      INT = 2
      DO 480 I = 1, 6
        ERRZ(I) = ( ZING(I)-SIMP(I) ) / 15.0
        IF ( ABS(ERRZ(I)/ZING(I)) .GT. 0.05 ) CKOUT = .TRUE.
C      ZING, SIMP ARE SIMPSON INTEGRALS WITH IDZ, IDZ/2 INCREMENTS
        ZING(I) = ZING(I) + ERRZ(I)
C      480      CORRECTED ZING IS NOW BOOLE INTEGRAL
        CONTINUE
C
C      ABOVE ZING(I) ARE THE REQUIRED INTEGRALS
C
C      490      IF ( .NOT. CKOUT ) GO TO 500
        WRITE (6,100) ZING
        IF ( .NOT. SIMPL ) WRITE (6,110) ERRZ
C
C      500      OZE = OMEG * ZE
        WKSQ = XK*XK + W*W
        T1 = XK*W / WKSQ
        T2 = W*W / WKSQ
C
        Y1R = GAM*ZING(2)-ZING(2) + ZING(4) + W*T1*ZING(6)
        Y1I = XK*T1*ZING(6)
C
        GO TO (530,510,520), IM
C
C      510      Y2R = -SNH*ER/W
        Y2I = -SNH*EI/W
        ERCON = SNH*ER
        EICON = SNH*EI
        GO TO 550
C
C      520      COZE = COSH(OZE)
        SOZE = SINH(OZE)
        GO TO 540
C
C      530      COZE = COS(OZE)

```

```

HYMN2410
HYMN2420
HYMN2430
HYMN2440
HYMN2450
HYMN2460
HYMN2470
HYMN2480
HYMN2490
HYMN2500
HYMN2510
HYMN2520
HYMN2530
HYMN2540
HYMN2550
HYMN2560
HYMN2570
HYMN2580
HYMN2590
HYMN2600
HYMN2610
HYMN2620
HYMN2630
HYMN2640
HYMN2650
HYMN2660
HYMN2670
HYMN2680
HYMN2690
HYMN2700
HYMN2710
HYMN2720
HYMN2730
HYMN2740
HYMN2750
HYMN2760
HYMN2770
HYMN2780
HYMN2790
HYMN2800
HYMN2810
HYMN2820
HYMN2830
HYMN2840
HYMN2850
HYMN2860
HYMN2870
HYMN2880
HYMN2890
HYMN2900
HYMN2910
HYMN2920
HYMN2930
HYMN2940
HYMN2950
HYMN2960
HYMN2970
HYMN2980
HYMN2990
HYMN3000
HYMN3010
HYMN3020
HYMN3030
HYMN3040
HYMN3050
HYMN3060
HYMN3070
HYMN3080
HYMN3090
HYMN3100
HYMN3110
HYMN3120
HYMN3130
HYMN3140
HYMN3150
HYMN3160
HYMN3170
HYMN3180
HYMN3190
HYMN3200
HYMN3210
HYMN3220
HYMN3230
HYMN3240
HYMN3250
HYMN3260
HYMN3270
HYMN3280
HYMN3290
HYMN3300
HYMN3310
HYMN3320
HYMN3330
HYMN3340
HYMN3350
HYMN3360
HYMN3370
HYMN3380
HYMN3390
HYMN3400
HYMN3410
HYMN3420
HYMN3430
HYMN3440
HYMN3450
HYMN3460
HYMN3470
HYMN3480
HYMN3490
HYMN3500
HYMN3510
HYMN3520
HYMN3530
HYMN3540
HYMN3550
HYMN3560
HYMN3570
HYMN3580
HYMN3590
HYMN3600
HYMN3610

```

```

      SOZE = -SIN(OZE)
      ECOM = SINH*ER/OMEG
      EICOM = SINH*EI/OMEG
      Y2R = -SINH*ER/WCOZE
      Y2I = -SINH*EI/WCOZE - OMEG/W*BOZE
      TEMP = GAM*ZING(1) + ZING(3) + W*Y1*ZING(5)
      Y3R = ECOM*KK*Y1*ZING(5) + EICOM*TEMP
      Y3I = EICOM*KK*Y1*ZING(5) - ECOM*TEMP
      Y6R = EICOM*ZING(1) + ZING(2)
      Y6I = -ECOM*ZING(1)
      *****
      CALCULATION OF FIRST-ORDER SOLUTION...
      H1R = ( Y1R+Y2R+Y3R ) / GAM
      H1I = ( Y1I+Y2I+Y3I ) / GAM
      HD = Y6R*Y6R + Y6I*Y6I
      HR = ( H1R*Y6R + H1I*Y6I ) / HD
      HI = ( H1I*Y6R - H1R*Y6I ) / HD
      THR(IW) = HR
      THI(IW) = HI
      IF ( .NOT. HRUN ) GO TO S20
      *****
      TERMS FROM HIGH-ORDER ANALYSIS ( STILL IN W-LOOP )
      INITIALIZE INTEGRALS, INTEGRANDS FOR Z=0.0
      DO 570 I = 1, 6
      AL(I) = 0.0
      DO 570 IZ = 1, IDZP
      GS(I,IZ) = 0.0
      DO 580 I = 1, 12
      OLD(I) = 0.0
      ZAP(I) = 0.0
      GL(I,1) = 0.0
      SLAM(I) = 0.0
      OLD(3) = -KK*OMEG2
      IF ( IM.EQ. 1 ) SOZE = -SOZE
      MOD = 1
      TEMP = -Y1*RHOL0
      GL( 9,1) = TEMP*KK*W*SOZE
      GL(10,1) = TEMP*KK*W*COZE
      GL(11,1) = TEMP*OMEG2*SOZE
      GL(12,1) = TEMP*OMEG2*COZE
      IF ( .NOT. TABLR ) GO TO S85
      CALL INT4 ( WIT, AVN, W, ANH )
      CALL INT4 ( WIT, BVN, W, BNH )
      CALL INT4 ( WIT, CVNR, W, CNHR )
      CALL INT4 ( WIT, CVNI, W, CNNI )
      BNH = TLOM * BNH
      CNHR = TLOM * CNHR
      CNNI = TLOM * CNNI
      YE = ANH - CNNI / (W*GAM)
      YF = ( BNH + CNHR ) / (W*GAM)
      H2R = Y6R*YE - Y6I*YF
      H2I = Y6R*YF + Y6I*YE
      HSSQ = H2R*H2R + H2I*H2I
      HA = ( H1R*H2R + H1I*H2I ) / HSSQ
      HB = ( H1I*H2R - H1R*H2I ) / HSSQ
      CALL INT4 ( WET, CRT, W, CR )
      CALL INT4 ( WET, CIT, W, CI )
      GO TO (590,610,630), IM
      DO 600 IZ = 1, IDZP
      ARG = OMEG*ZZ(IZ)
      STAB(IZ) = SIN( ARG )
      CTAB(IZ) = COS( ARG )
      SIGN = -1.0
      GO TO 650
      DO 620 IZ = 1, IDZP
      STAB(IZ) = ZZ(IZ)
      CTAB(IZ) = 1.0
      GL(11,1) = TEMP * ZE
      GL(12,1) = TEMP
      GO TO 650
      DO 640 IZ = 1, IDZP
      ARG = OMEG*ZZ(IZ)
      STAB(IZ) = SINH(ARG)
      CTAB(IZ) = COSH(ARG)
      SIGN = 1.0
      DO 780 IZ = 2, IDZP
      MOD = MOD + 1
      V3 = KK*RHOL(IZ) / RHO(IZ)
      V4 = DU(IZ) + V3
      V5 = QBAR(IZ)*V4 + RHO(IZ)*U(IZ)*DQ(IZ)
      V6 = ( RHOL(IZ) / UL(IZ)*DUL(IZ) - DROL(IZ) ) / RHO(IZ)
      V7 = ( 2.0*(D2U(IZ)-DU(IZ)) + V3 - KK*V4 )
      V8 = KK*ZIPS(IZ) - U(IZ) - 3.0*DU(IZ)
      V9 = V3*( DU(IZ) - DUL(IZ) - UL(IZ) / RHO(IZ)*DROL(IZ) )
      + DU(IZ)*DU(IZ)
      V10 = ( GAM*DQ(IZ) - DQ(IZ) + RHO(IZ)*D2U(IZ) + D2U(IZ) )
      + U(IZ) / RHO(IZ)
      V11 = U(IZ) / RHO(IZ)*DROL(IZ) / RHO(IZ)
      V12 = ( GAM*QBAR(IZ) - QBAR(IZ) ) * DU(IZ)
      V13 = ( V12 + D2U(IZ) ) / RHO(IZ)
      V14 = QBAR(IZ) / RHO(IZ)
      V17 = (GAM-1.0) * ( V16*V16 + U(IZ) / RHO(IZ)*DQ(IZ) )
      + RHO(IZ)
      V18 = (U(IZ)-UL(IZ))*DQ(IZ) + QBAR(IZ)*(DU(IZ)-DUL(IZ))
      + RHO(IZ)
      V19 = ( UL(IZ)-KK-DUL(IZ) ) / ( UL(IZ)*UL(IZ) ) * RHO(IZ)
      V20 = V19 + DROL(IZ) / UL(IZ)
      V21 = V16 - GAM*V16 - BN(IZ) - DU(IZ) / RHO(IZ)
      V22 = GAM - 1.0
      *****

```

```

      V23 = RHO(IZ) + 1.0
      V24 = RHO(IZ) - 1.0
      V25 = V22 + (QBAR(IZ)*DU(IZ) + U(IZ)*DQ(IZ))
      V26 = DU(IZ) + (V22*QBAR(IZ) + (GAM + V23)*DU(IZ))
      V27 = RHO(IZ)*V10/T2
      V28 = V22 + (QBAR(IZ)*(QBAR(IZ)/RHO(IZ) + DU(IZ))
      0      + 2.0*U(IZ)*DQ(IZ))
      1      V29 = RHO(IZ) * (D2U(IZ)*U(IZ) - UL(IZ))
      0      + DU(IZ)*(DU(IZ) - DUL(IZ))
      1      V30 = U(IZ)*D2U(IZ)
C
C      THE FUNCTIONS V1 ... V20 ARE INDEPENDENT OF W. HENCE WE COULD
C      TRADE CORE FOR TIME BY TAKING ALL OR SOME OUT OF W-LOOP AS
C      SUBSCRIPTED VARIABLES. LET S SEE FIRST WHAT CORE WE HAVE.
C
      ARG = W + V1(IZ)
      CWV = COS(ARG)
      SWV = SIN(ARG)
      XI10R = CWV*V2(IZ)/RHO(IZ)
      XI10I = SWV*V2(IZ)/RHO(IZ)
      ZETAR = CWV/V2(IZ)
      ZETAI = SWV/V2(IZ)
      XI14R = XI10R*DUL(IZ)
      XI14I = XI10I*DUL(IZ)
      OZEE = OMEG + (ZE-ZZ(IZ) )
      GO TO (660,670,680), IM
C
C 660      PO = CTAB(IZ)
      PPO = -OMEG*STAB(IZ)
      ST = SIN ( OZEE )
      CT = COS ( OZEE )
      GO TO 690
C
C 670      PO = 1.0
      PPO = 0.0
      ST = ZE-ZZ(IZ)
      CT = 1.0
      GO TO 690
C
C 680      PO = CTAB(IZ)
      PPO = OMEG*STAB(IZ)
      ST = SIN( OZEE )
      CT = COS( OZEE )
C
C 690      IJK = 0
      DO 700 JZ = IZ, IDZP
      IJK = IJK + 1
      GS(1,JZ) = (QBAR(IZ)*STAB(IJK)+QBAR(IZ-1)*STAB(IJK+1))
      0      * HDZ + GS(1,JZ)
      1      GS(2,JZ) = (QBAR(IZ)*CTAB(IJK)+QBAR(IZ-1)*CTAB(IJK+1))
      0      * HDZ + GS(2,JZ)
      1      GS(3,JZ) = (ZIP3(IZ)*STAB(IJK)+ZIP3(IZ-1)*STAB(IJK+1))
      0      * HDZ + GS(3,JZ)
      1      GS(4,JZ) = (ZIP3(IZ)*CTAB(IJK)+ZIP3(IZ-1)*CTAB(IJK+1))
      0      * HDZ + GS(4,JZ)
      1      GS(5,JZ) = (ZIP5(IZ)*STAB(IJK)+ZIP5(IZ-1)*STAB(IJK+1))
      0      * HDZ + GS(5,JZ)
      1      GS(6,JZ) = (ZIP5(IZ)*CTAB(IJK)+ZIP5(IZ-1)*CTAB(IJK+1))
      0      * HDZ + GS(6,JZ)
      1
C
C 700      CONTINUE
C
      P10R = -XK*W*GS(5,IZ) * T1
      P10I = ( GAM*GS(1,IZ)-GS(1,IZ)+GS(3,IZ)+W*T1*GS(5,IZ) ) * W
      P11R = 0.0
      P11I = -W*GS(1,IZ)
      IF ( LIMIT ) GO TO 710
      P10R = P10R/OMEG
      P10I = P10I/OMEG
      P11I = P11I/OMEG
      PP10R = -W*XK*T1 * GS(6,IZ)
      0      PP10I = (GAM*GS(2,IZ) - GS(2,IZ) + GS(4,IZ)
      1      + W*T1*GS(6,IZ) ) * W
C
C      PP11R = 0.0
      PP11I = -W*GS(2,IZ)
C
C      IF ( KNOT ) GO TO 730
C      EVALUATE INTEGRALS IN EXPRESSIONS FOR LAMDA5 ( AL(1) )
      XI16R = ( W*RHO(IZ)*ZETAR - V19*ZETAI ) * T1
      XI16I = ( W*RHO(IZ)*ZETAI - V19*ZETAR ) * T1
      T3 = ( W*T1*DROL(IZ)/RHO(IZ) + D2U(IZ) ) * PO
      G(1) = T3 * XI10R
      G(2) = T3 * XI10I
      T4 = OMEG2*PO + PPO
      G(3) = XI14R * T4
      G(4) = XI14I * T4
      G(5) = PPO * XI10R
      G(6) = PPO * XI10I
      G( 7) = XI14R * PP11I
      G( 8) = XI14I * PP11I
      G( 9) = XI14R * PP10R
      G(10) = XI14I * PP10R
      G(11) = XI14R * PP10I
      G(12) = XI14I * PP10I
C
C      DO 720 I = 1, 12
      ZAP(I) = ( G(I) + OLD(I) ) * HDZ + ZAP(I)
      0      OLD(I) = G(I)
      1      ( TRAPEZOIDAL RULE )
      2      VK1 = XK * ( T2*RHO(IZ)/RHO(IZ)*(V24*DU(IZ) - V3)
      3      + RHO(IZ) * (W*T1*RHO(IZ)/RHO(IZ)*DU(IZ)
      4      - DUL(IZ) - XK*ZETAR)
      5      - UL(IZ)*DROL(IZ) - U(IZ)/RHO(IZ)*DROL(IZ) )
      6      - RHO(IZ)/RHO(IZ)*(V22*QBAR(IZ) + V23*DU(IZ))
      7      VK2 = XK * ( T2*U(IZ)/RHO(IZ)*DROL(IZ)
      8      + XK*GAM*RHO(IZ)*ZETAI/W)
C
C 730      XI1R = T2/RHO(IZ) * (V25 - V26 - V27 - V28 + V29 + VK1)
      XI1I = T2 * (VK2 + V30)
      XI2I = ( GAM*V16 - V16 + DU(IZ) + T2*V4 ) * W
      XI3I = W*U(IZ) - T2/W*V7
      XI4I = T1*V6 + 2.0*W*U(IZ)
      XI5I = ( T2*V8 + DU(IZ)/RHO(IZ) ) / W
      XI2R = XI3R = XI4R = XI5R = 0
C
C
C      IF ( KNOT ) GO TO 740
      A1R = -XI16R*ZAP(8) - XI16I*ZAP(7)
      A1I = XI16R*ZAP(7) - XI16I*ZAP(8) + GAM*PO*V5*T1
      A2R = T1/W*(V16*V3-V5/RHO(IZ))*PO

```

HYNN4730
 HYNN4740
 HYNN4750
 HYNN4760
 HYNN4770
 HYNN4780
 HYNN4790
 HYNN4800
 HYNN4810
 HYNN4820
 HYNN4830
 HYNN4840
 HYNN4850
 HYNN4860
 HYNN4870
 HYNN4880
 HYNN4890
 HYNN4900
 HYNN4910
 HYNN4920
 HYNN4930
 HYNN4940
 HYNN4950
 HYNN4960
 HYNN4970
 HYNN4980
 HYNN4990
 HYNN5000
 HYNN5010
 HYNN5020
 HYNN5030
 HYNN5040
 HYNN5050
 HYNN5060
 HYNN5070
 HYNN5080
 HYNN5090
 HYNN5100
 HYNN5110
 HYNN5120
 HYNN5130
 HYNN5140
 HYNN5150
 HYNN5160
 HYNN5170
 HYNN5180
 HYNN5190
 HYNN5200
 HYNN5210
 HYNN5220
 HYNN5230
 HYNN5240
 HYNN5250
 HYNN5260
 HYNN5270
 HYNN5280
 HYNN5290
 HYNN5300
 HYNN5310
 HYNN5320
 HYNN5330
 HYNN5340
 HYNN5350
 HYNN5360
 HYNN5370
 HYNN5380
 HYNN5390
 HYNN5400
 HYNN5410
 HYNN5420
 HYNN5430
 HYNN5440
 HYNN5450
 HYNN5460
 HYNN5470
 HYNN5480
 HYNN5490
 HYNN5500
 HYNN5510
 HYNN5520
 HYNN5530
 HYNN5540
 HYNN5550
 HYNN5560
 HYNN5570
 HYNN5580
 HYNN5590
 HYNN5600
 HYNN5610
 HYNN5620
 HYNN5630
 HYNN5640
 HYNN5650
 HYNN5660
 HYNN5670
 HYNN5680
 HYNN5690
 HYNN5700
 HYNN5710
 HYNN5720
 HYNN5730
 HYNN5740
 HYNN5750
 HYNN5760
 HYNN5770
 HYNN5780
 HYNN5790
 HYNN5800
 HYNN5810
 HYNN5820
 HYNN5830
 HYNN5840
 HYNN5850
 HYNN5860
 HYNN5870
 HYNN5880
 HYNN5890
 HYNN5900
 HYNN5910
 HYNN5920
 HYNN5930

Report 20672-PIF, Appendix B

```

      T5 = W/UL(IZ) * RHOL(IZ)/UL(IZ)
      T6 = V20*ZETA1 - T5*ZETAR
      T7 = V20*ZETAR - T5*ZETA1
      T8 = W/RHO(IZ) * ( RHOL(IZ) - RHO(IZ)*RHOL(IZ) )
C
0      A4R = T1 * ( T8*( ZETA1*ZAP(5) + ZETAR*ZAP(6) )
1          - RHOL(IZ)*( ZETAR*ZAP(1) + ZETA1*ZAP(2) )
2          - T6*ZAP(3) + T7*ZAP(4) )
3          + XI16R*(ZAP( 9)-ZAP(12)) - XI16I*(ZAP(11)+ZAP(10))
C
0      A4I = T1 * ( T8*( ZETA1*ZAP(6) - ZETAR*ZAP(5) )
1          - RHOL(IZ)*( ZETAR*ZAP(2) - ZETA1*ZAP(1) )
2          - T7*ZAP(3) - T6*ZAP(4) )
3          + XI16R*(ZAP(11)+ZAP(10)) + XI16I*(ZAP( 9)-ZAP(12))
C
740      T9 = HA * P11I
      T10 = HB * P11I
      TEMP = -GAM*W*OBAR(IZ)
0      A1R = A1R + TEMP*(T9+P10I) + GAM*P0*(V18+T2*V5)
1          + XI2I*P11I + XI4I*PP11I
      A1I = A1I + TEMP*(T10-P10R)
      A2R = A2R + V16*(T10-P10R)
0      A2I = ( (V18+T2*V5)/RHO(IZ) - V16*(V3*T2-DU(IZ)) )/W*P0
1          -V16*(T9+P10I)
0      A4R = A4R + XI1R*P0 + XI4I*PP10I + XI2I*P10I
0      A4I = A4I + ( XI1I-OMEG2*XI5I )*P0 - XI3I*PP0 - XI4I*PP10R
1          - XI2I*P10R
C
C*****
C      SET UP INTEGRANDS ( SIMPSON RULE HERE )
C      DO 750 I = 1, 6
      GL(2*I-1,NOD) = AL(I)*ST
      GL(2*I ,NOD) = AL(I)*CT
      AL(I) = 0.0
750      CONTINUE
C
      GO TO (780,780+760), NOD
C
760      DO 770 I = 1, 12
      SLAM(I) = SLAM(I) + GL(I,1) + 4.0*GL(I,2) + GL(I,3)
C      WEIGHTED SUM FOR THREE ORDINATES
      GL(I,1) = GL(I,3)
770      CONTINUE
      NOD = 1
C
780      CONTINUE
C
C***** ENDS PRINCIPAL Z-LOOP *****
C      STILL DOING FOR IW
C
C*****
C      COMPLETE INTEGRATION
C      DO 790 I = 1, 12
      SLAM(I) = SLAM(I) * DZ/3.0
790      CONTINUE
C      IF ( LIMIT ) GO TO 800
C      CALCULATE DEFECT ( CONTRIBUTION OF INTEGRALS FROM Z=ZC TO Z=ZE )
      TEMP = 2.0*W*UE
      SLAM( 1) = SLAM( 1) + TEMP*PP11I*(CF-1.0)/OMEG2
      SLAM( 2) = SLAM( 2) + TEMP*PP11I*SF/OMEG
      SLAM( 9) = SLAM( 9) + TEMP*PP10I*(CF-1.0)/OMEG2
      SLAM(10) = SLAM(10) + TEMP*PP10I*SF/OMEG
      SLAM(11) = SLAM(11) - TEMP*PP10R*(CF-1.0)/OMEG2
1      -0.5*W*UE*( PSI*COZE-CTAB(IDZP)*SF )/OMEG
2      + 0.5*T2/W*UE*( PSI*SOZE-STAB(IDZP)*SF )*SIGN
      SLAM(12) = SLAM(12) - TEMP*PP10R*SF/OMEG
1      - 0.5*W*UE*( PSI*SOZE-STAB(IDZP)*SF )*SIGN
2      + 0.5*T2/W*UE*( PSI*COZE+CTAB(IDZP)*SF )/OMEG*SIGN
C
800      G21R = ANH*SLAM(1) + BNH*SLAM(5) + CNHR*SLAM(9) - CNHI*SLAM(7)
      G21I = ANH*SLAM(3) + BNH*SLAM(7) + CNHR*SLAM(7) + CNHI*SLAM(5)
      DG21R = ANH*SLAM(2) + BNH*SLAM(6) + CNHR*SLAM(6) - CNHI*SLAM(8)
      DG21I = ANH*SLAM(4) + BNH*SLAM(8) + CNHR*SLAM(8) + CNHI*SLAM(6)
C
C      THE FOLLOWING AVAILABLE BY EQUIVALENCE...
C      G2OR IS SLAM ( 9 )
C      G2OI IS SLAM (11)
C      DG2OR IS SLAM (10)
C      DG2OI IS SLAM (12)
C
C      FOR NONZERO OMEG, DIVISION BY OMEG IS IMPLICIT IN ERCON, EICON.
C      IAR, IAI, IBR, IBI ARE TYPE REAL.
      TEMP = UE * W * ZING(2)
0      IAR = H1R - DG2OR - ERCON*G2OI - EICON*G2OR
1          + ( ( CI*Y1I - CR*Y1R ) *W + CR*Y1I + CI*Y1R ) *W*UE
0      IAI = H1I - DG2OI + ERCON*G2OR - EICON*G2OI
1          - ( ( CR*Y1I + CI*Y1R ) *W + CR*Y1R - CI*Y1I ) *W*UE
      IBR = H2R + DG21R + ERCON*G21I + EICON*G21R + TEMP*( CI-W*CR )
      IBI = H2I + DG21I - ERCON*G21R + EICON*G21I - TEMP*( CR+W*CI )
C
      HTD = IBR*IBR + IBI*IBI
      HTR = ( IAR*IBR + IAI*IBI ) / HTD
      HTI = ( IAI*IBR - IAR*IBI ) / HTD
C
      THTR(IW) = HTR
      THTI(IW) = HTI
C
      IF ( .NOT. CKOUT ) GO TO 820
      WRITE (6,150)
      WRITE (6,160) W , IAR , IAI , IBR , IBI , ERCON , EICON ,
1          G2OR , G21R , DG2OR , DG21R , H1R , H2R , CR ,
2          G2OI , G21I , DG2OI , DG21I , H1I , H2I , CI
C
820      CONTINUE
C
C      END OF W-LOOP
C*****
C      KER = NW
      XOUT(9) = XNW
C
      IF ( HRUN ) GO TO 850
C
      DO 830 IW = 1, NW
      XOUT(IW+ 9) = WC (IW)
      XOUT(IW+39) = THR(IW)
      XOUT(IW+69) = THI(IW)
830      CONTINUE
      GO TO (880,840), KOUT
840      IF ( CKOUT ) CALL PAGE ( 70 )

```

```
WRITE (6,40)
WRITE (6,50) ( WC(I), THR(I), THZ(I), I = 1, NW )
GO TO 880
```

HYMNM7290
HYMNM7260
HYMNM7270
HYMNM7280
HYMNM7290
HYMNM7300
HYMNM7310
HYMNM7320
HYMNM7330
HYMNM7340
HYMNM7350
HYMNM7360
HYMNM7370
HYMNM7380
HYMNM7390
HYMNM7400
HYMNM7410
HYMNM7420
HYMNM7430
HYMNM7440
HYMNM7450
HYMNM7460
HYMNM7470
HYMNM7480
HYMNM7490
HYMNM7500
HYMNM7510
HYMNM7520
HYMNM7530
HYMNM7540
HYMNM7550
HYMNM7560
HYMNM7570
HYMNM7580
HYMNM7590
HYMNM7600
HYMNM7610


```

SUBROUTINE DDD(DIN,DOUT,CD,NER,ERR)
C
C PROGRAM D COMPUTE HTR,HTI + INTERPOLATE 40 POINTS
C 20 SEP 67 MODIFIED FOR TABULAR INJECTOR COEFFICIENTS
C
LOGICAL LOGIK,HRUN,TABLR
COMMON /PROLOG/ LOGIK(30)
COMMON /ABCD/ EXTRA(100), ABLOK(600), A , B , SPACE(3556),
1 WIT(17), AVN(17), BVN(17), CVNR(17), CVNI(17)
DIMENSION DIN(1),DOUT(1),A(133),B(133),OMEGA(1),HR(1),HI(1)
1,HTR(30),HTI(30),HTRINT(1),HTIINT(1), OMEGA(1)
2,DOM(30)
EQUIVALENCE (LOGIK(8),HRUN),(LOGIK(17),TABLR)
EQUIVALENCE (A(1),ANH),(A(2),BNH),(A(3),CNHRE),(A(4),CNHIM),
1(A(5),GAMMA),(A(6),XLRN),(A(7),XLON),(A(9),XNW),(A(10),OMEGA),
2(A(40),HR),(A(70),HI),(B(9),ONW),(B(10),OMGA),(B(51),HTRINT),
3(B(92),HTIINT), ( OMEGA, DOM )
C
10 FORMAT ( 21MO INPUT TO PROGRAM D // 10X8H GAMMA = F8.4,5X6HLR/N
1 F12.8, 5X6HLT/N = F12.8 )
20 FORMAT ( 18X3HANH12X3HBNH11X6HCNH RE 9X6HCNH IM // 9X 4F15.7 // )
30 FORMAT ( // 38H INJECTOR DISTRIBUTION COEFFICIENTS... //
117X5HOMEGA 11X3HANH 12X3HBNH 11X6HCNH RE 9X6HCNH IM // (9X5F15.7)
40 FORMAT (1MO, 19X,8HOMEGA(C),9X3H MR,13X3H MI )
50 FORMAT (1MO,19X, 8HOMEGA(C),9X3HMYR 13X3HMTI )
60 FORMAT(1H,10X,3F16.6)
70 FORMAT (1MO,20H PROGRAM D OUTPUT // 19X,8HOMEGA(C) 9X
16H HTR,10X,6H HTI // )
80 FORMAT (91HALL VALUES OF HTR ARE NEGATIVE- ( I.E. OUT OF RANGE OPMTHT
1INTEREST- WILL PROCEED TO NEXT CASE))
90 FORMAT(//,30X,69H FOLLOWING WILL BE INTERPOLATION WITHIN HTR HTI
1 TABLE GIVEN ABOVE )
100 FORMAT (19X,8H OMEGA ,9X6HMYRINT,10X,6HMTIINT )
110 FORMAT (11X,F10.5,10X,F10.5,10X,F10.5)
C
ERR=0.0
DO 100 I=1,133
120 DO 130 I=1,133
130 B(I)=0.0
NER=IFIX(XNW)
IF(NER)140,140,160
140 WRITE (6,150)NER
150 FORMAT (1MO,10X,31H NUMBER OF OMEGAS IN ERROR = ,3X,I4 )
GO TO 510
160 IF(NER-29)170,170,140
170 ONW = 40.0
IF ( HRUN ) GO TO 190
NWI = A(8) + 0.01
IF ( NWI .GT. 2 ) GO TO 180
ASSIGN 280 TO NT
TABLR = .FALSE.
ANH = AVN (1)
BNH = BVN (1)
CNHRE = CVNR(1)
CNHIM = CVNI(1)
GO TO 190
180 ASSIGN 270 TO NT
TABLR = .TRUE.
190 IF(CD-99.0)260,260,200
200 CALL PAGE ( 60 )
WRITE (6,10) GAMMA, XLRN, XLON
IF ( HRUN ) GO TO 230
IF ( TABLR ) GO TO 210
WRITE (6,20) ANH, BNH, CNHRE, CNHIM
GO TO 220
210 WRITE (6,30) ( WIT(I), AVN(I), BVN(I), CVNR(I), CVNI(I),
1 I = 1, NWI )
220 WRITE (6,40)
GO TO 240
230 WRITE (6,50)
240 DO 250 I = 1,NER
250 WRITE (6,60)OMEGA(I),HR(I),HI(I)
C
260 IF ( HRUN ) GO TO 350
DO 340 I=1,NER
W = OMEGA(I)
GO TO NT,(270,280)
270 CALL INT4 ( WIT, AVN , W, ANH )
CALL INT4 ( WIT, BVN , W, BNH )
CALL INT4 ( WIT, CVNR, W, CNHRE )
CALL INT4 ( WIT, CVNI, W, CNHIM )
280 DEN = GAMMA*W
X = ANH - CNHIM/DEN*XLON
Y = BNH / DEN * XLRN + CNHRE * XLON / DEN
SQD = X * X + Y * Y
HTR(I) = (X * HR(I) + Y * HI(I) ) / SQD
HTI(I) = (X * HI(I) - Y * HR(I) ) / SQD
CALL DVCHK (K000FX)
GO TO (310,290),K000FX
290 IF (CD-10.0) 340,300,300
300 IF (I-1) 330,320,330
310 C=10.0
320 LIN=NER+6
CALL PAGE (LIN)
WRITE (6,70)
330 WRITE (6,60)DOM(I),HTR(I),HTI(I)
340 CONTINUE
GO TO 370
C
350 DO 360 I = 1,NER
HTI(I) = HI(I)
360 HTR(I) = HR(I)
370 JOMEG1 = 0
JOMEG2=0
IF ( CD .LE. 99.0 ) CALL PAGE (60)
DO 390 I =1,NER
IF (HTR(I)) 390,390,380
380 JOMEG1 = I
GO TO 410
390 CONTINUE
IF (JOMEG1)400,400,410
400 WRITE (6,80)
ERR= -1.0
GO TO 320
410 DO 430 J =1,NER
IF (HTR(J)) 420,430,430
420 JOMEG2 = J
GO TO 440

```

Report 20672-PIF, Appendix B

430 CONTINUE	MTNT1200
JONES2 =NER	MTNT1210
440 DLTNEG = (DOM(JONES2) -DOM(JONES1))/ 39.0	MTNT1220
L=NER+1	MTNT1230
MTI(L)=0.0	MTNT1240
MYRI(L)=0.0	MTNT1250
DOMI(L)=0.0	MTNT1260
OMGA(I) =DOM(JONES1)	MTNT1270
DO 490 I=1,40	MTNT1280
CALL INTA (DOM(I),MYRI(I),OMGA(I),MYRIINT(I))	MTNT1290
CALL INTA (DOM(I),MTI(I),OMGA(I),MTIINT(I))	MTNT1300
IF (CD-10.0)480,450,450	MTNT1310
450 IF (I-1) 470,460,470	MTNT1320
460 IF (.NOT. MRUN) CALL PAGE (60)	MTNT1330
WRITE (6,90)	MTNT1340
WRITE (6,100)	MTNT1350
470 WRITE (6,60) OMGA(I),MYRIINT(I),MTIINT(I)	MTNT1360
480 OMGA(I+1) = OMGA(I) + DLTNEG	MTNT1370
490 CONTINUE	MTNT1380
DO 500 I=1,133	MTNT1390
500 DOUT (I) = B(I)	MTNT1400
IF(C) 510,520,510	MTNT1410
510 NER=0	MTNT1420
520 RETURN	MTNT1430
END	MTNT1440

Report 20672-PIF, Appendix B

SIBMAP	*ADMIN		*ADM0010
	* GLAUZ - ADAMS METHOD OF INTEGRATION		*ADM0020
	* FAP TO MAP CONVERSION HAZLETT, DEC 1963 , FORTRAN 4 PATTERSON JULY 64		*ADM0030
	ENTRY ADMSET		*ADM0040
	ENTRY ADMINT		*ADM0050
	ENTRY ADMCOR		*ADM0060
	ENTRY ADMPAR		*ADM0070
	ENTRY ADMRES		*ADM0080
ADMSET	SAVE 1		*ADM0090
	CLA* 3+4		*ADM0100
	STA BZ	N TO ADD OF BZ	*ADM0110
	ALS 2	4N	*ADM0120
	STA BP18	SAVE 4N, SET FLAG FOR RETURN	*ADM0130
	ADD* 3+4	+N	*ADM0140
	STA CF	5N	*ADM0150
	ADD 7+4	PUT IN	*ADM0160
	ADD BP18	+4N	*ADM0170
	STA CC	PUT IN DIFF TABLE LOC	*ADM0180
	CLA 4+4	F FUNCTION LOCATION	*ADM0190
	ADD* 3+4	+N	*ADM0200
	STA LF	FUNCTION VALUE LOC	*ADM0210
	CLA 5+4	DERIV LOC	*ADM0220
	ADD* 3+4	+N	*ADM0230
	STA LD	DERIV VALUE LOC	*ADM0240
	CLA 6+4	PARTIAL STEP LOC	*ADM0250
	ADD* 3+4	+N	*ADM0260
	STA CP	PARTIAL STEP LOC	*ADM0270
	CLA 7+4		*ADM0280
	ADD* 3+4	+N	*ADM0290
	STA LG	TEST VALUE LOC. 7+4 WAS PUT IN	*ADM0300
	ADD* 3+4	+N	*ADM0310
	STA CA	ACCURACY EXPONENT LOC	*ADM0320
	ADD* 3+4	+N	*ADM0330
	STA CK	OLD FCN. LOC.	*ADM0340
	ADD* 3+4		*ADM0350
	STA CQ		*ADM0360
	CLA 8+4		*ADM0370
	STA CX	X LOC	*ADM0380
	CLA 9+4		*ADM0390
	STA CH	H LOC	*ADM0400
	CLA 10+4		*ADM0410
	ADD* 3+4	+N	*ADM0420
	STA CD	ACCURACY INPUT TABLE	*ADM0430
	TRA RP20		*ADM0440
ADMRES	SAVE 1		*ADM0450
	STZ BP18		*ADM0460
BP20	STZ FLAG		*ADM0470
	LXA BZ+4	+N	*ADM0480
CD	CAL +4	ACCURACY INPUT+4	*ADM0490
	4N =03770000000000		*ADM0500
	TNZ +2	TEST FOR 0 ACCURACY INPUT	*ADM0510
	CLA =01520000000000	ACCURACY SET= +152	*ADM0520
	ADD =00220000000000		*ADM0530
CA	STO +4	ACCURACY EXPONENT+4	*ADM0540
	TIX CD+4+1		*ADM0550
	LXA CF+1	+5N	*ADM0560
BP	STZ* CC	DIFF TABLE+1	*ADM0570
	TIX BP+1+1		*ADM0580
	AXT 5+1		*ADM0590
	SXD CNT+1		*ADM0600
	CLA BP18		*ADM0610
	TNZ BP19		*ADM0620
	RETURN ADMRES		*ADM0630
BP19	RETURN ADMSET		*ADM0640
BP18	PZE		*ADM0650
ADMINT	SAVE		*ADM0660
	CLA FLAG		*ADM0670
	TNZ BZ		*ADM0680
	RETURN ADMINT		*ADM0690
BZ	AXT +4	+N	*ADM0700
BP2	CLA* LF	FUNCTION+4	*ADM0710
CK	STO +4	OLD FUNCTION+4	*ADM0720
	TIX BP2+4+1		*ADM0730
BF	AXT COEFP+4	PRED TABLE LOC	*ADM0740
	SXA CO+4		*ADM0750
	TSX COMP+4		*ADM0760
CX	CLA +	X	*ADM0770
CH	FAD +	H	*ADM0780
	STO* CX	STORE IN X	*ADM0790
	RETURN ADMINT		*ADM0800
COMF	SXA IR1+1		*ADM0810
	SXA IR2+2		*ADM0820
	SXA IR4+4		*ADM0830
	LXA BZ+4	N TO IN 4	*ADM0840
CF	AXT +1	5N IN 1	*ADM0850
CB	AXT 5+2		*ADM0860
	STZ TEMP		*ADM0870
CC	LDQ +1	DIFF TABLE+1	*ADM0880
CO	FMP +2	COEF+2	*ADM0890
	FAD TEMP		*ADM0900
	STO TEMP		*ADM0910
	TXI BP3+1+1	NEXT DIFF	*ADM0920
BP3	TIX CC+2+1	NEXT COEF	*ADM0930
	AXT 0+2		*ADM0940
LD	LDQ +4	DERIV+4	*ADM0950
	FMP* CO	COEF+2	*ADM0960
	FAD TEMP		*ADM0970
	LRS 35		*ADM0980
	FMP* CH	H	*ADM0990
IG	STO +4	TEST VALUE	*ADM1000
CCM	FAD* CK	OLD FUNCTION	*ADM1010
CM	STO* LF	FUNCTION+4	*ADM1020
	TIX CR+4+1	NEXT EQUATION	*ADM1030
IR4	AXT +4		*ADM1040
IR2	AXT +2		*ADM1050
IR1	AXT +1		*ADM1060
	TRA 1+4		*ADM1070
ADMCOR	SAVE J+2		*ADM1080
	CLA FLAG		*ADM1090
	TDF FIRST		*ADM1100
	STD TT	0 TO DECR TT	*ADM1110
	LXA BZ+4	N IN 4	*ADM1120
DA	CLA* LG	TEST VALUE+4	*ADM1130
CO	STO +4	PREDICTOR TEST VALUE+4	*ADM1140
	TIX DA+4+1		*ADM1150
	AXT COEFC+4	CORRECTOR TABLE LOC	*ADM1160
	SXA CO+4		*ADM1170
	TSX COMP+4		*ADM1180
	LXA BZ+4	N TO IN 4	*ADM1190
LF	CAL +4	FUNCTION+4	*ADM1200
	ANA =03770000000000	KEEP EXP ONLY	*ADM1210

	SUB	=000200000000	SHIFT EXP	*ADM1220
	UFA*	L6	TEST VALUE+4	*ADM1230
	UFS*	CQ	DEL YC - DEL YP	*ADM1240
	SSP			*ADM1250
	UFA*	CA		*ADM1260
	ANA	=0000777777776	DOUBLING TEST 0 DOUBLE	*ADM1270
	TZE	BP4		*ADM1280
	SKD	TT+4	NO DOUBLE FLAG OVER 0	*ADM1290
BP4	ANA	=00007777777600	HAVING TEST 0 NO HALVE	*ADM1300
	THZ	HALV	NO ZERO HALVE	*ADM1310
DE	TIX	LF+4+1		*ADM1320
	LXA	BZ+4	+M	*ADM1330
	LXD	CNT+1		*ADM1340
	TXL	BP3+1+0		*ADM1350
	TXI	BP4+1+1	REDUCE CNT BY 1	*ADM1360
BP6	SKD	CNT+1	SM	*ADM1370
BP5	LXA	CF+1		*ADM1380
LP	AKT	9+2		*ADM1390
	LDQ*	LD	DERIV+4	*ADM1400
	CLS*	CC	DIFF TABLE+1	*ADM1410
CPR	STO*	CC	DIFF TABLE+1	*ADM1420
	FAD*	CC		*ADM1430
	LRS	35		*ADM1440
CNT	TXH	BP7+2+2		*ADM1450
	LDQ	COEFF	0.	*ADM1460
BP7	TXI	BP4+1+1	NEXT DIFF	*ADM1470
BP8	TIX	CPR+2+1		*ADM1480
	TIX	LF+4+1		*ADM1490
TT	TXL	OUT+4+2	** ZERO DOUBLE	*ADM1500
	AKT	TDBL+6		*ADM1510
	SKA	TY+4		*ADM1520
	TSX	MAT+4		*ADM1530
	LDQ*	CH	M	*ADM1540
	FMP	THAL+1	2.0	*ADM1550
	STO*	CH	M	*ADM1560
OUT	RETURN	ADMCOR		*ADM1570
HALV	AKT	THAL+4	HAVING TABLE	*ADM1580
	SKA	TY+4		*ADM1590
	TSX	MAT+4		*ADM1600
	CLA*	CH	X	*ADM1610
	FSS*	CH	M	*ADM1620
	STO*	CH	X BACKED UP	*ADM1630
	LDQ*	CH	M	*ADM1640
	FMP	TPBL	.5	*ADM1650
	STO*	CH	NEW M	*ADM1660
	TSX	IR2+4	RESTORE IR1,IR2 DESTROYED BY MAT	*ADM1670
	TRA	BF		*ADM1680
FIRST	STL	FLAG	FLAG NOT = ZERO	*ADM1690
	SKA	IR1F+1		*ADM1700
	LXA	BZ+4	M	*ADM1710
	LXA	CF+1	SM	*ADM1720
BP10	CLA*	LD	DERIV+4	*ADM1730
	STO*	CC	DIFF TABLE+1	*ADM1740
	TXI	BP1+1+5		*ADM1750
BP9	TIX	BP10+4+1		*ADM1760
IR1F	AKT	+1		*ADM1770
	TRA	BZ		*ADM1780
MAT	LXA	CF+1	SM	*ADM1790
	SKA	IRAM+4		*ADM1800
TM	AKT	4+4	4	*ADM1810
	AKT	9+2	9	*ADM1820
TV	SKD	TU+4	STORE INA INSHIFT LOC	*ADM1830
	TXI	BP11+1+1	MOVE PAST Y OR PAST DIFF.	*ADM1840
BP11	STZ	TEMP		*ADM1850
TX	LDQ*	CC	DIFF TABLE+1	*ADM1860
TY	FMP	+2	MAT CORP+2	*ADM1870
	FAD	TEMP		*ADM1880
	STO	TEMP		*ADM1890
	TXI	BP12+1+1	MOVE TO NEXT DIFF	*ADM1900
BP12	TXI	BP14+2+1	MOVE TO NEXT COEF	*ADM1910
BP14	TIX	TX+4+1	GO FOR MORE TERMS	*ADM1920
TU	TXI	TZ+1+2	MOVE BACK TO ORIG DIFF	*ADM1930
TZ	STO*	CC	DIFF TABLE+1	*ADM1940
	LXD	TU+4		*ADM1950
	TIX	TV+4+1		*ADM1960
	TIX	TM+1+1	MOVE TO Y TERM OR ALL THROUGH	*ADM1970
IR4M	AKT	+4		*ADM1980
	TRA	1+4		*ADM1990
ADMPAR	SAVE			*ADM2000
	SKA	IR2+2		*ADM2010
	SKA	IR1+1		*ADM2020
	CLA*	3+4		*ADM2030
	FSS*	CH	XP-X	*ADM2040
	FDP*	CH	XP-X /M +P	*ADM2050
	STQ	TEMPA-5	P TO TEMPA-5	*ADM2060
	STZ	TEMPA		*ADM2070
	AKT	-4+4	GENERATE POWERS OF P	*ADM2080
BP16	FMP	TEMPA-5		*ADM2090
	STO	TEMPB-4+4		*ADM2100
	LRS	35		*ADM2110
	TXI	BP15+4+1		*ADM2120
BP15	TXH	BP16+4+0		*ADM2130
	AKT	5+1		*ADM2140
	AKT	CPP+4		*ADM2150
	SKA	TX+4		*ADM2160
	SKA	TZ+4		*ADM2170
	AKT	TPBL+4		*ADM2180
	SKA	TY+4		*ADM2190
	TSX	MAT+1+4	AVOIDS SM TO IN1	*ADM2200
	AKT	CC+4		*ADM2210
	SKA	TX+4		*ADM2220
	SKA	TZ+4		*ADM2230
	AKT	1+1		*ADM2240
	AKT	4+2		*ADM2250
CPP	CLA	TEMPB+1+1		*ADM2260
	STO	TEMPA+2		*ADM2270
	TXI	BP17+1+1		*ADM2280
BP17	TIX	CPP+2+1		*ADM2290
	AKT	TEMPA+4		*ADM2300
	SKA	CO+4		*ADM2310
	AKT	LF+4		*ADM2320
	SKA	CCM+4		*ADM2330
	AKT	CP+4		*ADM2340
	SKA	CM+4		*ADM2350
	TSX	COMP+2+4		*ADM2360
	AKT	LF+4		*ADM2370
	SKA	CM+4		*ADM2380
	AKT	CK+4		*ADM2390
	SKA	CCM+4		*ADM2400
CP	RETURN	ADMPAR		*ADM2410
	PZE	0+4		*ADM2420

FLAG	PZE					*ADM2430
	DEC	1.	1			*ADM2440
	DEC	.5	1/2			*ADM2450
	OCT	177652525253	.4166666667	5/12		*ADM2460
	DEC	.375	3/8			*ADM2470
	OCT	177544764477	.3486111111	251/720		*ADM2480
COEFP	DEC	0.				*ADM2490
	OCT	200515405541	.651388889	469/720		*ADM2500
	OCT	176466026603	.151388889	109/720		*ADM2510
	DEC	.0680555556		49/720		*ADM2520
	OCT	173660266027	.026388889	19/720		*ADM2530
	DEC	0.	.00			*ADM2540
COEFC	OCT	177544764477	.348611111	251/720		*ADM2550
	DEC	.00833333333		6/720		*ADM2560
	DEC	.0625		45/720 = 1/16		*ADM2570
	DEC	.152777778		110/720		*ADM2580
	DEC	.125		90/720 = 1/8		*ADM2590
	DEC	.0416666667		1/24		*ADM2600
	DEC	.166666667		1/6		*ADM2610
	DEC	.166666667		1/6		*ADM2620
	DEC	.166666667		1/6		*ADM2630
	DEC	.25		1/4		*ADM2640
TPBL	DEC	.5				*ADM2650
	DEC	.125				*ADM2660
	DEC	.0625				*ADM2670
	DEC	.0390625				*ADM2680
	DEC	.25				*ADM2690
	DEC	.125				*ADM2700
	DEC	.078125				*ADM2710
	DEC	.125				*ADM2720
	DEC	.09375				*ADM2730
THAL	DEC	.0625				*ADM2740
	DEC	2.				*ADM2750
	DEC	-1.				*ADM2760
	DEC	0				*ADM2770
	DEC	0				*ADM2780
	DEC	4.				*ADM2790
	DEC	-4.				*ADM2800
	DEC	1.				*ADM2810
	DEC	8.				*ADM2820
	DEC	-12.				*ADM2830
TDBL	DEC	16.				*ADM2840
TEMP	BSS	11				*ADM2850
TEMPA	SYN	TEMP+6				*ADM2860
TEMPB	SYN	TEMP+10				*ADM2870
	END					*ADM2880

Report 20672-PIF, Appendix B

```

SIMPTC NOZMIT LIST,M94
SUBROUTINE CCC(DIN,DOUT,WC,CODE,NER)
C*****
C***** THIS PROGRAM WAS WRITTEN FROM A REPORT ON NOZZLE ADMITTANCE*****
C***** THEORY FROM PRINCETON UNIVERSITY. THE ANALYSIS WAS DONE BY*****
C***** CARL LUNDELIUS AND THE PROGRAMMING BY JERRY HOWARD, JOB 8052*****
C*****
C NOZMIT MODIFIED 25 JUL 67 TO SUPPLY CR1,C11 IN PLACE OF BR1,B11.
C*****
C
LOGICAL LOGIK, SL1, SL2, EORJ
COMMON /ARCDF/ EXTRA(100), ABLOK(600)
1 , XX , U2TBL , DESIRE , RAT , RAC , RCC
2 , RCT , ALFA , G , KN , Y , YP
3 , YOUT , TEMP , E , XTABLE , YTABLE , A
4 , R , AM , AP , AMP , Z2 , AMM
5 , AMP2 , CALFA , CTALFA , DELAM , DELTZ , FKN
6 , G1 , G2 , G3 , G4 , JPLAG1 , KMM1
7 , K , NN , P1 , PROD , RSTA1 , RSTA2
8 , SALFA , T1 , T2 , T3 , XINT , XK
9 , ZZ1 , ZZ2 , ZZ3 , A1 , ABC , ABD
COMMON /ABCF/
1 A11 , ALPHA1 , ALPHAR , AR1 , B101 , B102
2 , B10 , B1 , B2 , B3 , B4 , B5
3 , B6 , B7 , B8 , B91 , B92 , B9
4 , B11 , BR1 , C2 , C3 , CWI1 , CHIR
5 , C11 , CR1 , C , D10 , D11 , D1
6 , D2 , D3 , D4 , D5 , D6 , D7
7 , D8 , D9 , DC2 , D , DU2 , EI
8 , ER , F31 , F3R , F1 , FR , H1
9 , H , I , IWO , IW , INW , J
COMMON /ABCF/
1 MDESIR , NK , NP , S2 , S , TY
2 , U2 , U , W2 , W , X101 , X10R
3 , X121 , X12R , X1 , XJ1 , XJR , XMNEW
4 , XMOLD , XNEW , XOLD , XPT , X , Z1
5 , ZR
COMMON /PROLOG/ LOGIK(50), SL1, SL2, EORJ
C
DIMENSION XX(200),U2TBL(200),XTABLE(200),YTABLE(200),ZZ(200)
DIMENSION Y(8),YP(8),YOUT(8),TEMP(72),E(8)
DIMENSION A(200),R(200),AM(200),AP(200),AMP(200)
DIMENSION DIN(1), DOUT(1),WC(1)
C
C*****
C
C
C NER = 0
C *****
C READ INPUT*
C *****
G = DIN(1)
NOMEG=WC(2)+2.0001
MDESIR = DIN(2) + .0001
SEO=.5*(6+1.0)*SQRT(DIN(4)*DIN(7))
IF (CODE) 10,20,30
10 NER = 1
20 RETURN
30 IF(WC(1))40,50,40
40 WCONST=DOUT(3)/(6.2831853*DOUT(1))
GEO=SEO/DOUT(1)
GO TO 60
50 WCONST=DOUT(3)/(6.2831853*DOUT(2))
GEO=SEO/DOUT(2)
60 IF(CODE-99.0)100,100,70
C *****
C PRINT OUT INPUT*
C *****
70 CALL PAGE(5)
WRITE (6,80)
80 FORMAT (1H0,75H PROGRAM C INPUT - CALCULATES NOZZLE ADMITTANCE
1COEFFICIENTS USING 8052 )
WRITE (6,90)G, MDESIR
90 FORMAT (1H0,5X,3H G =,F9.3,11H , MDESIR =,I2 )
100 CONTINUE
C *****
C MDESIR=1,INPUT TABLE,INPUT DESIRE MDESIR=2,CALCULATE TABLE,INPUT*
C DESIRE MDESIR=3,CALCULATE TABLE,CALCULATE DESIRE (AT LAST POINT)*
C *****
GO TO (150,110,110),MDESIR
110 RAT = DIN(4)
RAC = DIN(5)
RCC = DIN(6)
RCT = DIN(7)
ALFA = DIN(8)
KN = DIN(9) + .0001
IF (CODE - 99.0) 140,140,120
120 CALL PAGE (1)
WRITE (6,130)RAT, RAC, RCC, RCT, ALFA, KN
130 FORMAT (1H ,5X5HRAT =,F7.3,6H,RAC =,F7.3,6H,RCC =,F7.3,6H,RCT =,
1 F7.3, 7H,ALFA = F7.3,5H,KN = I4 )
140 CONTINUE
CALL TBLCAL
KN = KN/2 + 1
GO TO 190
C *****
C READ VELOCITY POTENTIAL TABLE, FIRST POINT IS (0,1)*
C *****
150 J = 10
DO 170 I = 1,200
I = I
XX(I) = DIN(J)
U2TBL(I) = DIN(J+1)
J = J+2
IF (I) 170,170,160
160 IF ( XX(I) ) 170,180,180
170 CONTINUE
C *****
C KN = COUNT OF TOTAL NO. OF POINTS IN THE TABLE.*
C *****
180 KN = I - 1
190 IF(CODE-199.0)240,240,200
200 CALL PAGE(70)
WRITE (6,220)
KKK=KN/2+1
DO 210 I=1,KKK
KKK=KKK+1
VOL1=SQRT(U2TBL(I))
VOL2=SQRT(U2TBL(KKK))
WRITE (6,230)I,ZZ(2*I-1),XX(I),VOL1,KKK,ZZ(2*KKK-1),XX(KKK),VOL2
210 CONTINUE

```

Report 20672-PIF, Appendix B

```

220 FORMAT(///,40X, 25HVELOCITY POTENTIAL TABLE ,///,35X, 46H2 = AXIAL PNOZM1210
POSITION IN NOZZLE (INCHES) ,///,35X,39H2 = VELOCITY POTENNOZM1220
TIAL (NONDIMENSIONAL) ,///,35X, 69HV = AXIAL VELOCITY (UNDIMENSIONALNOZM1230
IZED BY SPEED OF SOUND AT THROAT) NOZM1240
A ,///,5X,5HPPOINT,11X,1HZ,16X,1HX,15X,1HV,16X,5HPPOINT,11X,1HZ,16X,1HNOZM1250
5X,16X,1HV,///) NOZM1260
230 FORMAT(6X,13,6X,3(E12.5,5X),6X,13,6X,2(E12.5,5X),E12.5,/) NOZM1270
240 CONTINUE NOZM1280
***** NOZM1290
***** NOZM1300
***** NOZM1310
***** NOZM1320
***** NOZM1330
***** NOZM1340
***** NOZM1350
***** NOZM1360
***** NOZM1370
***** NOZM1380
***** NOZM1390
***** NOZM1400
***** NOZM1410
***** NOZM1420
***** NOZM1430
***** NOZM1440
***** NOZM1450
***** NOZM1460
***** NOZM1470
***** NOZM1480
***** NOZM1490
***** NOZM1500
***** NOZM1510
***** NOZM1520
***** NOZM1530
***** NOZM1540
***** NOZM1550
***** NOZM1560
***** NOZM1570
***** NOZM1580
***** NOZM1590
***** NOZM1600
***** NOZM1610
***** NOZM1620
***** NOZM1630
***** NOZM1640
***** NOZM1650
***** NOZM1660
***** NOZM1670
***** NOZM1680
***** NOZM1690
***** NOZM1700
***** NOZM1710
***** NOZM1720
***** NOZM1730
***** NOZM1740
***** NOZM1750
***** NOZM1760
***** NOZM1770
***** NOZM1780
***** NOZM1790
***** NOZM1800
***** NOZM1810
***** NOZM1820
***** NOZM1830
***** NOZM1840
***** NOZM1850
***** NOZM1860
***** NOZM1870
***** NOZM1880
***** NOZM1890
***** NOZM1900
***** NOZM1910
***** NOZM1920
***** NOZM1930
***** NOZM1940
***** NOZM1950
***** NOZM1960
***** NOZM1970
***** NOZM1980
***** NOZM1990
***** NOZM2000
***** NOZM2010
***** NOZM2020
***** NOZM2030
***** NOZM2040
***** NOZM2050
***** NOZM2060
***** NOZM2070
***** NOZM2080
***** NOZM2090
***** NOZM2100
***** NOZM2110
***** NOZM2120
***** NOZM2130
***** NOZM2140
***** NOZM2150
***** NOZM2160
***** NOZM2170
***** NOZM2180
***** NOZM2190
***** NOZM2200
***** NOZM2210
***** NOZM2220
***** NOZM2230
***** NOZM2240
***** NOZM2250
***** NOZM2260
***** NOZM2270
***** NOZM2280
***** NOZM2290
***** NOZM2300
***** NOZM2310
***** NOZM2320
***** NOZM2330
***** NOZM2340
***** NOZM2350
***** NOZM2360
***** NOZM2370
***** NOZM2380
***** NOZM2390
***** NOZM2400
***** NOZM2410

```

Report 20672-PIF, Appendix B

```

      B3=W*U2
      B4=.25*(W2-U*C2*(G/(G-1.0))*S2)
      B5=.25*(G-1.0)*U2*DU2*W/C2
C
      ABD=Y(7)*Y(7)-Y( 8)*Y( 8)
      YP(7)=(B2*Y(7)-B3*Y( 8)-B4)/B1-ABD
      YP( 8)=(B3*Y(7)+B2*Y( 8)+B5)/B1-2.0*Y(7)*Y( 8)
C
410 YP(1)=.5*(DU2-W*Y(2)/U2)
      YP(2)=.5*W*Y(1)/U2
      D1=-Y(3)*Y(7)+Y(4)*Y( 8)-W*(.5/U2+2.0/((G+1.0)*(1.0-U2)))
      D2=S2*C2*(1.0/(G-1.0))*Y(2)/(2.0*W*U)
      D3=(-W*Y(2)/U2+DU2*(1.0+(G-1.0)*Y(1)/C2))/(2.0*C2)
      YP(3)=D1+D2+D3
C
      D4=-Y(4)*Y(7)-Y(3)*Y( 8)-W*(.5/U2+2.0/((G+1.0)*(1.0-U2)))
      D5=-S2*C2*(1.0/(G-1.0))*U*((1.0-U2)/(2.0*U2)+Y(1)/U2)/(2.0*W)
      D6=(W*Y(1)/U2+DU2*(G-1.0)*Y(2)/C2)/(2.0*C2)
      YP(4)=D4+D5+D6
C
      D7=S2*C2*(1.0/(G-1.0))/(4.0*U)-Y(5)*Y(7)
      D8=Y(6)*Y( 8)-W*(.5/U2+2.0/((G+1.0)*(1.0-U2)))
      YP(5)=D7+D8
C
      ABC=-Y(6)*Y(7)
      YP(6)=ABC-Y(5)*Y( 8)-W*(.5/U2+2.0/((G+1.0)*(1.0-U2)))
C
      CALL ADMCOR
C
420 XMNEW=U/C
      XNEW=X
C
      IF(XMNEW-DESIRE)430,500,440
C *****
C IF OUR CALCULATED MACH NUMBER IS CLOSE ENOUGH TO DESIRE WE WILL STOP*
C *****
430 IF(ABS(XMNEW-DESIRE)-1.E-5)500,500,470
440 IF(XM-XX(KN))450,460,460
450 XNEW = XX(KN)
      GO TO 500
460 XMOLD = XMNEW
      XOLD=XNEW
      GO TO 380
C *****
C PASSED DESIRED MACH NUMBER *
C LINEAR INTERPOLATION TO GET X CORRESPONDING TO DESIRED MACH*
C *****
470 XPT=XOLD+(XNEW-XOLD)/(XMNEW-XMOLD)*(DESIRE-XMOLD)
      XOLD = XNEW
      XMOLD = XMNEW
      XNEW = XPT
      CALL INT4(XTABLE(1),YTABLE(1),XNEW,U2)
      C2 = .5*(G+1.0-U2*(G-1.0))
      C = SQRT(C2)
      U = SQRT(U2)
      XMNEW = U/C
      I = I+1
      IF(I-15)430,480,480
480 WRITE (6,490)
490 FORMAT(72H0 ITERATION-SCHEME DOES NOT CONVERGE AFTER 10 ITERATIONS)
      I = SEE PROGRAMMER)
      GO TO 10
500 CALL ADMPAR(XNEW)
C
C *****
C COMPUTE ADMITTANCE COEFFICIENTS AND PRINT FINAL RESULTS*
C *****
510 CALL INT4D (XTABLE(1),YTABLE(1),XNEW,U2,DU2)
520 C2=.5*(G+1.0-U2*(G-1.0))
      C=SQRT(C2)
      U=SQRT(U2)
C
      DC2=-.5*(G-1.0)*DU2
      D=SQRT(2.0/(G+1.0))*U*C2/((C2/(.5*(G+1.0)))+(1.0*G/(G-1.0)))
      D9=(1.0-U2)*(G+1.0)
      F3R=YOUT(1)/C2
      F3I=YOUT(2)/C2
      XI2R=2.0*YOUT(3)/D9
      XI2I=2.0*YOUT(4)/D9
      XI0R=2.0*YOUT(5)/D9
      XI0I=2.0*YOUT(6)/D9
      ZR=YOUT(7)
      ZI=YOUT( 8)
      ER=C2*XI0R-ZR
      EI=C2*XI0I-ZI
      FR=U2*C2*XI0R-ZR*U2
      FI=U2*C2*XI0I-ZI*U2-.5*W
      DIO=FR*FR+FI*FI
      ARI= D*(ER*FR+EI*FI)/DIO
      AII= D*(EI*FR-ER*FI)/DIO
      IF(I)540,530,540
530 G1=W*C2*SQRT(U/(C2*(1.0/(G-1.0))))
      GO TO 550
540 G1=W*C2*SQRT(U/(C2*(1.0/(G-1.0))))/5
550 BR1= G1*(FR*XI0I+FI*XI0R)/DIO
      BI1= G1*(FR*XI0R+FI*XI0I)/DIO
      HI=U2*C2*SQRT(2.0/(G+1.0))
      XJR=F3I*ZR-F3I*ZI+.5*(1.0-U2)*XI0R+.5*W*XI2I
      XJI=F3I*ZR+F3R*ZI+.5*(1.0-U2)*XI0I-.5*W*XI2R
      CR1 = HI*(XJR+FR+XJI*FI)/DIO
      CI1 = HI*(XJI+FR-XJR*FI)/DIO
C
560 ALPHAR = -ARI/DESIRE
      ALPHA1 = -AII/DESIRE
      CMIR = -CR1/DESIRE
      CTI1 = -CI1/DESIRE
      TT = (W/(5*SQRT(.5*(G+1.0))))/SQRT(U*(.5*(G+1.0)-U2*(G-1.0)/2.0))*
      I(1.0/(G-1.0))
      T1 = ARI*TT - BI1
      T2 = AII*TT + BR1
C
C *****
C CASE IS COMPLETED
C *****
C
      FOR S=0 ADM COEF ARE ALPHA FOR 8005 LONGITUDINAL
C
      FOR S=N ADM COEF ARE T FOR 999 TRANSVERSE
C
      IF(I)580,570,580

```



```

570 DOUT(IWO+1)=ALPHAR                                NOZM3630
DOUT(IWO+101)=ALPHAI                                  NOZM3640
DOUT(IWO)=W/GEO                                         NOZM3650
DOUT(IWO+100)=W/GEO                                     NOZM3660
GO TO 590                                               NOZM3670
580 CONTINUE                                           NOZM3680
DOUT(IW+19)=W/GEO                                       NOZM3690
DOUT(IW+49)=T1                                          NOZM3700
DOUT(IW+79)=T2                                          NOZM3710
DOUT(IW+109)=CR1                                       NOZM3720
DOUT(IW+139)=C11                                       NOZM3730
590 IWO=IWO+2                                           NOZM3740
IF (I CODE - 9.0) 660,660,600                         NOZM3750
600 CONTINUE                                           NOZM3760
KKKN=(2*IW)+1                                          NOZM3770
IF (NOMEG-KKKN)610,620,620                             NOZM3780
610 KKKN=KKKN-1                                         NOZM3790
620 KCOUNT=KCOUNT+4                                    NOZM3800
IF (KCOUNT-KPAGE)640,640,630                          NOZM3810
630 CALL PAGE(70)                                       NOZM3820
WRITE (6,530)                                          NOZM3830
KCOUNT=0                                               NOZM3840
KPAGE=48                                              NOZM3850
640 *****                                           NOZM3860
C PRINT FINAL RESULTS*                               NOZM3870
650 *****                                           NOZM3880
660 WRITE (6,650)NC(1),WC(KKKN),DESIRE,AR1,A11,BR1,B11,CR1,C11,S,W,G,AN NOZM3890
LPMAR,ALPHAI,T1,T2,CHIR,CHII                          NOZM3900
660 FORMAT(2(3X,F7.4,2X,F7.4,3X,F7.4,6E16.5//)        NOZM3910
PCCPS=(WCONST*WC(KKKN))*12.0                         NOZM3920
WRITE (6,670)PCCPS                                    NOZM3930
680 CONTINUE                                           NOZM3940
670 FORMAT(4X,BNFC(CPS)=F10.4//)                     NOZM3950
DOUT(205)=DESIRE                                       NOZM3960
IF(S) 690,680,690                                     NOZM3970
690 DOUT(1)=NP                                          NOZM3980
DOUT(101)=NP                                           NOZM3990
RETURN                                                NOZM4000
DOUT(16)=0.0                                           NOZM4010
DOUT(IW+21)=0.0                                         NOZM4020
DOUT(IW+31)=0.0                                         NOZM4030
DOUT(IW+41)=0.0                                         NOZM4040
DOUT(IW+111)=0.0                                       NOZM4050
DOUT(IW+141)=0.0                                       NOZM4060
RETURN                                                NOZM4070
END                                                    NOZM4080

```

Report 20672-PIF, Appendix B

```

SIBPTC VELPOT LIST,M94
SUBROUTINE TBLCAL
C TBLCAL SUBROUTINE CALCULATES XX VS U2TBL FROM NOZZLE GEOMETRY
C SIMPSON'S RULE IS USED WITH KN INPUT ODD AND CHANGED TO KN/2+1 IN MAIN
C
LOGICAL LOGIK, SL1, SL2, EORJ
COMMON /PROLOG/ LOGIK(10), SL1, SL2, EORJ
C
COMMON /ABCD/ EXTRA(100), ABLOK(600)
1 , XX , U2TBL , DESIRE , RAT , RAC , RCC
2 , RCT , ALFA , G , KN , Y , YP
3 , YOUT , TEMP , E , YTABLE , YTABLE , A
4 , R , AM , AP , AMP , ZZ , AMM
5 , AMP2 , CALFA , CTALFA , DELAM , DELTZ , FKN
6 , G1 , G2 , G3 , G4 , JFLAG1 , KNM1
7 , K , NM , P1 , PROD , RSTA1 , RSTA2
8 , SALFA , T1 , T2 , T3 , XINT , XK
9 , ZZ1 , ZZ2 , ZZ3 , A1 , ABC , ABD
COMMON /ABCD/
1 , A11 , ALPHA1 , ALPHAR , AR1 , B101 , B102
2 , B10 , B1 , B2 , B3 , B4 , B5
3 , B6 , B7 , B8 , B9 , B92 , B9
4 , B11 , BR1 , C2 , C3 , CH1 , CHIR
5 , C11 , CR1 , C , D10 , D11 , D1
6 , D2 , D3 , D4 , D5 , D6 , D7
7 , D8 , D9 , DC2 , D , DU2 , E1
8 , ER , F31 , F3R , F1 , FR , H1
9 , H , I , IWO , IW , IWW , J
COMMON /ABCD/
1 , MDESIR , NK , NP , S , S , TT
2 , U2 , U , W2 , W , X101 , X10R
3 , X121 , X12R , X1 , XJR , XNEW
4 , XNOLD , XNEW , XOLD , XPT , X , Z1
5 , ZR
C
DIMENSION XX(200),U2TBL(200),XTABLE(200),YTABLE(200),ZZ(200)
DIMENSION Y(8),YP(8),YOUT(8),TEMP(72),E(8)
DIMENSION A(200),R(200),AM(200),AP(200),AMP(200)
C
FKN = KN
KNM1 = KN - 1
DELAM = 1.0/(FKN+1.0)
PI = 3.1415927
ZZ(1) = 0.0
C
DO 10 J = 1,200
ZZ(J) = 0.0
A(J) = 0.0
R(J) = 0.0
AMP(J) = 0.0
AM(J) = 0.0
XX(J) = 0.0
U2TBL(J) = 0.0
10 AP(J) = 0.0
C
R(1) = RAT
A(1) = PI*R(1)**2
U2TBL(1) = 1.0
R(KN) = RAC
ALFA = ALFA*.01799329
CALFA = COS(ALFA)
SALFA = SIN(ALFA)
CTALFA = CALFA/SALFA
RSTA1 = RAT+RCT*(1.0-CALFA)
RSTA2 = RAC-RCC*(1.0-CALFA)
ZZ1 = RCT+SALFA
ZZ2 = ZZ1+CTALFA*(RSTA2-RSTA1)
ZZ3 = ZZ2+RCC*SALFA
DELTZ = ZZ3/(FKN-1.0)
C
JFLAG1 = 1
C
DO 80 I = 2,KNM1
ZZ(I) = ZZ(I-1) + DELTZ
GO TO (20,40,60),JFLAG1
20 R(I) = RAT+RCT-SQRT(RCT**2-ZZ(I)**2)
IF(R(I)-RSTA1)70,70,30
30 JFLAG1 = 2
40 R(I) = RSTA1+(RSTA2-RSTA1)*(ZZ(I)-ZZ1)/(ZZ2-ZZ1)
IF(R(I) - RSTA2)70,70,50
50 JFLAG1 = 3
60 R(I) = RAC-RCC+SQRT(RCC**2-(ZZ3-ZZ(I))**2)
70 A(I) = PI*R(I)**2
80 CONTINUE
C
ZZ(KN) = ZZ(KNM1) + DELTZ
A(KN) = PI*RAC**2
AMM = 1.0+ DELAM
G1 = 2.0/(G + 1.0)
G2 = (G - 1.0)/2.0
G3 = (G + 1.0)/(2.0*G - 2.0)
G4 = 1.0/G1
C
DO 90 J = 1,KN
AMM = AMM - DELAM
AM(J) = AMM
AP(J) = (A(J)/AMM)*(G1*(1.0+G2*AMM**2))**G3
90 CONTINUE
C
DO 100 K = 2,KN
CALL INTG(AP(1),AM(1),A(K),AMP(K))
AMP2 = AMP(K)**2
U2TBL(K) = (G4*AMP2)/(1.0+G2*AMP2)
100 CONTINUE
C
DESIRE = AMP(KN)
XINT = 0.0
NM = KN - 2
K = 1
XK = SQRT(G1*RAT/RECT)
PROD = 2.0*XK*DELTZ/3.0
DO 110 J = 1,NM+2
T1 = SQRT(U2TBL(J))
T2 = SQRT(U2TBL(J+1))
T3 = SQRT(U2TBL(J+2))
XINT = XINT + PROD*(T1+.0*T2+T3)
K = K + 1
XX(K) = -XINT/RAT
U2TBL(K-1) = U2TBL(J)
110 CONTINUE

```

Report 20672-PIF, Appendix B

```
      U2TBL(K) = U2TBL(KN)  
C*****  
      RETURN  
      END
```

```
VELP1210  
VELP1220  
VELP1230  
VELP1240
```

Report 20672-PIF, Appendix B

```

SIBFTC LONGIT LIST=494
SUBROUTINE LONGI
C
COMMON /ABCD / DINP(400)
DIMENSION
1 EXTRA(100),DISTL(20),DISTM(20),AMIT(90),
2 TAB(150,3), OMG(150), ALFR(150), ALFI(150), W(27)
EQUIVALENCE
1 (EXTRA(11),GAMMA), (DINP(107), U1BAR 1, (EXTRA(23), W 1,
2 (EXTRA(14),RAC), (EXTRA(15), FLCM), (EXTRA(16),SOUND,CO),
3 (DINP(17),ULM ), (DINP(18),ZK ),
4 (EXTRA(20),ELNOZ), (EXTRA(51),DISTL), (EXTRA(71),DISTM),
5 (DINP(11), EXTRA),
6 (DINP(151),TAB,OMG), (DINP(301),ALFR), (DINP(451),ALFI),
7 (DINP(601),AMIT)
C
C
10 FORMAT (21X F7.1, 11X F10.5, 10X F10.5, 10X F10.5)
20 FORMAT ( / 11X 30M RESULTS FOR LONGITUDINAL MODE //21X7HFC(CPS)
1 15X5HOMEGA14X7HTAU(5)16X1MN )
30 FORMAT ( //8H U1BAR =,E15.8,9X,7HGMMA =,E15.8,3X,7HX =,E15.8,
1X,3HX =,E15.8,4X5HULM =E15.8 )
C
CALL PAGE (60)
NINC = 10
EIN = 1.0E-4
CALL INT4 ( DISTL(1), DISTM(1), ELCH, EDIST )
CALL INTGR ( 0.0, ELCH, X, NINC )
CALL INT4 ( DISTL(1), DISTM(1), K , UOFX )
CALL INTGS ( UOFX, SUMM, EIN, MINC )
XX = 1.0 - SUMM/(EDIST*ELCH)
ULO = ULM / SOUND
WRITE (6,30)U1BAR, GAMMA, ZK, XX, ULM
WRITE (6,20)
U1BAR2=U1BAR*U1BAR
T1BAR=1.0-.5*(GAMMA-1.0)*U1BAR2
C1BAR=SQRT(T1BAR)
ZETA1B=1.0/(T1BAR-GAMMA*U1BAR2*(ZK-1.0))
ASTAR=2.0*C1BAR/(C1BAR**2-U1BAR2)
C
50 NOMEQ = EXTRA(22) + .001
IJ = NOMEQ-1
KK = 1
IK = 5*IJ + 1
DO 60 J = 1, IJ
OMG(KK) = W(IJ)
DELT = 0.2*(W(IJ+1)-W(IJ))
KK = KK+1
DO 60 I = 1, 4
OMG(KK) = OMG(KK-1) + DELT
KK = KK + 1
60 CONTINUE
OMG(KK) = W(NOMEQ)
DO 70 KK = 1, IK
CALL INT4 ( AMIT(1), AMIT(31), OMG(KK), ALFR(KK) )
CALL INT4 ( AMIT(1), AMIT(61), OMG(KK), ALFI(KK) )
70 CONTINUE
DO 130 I = 1, IK
IF ( I .EQ. 51 .OR. I .EQ. 101 ) CALL PAGE ( 60 )
OMEGA=TAB(I,1)
ALPRE=TAB(I,2)
ALPIM=TAB(I,3)
DENB=(C1BAR-U1BAR*ALPRF)**2+U1BAR2*ALPIM*ALPIM
BRE=(C1BAR-C1BAR-U1BAR2*(ALPRE*ALPRE+ALPIM*ALPIM))/DENB
BIN=2.0*C1BAR*U1BAR*ALPIM/DENB
UL=ULO-ZK*XX
ZETA1B=ZETA1B*U1BAR/UL
A=2.0*ZETA1B*U1BAR*GAMMA*ZK/OMEGA
B=T1BAR/GAMMA+U1BAR2/GAMMA
C=2.0*U1BAR*C1BAR/GAMMA
D=1.0+ZETA1B*ZK/OMEGA
PHI=OMEGA*ASTAR*(1.0-XX)
THETA=2.0*OMEGA*XX
SINPHI=SIN(PHI)
COSPHI=COS(PHI)
SINTH=SIN(THETA)
COSTH=COS(THETA)
CR=1.0+BRE*COSPHI-BIN*SINPHI
CI=BIN*COSPHI+BRE*SINPHI
DR=1.0-BRE*COSPHI+BIN*SINPHI
DI=-BIN*COSPHI-BRE*SINPHI
ER=1.0-COSTH
EI= SINTH
FR=1.0+COSTH
FI=-SINTH
CAPI=(FR/GAMMA)*(U1BAR*CR-C1BAR*DR)-(FI/GAMMA)*(U1BAR*CI-C1BAR*DI)
1+(D*B-U1BAR*A)*(ER*CR-EI*CI)+(C1BAR*A-C*D)*(ER*DR-FI*DI)
CAPJ=(FI/GAMMA)*(U1BAR*CR-C1BAR*DR)+(FR/GAMMA)*(U1BAR*CI-C1BAR*DI)
1+(D*B-U1BAR*A)*(ER*CI+EI*CR)+(C1BAR*A-C*D)*(ER*DI+EI*DR)
CAPK=FR*(B*CR-C*DR)-FI*(R*CI-C*DI)
CAPL=FI*(B*CR-C*DR)+FR*(B*CI-C*DI)
DENMN=CAPK*CAPK+CAPL*CAPL
CAPM=(CAPK*CAPI+CAPL*CAPJ)/DENMN
CAPN=(CAPK*CAPJ-CAPL*CAPI)/DENMN
SE=UL*GAMMA*(1.0+ZETA1B-ZETA1R)
T=.5*(CAPM*CAPM+CAPN*CAPN)/CAPM
ZN=T/SE
COSOD=1.0-CAPM/T
SINOD = CAPN /T
OMDEL = ATAN(SINOD/COSOD)
IF ( SINOD) 80,110,110
80 IF (COSOD) 100,100,90
90 OMDEL=6.2831853*OMDEL
GO TO 120
100 OMDEL=3.1415927*OMDEL
GO TO 120
110 IF (COSOD) 100,120,120
120 DELTA=OMDEL/OMEGA
C
NON-DIMENSIONALIZED RESULTS
TAUMS = DELTA*ELCH/SOUND*81.333333
FREQ = OMEGA*SOUND/ELCH*12.0/6.2831853
WRITE (6,10) FREQ, OMEGA, TAUMS, ZN
130 CONTINUE
RETURN
END

```

```

SIBFTC NTAU LIST,M94
SUBROUTINE PFF ( FIN, FOUT, CF, NER, W )
C*****
DIMENSION FIN(1),FOUT(1),A(133),B(133),OMGA(1),XN(1),TAU(1),OMX(1)
1,HTINT(1),MTINT(1)
DIMENSION XNNEW(41),FCCPS(41),W (1)
COMMON /ABCD/ / EXTRA(100), ABLOK(400), A , B, XNNEW, FCCPS
EQUIVALENCE (A(9),ONW),(A(10),OMGA),(A(91),MTRINT),(A(92),MTINT),
1(B(9),XNW),(B(10),OMX),(B(51),TAU),(B(92),XN)
C
C
CONST=FOUT(101)
XNMIN=1000.0
CALL PAGE(70)
CALL DVCHK (K000FX)
DO 20 I=1,133
A(I) =FIN(I)
B(I)=0.0
NER=IPIX(ONW)
XNW=ONW
IF(CF-99.0)70,70,90
30 CALL PAGE (44)
WRITE (6,40)
40 FORMAT (1H0,50H PROGRAM F INPUT SOLVE FOR N(W) AND TAU(W)
1//19X,8H(OMGA)D,9X,6HMTINT,10X,6HMTINT)
DO 50 I =1,40
50 WRITE (6,60)OMGA(I),MTRINT(I), MTINT(I)
60 FORMAT(1H ,10X,3F16.6)
70 CONTINUE
DO 120 I =1,40
XN(I)=(MTRINT(I)*MTRINT(I) + MTINT(I)*MTINT(I))/(2.0*MTRINT(I))
DNOM = XN(I) - MTRINT(I)
CALL QUAD (DNOM,MTINT(I),TAU(I))
TAU(I)=(TAU(I)+A(I)*83.333333)/(A(2)+OMGA(I))
C A(1)=L,A(2)=CO
OMX(I)=OMGA(I)
CALL DVCHK (K000FX)
GO TO (80,90),K000FX
80 NER=0
GO TO 220
90 IF(XN(I))120,120,100
100 IF(XN(I)-XNMIN) 110,120,120
110 XNMIN=XN(I)
IMIN=I
120 CONTINUE
DO 190 I=1,100
FOUT(I) = B(I)
IF ( CF-9.0 ) 180,180,140
140 CALL PAGE (45)
WRITE (6,150)
150 FORMAT(1H0,20H PROGRAM F OUTPUT //21X,7HFC(CPS),13X,8H(OMGA)D,
113X,7HTAU(MS),16X,1HM )
DO 160 I=1,40
FCCPS(I)=CONST*OMX(I)
160 WRITE (6,170)FCCPS(I),OMX(I),TAU(I),XN(I)
170 FORMAT(21X,F7.1 ,11X,F10.5,10X,F10.5,10X,F10.5)
180 HTINT(41) = 0.0
MTRINT(41)=0.0
XN(41)=0.0
OMX(41)=0.0
FCCPS(41)=0.0
190 FORMAT(56X,5HNMIN=F10.5,/36X,8HTAU(MS)=F10.5,/36X,9H(OMGA)D=F10.5,
10.5,/36X,8HFC(CPS)=F10.1)
DO 200 I =1,40
200 CALL INT4D(OMX(I),XN(I),OMX(I),SAVNOT,XNNEW(I))
XNNEW(41)=0.0
CALL INT4(XNNEW(1),OMX(1),0.0,DOMMIN)
FCMIN=CONST*DOMMIN
CALL INT4(FCCPS(1),MTRINT(1),FCMIN,MTR1)
CALL INT4(FCCPS(1),MTINT(1),FCMIN,MT11)
MTRMIN=MTR1*MTR1+MT11*MT11/(2.0*MTR1)
DNOM=MTRMIN-MTR1
CALL QUAD(DNOM,MT11,TAUMIN)
TAUMIN=(TAUMIN+A(1)*83.333333)/(A(2)+DOMMIN)
CALL PAGE (8)
WRITE (6,210)
210 FORMAT(//21X,50H THE FOLLOWING ARE VALUES INTERPOLATED AT SLOPE OFNTAU
1 N=0.0 //)
WRITE (6,190)MTRMIN,TAUMIN,DOMMIN,FCMIN
220 RETURN
END

```

```

SIBFTC QUADR LIST,M94
SUBROUTINE QUAD (A,B,ANGLE)
IF(B) 10,90,80
10 IF(A) 20,30,40
20 ROTATE = 3.1415927
GO TO 110
30 ANGLE = 4.7123890
GO TO 120
40 ROTATE = 6.2831853
GO TO 110
50 IF (A) 60,70,70
60 ANGLE = 3.1415927
GO TO 120
70 ANGLE = 0.0
GO TO 120
80 IF(A) 20,90,100
90 ANGLE = 1.5707963
GO TO 120
100 ROTATE = 0.0
110 ANGLE = ATAN(B/A) + ROTATE
120 RETURN
END

```

```

SIBFTC KORE LIST,M94
SUBROUTINE CORE(X,N,CODE)
DIMENSION X(1)
IF(CODE-900.0)40,10,10
10 CODE=100.0
CALL PAGE(70)
WRITE (6,20)
20 FORMAT(10X,37HINPUT DATA DUMP FOR PROGRAM FAILIER //)
WRITE (6,30)X(1),I=1,N)
30 FORMAT(9X,10(F10.4,2X))
40 RETURN
END

```

Report 20672-PIF, Appendix B

```

SORIGIN      ALODE,REW
$INCLUDE     JECTOR

SIBFTC INJ    LIST,M94
SUBROUTINE INJCTR
C
COMMON /PROLOG/ LOGIK(38), HEAD(12), SL1, SL2, EORJ
COMMON /JECTOR/ EJDATA( 9600)
C
EQUIVALENCE (LOGIK(5),ERUN), (LOGIK(10),JRUN), (LOGIK(9),IRUN)
LOGICAL LOGIK, ERUN, JRUN, SL1, SL2, EORJ, IRUN
DIMENSION HEAD(12)
C
IF ( SL1 ) GO TO 20
DO 10 I = 1, 9600
10  EJDATA(I) = 0.0
SL1 = .TRUE.
GO TO 30
C
20 READ (13) EJDATA
BACKSPACE 13
30 CALL AS138 ( EJDATA, HEAD, NE )
IF ( NE .NE. 1 ) CALL EXIT
WRITE (13) EJDATA
BACKSPACE 13
IF ( .NOT. JRUN ) GO TO 40
CALL JJJ
40 IF ( ERUN .OR. IRUN ) CALL INJDIS
C
50 RETURN
END
INJ 10
INJ 20
INJ 30
INJ 40
INJ 50
INJ 60
INJ 70
INJ 80
INJ 90
INJ 100
INJ 110
INJ 120
INJ 130
INJ 140
INJ 150
INJ 160
INJ 170
INJ 180
INJ 190
INJ 195
INJ 196
INJ 200
INJ 210
INJ 220
INJ 230
INJ 240
INJ 250

SIBFTC JECT   LIST,M94
SUBROUTINE JJJ
C
***** DECK MODIFIED 20 AUG 67 *****
C
DIMENSION THET1(1450), R1(1450), THU(1000)
DIMENSION NELE(1000),X(1000),Y(1000),NTYPEE(1000),R(22)
1,THETA(182),AS(20),WTE(1000),AAX(1000),AAP(1000),MBAND(1000),XMR(
21000),XMUTOT(20),AXTY(200),AFTY(200),XX(1000),YY(1000)
COMMON /JECTOR/ DATA ( 9600)
C
EQUIVALENCE (DATA(3),XM), (DATA(4),XN)
EQUIVALENCE (DATA(1021),THET1), (DATA(2471),R1), (DATA(3921),THU)
EQUIVALENCE (NTYPEE,DATA(2001)), (AXTY,DATA(1001)), (AFTY,DATA(1201))
1, (DATA(1921),XX), (DATA(2921),YY), (DATA(4921),XMUTOT)
C
NERROR=0
SECT=DATA(5)
WT=DATA(9573)
RINJ=DATA(9574)
XMR=DATA(9575)
PFC=DATA(9576)
DFFC=DATA(9577)
NT=DATA(9578)+.0001
POLAR=DATA(9572)
NE=DATA(9571)+.0001
ROX=DATA(9579)
ROF=DATA(9580)
EMUMAX=5.0
PXADJ=1.0
PFADJ=1.0
CDX=DATA(9585)
CDF=DATA(9586)
XFC=DATA(9591)
DXFC=DATA(9592)
PFPC = DATA(9589)/100.0
PXFC = DATA(9590)/100.0
IF (XM .EQ. 0.0) XM = 70.0
IF (XN .EQ. 0.0) XN = 180.0
R=19
R1=6.2831853/4.0
R1=DATA(3221)/20.30+30
ROTATE=3.1415926/SECT
GO TO 40
30 ROTATE=0.0
40 IF (POLAR .EQ. 0.0)
50 IF (SECT=1.0) ROTATE=0.0
60 DO 70 I=1,NE
KK=K+1
NELE(I)=DATA(KK)+.0001
X(I)=DATA(KK+1)
Y(I)=DATA(KK+2)
NTYPEE(I)=DATA(KK+3)+.0001
SAVE=SQRT(X(I)*X(I)+Y(I)*Y(I))
Y(I)=(ATAN(Y(I)/X(I)))+ROTATE
X(I)=SAVE
K=K+4
70 CONTINUE
GO TO 220
80 DO 170 I=1,NF
KK=K+1
NELE(I)=DATA(KK)+.0001
X(I)=DATA(KK+1)
Y(I)=DATA(KK+2)
NTYPEE(I)=DATA(KK+3)+.0001
C
THE FOLLOWING SEGMENT OF CODING REPLACES SUBROUTINE MOVXY...
90 IF ( Y(I) ) 90,130,140
100 IF ( X(I) ) 100,110,120
100 ROTATE = 3.1415927
GO TO 160
110 X(I) = 1.0E-15
120 ROTATE = 6.2831853
GO TO 160
130 ROTATE = 0.0
GO TO 160
140 IF ( X(I) ) 100,150,130
150 X(I) = 1.0E-15
ROTATE = 0.0
160 SAVE = SQRT ( X(I)*X(I)+Y(I)*Y(I) )
SAVE=SQRT(X(I)*X(I)+Y(I)*Y(I))
Y(I)=(ATAN(Y(I)/X(I)))+ROTATE
X(I)=SAVE
K=K+4
170 CONTINUE
GO TO 220
JJJ 10
JJJ 20
JJJ 30
JJJ 40
JJJ 50
JJJ 60
JJJ 70
JJJ 80
JJJ 90
JJJ 100
JJJ 110
JJJ 120
JJJ 130
JJJ 140
JJJ 150
JJJ 160
JJJ 170
JJJ 180
JJJ 190
JJJ 200
JJJ 210
JJJ 220
JJJ 230
JJJ 240
JJJ 250

```

Report 20672-PIF, Appendix B

```

180 IF (SECT-1,0)190,190,200 JECT 990
190 ROTATE=0.0 JECT 900
200 DO 210 I=1,NE JECT 910
      KK=K+1 JECT 920
      NELE(I)=DATA(KK)+.0001 JECT 930
      X(I)=DATA(KK+1) JECT 940
      Y(I)=(DATA(KK+2)*.0174532)+ROTATE JECT 950
      NTYPEE(I)=DATA(KK+3)+.0001 JECT 960
      K=K++ JECT 970
210 CONTINUE JECT 980
C----- JECT 990
C CALCULATING AREAS OF ELEMENTS JECT1000
C----- JECT1010
220 NN=994 JECT1020
      DO 280 I=1,NT JECT1030
      KK=NN+1 JECT1040
      NST=DATA(KK)+.0001 JECT1050
      KK1=KK+1 JECT1060
      JJ=KK1 JECT1070
      NX=DATA(KK1)+.0001 JECT1080
      AXTY(NST)=0.0 JECT1090
      IF (NX)230,250,230 JECT1100
230 DO 240 JX=1,NX JECT1110
      JJ=KK1+JX JECT1120
      AXTY(NST)=AXTY(NST)+(,7853981*(DATA(JJ)*DATA(JJ))) JECT1130
240 CONTINUE JECT1140
250 NN1=JJ+1 JECT1150
      NN=NN1 JECT1160
      NF=DATA(NN1)+.0001 JECT1170
      AFTY(NST)=0.0 JECT1180
      IF (NF)260,280,260 JECT1190
260 DO 270 JF=1,NF JECT1200
      NN=NN1+JF JECT1210
      AFTY(NST)=AFTY(NST)+(,7853981*(DATA(NN)*DATA(NN))) JECT1220
270 CONTINUE JECT1230
280 CONTINUE JECT1240
      AXTOT=0.0 JECT1250
      AFTOT=0.0 JECT1260
      DO 290 I=1,NE JECT1270
      NN=NTYPEE(I) JECT1280
      AAX(I)=AXTY(NN) JECT1290
      AAF(I)=AFTY(NN) JECT1300
      AXTOT=AXTOT+AAX(I) JECT1310
      AFTOT=AFTOT+AAF(I) JECT1320
290 CONTINUE JECT1330
      AXTOT=AXTOT*SECT JECT1340
      AFTOT=AFTOT*SECT JECT1350
C----- JECT1360
C CALCULATING RADII AND ANGLE BOUNDRIES JECT1370
C----- JECT1380
300 NPTS=180.0/SECT JECT1390
      TPS=NPTS JECT1400
      DELTH=THFNL/TPS JECT1410
      AREA = 3.141592 * RINJ**2 JECT1420
      ASECT = AREA/(XM*XM) JECT1430
      R(1) = 0.0 JECT1440
      ANP = ASECT * 180.0 / 3.141592 JECT1450
      DO 310 I = 2,21 JECT1460
      R(I) = SORT ( ANP + R(I-1)**2) JECT1470
310 CONTINUE JECT1480
      R(22) = 0.0 JECT1490
      XNUM=0.0 JECT1500
      NPTS1=NPTS+1 JECT1510
      DO 320 J=2,NPTS1 JECT1520
      XNUM=XNUM+1.0 JECT1530
      THETA(J)=DELTH*XNUM JECT1540
320 CONTINUE JECT1550
C----- JECT1560
C CALCULATING WEIGHT FLOW JECT1570
C----- JECT1580
      WFT1=WT/(XMR+1.0) JECT1590
      WXT1=WT-WFT1 JECT1600
      WFT2=WFT1 JECT1610
      WXT2=WXT1 JECT1620
      IF (PFFC)340,340,330 JECT1630
330 WFT2=WFT1*(1.0-PFFC) JECT1640
340 IF (PXFC)360,360,350 JECT1650
350 WXT2=WXT1*(1.0-PXFC) JECT1660
360 SIGMEN=WT/(3.141592*RINJ*RINJ) JECT1670
370 AXTHMAX=AXTOT JECT1680
      AXTHMIN=AXTOT JECT1690
      AFTHMAX=AFTOT JECT1700
      AFTHMIN=AFTOT JECT1710
380 AFFC=0.0 JECT1720
      AXFC=0.0 JECT1730
      IF (DFFC)400,400,390 JECT1740
390 AFFC=FFC*,785398*DPFFC*DPFFC JECT1750
      AFTHMIN=AFTHMIN-AFFC JECT1760
      AFTHMAX=AFTHMAX-AFFC JECT1770
400 IF (DXFC)420,420,410 JECT1780
410 AXFC=XFC*,785398*DXFC*DXFC JECT1790
      AXTHMIN=AXTHMIN-AXFC JECT1800
      AXTHMAX=AXTHMAX-AXFC JECT1810
420 AXNOM=(AXTHMAX+AXTHMIN)/2.0 JECT1820
      AFNOM=(AFTHMAX+AFTHMIN)/2.0 JECT1830
      IF (DFFC+DXFC)440,440,430 JECT1840
430 WXT2=(WXT2+AXNOM)/(AXNOM+AXFC) JECT1850
      WFT2=(WFT2+AFNOM)/(AFNOM+AFFC) JECT1860
440 XMR1=WXT2/WFT2 JECT1870
450 ETOF=0.0 JECT1880
      ETFF=0.0 JECT1890
      QX=WXT2/AXTOT JECT1900
      QP=WFT2/AFTOT JECT1910
      CALL DVCHK (K000FX) JECT1920
460 DO 480 I=1,NE JECT1940
      NBAND(I)=0 JECT1950
      WFE1=AAF(I)*QF JECT1960
      WXE1=AAX(I)*QX JECT1970
      WTE(I)=WFE1+WXE1 JECT1980
      XMRE(I)=WXE1/WFE1 JECT1990
      ETOF=ETOF+WXE1 JECT2000
      ETFF=ETFF+WFE1 JECT2010
      CALL DVCHK (K000FX) JECT2020
      GO TO (470,480),K000FX JECT2030
470 NBAND(I)=1 JECT2040
480 CONTINUE JECT2050
      ETOF=SECT*ETOF JECT2060
      ETFF=SECT*ETFF JECT2070
      WMRELH=ETOF/ETFF JECT2080
      AXXTY=AXTOT+AXFC JECT2090
      AFTTY=AFTOT+AFFC JECT2100

```

IF T21210
JEC T21212
JEC T21310
JEC T21312
JEC T21410
JEC T21510
JEC T21610
JEC T2170
JEC T2180
JEC T2190
JEC T2200
JEC T2210
JEC T2220
JEC T2230
JEC T2240
JEC T2250
JEC T2260
JEC T2270
JEC T2280
JEC T2290
JEC T2300
JEC T2310
JEC T2320
JEC T2330
JEC T2340
JEC T2350
JEC T2360
JEC T2370
JEC T2380
JEC T2390
JEC T2400
JEC T2410
JEC T2420
JEC T2430
JEC T2440
JEC T2450
JEC T2460
JEC T2470
JEC T2480
JEC T2490
JEC T2500
JEC T2510
JEC T2520
JEC T2530
JEC T2540
JEC T2550
JEC T2560
JEC T2570
JEC T2580
JEC T2590
JEC T2600
JEC T2610
JEC T2620
JEC T2630
JEC T2640
JEC T2650
JEC T2660
JEC T2680
JEC T2690
JEC T2700
JEC T2710
JEC T2720
JEC T2730
JEC T2740
JEC T2750
JEC T2760
JEC T2770
JEC T2780
JEC T2800
JEC T2810
JEC T2820
JEC T2830
JEC T2840
JEC T2850
JEC T2860
JEC T2870
JEC T2880
JEC T2890
JEC T2900
JEC T2910
JEC T2920
JEC T2930
JEC T2940
JEC T2950
JEC T2960
JEC T2970
JEC T2980
JEC T2990
JEC T3000
JEC T3010
JEC T3020
JEC T3030
JEC T3040
JEC T3050
JEC T3060
JEC T3080
JEC T3090
JEC T3100
JEC T3110
JEC T3120
JEC T3130
JEC T3140
JEC T3150
JEC T3160
JEC T3170
JEC T3180
JEC T3190
JEC T3200
JEC T3210
JEC T3220
JEC T322A
JEC T3230
JEC T3240
JEC T3250
JEC T3260
JEC T3270

JECT1210
 JECT12130
 JECT12140
 JECT12150
 JECT12160
 JECT12170
 JECT12180
 JECT12190
 JECT12200
 JECT12210
 JECT12220
 JECT12230
 JECT12240
 JECT12250
 JECT12260
 JECT12270
 JECT12280
 JECT12290
 JECT12300
 JECT12310
 JECT12320
 JECT12330
 JECT12340
 JECT12350
 JECT12360
 JECT12370
 JECT12380
 JECT12390
 JECT12400
 JECT12410
 JECT12420
 JECT12430
 JECT12440
 JECT12450
 JECT12460
 JECT12470
 JECT12480
 JECT12490
 JECT12500
 JECT12510
 JECT12520
 JECT12530
 JECT12540
 JECT12550
 JECT12560
 JECT12570
 JECT12580
 JECT12590
 JECT12600
 JECT12610
 JECT12620
 JECT12630
 JECT12640
 JECT12650
 JECT12660
 JECT12670
 JECT12680
 JECT12690
 JECT12700
 JECT12710
 JECT12720
 JECT12730
 JECT12740
 JECT12750
 JECT12760
 JECT12770
 JECT12780
 JECT12790
 JECT12800
 JECT12810
 JECT12820
 JECT12830
 JECT12840
 JECT12850
 JECT12860
 JECT12870
 JECT12880
 JECT12890
 JECT12900
 JECT12910
 JECT12920
 JECT12930
 JECT12940
 JECT12950
 JECT12960
 JECT12970
 JECT12980
 JECT12990
 JECT13000
 JECT13010
 JECT13020
 JECT13030
 JECT13040
 JECT13050
 JECT13060
 JECT13070
 JECT13080
 JECT13090
 JECT13100
 JECT13110
 JECT13120
 JECT13130
 JECT13140
 JECT13150
 JECT13160
 JECT13170
 JECT13180
 JECT13190
 JECT13200
 JECT13210
 JECT13220
 JECT13222
 JECT13224
 JECT13225
 JECT13230
 JECT13240
 JECT13250
 JECT13260
 JECT13270

Report 20672-PIF, Appendix B

```

      XXX = XXY * ASECT                                JECT3290
      J=J                                                JECT3300
      DO 710 I=1,NE                                     JECT3310
      IF (X(I) .LE. R(J+1) .AND. X(I) .GT. R(J)) TOTW = TOTW + WTE(I) JECT3320
710  CONTINUE                                           JECT3330
      XMUTOT(J) = TOTW*AJ5                               JECT3340
      IF(XMUTOT(J)-XMUMAX)730,730,720                  JECT3350
720  XMUMAX=XMUTOT(J)                                   JECT3360
730  CONTINUE                                           JECT3370
      CALL PAGE(70)                                       JECT3380
      WRITE (6,790)                                       JECT3390
      DO 740 J=1,20                                       JECT3400
      XXMAX=XMUTOT(J)/XMUMAX                             JECT3410
      WRITE (6,750)R(J+1),XMUTOT(J),XXMAX              JECT3420
740  CONTINUE                                           JECT3430
      RETURN                                              JECT3440
750  FORMAT(32X,F6.3,14X,F7.3,13X,F6.4)                JECT3450
760  FORMAT(//,5X,28HA,,,PROPELLANT ORFICE AREAS,/,9X,34HELEMENT TOTAL JECT3460
      1L OXIDIZER AREA =,F11.8,8H SQ. IN.,15X,30HELEMENT TOTAL FUEL JECT3470
      2AREA =,F11.8,8H SQ. IN.,/,9X,34HTOTAL OXIDIZER FILM COOLING AJECT3480
      3REA =,F11.8,8H SQ. IN.,15X,30HTOTAL FUEL FILM COOLING AREA =,F11.8JECT3490
      4,8H SQ. IN.,/,9X,34HINJECTOR TOTAL OXIDIZER AREA =,F11.8,8H SJECT3500
      5, IN.,15X,30HINJECTOR TOTAL FUEL AREA =,F11.8,8H SQ. IN.,/,5XJECT3510
      6,54HB,,,INJECTOR PRESSURE DROPS FOR ABOVE INJECTOR DESIGN,/,9X, JECT3520
      724HOXIDIZER PRESSURE DROP =,F6.1,3HPSI,35X,20HFUEL PRESSURE DROP =JECT3530
      8F6.1,4H PSI,/,5X,7HMC,,,PROPELLANT FLOWS AND INJECTOR VELOCITIJECT3540
      9ES FOR ABOVE INJECTOR DESIGN,/)                  JECT3550
770  FORMAT(//,48X,19HTOTAL WEIGHT FLOW =,F6.1,7H LB/SEC,/,42X,39HAVERAGJECT3560
      1E MIXTURE RATIO OF THE ELEMENTS =,F7.3,/,41X,40HOVERALL MIXTURE RAJECT3570
      2TIO FOR THE INJECTOR =,F7.3,/,9X,34HELEMENT TOTAL OXIDIZER FLOW JECT3580
      3 =,F6.1,7H LB/SEC,21X,26HELEMENT TOTAL FUEL FLOW =,F6.1,7H LB/JECT3590
      4SEC,/,9X,34HTOTAL OXIDIZER FILM COOLING FLOW =,F6.1,7H LB/SEC,21X,JECT3600
      526HTOTAL FUEL FILM COOLING =,F6.1,7H LB/SEC,/,9X,34HINJECTOR TOTAJECT3610
      6L OXIDIZER FLOW =,F6.1,7H LB/SEC,21X,25HINJECTOR TOTAL FUEL FLJECT3620
      7OW=,F7.1,7H LB/SEC,/,9X,37HOXIDIZER OVERALL INJECTION VELOCITY =,FJECT3630
      86.1,7H FT/SEC,18X,33HFUEL OVERALL INJECTION VELOCITY =,F6.1,7H FT/JECT3640
      9SEC,/)                                           JECT3650
780  FORMAT(9X,23HFUEL LOSS COEFFICIENT =,F5.3,/,9X,27HPERCENT FUEL FILJECT3660
      1M COOLING =,F5.1,/,9X,31HPERCENT OXIDIZER FILM COOLING =,F5.1,/,9XJECT3670
      2,38HDIAMETER OF FUEL FILM COOLING ORFICE =,F7.5,75H IN. (NOTE,,THIJECT3680
      35 MIGHT BE AN EQUIVALENT DIAMETER FOR MULTIPLE-ROW COOLING),/,9X,JECT3690
      442HDIAMETER OF OXIDIZER FILM COOLING ORFICE =,F7.5,21H IN. (SEE ABJECT3700
      5OVE NOTE),/,9X,51HNUMBER OF FUEL FILM COOLING ORFICES PER INJECTOJECT3710
      6R =,F5.0,/,9X,54HNUMBER OF OXIDIZER FILM COOLING ORFICES PER INJECJECT3720
      7TOR =,F5.0,/,9X,18HOXIDIZER DENSITY =,F7.2,4H PCF,/,9X,14HFUEL DENJECT3730
      8SITY =,F6.1,4H PCF,/)                          JECT3740
790  FORMAT(//,3X,114HSECTION 4,,RESULTANT FLOW DISTRIBUTION (MU) AS JECT3750
      1A FUNCTION OF ONLY THE RADIUS, I.E., AVERAGE OF MU IN A RADIAL BANJECT3760
      2D, //,32X,6HRADIUS,15X,5HMU(R),11X,13HMU(R)/MU(MAX),/,34X,3HINJECT3770
      3,/)                                              JECT3780
800  FORMAT(13X,13,18X,12,4X,4(10X,F10.5))            JECT3790
810  FORMAT(//,2X, 49HSECTION 2,,, ELEMENT LOCATION AND INJECTION TYPEJECT3800
      1,/,/,11X, 7HELEMENT,15X, 4HTYPE,17X,1HR,17X, 5HTHETA,17X,1HX,19X,1JECT3810
      2HY,/,13X, 3HNO.,18X, 3HNO.,14X, 8H(INCHES),12X, 8H(DEGREE),12X, 8HJECT3820
      3(INCHES),12X,8H(INCHES),/)                      JECT3830
820  FORMAT(//,3X, 74HSECTION 1,,,MISCELLANEOUS INFORMATION FOR INJECJECT3840
      1TOR DESIGNED BY PROJECTS ,/)                  JECT3850
830  FORMAT(//,5X, 46HD,,,,,INPUT INFORMATION USED IN COMPUTATIONS ,/JECT3860
      1/,9X, 23HTOTAL PROPELLANT FLOW =,F6.1,7H LB/SEC,/,9X, 59HTOTAL NUMJECT3870
      2BER OF ELEMENT TYPES (SYMMETRICAL SECTION ONLY) = ,13,/,9X, 54HTOTJECT3880
      3AL NUMBER OF ELEMENTS (SYMMETRICAL SECTION ONLY) = ,14,/,9X, 27HOXJECT3890
      4IDIZER LOSS COEFFICIENT =,F5.3,)              JECT3900
840  FORMAT(//,2X, 78HSECTION 3,,,TYPE DESCRIPTION,ORIFICE AREA, PROPEJECT3910
      1LLANT FLOW, AND MIXTURE RATIO,/,3X, 84HTYPE *----- OXIDIZER JECT3920
      2ORIFICE DATA -----**----- -- FUEL ORIFICE DATA ----- *,/,93X,JECT3930
      3 5HTOTAL,5X, 5HTOTAL,5X, 5HTOTAL,4X, 7HMIXTURE,/,12X, 6HNUMBER,34XJECT3940
      4, 6HNUMBER,33X, 8HOXIDIZER,4X, 4HFUEL,3X,10HPROPELLANT,3X, 5HRATIOJECT3950
      5,/,14X,2HOF,5X, 8HDIAMETER,4X, 4HAREA,6X, 4HFLOW,7X,2HOF,5X, 8MDIAJECT3960
      6METER,4X, 4HAREA,6X, 4HFLOW,6X, 4HAREA,6X, 4HAREA,4X, 9HFLOW RATE,JECT3970
      7,11X, 7HORIFICE,6X,3HIN.,5X, 7H5Q. IN.,4X, 6HLB/SEC,3X, 8HORIFICEJECT3980
      85,5X, 3HIN.,4X, 7H5Q. IN.,4X, 6HLB/SEC,3X, 7H5Q. IN.,3X, 7H5Q. IN,JECT3990
      9,4X, 6HLB/SEC,/)                               JECT4000
850  FORMAT(3X,13,7X,12)                               JECT4010
860  FORMAT(22X,F6.4,3X,F8.6,2X,F8.6)                 JECT4020
870  FORMAT(54X,12)                                    JECT4030
880  FORMAT(62X,F6.4,3X,F8.6,2X,F8.6)                 JECT4040
890  FORMAT(91X,F8.5,2X,F8.5,2X,F8.4,3X,F7.4)         JECT4050
900  FORMAT(91X,F8.5,2X,F8.5,2X,F8.3,2X,8HINFINITY)    JECT4060
910  FORMAT (///10X)5HELEMENT RESULTS )              JECT4070
920  FORMAT (32X15,11XF10.3,10XF10.4,11XF10.4 )      JECT4080
930  FORMAT (//31X7HELEMENT14X6HRADIUS15X5HANGLE11X12HDISTRIBUTION/90X JECT4090
      11HCOEFFICIENT/34X3HNO.35X7HRADIANS15X2HMU// ) JECT4100
      END                                              JECT4110

```

```

91BPTC INJDS LIST,M94
SUBROUTINE INJDIS
C
C ***** DECK MODIFIED 20 AUG 67 *****
C
REAL IPP,IPR,IPT,INTEG,IPX
INTEGER DSCR, TIME
LOGICAL LOGIK, SL1, SL2, EORJ, IRUN
COMMON /PROLOG/ LOGIK(50), SL1, SL2, EORJ
COMMON /JECTOR/ DATA ( 9600)
COMMON GAMMA, NW, WC, AVN, BVN, CVNR, CVNI, CE, CI
DIMENSION
1 U (1000), AVN ( 30), BVN ( 30), CVNR ( 30), INJD 130
2 CVNI ( 30), RR (1000), THATA (1000), FIRST ( 30), INJD 140
3 SECOND ( 30), Z ( 2), WC ( 30), INJD 150
4 IPP(50), OPP(50), IPR(50), OPR(50), IPT(50), OPT(50), INJD 160
5 X (1000), Y (1000) INJD 170
EQUIVALENCE ( IRUN, LOGIK(9) ), INJD 180
1 (E1 ,DATA(1)), (XM ,DATA(3)), INJD 190
2 (XN ,DATA(4)),(V ,DATA(6)),(SVN ,DATA(8)), INJD 200
3 (POO ,DATA(12)), (Z1 ,DATA(15)), INJD 210
4 (RR, X, DATA(1921) ),(THATA, Y, DATA(2921)), INJD 220
5 (U ,DATA(5921)), INJD 230
6 (IPP ,DATA(20)), INJD 240
7 (OPP ,DATA(70)),(IPR ,DATA(120)), (OPR ,DATA(170)), INJD 250
8 (IPT ,DATA(220)),(OPT ,DATA(270)),(IFLP,DATA(9596)), INJD 260
9 (TFLR,DATA(9597)),(TFLT,DATA(9598)) INJD 270
C
10 FORMAT (//12X30RESULTS OF DESCRIBING FUNCTION // 23X10ELEMENT INJD 290
1 6HRADIUS4X5SHANGLE3X10HFRACTIONAL /13X5HOMEGA7X3HNO.7X3H 7X3HRAIDINJD 300
2 4X9FLOW-RATE10X2HFP12X2HFR12X2HFT // ) INJD 310
20 FORMAT (10XF9.4,19.F11.3,F10.4,F11.5,2X3F14.6 I INJD 320
30 FORMAT (// 12X41HRESULTS OF INJECTION DISTRIBUTION EFFECTS // INJD 330
143X5HOMEGA6X3HAVNBX3HBVN7X3HCVN7X3HCVN / 48X316X4HREAL1,6X4HIMAG/ INJD 340
2/ ) INJD 350
40 FORMAT (39X5F10.4 ) INJD 360
50 FORMAT ( 44X5SHALL 4F10.4 ) INJD 370
60 FORMAT ( // 5X39HINPUT TO INJECTION DISTRIBUTION PROGRAM//10X9HCONTINJD 380
15TANT5//14X10HNUMBER OF OMEGAS = 13//14X20HNUMBER OF ELEMENTS =15,INJD 390
1 15H FOR EACH OF 14. 20H SYMMETRIC SECTIONS. INJD 391
2//14X22HRAIDIAL DIVISIONS(XM) = F5.0//14X24HANGULAR DIVISIONS (XN) INJD 400
3=F5.0//14X27HACOUSTIC MODE NUMBER(SVN) =F7.4//14X30HORDER OF BESSEINJD 410
4L FUNCTIONS(IV) = F3.0//14X17HINJECTOR RADIUS =F8.3,5H. IN.//14X32HINJD 420
5SRATIO OF SPECIFIC HEATS(GAMMA) =F7.4//14X39HMAXIMUM PRESSURE AMPLITUDINJD 430
6TUDE RATIO(POO) =F7.3//14X39HTRANSFER FUNCTIONS FOR LINEAR OPERATINJD 440
7ION//20X16HPRESSURE(TFLP) =F7.3//20X23HRAIDIAL VELOCITY(TFLR) =F7.3INJD 450
8//20X27HTANGENTIAL VELOCITY(TFLT) =F7.3 ) INJD 460
70 FORMAT (// 10X17HINPUT FREQUENCIES ) INJD 470
80 FORMAT (// 7X 5F20.4 ) INJD 480
90 FORMAT (//10X19HELEMENT INFORMATION ) INJD 490
100 FORMAT (//31X7HELEMENT14X6HRADIUS15X5SHANGLE11X12HDISTRIBUTION/90X INJD 500
111HCOEFFICIENT/34X3HNO.17X3HIN.15X7HRAIDIAN51X2HNU// ) INJD 510
110 FORMAT (32X15.11XF10.3,10XF10.4,11XF10.4 ) INJD 520
120 FORMAT (1H1//26H TABULAR NONLINEAR EFFECTS//11X8HPRESSURE11X10HCOMINJD 530
1BUSTION12X6HRAIDIAL12X10HCOMBUSTION10X10HTANGENTIAL10X10HCOMBUSTIONINJD 540
2/51X8HVELOCITY32X8HVELOCITY/ 9X 3(12HPERTURBATION19X4HGA1N12X) ) INJD 550
130 FORMAT ( 6(F18.3,2X) ) INJD 560
140 FORMAT (//33X65H***** THESE VALUES PERTAIN TO A STANDING MOINJD 570
1DE ***** ) INJD 580
150 FORMAT (//33X65H***** THESE VALUES PERTAIN TO A SPINNING MOINJD 590
1DE ***** ) INJD 600
160 FORMAT (23X42HTHE VALUE OF IZZIT IS ZERO AND NOT ALLOWED) INJD 610
170 FORMAT(23X45HVALUE OF BESSEL ARGUMENT TOO HIGH OR LOW Z = F10.4) INJD 620
C
180 DSCR = 1 INJD 640
IF ( .NOT. IRUN ) GO TO 190 INJD 650
CE = 100.0 INJD 660
DSCR = 2 INJD 670
GO TO 200 INJD 680
190 NW = 1 INJD 690
WC(1) = 1.0 INJD 700
200 TIME = 1 INJD 710
RINJ = DATA(9574) INJD 720
NE = DATA(9571) + 0.0001 INJD 730
NS = DATA(5) + 0.0001 INJD 731
NUMBR = DATA(9599) + 0.0001 INJD 740
IZZIT = DATA(2) INJD 750
K = V + 0.0001 INJD 760
KK = K + 1 INJD 770
L = 2*K - 1 INJD 780
M = L + 2 INJD 790
N = M + 2 INJD 800
IF ( E1 .LE. 0.0 ) E1 = 0.0001 INJD 810
IF ( NUMBR .LE. 0 ) NUMBR = 10 INJD 820
IF ( CE .LE. 99.0 ) GO TO 260 INJD 830
CALL PAGE ( 70 ) INJD 840
WRITE (6,60) NW,NE,NS,XM,XN,SVN,V,RINJ,GAMMA,POO,TFLP,TFLR,TFLT INJD 850
GO TO (220,210), DSCR INJD 860
210 WRITE (6,70) INJD 870
WRITE (6,80) (WC(IW), IW = 1,NW) INJD 880
220 LINKNT = 0 INJD 890
DO 240 J = 1,NE INJD 900
IF (LINKNT .GT. 0) GO TO 230 INJD 910
CALL PAGE ( 70 ) INJD 920
WRITE (6,90) INJD 930
WRITE (6,100) INJD 940
LINKNT = 50 INJD 950
230 WRITE (6,110) J, RR(J), THATA(J), U(J) INJD 960
LINKNT = LINKNT - 1 INJD 970
240 CONTINUE INJD 980
GO TO (260,250), DSCR INJD 990
250 WRITE (6,120) INJD1000
WRITE (6,130) (IPP(I),OPP(I),IPR(I),OPR(I),IPT(I),OPT(I),I=1,50) INJD1010
CXXXXXXXXXXXXXXXXXXXXXXXXXXXXXXXXXXXXXXXXXXXXXXXXXXXXXXXXXXXXXXXXXXXXXXXXXINJD1020
C RUNNING DESCRIBING FUNCTION IMPLIES THAT THE EXPANSION INJD1030
C COEFFICIENTS AVN, BVN, AND CVN ARE FUNCTIONS OF THE FREQUENCY,OMEGA.INJD1040
C THEREFORE, AN OMEGA LOOP MUST BE ESTABLISHED. OTHERWISE, THIS LOOP INJD1050
C IS GONE THROUGH ONLY ONCE. INJD1060
CXXXXXXXXXXXXXXXXXXXXXXXXXXXXXXXXXXXXXXXXXXXXXXXXXXXXXXXXXXXXXXXXXXXXXXXXXINJD1070
260 DO 470 IW = 1, NW INJD1080
WCR = WC(IW) INJD1090
VCO = POO/(GAMMA*WCR) INJD1100
SUMP = 0.0 INJD1110
SUMR = 0.0 INJD1120
SUMT = 0.0 INJD1130
LINKNT = 0 INJD1140
DO 450 J = 1, NE INJD1150
R = RR(J)/RINJ INJD1160
ETA = U(J)/(XM*KN) INJD1170
C ***** INJD1180
C THE CALL TO BESSEL REQUIRES THE DEFINITION OF THE REAL PORTION INJD1190

```

```

C OF THE ARGUMENT, Z(1), AND THE IMAGINARY PORTION, Z(2), FOR A INJD1200
C GIVEN ORDER V, THE OUTPUT OF BESSEL GIVES J0R(Z1), J0I(Z2), J1R(Z1), INJD1210
C J1I(Z2), ..., JVR(Z1), JVI(Z2). THEREFORE, THE ANSWERS WILL BE INJD1220
C STORED IN THE FOLLOWING FASHION, J(V-1) = FIRST(L), J(V) = INJD1230
C FIRST(M), AND J(V+1) = FIRST(N). INJD1240
C***** INJD1250

      KERR = 0 INJD1260
      Z(1) = SVN*R INJD1270
      Z(2) = 0.0 INJD1280
      CALL BESSEL ( FIRST(1), SECOND(1), KK, Z(1), KERR ) INJD1290
      IF ( KERR ) 270,270,550 INJD1300
270 SIVN = FIRST(M) INJD1310
      DSIVN = ( V*FIRST(M) - Z(1)*FIRST(N) )/R INJD1320
      Z(1) = SVN INJD1330
      Z(2) = 0.0 INJD1340
      CALL BESSEL ( FIRST(1), SECOND(1), KK, Z(1), KERR ) INJD1350
      IF ( KERR ) 280,280,550 INJD1360
280 GO TO (290,320), TIME INJD1370
290 IF ( K ) 300,300,310 INJD1380
300 D = ( FIRST(M)*FIRST(M) + FIRST(L)*FIRST(L) ) / 2.0 INJD1390
      GO TO 320 INJD1400
310 D = ( FIRST(M)*FIRST(M) - FIRST(L)*FIRST(N) ) * 3.14159 / (2.0*DATA(5)) INJD1410
320 IF ( IZZIT ) 330,360,340 INJD1420
CXXXXXXXXXXXXXXXXXXXXXXXXXXXXXXXXXXXXXXXXXXXXXXXXXXXXXXXXXXXXXXXXXXXXXXXXX INJD1430
C IZZIT IS NEGATIVE FOR STANDING MODES AND POSITIVE FOR SPINNING MODES INJD1440
CXXXXXXXXXXXXXXXXXXXXXXXXXXXXXXXXXXXXXXXXXXXXXXXXXXXXXXXXXXXXXXXXXXXXXXXXX INJD1450
330 VT = V*THATA(J) INJD1460
      CVT = COS(VT) INJD1470
      SVT = SIN(VT) INJD1480
      GO TO 350 INJD1490
340 CVT = 1.0 INJD1500
      SVT = 1.0 INJD1510
350 FP = 1.0 INJD1520
      FR = 1.0 INJD1530
      FT = 1.0 INJD1540
      GO TO (420,360), DSCRB INJD1550
360 PO = ABS(POO*SIVN*CVT) INJD1560
      VO = ABS(VOO*DSIVN*CVT) INJD1570
      WO = ABS(WOO*SIVN*V*SVT/R) INJD1580
      A = -9.14199 INJD1590
      B = -A INJD1600
      IF ( TFLP ) 370,380,370 INJD1610
370 SAVEP = 1.0/(3.14159*PO*TFLP) INJD1620
      CALL INTEGR(A,B,PSI,NUMBR) INJD1630
      CPSI = COS(PSI) INJD1640
      IPX = PO*CPSI INJD1650
      CALL INTA(IPT(1), OPP(1), IPX, OPX) INJD1660
      F = OPX*CPSI INJD1670
      CALL INTGS(F,INTEG,E1,MM) INJD1680
      FP = SAVEP*INTEG INJD1690
380 IF ( TFLR ) 390,400,390 INJD1700
390 SAVER = 1.0/(3.14159*VO*TFLR) INJD1710
      CALL INTEGR(A,B,PSI,NUMBR) INJD1720
      CPSI = COS(PSI) INJD1730
      IPX = VO*CPSI INJD1740
      CALL INTA(IPT(1), OPR(1), IPX, OPX) INJD1750
      F = OPX*CPSI INJD1760
      CALL INTGS(F,INTEG,E1,MM) INJD1770
      FR = SAVER*INTEG INJD1780
400 IF ( TFLT ) 410,420,410 INJD1790
410 SAVET = 1.0/(3.14159*VT*TFLT) INJD1800
      CALL INTEGR(A,B,PSI,NUMBR) INJD1810
      CPSI = COS(PSI) INJD1820
      IPX = WO*CPSI INJD1830
      CALL INTA(IPT(1), OPT(1), IPX, OPX) INJD1840
      F = OPX*CPSI INJD1850
      CALL INTGS(F,INTEG,E1,MM) INJD1860
      FT = SAVET*INTEG INJD1870
420 TERMP = ETA*FP*SIVN**2*CVT**2 INJD1880
      SUMP = SUMP + TERMP INJD1890
      TERMR = ETA*FR*SIVN*DSIVN*CVT**2 INJD1900
      SUMR = SUMR + TERMR INJD1910
      TERMT = -ETA*FT*SIVN**2*CVT*V*SVT/R INJD1920
      SUMT = SUMT + TERMT INJD1930
      TIME = 2 INJD1940
      GO TO (450,430), DSCRB INJD1950
430 IF ( LINKNT .GT. 0 ) GO TO 440 INJD1960
      CALL PAGE ( 70 ) INJD1970
      WRITE (6,10) INJD1980
      LINKNT = 50 INJD1990
440 WRITE (6,20) WCR, J, R, THATA(J), ETA, FP, FR, FT INJD2000
      LINKNT = LINKNT - 1 INJD2010
450 CONTINUE INJD2020
      DD = D INJD2030
      IF ( IZZIT .GT. 0 ) DD = D/2.0 INJD2040
      AVN(IW) = SUMP/DD INJD2050
      BVN(IW) = SUMR/DD INJD2060
      IF ( IZZIT .GT. 0 ) GO TO 460 INJD2070
      CVNR(IW) = SUMT/DD INJD2080
      CVNI(IW) = 0.0 INJD2090
      GO TO 470 INJD2100
460 CVNR(IW) = 0.0 INJD2110
      CVNI(IW) = SUMT/DD INJD2120
470 CONTINUE INJD2130
      IF ( CE .LT. 10.0 ) GO TO 530 INJD2140
      CALL PAGE ( 70 ) INJD2150
      WRITE (6,30) INJD2160
      GO TO (480,490), DSCRB INJD2170
480 WRITE (6,50) AVN(1), BVN(1), CVNR(1), CVNI(1) INJD2180
      GO TO 500 INJD2190
490 WRITE (6,40) ( WC(I), AVN(I), BVN(I), CVNR(I), CVNI(I), I=1,NW ) INJD2200
500 IF ( IZZIT ) 510,560,520 INJD2210
510 WRITE(6,140) INJD2220
      GO TO 530 INJD2230
520 WRITE (6,150) INJD2240
530 CONTINUE INJD2250
540 RETURN INJD2260
550 WRITE (6,170) Z(1) INJD2270
      GO TO 540 INJD2280
560 WRITE (6,160) INJD2290
      GO TO 540 INJD2300
      END INJD2310

```

Report 20672-PIF, Appendix B

```

SIGNAP BSS      LIST,REF,DECK
*      MAP
*      PNC      ON
*      ENTRY    BESSEL
*      LBL      BESSEL,X
*      CALL BESSEL (FIRST,SECOND,N,ARG,KODE)
*
*      FIRST = FIRST LOCATION OF ASCENDING STORING SEQUENCE FOR JN(Z),
*              OR IN(Z),
*      SECOND = FIRST LOCATION OF ASCENDING STORING SEQUENCE FOR YN(Z),
*              OR KN(Z),
*      N      = HIGHEST INTEGRAL ORDER DESIRED FOR BOTH JN(Z) AND YN(Z),
*              OR IN(Z) AND KN(Z),
*      ARG    = LOCATION OF Z = X+I*Y WITH X=ARG(1) AND Y=ARG(2),
*      KODE   = +0, COMPUTE JN(Z) AND YN(Z),
*              = -1, COMPUTE IN(Z) AND KN(Z),
*      DIMENSIONS REQUIREMENTS FIRST(300),SECOND(2*N+2),ARG(2)
*
COMMON BSS      20
BESSEL SNA      BSA+4
SNA      BSA+1,1
SNA      BSA+2,2
TXI      BSS1+4,-2
BESS1 CAL      1+4
STA      BSSP+1
CAL      2+4
ALS      18
STD      BSSP+1
LDQ      3+4
STQ      BSSP+2
CAL      5+4
STP      BSSP+1
CLA      4+4
STA      BSS2
ADD      =1
STA      BSS3
BESS2 CLA      =0
LDQ      =,SE-5
TLQ      BSS3
TRA      ERRR1
BESS3 LDQ      =0
TSX      BFFB,4
BESS4 PZE      =0,,00      L(J),L(Y)
PZE      =0      N
TRA      ERRR2      ERROR,,BFBF
PXD      0,0
BS4 AXI      =0,4
AXI      =0,1
AXI      =0,2
STQ      7+4
TRA      1+4
ERRR1 CLA      =1
TRA      BSA
ERRR2 CLA      =2
TRA      BSA
*      REM ALL ORDERS OF THE BESSEL FUNCTIONS Y SUB K TIMES (Z)
*      AND J SUB K TIMES (Z) FOR COMPLEX Z
BFBF STI      BFB1
LDI      1+4
LFT      400000
XCA
SXD      G20+1
SXD      G21+2
SXD      G22+4
STQ      COMMON+15
STQ      COMMON+16
CLA      0
STQ      CL
CLA      8
STQ      CL+1
CLA      TRA1
STQ      8
EFTM
R23 CAL      1+4
STA      BPR1
COM
ACL      L11
STQ      COMMON+17
CLA      2+4
ALS      18
STD      BFR1
CLA      COMMON+15
LDQ      COMMON+16
TSX      BFFB,4
BFR1 PZE      =0,0,,00
G20 TXL      BFBX,0,0
LDQ      COMMON+15
B61 FMP      COMMON+15
STQ      COMMON+5
LDQ      COMMON+16
FMP      COMMON+16
FAD      COMMON+5
FDM      LOC4
STQ      COMMON+5
CLA      COMMON+5
CALL ALQ6(COMMON+5)
TRA      G21+1
G21 TXL      BFBX,0,0
FDM      LOC2
XCA
FAD      OILER
STQ      COMMON+8      RL+GAM
LDQ      COMMON+15
CLA      SMCON
LRS      0
TLQ      R2
TRA      R3
R2 LDQ      COMMON+16
CLA      PIV2
LLS      0
G22 TXL      R4,0,0
R3 CLA      COMMON+16
FDP      COMMON+15
STQ      COMMON
CALL ATAN(COMMON)
LDQ      COMMON+15
TOP      R4
STQ      COMMON
CLA      LPI
LDQ      COMMON+16
LLS      0

```

	FAD	COMMON		BESS1220
	STO	COMMON+9		BESS1230
R4	LXA	COMMON+17.1		BESS1240
	CLA	0+1		BESS1250
	LDO	1+1		BESS1260
	TSX	MULT.4		BESS1270
	STO	COMMON+4		BESS1280
	STO	COMMON+5		BESS1290
	STZ	COMMON+8		BESS1300
	STZ	COMMON+9		BESS1310
	LXD	A38.2		BESS1320
	SXD	B68.2		BESS1330
B63	CLA	LOC1		BESS1340
R10	STO	COMMON+6		BESS1350
	FAD	LOC1		BESS1360
	STO	COMMON+7		BESS1370
	CLA	8+1		BESS1380
B64	FDP	COMMON+7		BESS1390
	STO	COMMON+10		BESS1400
	CLA	4+1		BESS1410
	FDP	COMMON+6		BESS1420
	STO	COMMON+11		BESS1430
	CLA	COMMON+11		BESS1440
B65	FSB	COMMON+10		BESS1450
	FAD	COMMON+8		BESS1460
	STO	COMMON+8		BESS1470
	CLA	9+1		BESS1480
B66	FDP	COMMON+7		BESS1490
	STO	COMMON+11		BESS1500
	CLA	9+1		BESS1510
	FDP	COMMON+6		BESS1520
	STO	COMMON+10		BESS1530
	CLA	COMMON+10		BESS1540
B67	FSB	COMMON+11		BESS1550
	FAD	COMMON+9		BESS1560
	STO	COMMON+9		BESS1570
	CLA	COMMON+6		BESS1580
	FAD	LOC2		BESS1590
	TXI	B68.1,-8		BESS1600
B68	TXH	R10.1,+9		BESS1610
Z60	LDO	COMMON+6		BESS1620
	FMP	LOC2		BESS1630
	FAD	COMMON+4		BESS1640
	XCA			BESS1650
	FMP	TVPI		BESS1660
	LXD	COMMON+17.2		BESS1670
	LXA	COMMON+17.1		BESS1680
	STO	0+2	RVZ	BESS1690
	LDO	COMMON+9		BESS1700
	FMP	LOC2		BESS1710
	FAD	COMMON+5		BESS1720
	XCA			BESS1730
	FMP	TVPI		BESS1740
	STO	1+2	TVZ	BESS1750
	LXD	G22.4		BESS1760
	CLA	2+4		BESS1770
	TZE	EXIT		BESS1780
	TSX	YM2.4		BESS1790
	LXD	G22.4		BESS1800
	CLA	2+4		BESS1810
	LWS	1		BESS1820
	TZE	EXIT		BESS1830
	LLS	1		BESS1840
	COM			BESS1850
	ACL	L1		BESS1860
	ALS	19		BESS1870
	ACL	COMMON+17	-L(VSUBN)	BESS1880
	TXI	AB80.1,-2		BESS1890
AB80	TXI	B71.2,-2		BESS1900
B71	STD	R15		BESS1910
	STD	B75		BESS1920
	CLA	COMMON+16		BESS1930
	LDO	LSIX		BESS1940
	LLS	0		BESS1950
	TLQ	METH2		BESS1960
	CLA	L2		BESS1970
R14	FAD	LOC1		BESS1980
	STO	COMMON+5		BESS1990
	ACL	C2		BESS2000
	STO	COMMON+8		BESS2010
	STZ	COMMON+9		BESS2020
	CLA	COMMON+15		BESS2030
	LDO	COMMON+16		BESS2040
	TSX	DIV.4		BESS2050
	STO	COMMON+8		BESS2060
	STO	COMMON+9		BESS2070
	CLA	0+2		BESS2080
	LDO	1+2		BESS2090
	TSX	MULT.4		BESS2100
	STO	COMMON+8		BESS2110
F21	FSB	0-2.2		BESS2120
	STO	2+2		BESS2130
	CLA	COMMON+8		BESS2140
	FSB	0-1.2		BESS2150
	STO	3+2		BESS2160
	CLA	COMMON+5		BESS2170
	TXI	R15.2,-2		BESS2180
R15	TXH	R14.2,+4		BESS2190
YMX	TXL	EXIT.0,+4		BESS2200
METH2	TSX	YM22.4		BESS2210
	TXI	B74.1,-2		BESS2220
B74	TXI	B75.2,-2		BESS2230
B75	TXH	METH2.2,+4		BESS2240
EXIT	LXD	G22.4		BESS2250
	TRA	BF8		BESS2260
B80	LXD	G21.2		BESS2270
	LXD	G20.1		BESS2280
	CLA	CL		BESS2290
	STO	0		BESS2300
	CLA	CL+1		BESS2310
	STO	8		BESS2320
	TRA	4+4		BESS2330
BFBX	CLA	COMMON+15		BESS2340
	LDO	COMMON+16		BESS2350
	LXD	G22.4		BESS2360
	TXI	B80.4+1		BESS2370
YM2	SXD	YMX.4		BESS2380
	CLA	TVPI		BESS2390
	STO	COMMON+8		BESS2400
	STZ	COMMON+9		BESS2410
	CLA	COMMON+10		BESS2420

Report 20672-PIF, Appendix B

	LDQ	COMMON+16		RE552430
	TSX	DIV+4		RE552440
	STQ	COMMON+6		RE552450
	STQ	COMMON+7		RE552460
	TRA	YMS		RE552470
YM22	SKD	YMX+4		RE552480
YM5	CLA	COMMON+6		RE552490
	LDQ	COMMON+7		RE552500
	STQ	COMMON+8		RE552510
	STQ	COMMON+9		RE552520
	CLA	0+1		RE552530
	LDQ	1+1		RE552540
	TSX	DIV+4		RE552550
	STQ	COMMON		RE552560
	STQ	COMMON+1		RE552570
	CLA	2+1		RE552580
	STQ	COMMON+8		RE552590
	CLA	3+1		RE552600
	STQ	COMMON+9		RE552610
	CLA	0+1		RE552620
	LDQ	1+1		RE552630
	TSX	DIV+4		RE552640
	STQ	COMMON+8		RE552650
	STQ	COMMON+9		RE552660
	CLA	0+2		RE552670
	LDQ	1+2		RE552680
	TSX	MULT+4		RE552690
	STQ	COMMON+3		RE552700
	FSB	COMMON		RE552710
	STQ	2+2		RE552720
	CLA	COMMON+3		RE552730
	FSB	COMMON+1		RE552740
	STQ	3+2		RE552750
	LXD	YMX+4		RE552760
	TRA	1+4		RE552770
LOC4	DEC	4.		RE552780
L11	OCT	1000001		RE552790
OTLER	DEC	.5772156649		RE552800
LSIX	DEC	6.		RE552810
PIV2	DEC	1.570796325		RE552820
LPI	DEC	3.14159265		RE552830
TVPI	DEC	.63661977236		RE552840
CL	BSS	2		RE552850
BF8	LDI	BF81		RE552860
	CLA	1+4		RE552870
	TPL	B80	EXIT	RE552880
	STA	BF82	L(I)	RE552890
	ACL	BF84		RE552900
	STA	BF82+1	L(I)+1	RE552910
	ARS	18		RE552920
	STA	BF83	L(Y)	RE552930
	ACL	BF84		RE552940
	STA	BF83+1	L(Y)+1	RE552950
	CAL	2+4		RE552960
	ADD	BF84		RE552970
	PAX	+1		RE552980
	AXT	0+2		RE552990
BF86	CLS*	BF82+1	-IJ	RE553000
	FSB*	BF83	-RY	RE553010
	XCA			RE553020
	FMP	BF85		RE553030
	STO*	BF83	RK0	RE553040
	CLA*	BF82	RJ	RE553050
	FSB*	BF83+1	-IJ	RE553060
	XCA			RE553070
	FMP	BF85		RE553080
	STO*	BF83+1	IK0	RE553090
	TNX	B80+1,1		RE553100
	TXI	RE553+2,-2		RE553110
RE559	CLS*	BF82	-RJ	RE553120
	FAD*	BF83+1	IY	RE553130
	XCA			RE553140
	FMP	BF85		RE553150
	XCA			RE553160
	CLS*	BF83	-RY	RE553170
	STO*	BF83	RK1	RE553180
	FSB*	BF82+1	-IJ	RE553190
	XCA			RE553200
	FMP	BF85		RE553210
	STO*	BF83+1	IK1	RE553220
	CLS*	BF82		RE553230
	LDQ*	BF82+1		RE553240
	STO*	BF82+1		RE553250
	STO*	BF82		RE553260
	TNX	B80+1,1		RE553270
	TXI	RE556+2,-2		RE553280
BESS6	CLA*	BF82+1	IJ	RE553290
	FAD*	BF83	RY	RE553300
	XCA			RE553310
	FMP	BF85		RE553320
	STO*	BF83	RK2	RE553330
	CLS*	BF82	-RJ	RE553340
	STO*	BF82		RE553350
	FAD*	BF83+1	IY	RE553360
	XCA			RE553370
	FMP	BF85		RE553380
	STO*	BF83+1		RE553390
	CLS*	BF82+1		RE553400
	STO*	BF82+1		RE553410
	TNX	B80+1,1		RE553420
	TXI	RE557+2,-2		RE553430
BESS7	CLA*	BF82	RJ	RE553440
	FSB*	BF83+1	-IJ	RE553450
	XCA			RE553460
	FMP	BF85		RE553470
	XCA			RE553480
	CLA*	BF83	RY	RE553490
	STO*	BF83	RK3	RE553500
	FAD*	BF82+1	IJ	RE553510
	XCA			RE553520
	FMP	BF85		RE553530
	STO*	BF83+1	IK3	RE553540
	CLS*	BF82+1		RE553550
	LDQ*	BF82		RE553560
	STO*	BF82		RE553570
	STO*	BF82+1		RE553580
	TNX	B80+1,1		RE553590
	TXI	BF86+2,-2		RE553600
BF81	PZF	**0	INDICATORS	RE553610
BF82	PZE	**0+2	L(I)	RE553620
	PZE	**0+2		RE553630

BF83	PZE	**0.2	L(Y)	BESS3640
	PZE	**0.2		BESS3650
BF86	DEC	1		BESS3660
BF85	DEC	1.57079633	PI/2	BESS3670
BF7F	STO	COMMON+5		BESS3680
	STQ	COMMON+6		BESS3690
	SXD	XR4.4		BESS3700
	SXD	COMMON+14.2		BESS3710
	SXD	XR1.1		BESS3720
	CLA	0		BESS3730
	STO	LFST		BESS3740
	CLA	8		BESS3750
	STO	LFST+1		BESS3760
	CLA	TRA1		BESS3770
	STO	8		BESS3780
	EPTM			BESS3790
	CLA	1.4		BESS3800
	TPL	A21		BESS3810
	CLS	COMMON+6		BESS3820
	LDQ	COMMON+5		BESS3830
	STQ	COMMON+6		BESS3840
	STO	COMMON+5		BESS3850
A21	CLA	COMMON+5		BESS3860
	LDQ	SMCON		BESS3870
	LLS	0		BESS3880
	TLO	A53		BESS3890
	LDQ	TEN		BESS3900
XR1	TXL	A119.0.8		BESS3910
A53	CLA	COMMON+6		BESS3920
F23	FDP	COMMON+5		BESS3930
A119	CLA	LTN5		BESS3940
	LRS	0		BESS3950
	STO	COMMON+7	TAN(ARG)	BESS3960
	TLO	F1		BESS3970
A22	CLA	COMMON+6		BESS3980
	TSX	HY3P.4		BESS3990
XR4	TXL	ERR2.0.8		BESS4000
	STQ	COMMON+3		BESS4010
	STO	COMMON+4		BESS4020
	CLA	COMMON+5		BESS4030
	CALL	COS(COMMON+5)		BESS4040
	XCA			BESS4050
F74	FMP	COMMON+3		BESS4060
	STO	COMMON+3	R(COS(Z))	BESS4070
	CLA	COMMON+5		BESS4080
	CALL	SIN(COMMON+5)		BESS4090
	XCA			BESS4100
F25	FMP	COMMON+4		BESS4110
	CHS			BESS4120
	STO	COMMON+4	I(COS(Z))	BESS4130
F1	CLA	COMMON+5		BESS4140
	LDQ	COMMON+6		BESS4150
	SSP			BESS4160
	LRS	0		BESS4170
	TLO	A23		BESS4180
A23	XCA			BESS4190
	STO	COMMON+9		BESS4200
	XCA			BESS4210
	FMP	L3V2		BESS4220
	STQ	COMMON+8	3/2P	BESS4230
	LXD	XR4.4		BESS4240
	GAL	1.4		BESS4250
	COM			BESS4260
	ACL	L1		BESS4270
	STA	COMMON	(-J)	BESS4280
	ALS	18		BESS4290
	STD	A10		BESS4300
	CLA	1.4		BESS4310
	ARS	18		BESS4320
	SSP			BESS4330
	ADD	C1		BESS4340
	FAD	C1	FLOATING N	BESS4350
	LDQ	COMMON+8		BESS4360
	TLO	A24		BESS4370
A24	CLA	COMMON+8		BESS4380
	FAD	TEN		BESS4390
	UFA	C1	N PRIME=MAX(3/2P*N)+10	BESS4400
	STO	COMMON+10		BESS4410
	FAD	C1		BESS4420
	STO	COMMON+1		BESS4430
	CAL	COMMON+10		BESS4440
	ALS	1		BESS4450
	COM			BESS4460
	ADW	L1		BESS4470
	ADW	COMMON		BESS4480
	STA	COMMON+2		BESS4490
	ALS	18		BESS4500
	STD	A41	-(J+2NPR+2)	BESS4510
	STD	A32		BESS4520
	STD	A45		BESS4530
	STD	A38		BESS4540
	CLA	COMMON+9		BESS4550
	TZE	BF7X		BESS4560
	CLA	COMMON+6		BESS4570
	SSP			BESS4580
	LDQ	LOC25		BESS4590
	TLO	A68		BESS4600
	CLA	A2		BESS4610
	TRA	A69		BESS4620
A68	CLA	A21		BESS4630
A69	LXA	COMMON+2.1		BESS4640
	STO	2.1		BESS4650
	STO	3.1		BESS4660
	STZ	4.1		BESS4670
	STZ	5.1		BESS4680
	CLA	COMMON+1		BESS4690
	FAD	LOC1		BESS4700
BF7Y	STO	COMMON+1		BESS4710
	ACL	C2		BESS4720
	STO	COMMON+8		BESS4730
	STZ	COMMON+9		BESS4740
	CLA	2.1		BESS4750
	LDQ	3.1		BESS4760
	TSX	MULT.4		BESS4770
	STO	COMMON+8		BESS4780
	STO	COMMON+9		BESS4790
	CLA	COMMON+5		BESS4800
	LDQ	COMMON+6		BESS4810
	TSX	DIV.4		BESS4820
	STO	COMMON+10		BESS4830
FF20	F58	4.1		BESS4840

Report 20672-PIF, Appendix B

	STO	0.1	BE554850
	CLA	COMMON+10	BE554860
	TXI	1.1	BE554870
	TXI	1.1	BE554880
	CLA	COMMON+1	BE554890
	FSR	LOC1	BE554900
	TXI	A10+1.2	BE554910
A10	TXL	BE7Y+1.2	BE554920
	CLA	LTN5	BE554930
A64	LDQ	COMMON+7	BE554940
	LXA	COMMON+1	BE554950
	STZ	COMMON+10	BE554960
	STZ	COMMON+11	BE554970
	TLO	A60	BE554980
	CLA	LF5P4	BE554990
	TRA	A61	BE555000
A60	CLA	LFAD4	BE555010
A61	STO	A62	BE555020
	ACL	L1	BE555030
	STO	A63	BE555040
	CLA	0.1	BE555050
A62	HPR		BE555060
	FAD	COMMON+10	BE555070
	STO	COMMON+10	BE555080
	CLA	1.1	BE555090
A63	HPR		BE555100
	CLA	COMMON+11	BE555110
	TXI	COMMON+11	BE555120
	TXI	A32+1.2	BE555130
A32	TXH	A65+1.2	BE555140
	LXA	COMMON+1	BE555150
	XCA		BE555160
	FMP	LOC1	BE555170
	FSR	1.1	BE555180
	STO	COMMON+11	BE555190
	LDQ	COMMON+10	BE555200
	FMP	LOC2	BE555210
	FSR	0.1	BE555220
	STO	COMMON+10	BE555230
	CLA	COMMON+7	BE555240
	LDQ	LTN5	BE555250
	TLO	A33	BE555260
	CLA	LOC1	BE555270
	STO	COMMON+3	BE555280
	STZ	COMMON+4	BE555290
A33	CLA	COMMON+3	BE555300
	LDQ	COMMON+4	BE555310
	STO	COMMON+8	BE555320
	STO	COMMON+9	BE555330
	CLA	COMMON+10	BE555340
	LDQ	COMMON+11	BE555350
	TSX	DIV+2.4	BE555360
	STO	COMMON+8	BE555370
	STO	COMMON+9	BE555380
A34	CLA	0.1	BE555390
	LDQ	1.1	BE555400
	TSX	MULT+4	BE555410
	STO	0.1	BE555420
	STO	1.1	BE555430
	TXI	A45+1.2	BE555440
A45	TXH	A34+1.2	BE555450
	LXA	COMMON+2.1	BE555460
	LXD	LZ+2	BE555470
A37	STZ	0.1	BE555480
	TXI	A35+2.1	BE555490
A35	TXI	A36+1.2	BE555500
A36	TXH	A37+2.1	BE555510
	LXD	XP4+4	BE555520
	CLA	1.4	BE555530
	TDL	0.7	BE555540
	LXA	COMMON+2	BE555550
A39	CLS	2.2	BE555560
	LDQ	3.2	BE555570
	STO	2.2	BE555580
	STO	3.2	BE555590
	CLS	4.2	BE555600
	STO	4.2	BE555610
	CLS	5.2	BE555620
	STO	5.2	BE555630
	CLS	7.2	BE555640
	LDQ	6.2	BE555650
	STO	7.2	BE555660
	STO	8.2	BE555670
	TXI	A38+2.1	BE555680
A38	TXH	A39+2.1	BE555690
D7	LXD	XR4+4	BE555700
A40	LXD	COMMON+14.2	BE555710
	LXD	XR1+1	BE555720
	CLA	LFST	BE555730
	STO	0	BE555740
	CLA	LFST+1	BE555750
	STO	0	BE555760
	TRA	1.4	BE555770
FDP2	CLA	COMMON+5	BE555780
	LDQ	COMMON+6	BE555790
	LXD	XR4+4	BE555800
	TXI	A40+4.1	BE555810
BF7X	LXA	COMMON+1	BE555820
	CLA	LOC1	BE555830
	STO	0.1	BE555840
A42	STZ	1.1	BE555850
	TXI	A41+1.2	BE555860
A41	TXH	A42+1.2	BE555870
MULX	TXL	D7+0.2	BE555880
DIV	STO	COMMON+10	BE555890
	STO	COMMON+11	BE555900
	SEP		BE555910
	LR5	0	BE555920
	TLO	RP1	BE555930
	XCA		BE555940
	TFF	FRR2	BE555950
	CLA	COMMON+10	BE555960
D30	FDP	COMMON+11	BE555970
D31	STO	COMMON+12	BE555980
D32	FMP	COMMON+12	BE555990
D34	FAD	LOC1	BE556000
	XCA		BE556010
	FMP	COMMON+11	BE556020
	STO	COMMON+13	BE556030
	LDQ	COMMON+12	BE556040
	FMP	COMMON+8	BE556050

D35	FAD	COMMON+9		BESS6060
F31	FDP	COMMON+13		BESS6070
	STQ	COMMON+11		BESS6080
	LDO	COMMON+12		BESS6090
D36	FMP	COMMON+9		BESS6100
	FSR	COMMON+8		BESS6110
DEF	TXL	RR3+0,*		BESS6120
RR1	CLA	COMMON+11		BESS6130
D37	FDP	COMMON+10		BESS6140
D39	STQ	COMMON+12		BESS6150
B88	FMP	COMMON+12		BESS6160
D40	FAD	LOC1		BESS6170
	XCA			BESS6180
	FMP	COMMON+10		BESS6190
	STQ	COMMON+13	DEN	BESS6200
	LDO	COMMON+12		BESS6210
	FMP	COMMON+9		BESS6220
D41	FAD	COMMON+8		BESS6230
F30	FDP	COMMON+13		BESS6240
	STQ	COMMON+11		BESS6250
	LDO	COMMON+12		BESS6260
D42	FMP	COMMON+8		BESS6270
D44	CHS			BESS6280
	FAD	COMMON+9		BESS6290
RR3	FDP	COMMON+13		BESS6300
	CLA	COMMON+11		BESS6310
	TRA	1+4		BESS6320
MULT	STQ	COMMON+10		BESS6330
	STQ	COMMON+11		BESS6340
	FMP	COMMON+9		BESS6350
MT1	STQ	COMMON+12	BD	BESS6360
	LDO	COMMON+11		BESS6370
	FMP	COMMON+8		BESS6380
MT2	STQ	COMMON+11	AD	BESS6390
	LDO	COMMON+10		BESS6400
	FMP	COMMON+8		BESS6410
	FSB	COMMON+12		BESS6420
MT3	STQ	COMMON+12		BESS6430
	LDO	COMMON+10		BESS6440
	FMP	COMMON+9		BESS6450
	FAD	COMMON+11		BESS6460
MT4	XCA			BESS6470
	CLA	COMMON+12		BESS6480
	TRA	1+4		BESS6490
SPILL	STQ	SVE		BESS6500
	STQ	SVE+1		BESS6510
	CLA	0		BESS6520
	LRS	21		BESS6530
	LBT			BESS6540
	TRA	SP1	FAD,FSB,FMP O.F. OR U.F.	BESS6550
	RND		FDP U.F. OR O.F.	BESS6560
	LBT			BESS6570
	TRA	ERR2	OVERFLOW	BESS6580
	LLS	3		BESS6590
	LBT			BESS6600
	TRA	GOK		BESS6610
	LDO	LZ		BESS6620
GOK	TRA*	0		BESS6630
	LDO	SVE+1		BESS6640
	TRA*	0		BESS6650
SP1	LLS	1		BESS6660
	LBT			BESS6670
	TRA	SP2		BESS6680
	TRA	ERR2	O.F.	BESS6690
SP2	LLS	1		BESS6700
	TZE	OK		BESS6710
	CLA	LZ		BESS6720
	TRA*	0		BESS6730
OK	CLA	SVE		BESS6740
	TRA*	0		BESS6750
SVE	BSS	2		BESS6760
IF57	BSS	2		BESS6770
TRA1	TRA	SPILL		BESS6780
CON2	OCT	20077777777		BESS6790
AZ	OCT	14000000000		BESS6800
AZ1	OCT	1004000000000		BESS6810
TEN	DEC	10.		BESS6820
LOC25	DEC	25.		BESS6830
C1	OCT	2330000000000		BESS6840
C2	OCT	10000000000		BESS6850
LOC1	DEC	1.		BESS6860
LZ	PZE	0		BESS6870
L1	DEC	1		BESS6880
L2	DEC	2		BESS6890
LIN5	DEC	.03492		BESS6900
LOC2	DEC	2.		BESS6910
L3V2	DEC	1.5		BESS6920
LFSB4	FSB	4+1		BESS6930
LFAD4	FAD	4+1		BESS6940
SMCON	OCT	10400000000		BESS6950
HY3F	LAS	HY3F1	10 EXP-4	BESS6960
	TRA	HY3F1+3	UNDERFLOW IMPOSSIBLE	BESS6970
HY3F1	TXI	HY3F1+1.0+26531	OCT 1636430..... = 1E-4	BESS6980
	LDO	HY3F2	SMALL ARGUMENT APPROXIMATION	BESS6990
	TRA	2+4		BESS7000
	STQ	COMMON		BESS7010
	SSP			BESS7020
	LDO	HY3F3	B8.028	BESS7030
	TLO	1+4	ERROR	BESS7040
	LDO	HY3F4	LN 2/2	BESS7050
	TLO	HY3FA		BESS7060
	LDO	COMMON		BESS7070
	FMP	COMMON		BESS7080
	STQ	COMMON+1	X SQUARED	BESS7090
	FAD	HY3F5	30	BESS7100
	XCA			BESS7110
	FMP	COMMON+1	X SQ	BESS7120
	FAD	HY3F6	360	BESS7130
	FDP	HY3F7	720	BESS7140
	FMP	COMMON+1	X SQ	BESS7150
	FAD	HY3F2	1	BESS7160
	STQ	COMMON+2	COSH X	BESS7170
	CLA	COMMON+1	X SQ	BESS7180
	FAD	HY3F8	42	BESS7190
	XCA			BESS7200
	FMP	COMMON+1	X SQ	BESS7210
	FAD	HY3F9	840	BESS7220
	FDP	HY3F10	9040	BESS7230
	FMP	COMMON+1	X SQ	BESS7240
	XCA			BESS7250
	FMP	COMMON		BESS7260

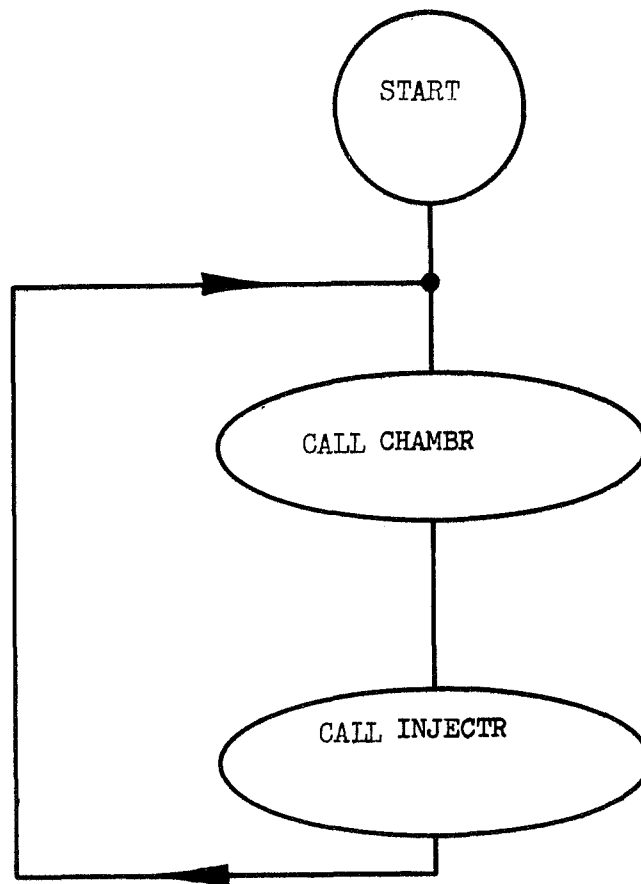
Report 20672-PIF, Appendix B

	FAD	COMMON		HESS7270
	TRA	HY3F7		HESS7280
HY3FA	LRS	27	COMPUTE EXPONENTIAL	HESS7290
	SUR	HY3F11		HESS7300
	STA	BE358		HESS7310
	MPY	HY3F12		HESS7320
BE358	LRS	*		HESS7330
	ALS	27		HESS7340
	STO	COMMON+4		HESS7350
	LRS	4		HESS7360
	STQ	COMMON+1	4.31	HESS7370
	MPY	COMMON+1	4.31	HESS7380
	STQ	COMMON+2	4+4+8.27	HESS7390
	ADD	HY3F13	8.27	HESS7400
	STO	COMMON+3	8.27	HESS7410
	CLA	HY3F14	12.23	HESS7420
	DVP	COMMON+3	8.27	HESS7430
	STQ	COMMON+3	4.31	HESS7440
	LDO	COMMON+2	8.27	HESS7450
	MPY	HY3F15	0.38	HESS7460
	LLS	4	4.31	HESS7470
	SUB	COMMON+3	4.31	HESS7480
	ADD	HY3F16	4.31	HESS7490
	SUR	COMMON+1	4.31	HESS7500
	STO	COMMON+3	4.31	HESS7510
	CLA	COMMON+1	9.31 (2P)	HESS7520
	LDO	HY3F2		HESS7530
	VDP	COMMON+3.0.27		HESS7540
	XCA			HESS7550
	ORA	HY3F17		HESS7560
	FAD	HY3F2		HESS7570
	ADD	COMMON+4		HESS7580
	SUB	HY3F18	EXP X IN AC, DIVIDE BY 2	HESS7590
	STO	COMMON+4		HESS7600
	CLA	HY3F19	1/4	HESS7610
	FDP	COMMON+4	EXP X/2	HESS7620
	STO	COMMON+1	EXP -X 12	HESS7630
	XCA			HESS7640
	FAD	COMMON+4		HESS7650
	STO	COMMON+2		HESS7660
	CLA	COMMON+4		HESS7670
	FSB	COMMON+1	SIN X IN AC	HESS7680
	LDO	COMMON		HESS7690
	LLS	0	SINH X IN AC	HESS7700
HY3FC	LDO	COMMON+2		HESS7710
	TRA	2.4	EXIT	HESS7720
HY3F2	DEC	1.		HESS7730
HY3F3	DEC	88.028		HESS7740
HY3F4	OCT	177542710900	LN 2/2, ERROR = 0.0000000095	HESS7750
HY3F5	DEC	90.		HESS7760
HY3F6	DEC	360.		HESS7770
HY3F7	DEC	720.		HESS7780
HY3F8	DEC	42.		HESS7790
HY3F9	DEC	840.		HESS7800
HY3F10	DEC	5040.		HESS7810
HY3F11	OCT	242		HESS7820
HY3F12	DEC	1.442695040981		HESS7830
HY3F13	DEC	87.41749720288	A	HESS7840
HY3F14	DEC	617.9722695812	B	HESS7850
HY3F15	DEC	0.0346373590380	C	HESS7860
HY3F16	DEC	9.954595787184	D	HESS7870
HY3F17	OCT	201000000000		HESS7880
HY3F18	OCT	10000000000		HESS7890
HY3F19	DEC	0.25		HESS7900
	END			HESS7910

SENTRY V8050

SDATA

"MAIN" PROGRAM, DECK = V8050

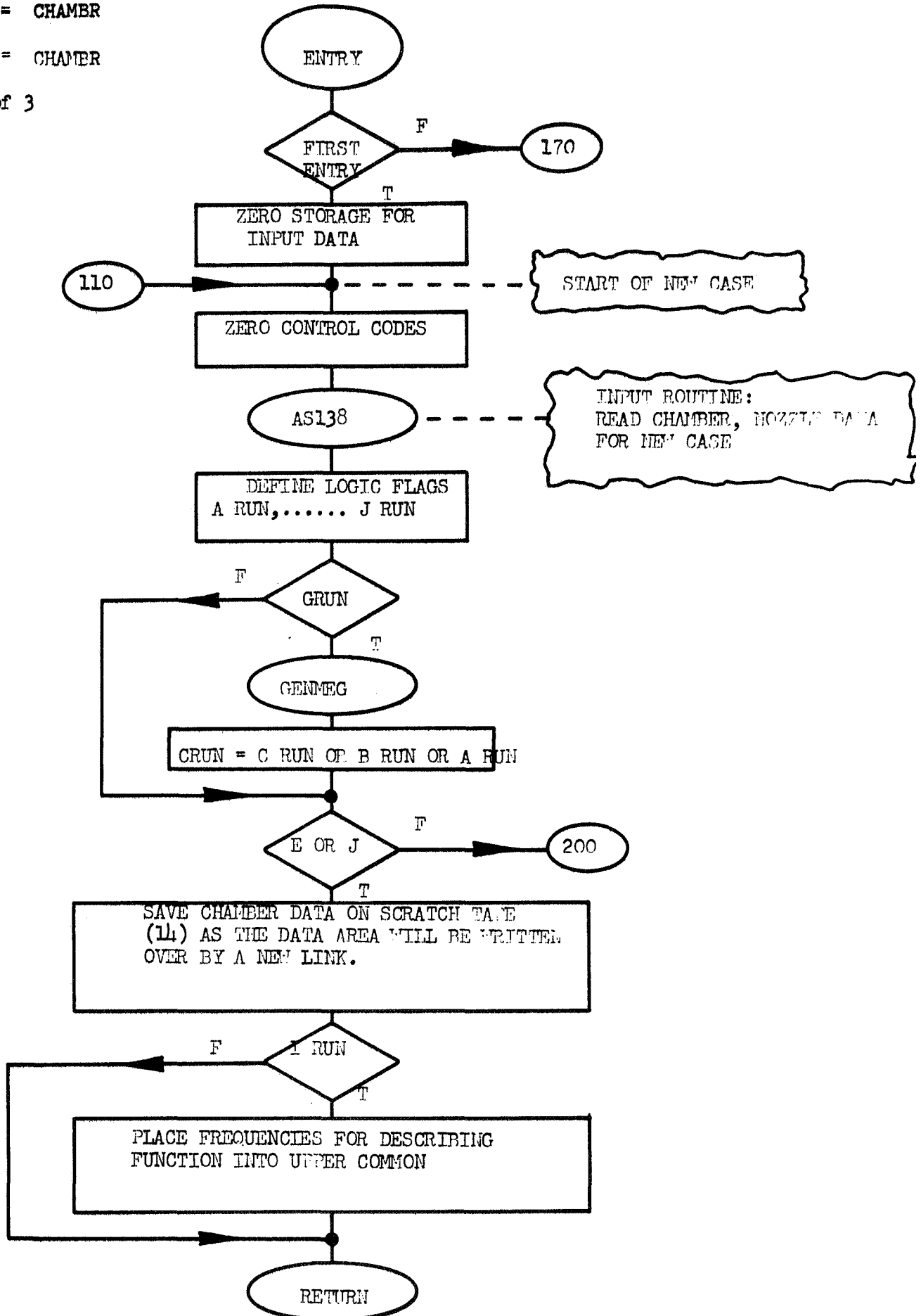


NOTE: SUBROUTINE CHAMBER PERFORMS MOST OF THE LOGICAL AND CONTROL FUNCTIONS OF AN AUTONOMOUS MAIN PROGRAM. CONTROL IS RETURNED TO THIS PROGRAM IF AND ONLY IF AN INJECTOR ROUTINE IS REQUIRED.

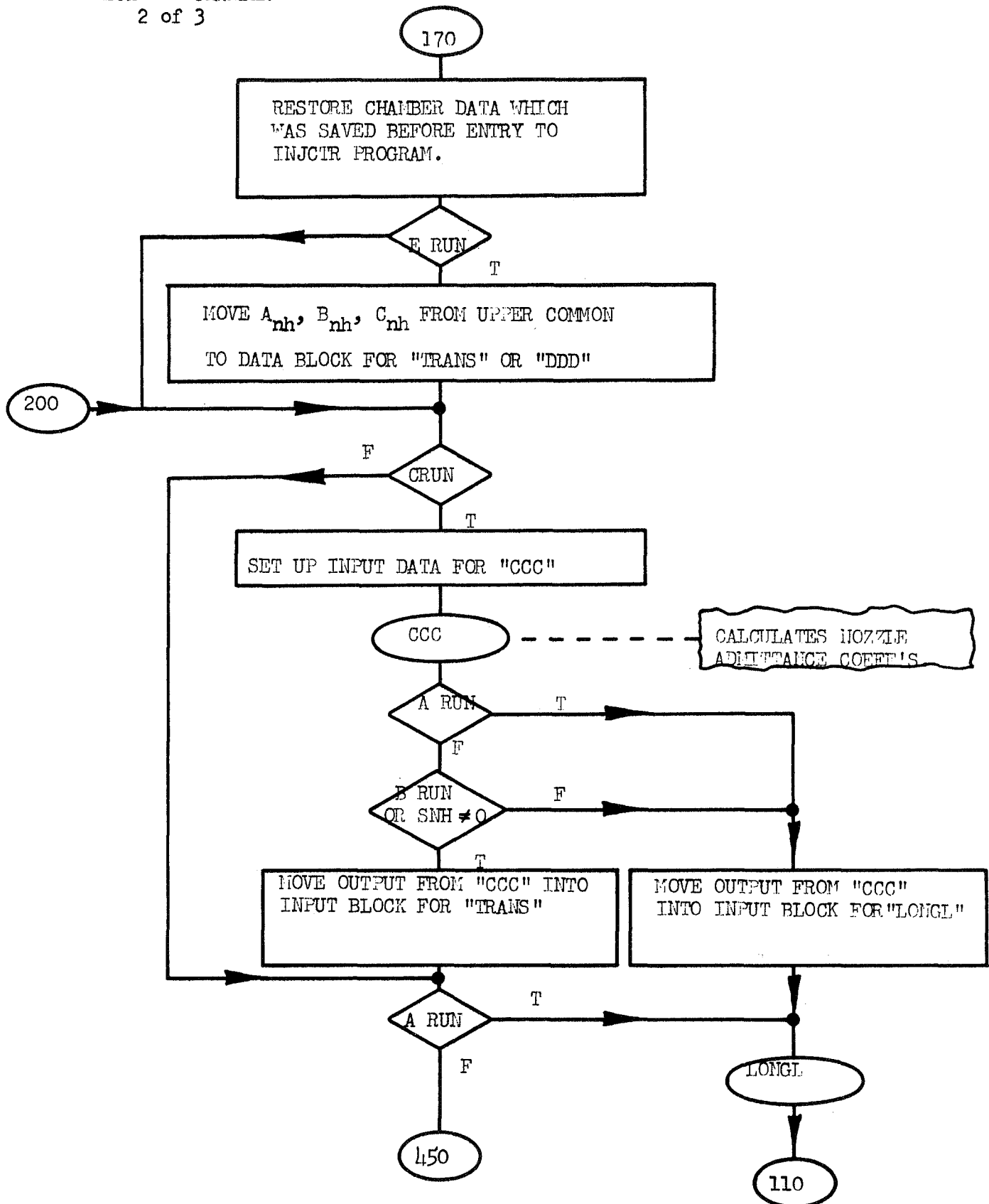
ENTRY = CHAMBR

DECK = CHAMER

1 of 3

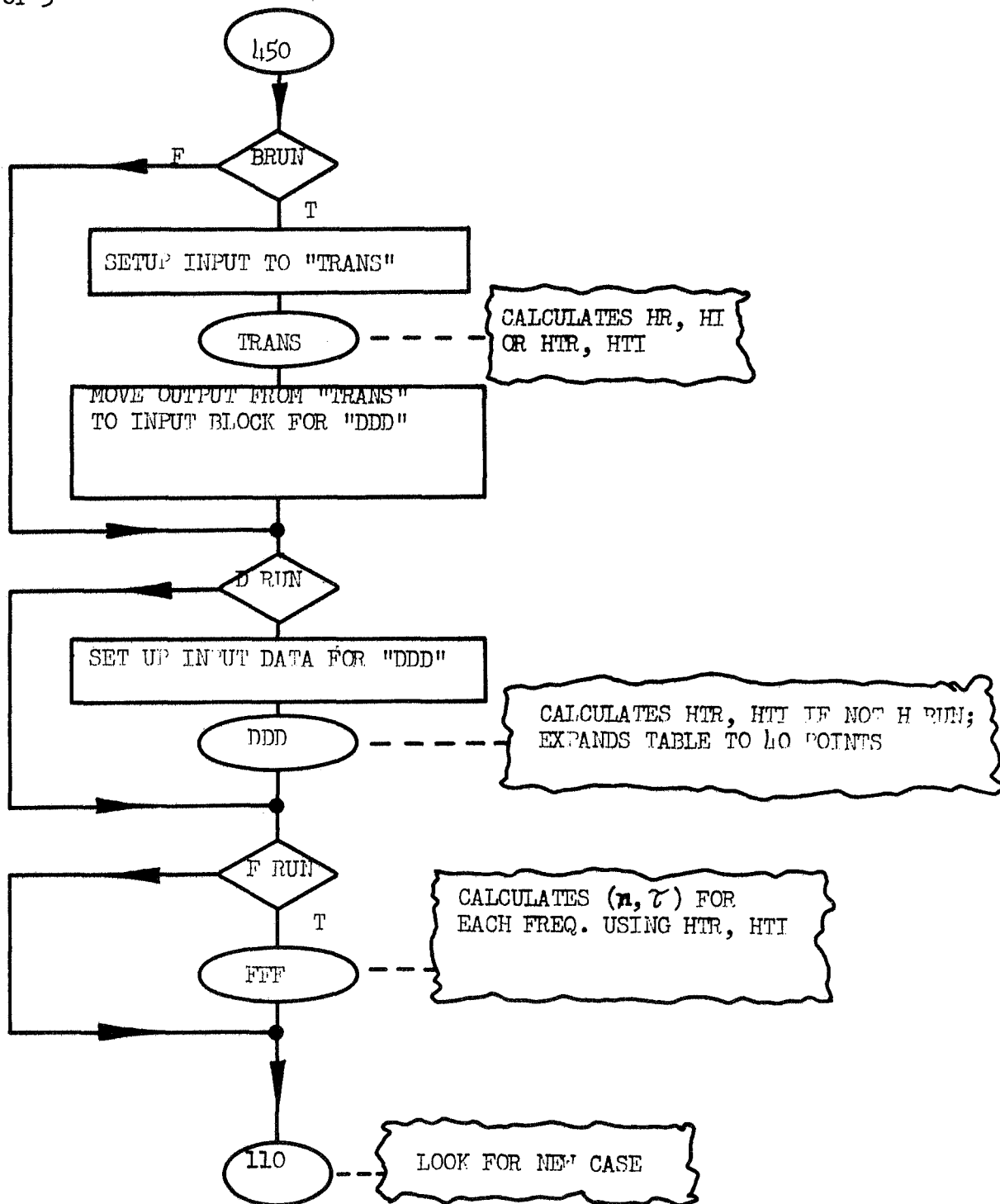


DECK = CHAMBER
2 of 3



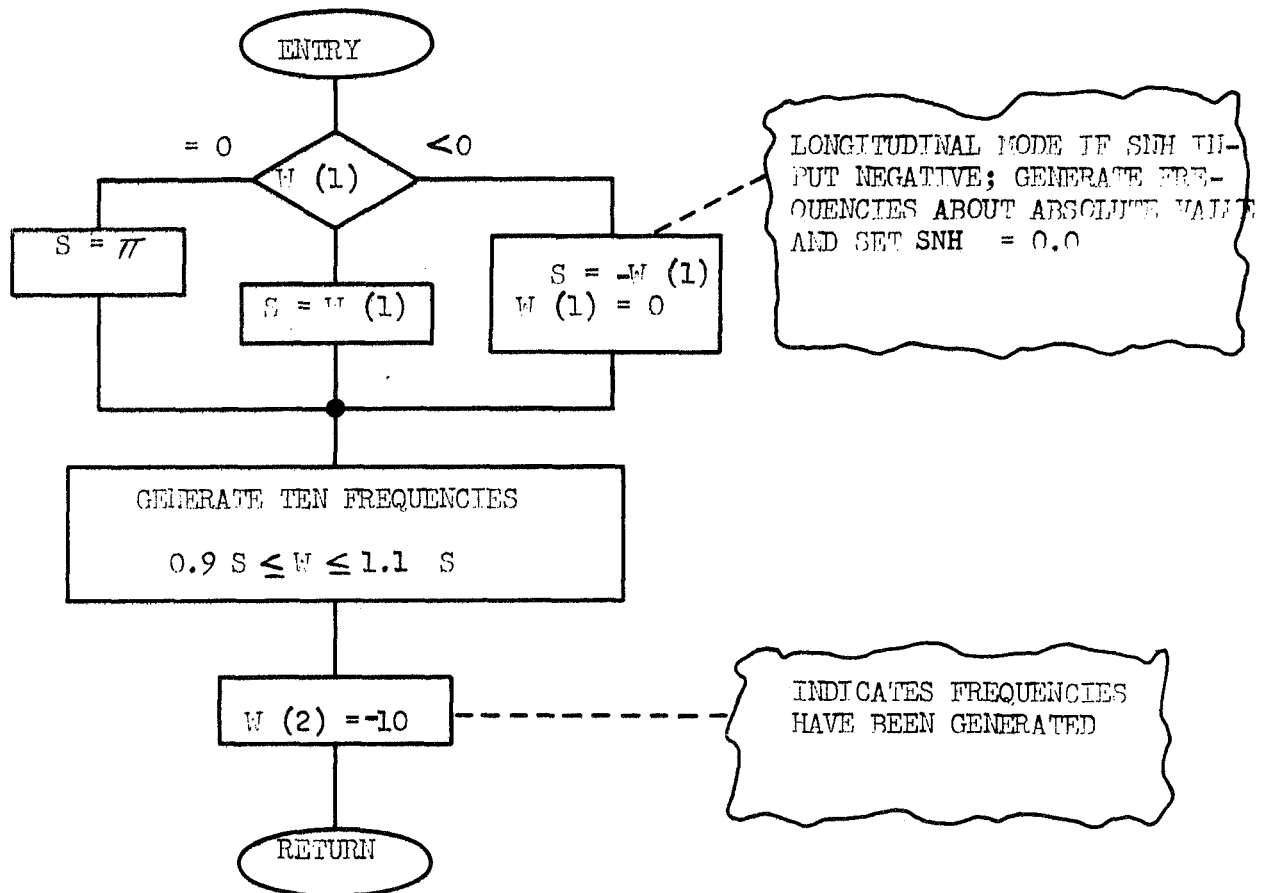
DECK = CHAMBER

3 of 3



ENTRY = GEMMEG

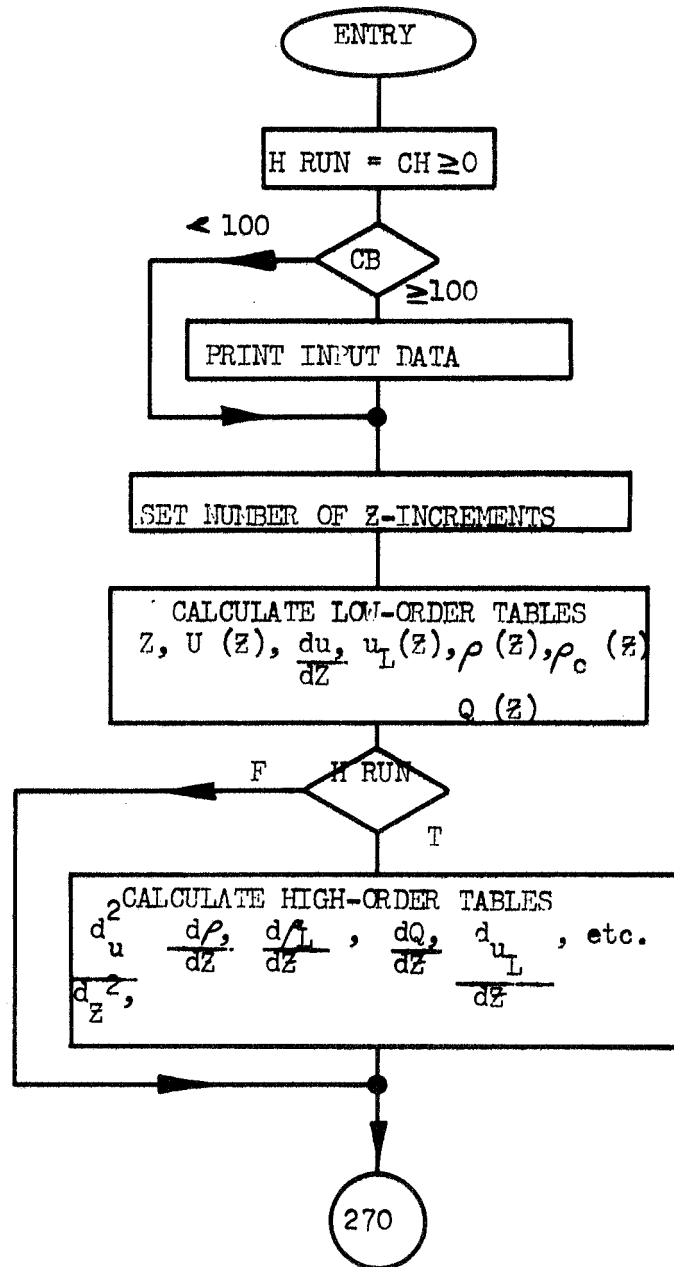
DECK = WGEN



ENTRY = TRANS

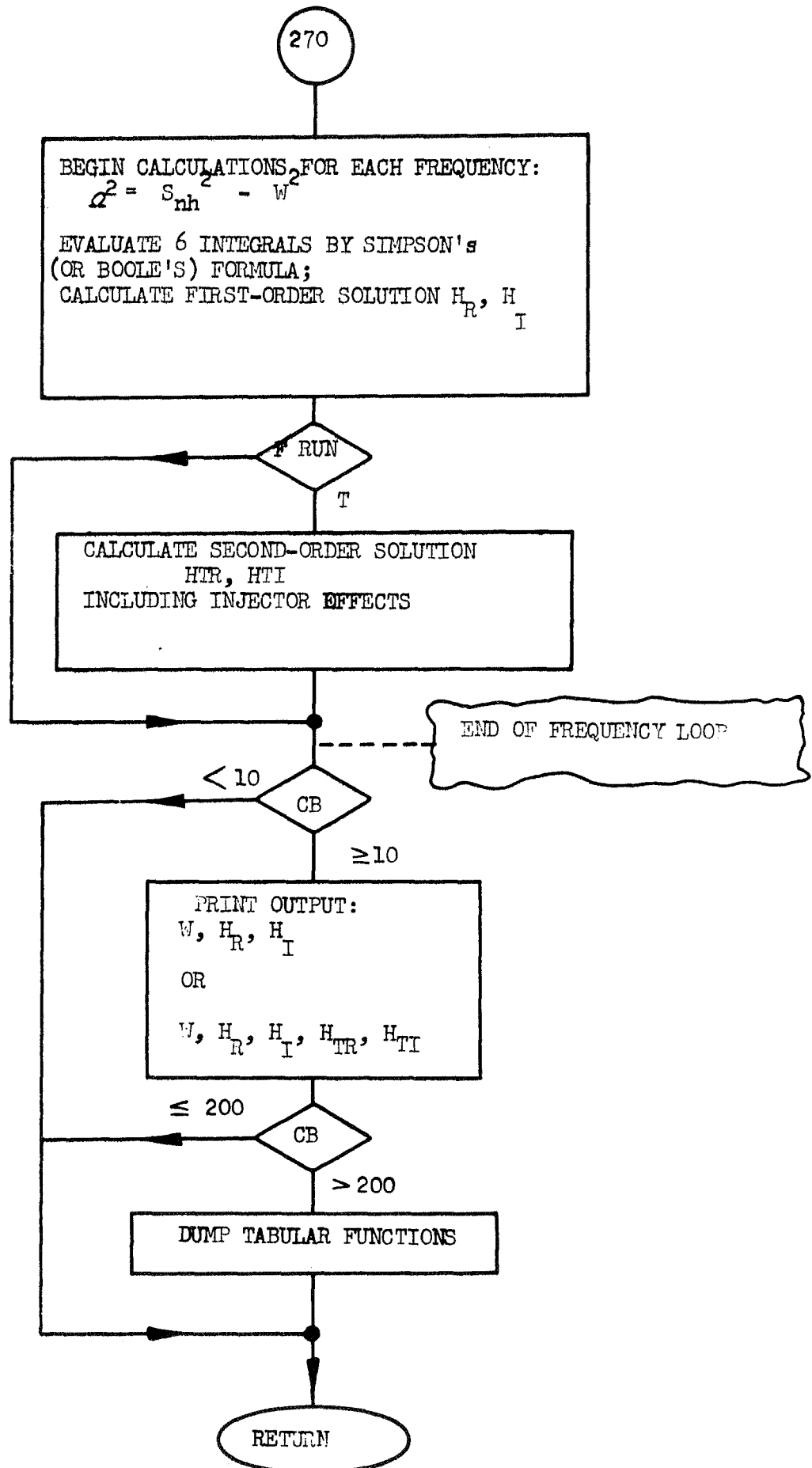
DECK = HYMN

1 of 2

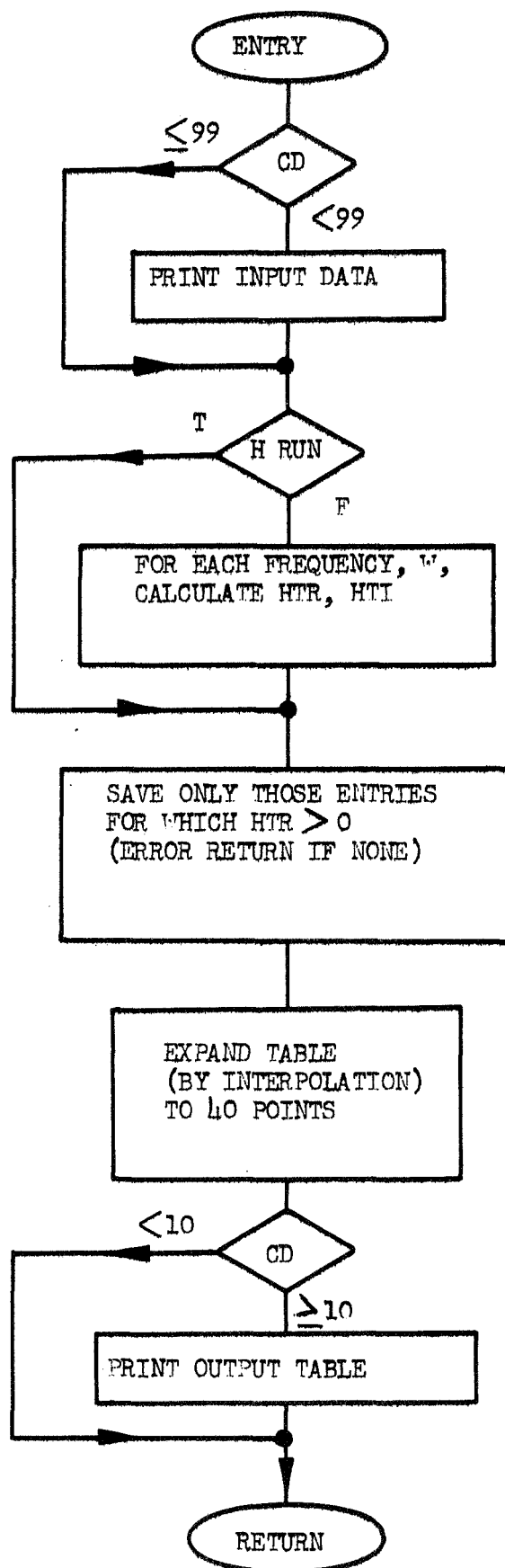


DECK = HYMN

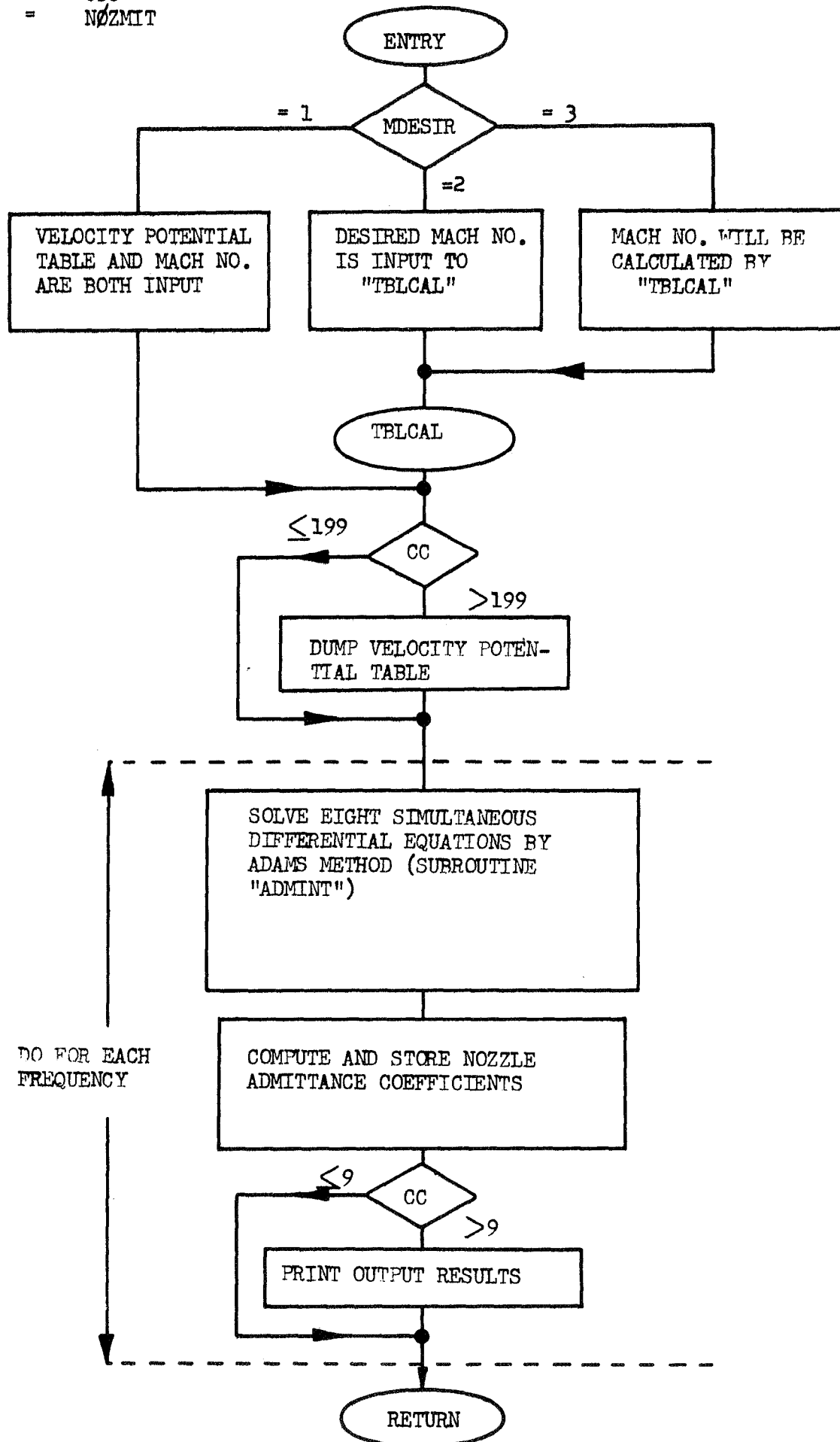
2 of 2



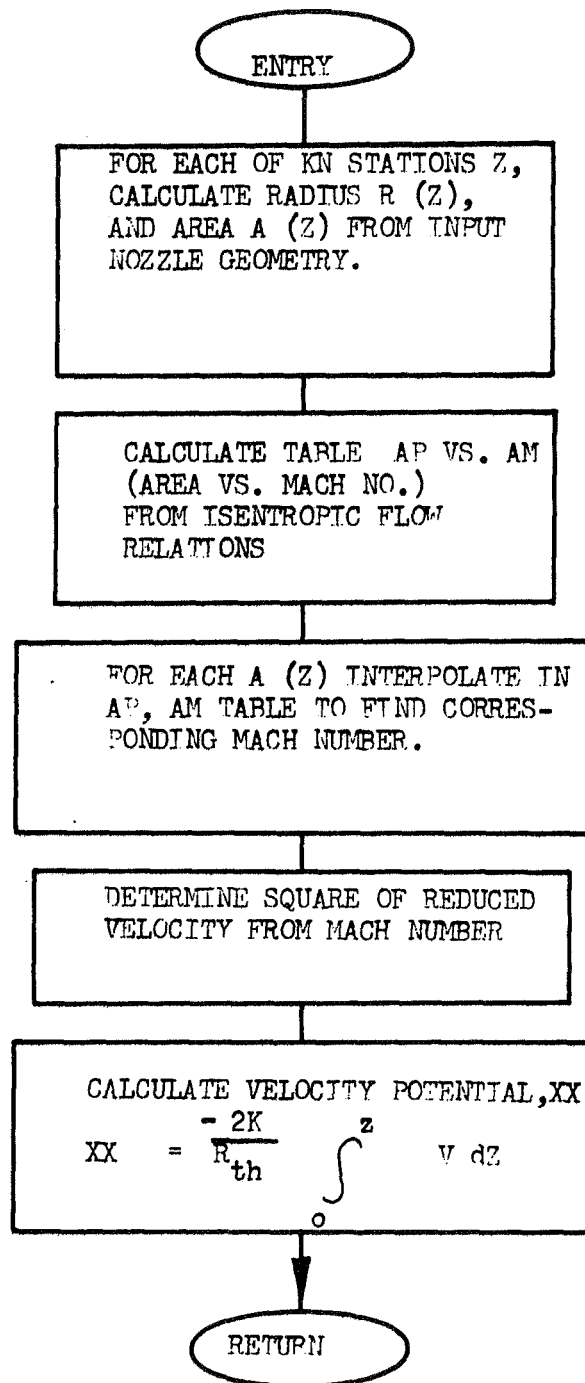
ENTRY " DDD
DECK " HTINT



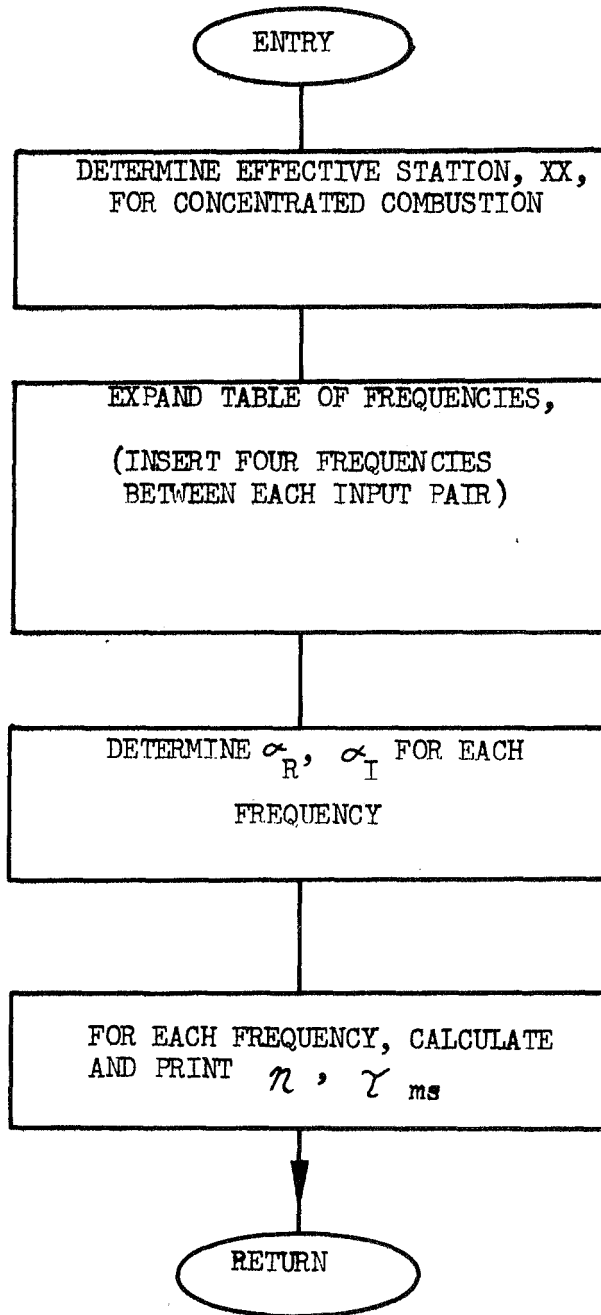
ENTRY = CCC
DECK = NOZMIT



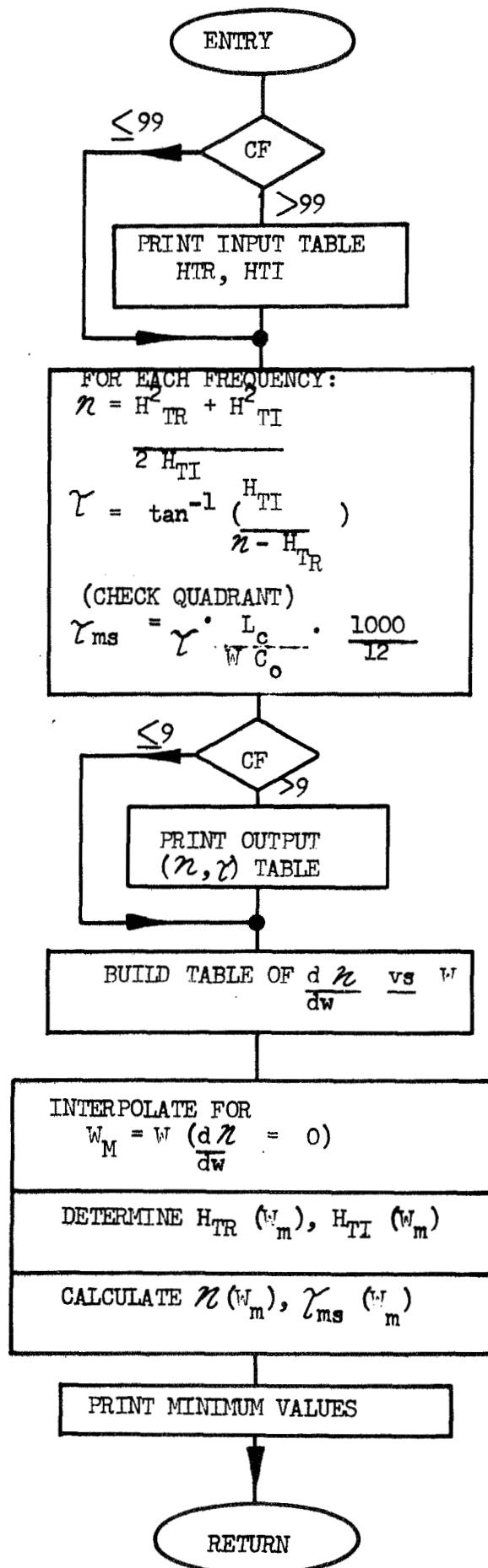
ENTRY = TELCAL
DECK = VELPOT



ENTRY = ~~L~~ONGL
DECK = ~~L~~ONGIT

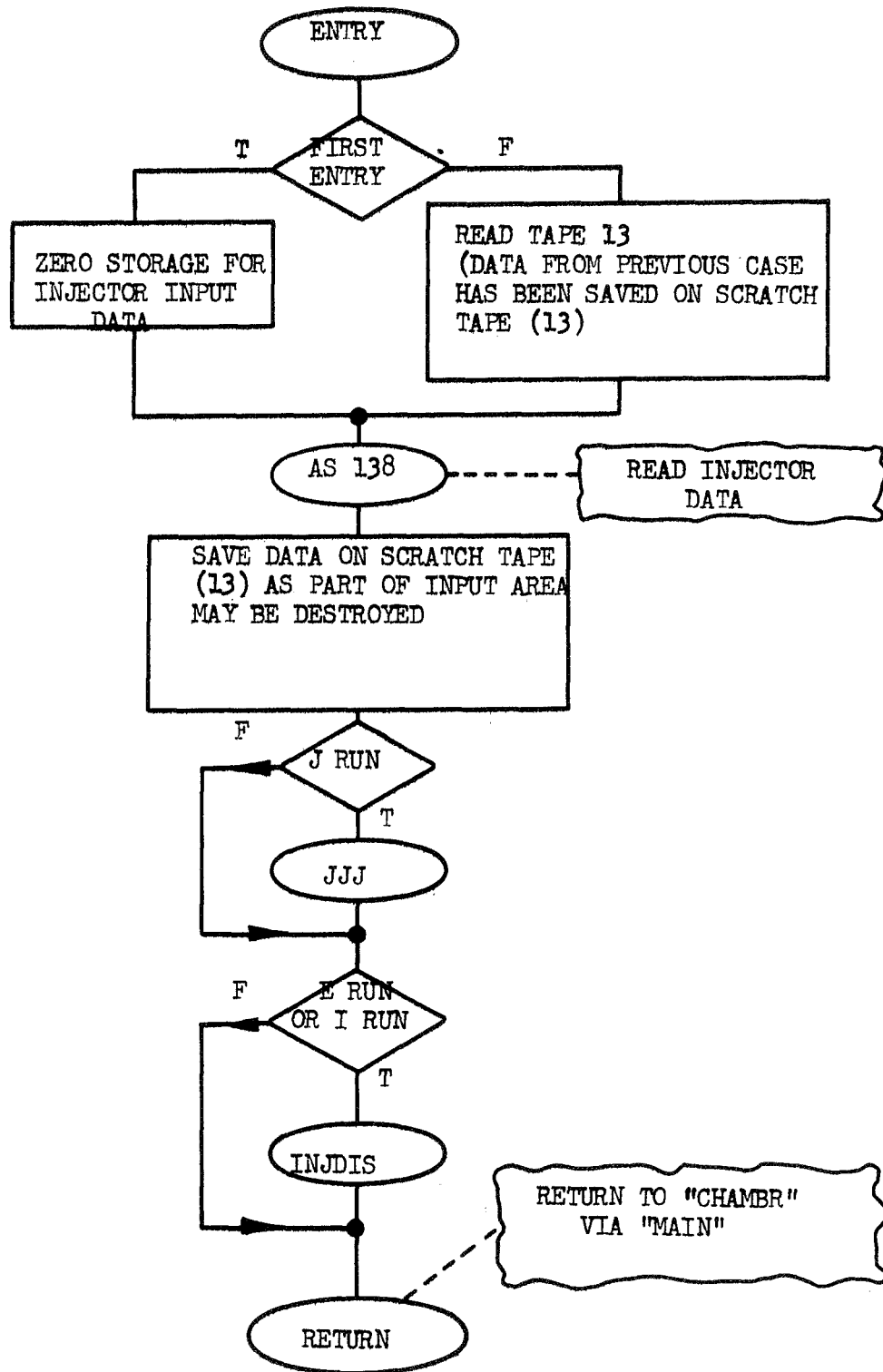


ENTRY = FFF
DECK = NTAU

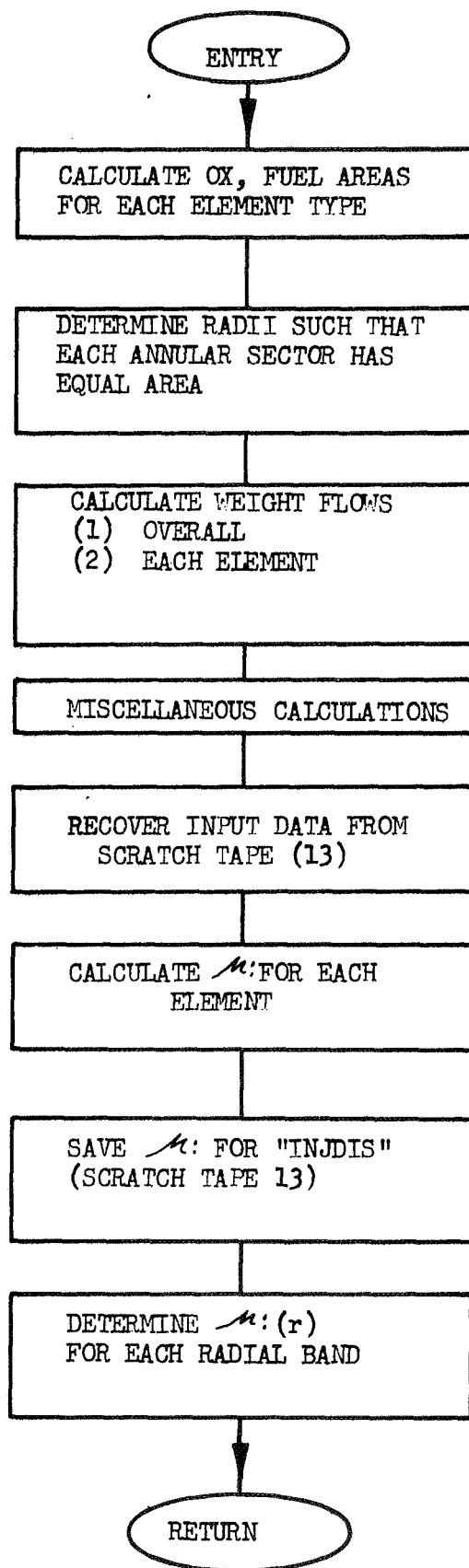


ENTRY = INJCTR

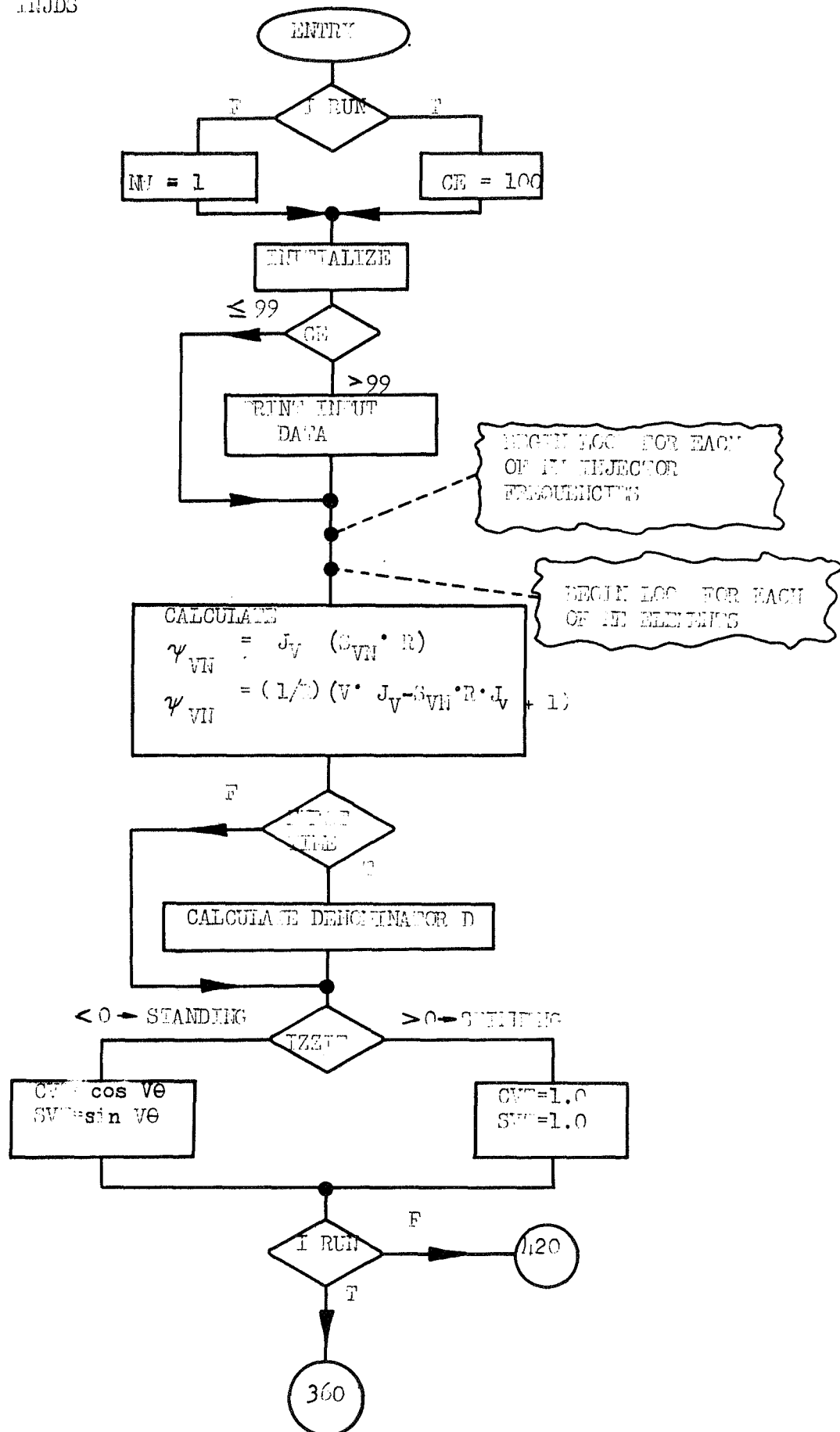
DECK = INJ



ENTRY = JJJ
DECK = JECT

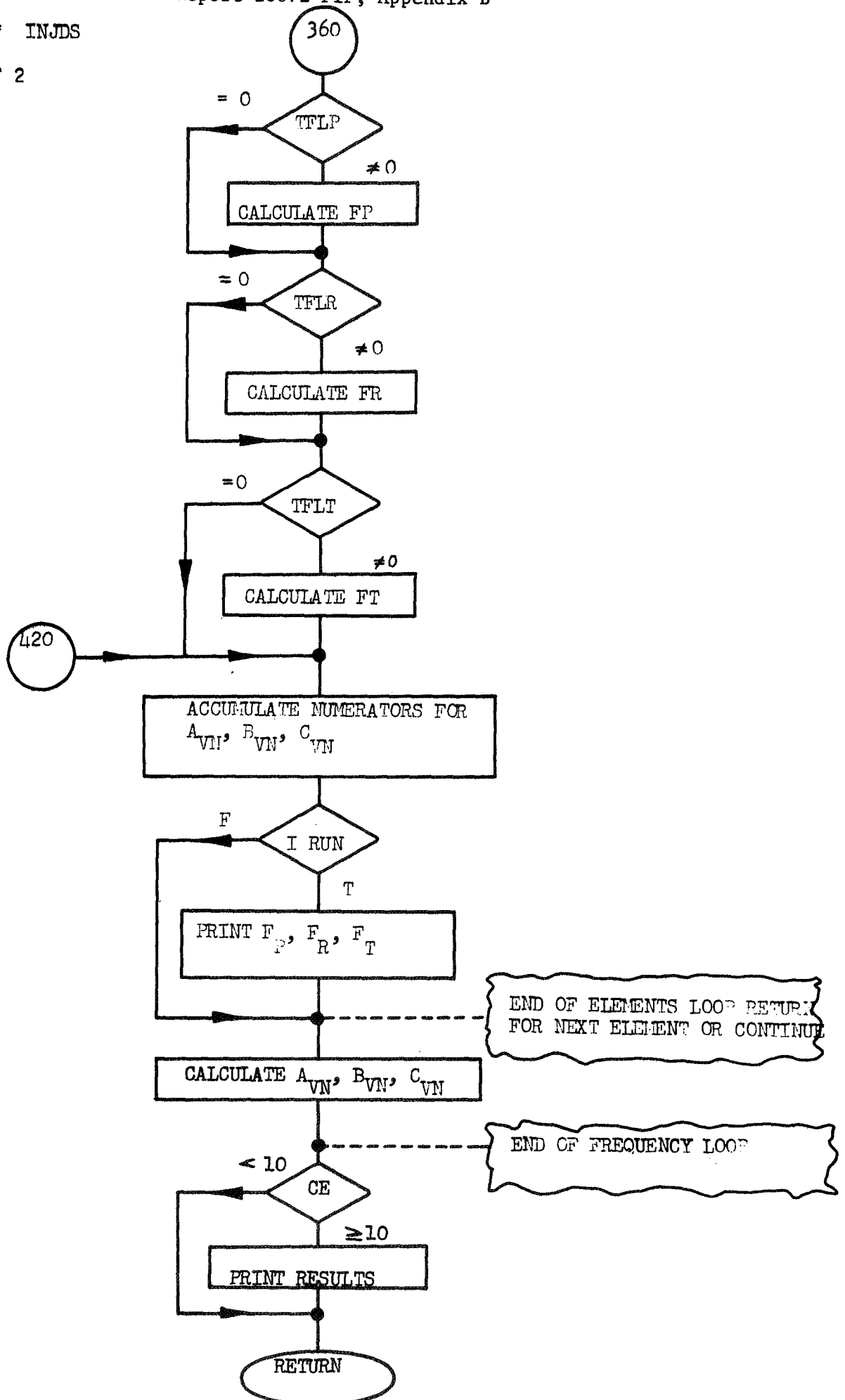


ENTRY = INJDIC
DECK = INJDS



DECK = INJDS

2 of 2



III. REFERENCES

1. Wieber, P. R., and Mickelsen, W., Effect of Transverse Acoustic Oscillations on the Vaporization of a Liquid-Fuel Droplet, NASA TN D-287, May 1960.
2. Reardon, F. H., An Investigation of Transverse Mode Combustion Instability in Liquid Propellant Rocket Motors, Princeton University Aeronautical Engineering Report No. 550, June 1961.
3. Crocco, L., and Sirignano, W. A., Behavior of Supercritical Nozzles Under Three Dimensional Oscillatory Conditions, to be published as an AGARDograph.
4. Culick, F. E. C., Stability of High Frequency Pressure Oscillations in Gas and Liquid Rocket Combustion Chambers, M. I. T. Aerophysics Laboratory Report No. 480, June 1961.
5. Crocco, L., and Cheng, S. I., Theory of Combustion Instability in Liquid Propellant Rocket Motors, AGARDograph No. 8, Butterworths Scientific Pub., Ltd., London, 1956.
6. Zinn, B. T., A Theoretical Study of Nonlinear Transverse Combustion Instability in Liquid Propellant Rocket Motors, Technical Report No. 732, Department of Aerospace and Mechanical Sciences, Princeton University, May 1966.
7. Scala, S. M., Transverse Wave and Entropy Wave Combustion Instability in Liquid Propellant Rockets, Princeton University Aeronautical Engineering Report No. 380, April 1957.
8. Crocco, L., "The Relevance of a Characteristic Time in Combustion Instability," Second ICRPG Combustion Conference, CPIA Publication No. 105, May 1966.

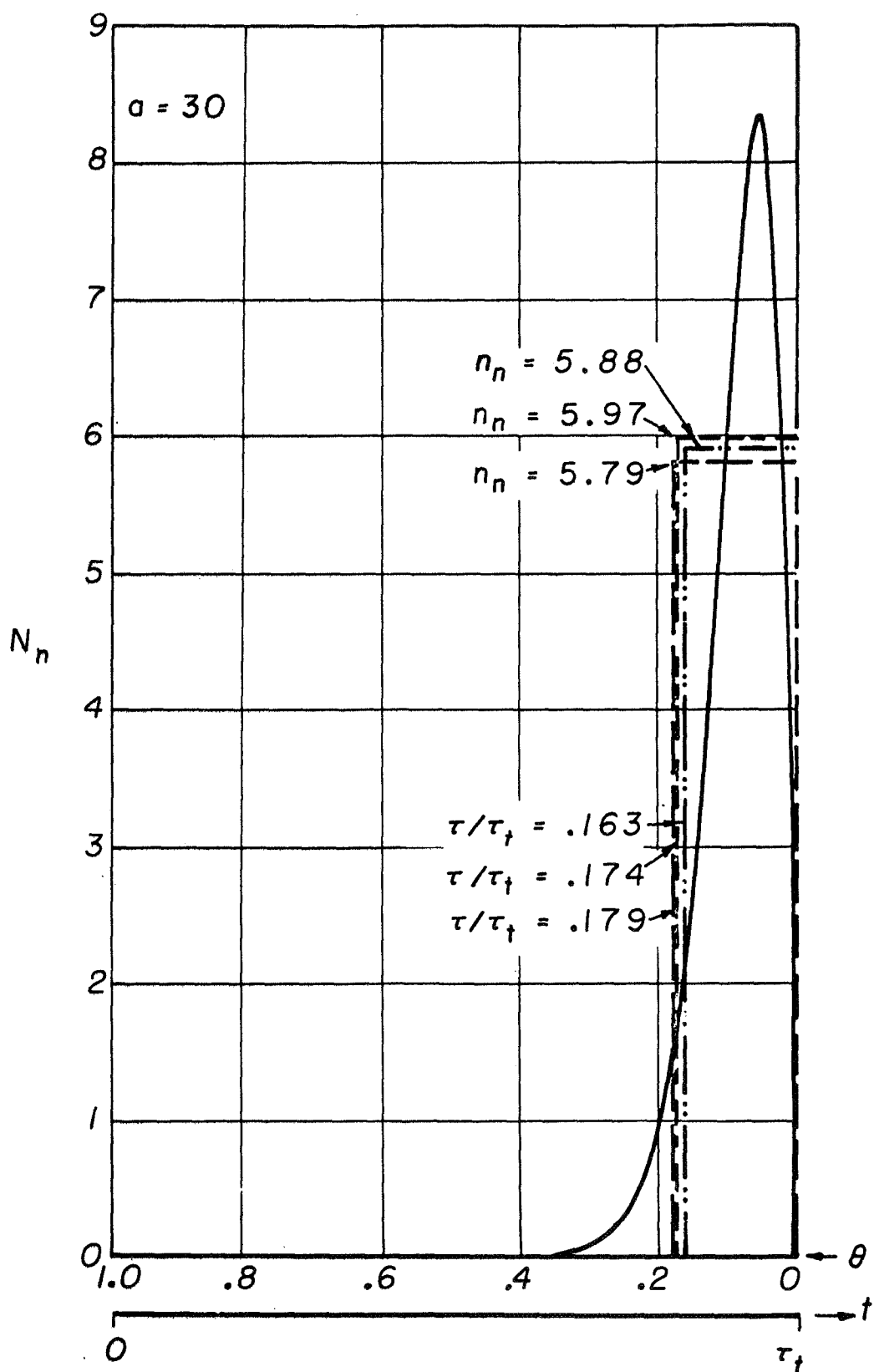


Figure 1. The General Interaction Index for Two Types of Combustion Sensitivities

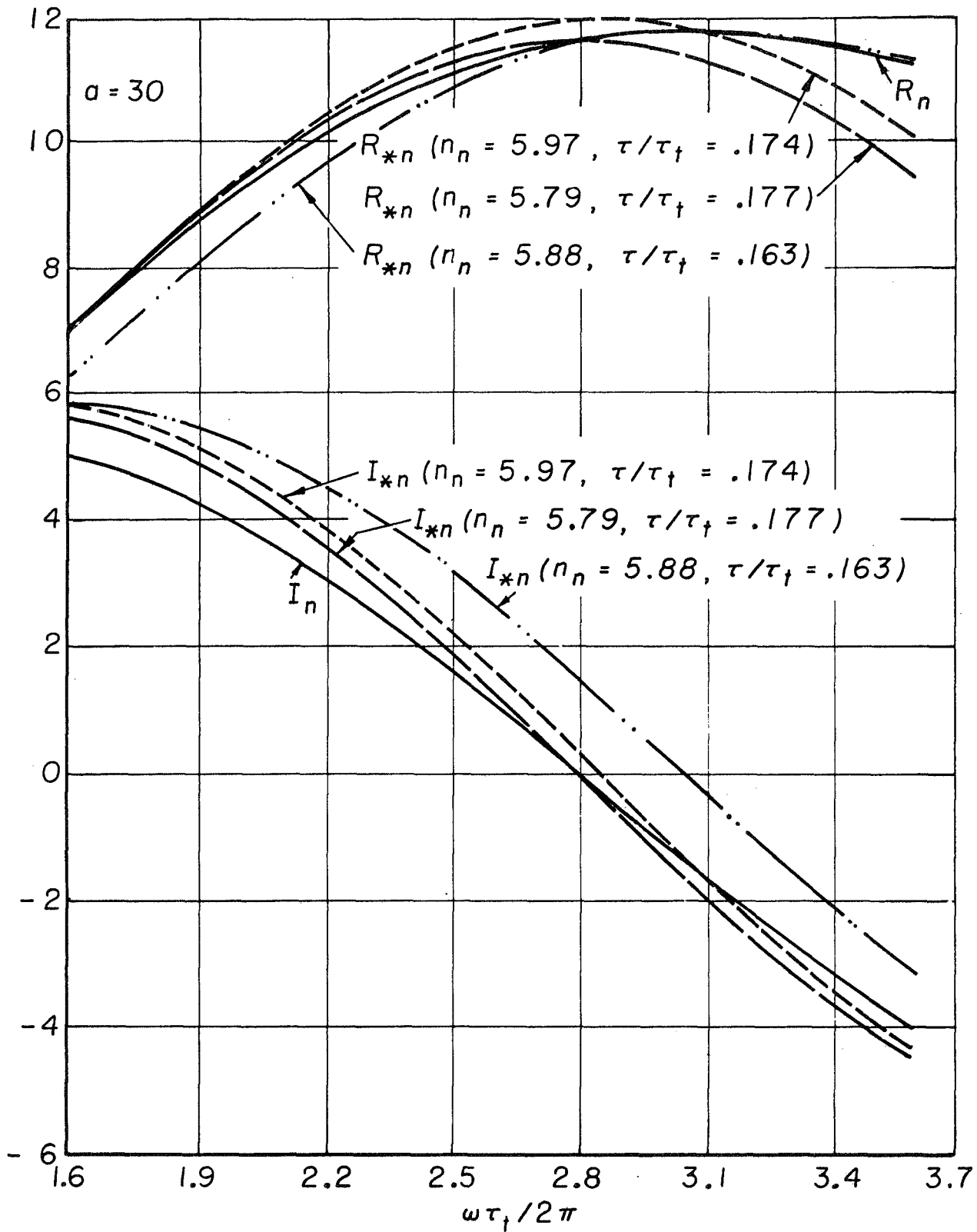
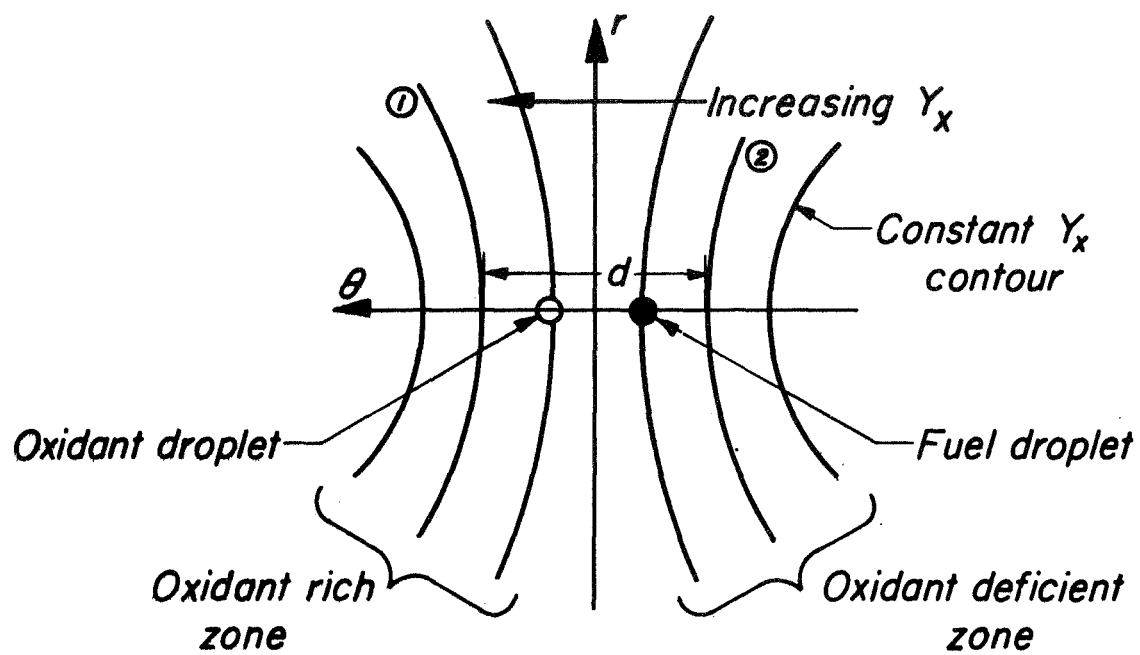
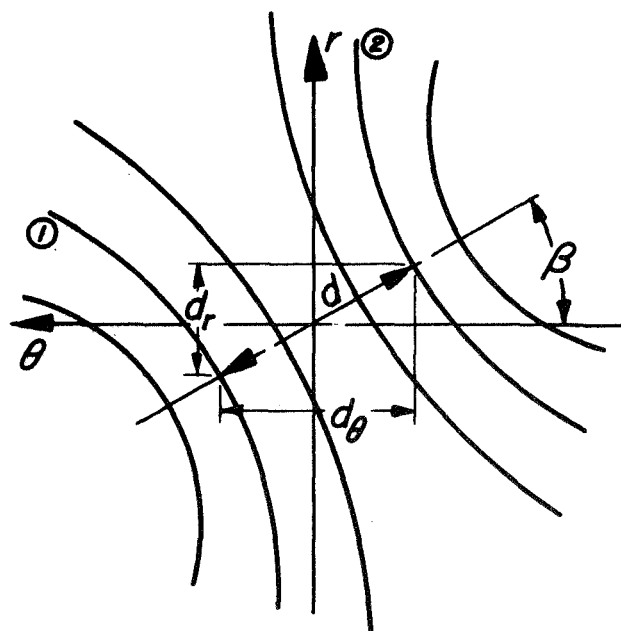


Figure 2. The Variation of the Feedback Factors R_n and I_n with Frequency

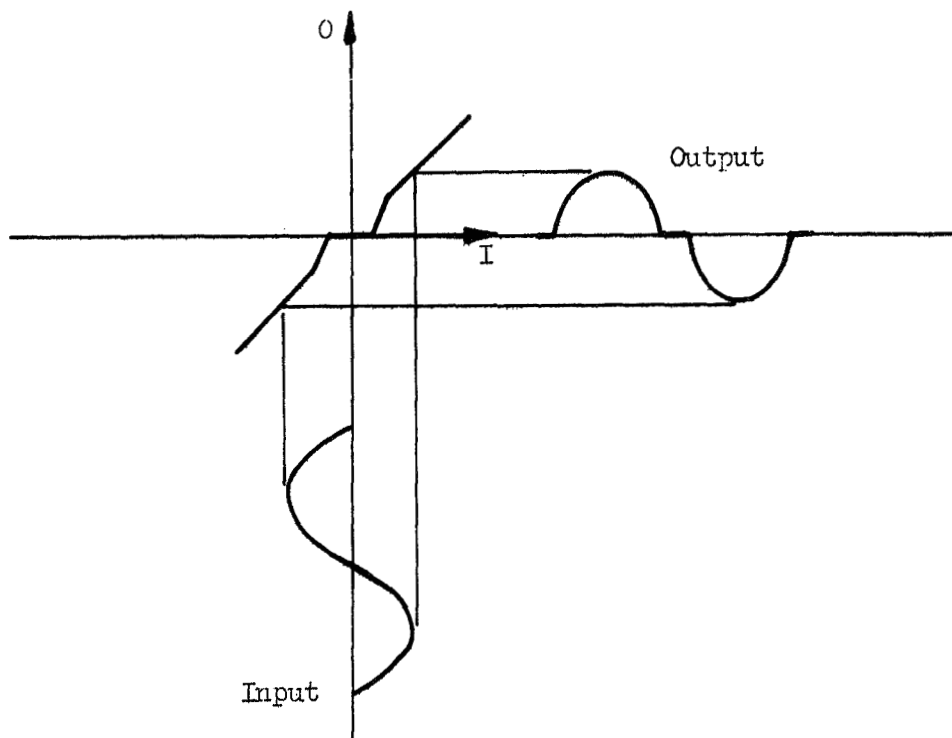


(a) Spray produced by tangentially oriented injector spud

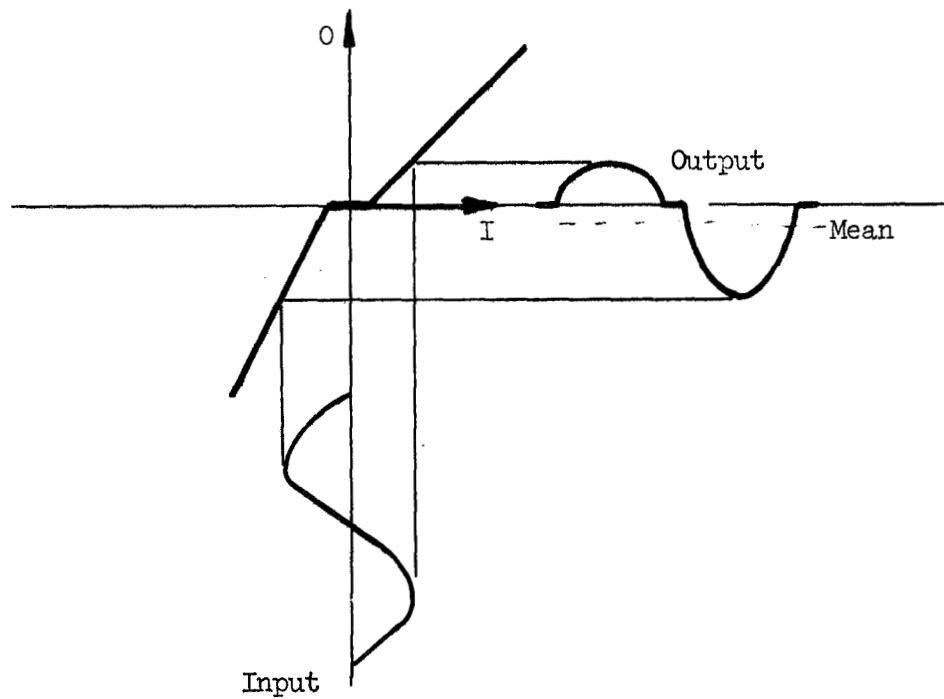


(b) Spray produced by rotated spud

Figure 3. Sprays Produced by Various Orientations of the Injector Spud



(a) Response Function with Odd-Symmetry



(b) Asymmetric Response Function

Figure 4. Examples of Nonlinear Response Functions

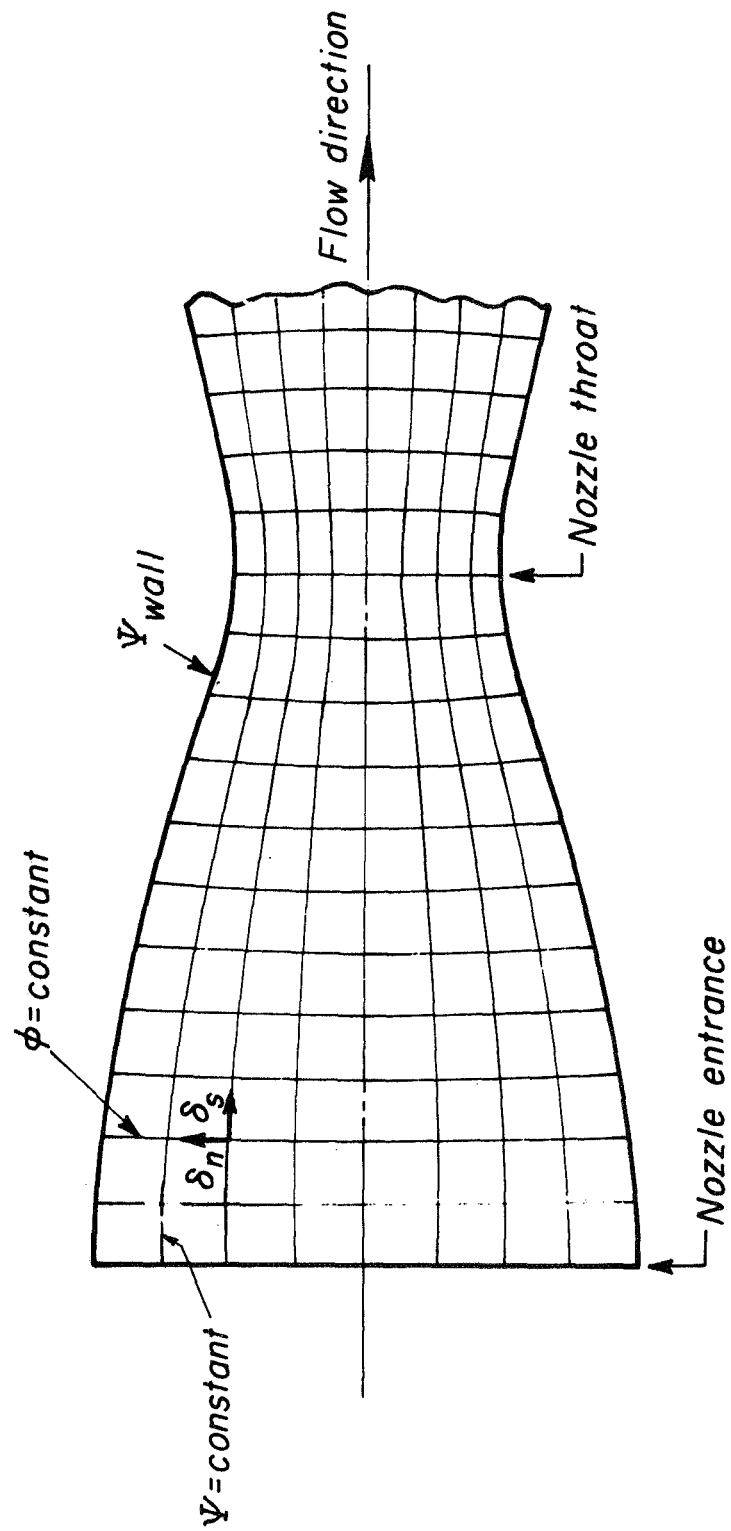


Figure 5. Exhaust Nozzle Coordinate System

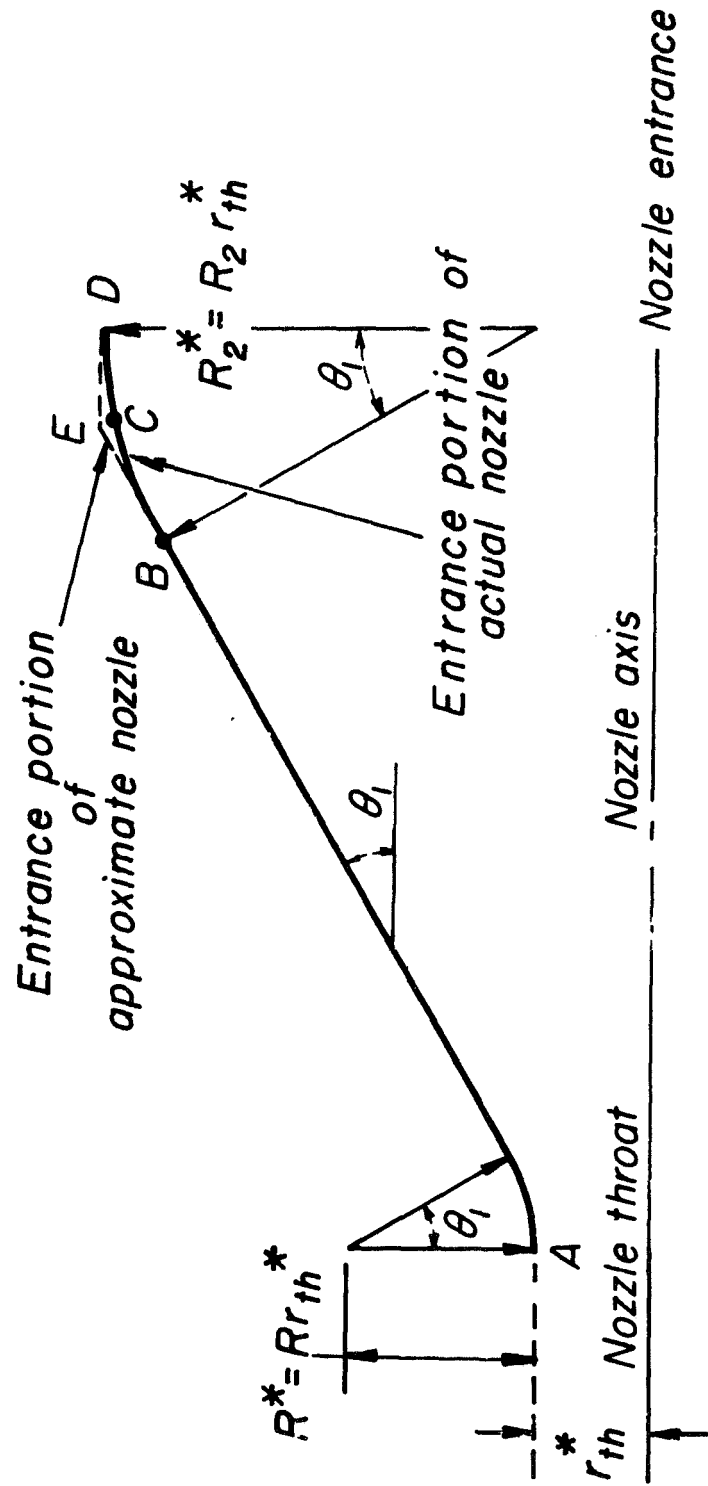


Figure 6. Nozzle Geometry and Comparison of Entrance Portions of Approximate And Actual Nozzle Geometries

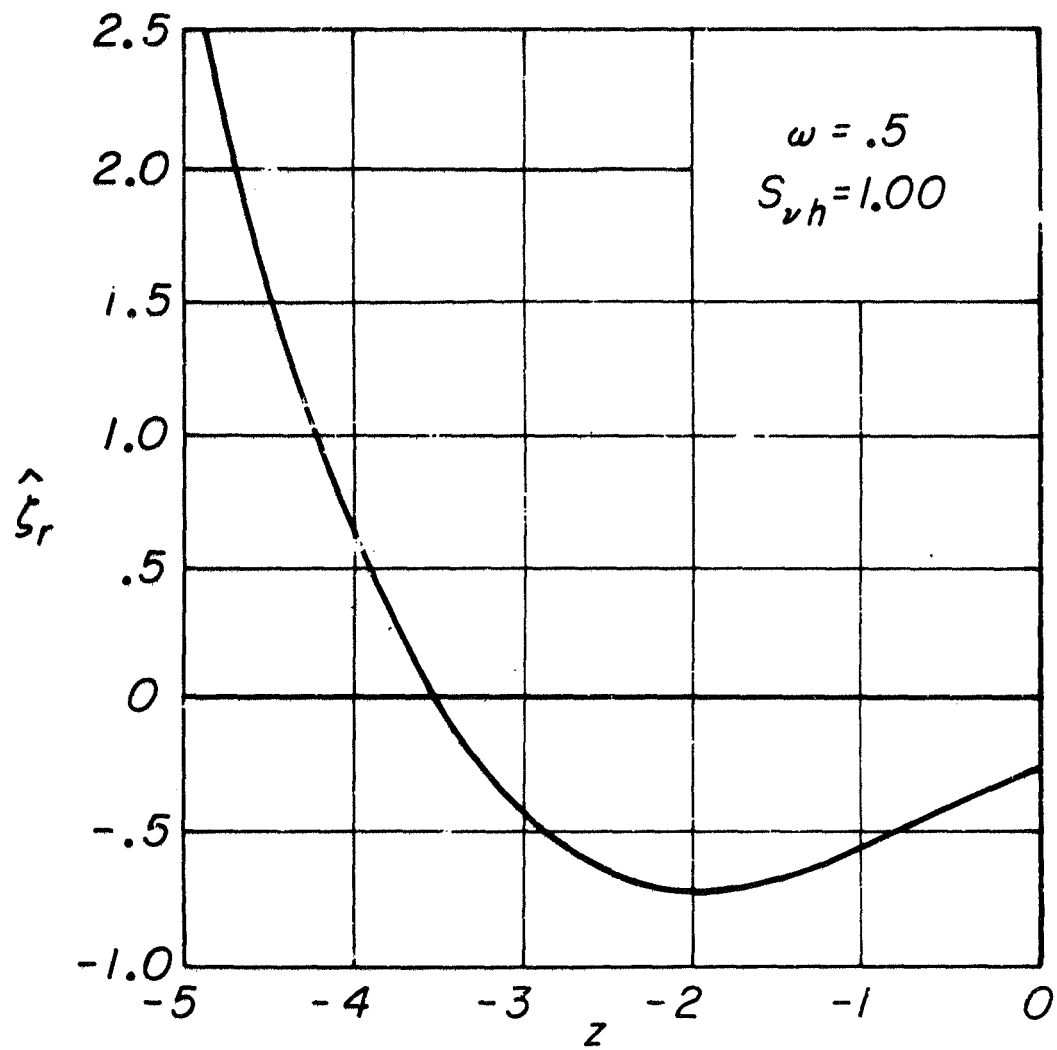


Figure 7. Real Part of ξ Versus Axial Distance

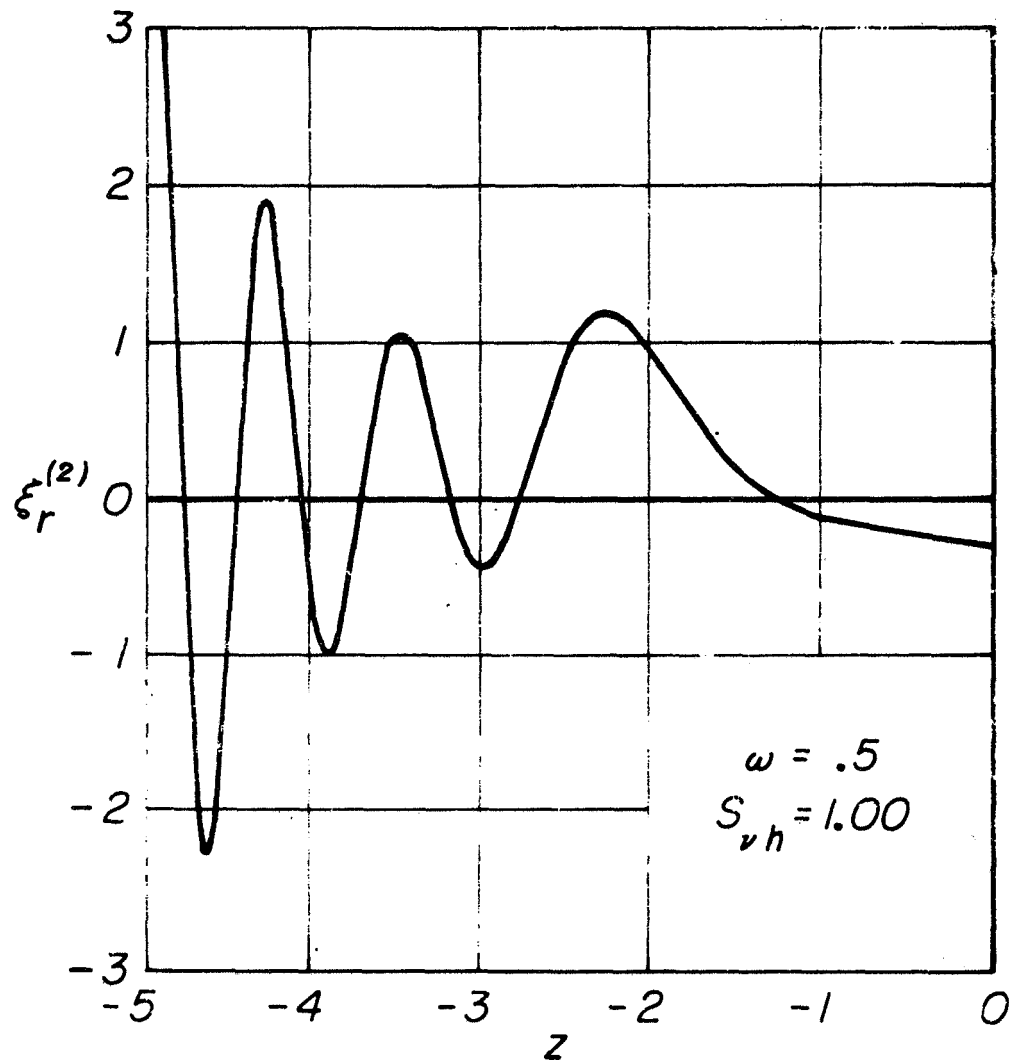


Figure 8. Real Part of $\xi^{(2)}$ Versus Axial Distance

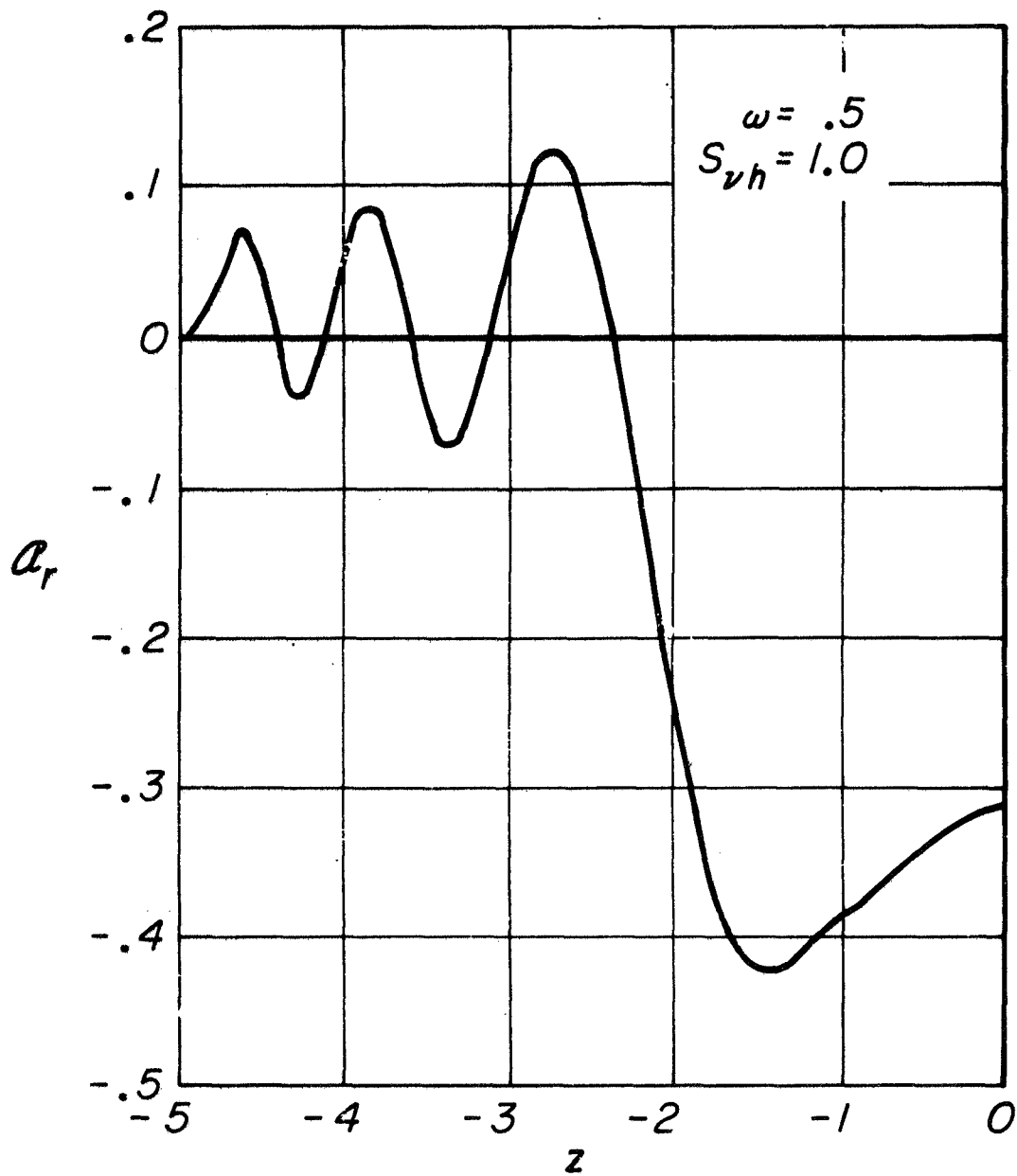


Figure 9. Real Part of Pressure Admittance Coefficient Versus Axial Distance

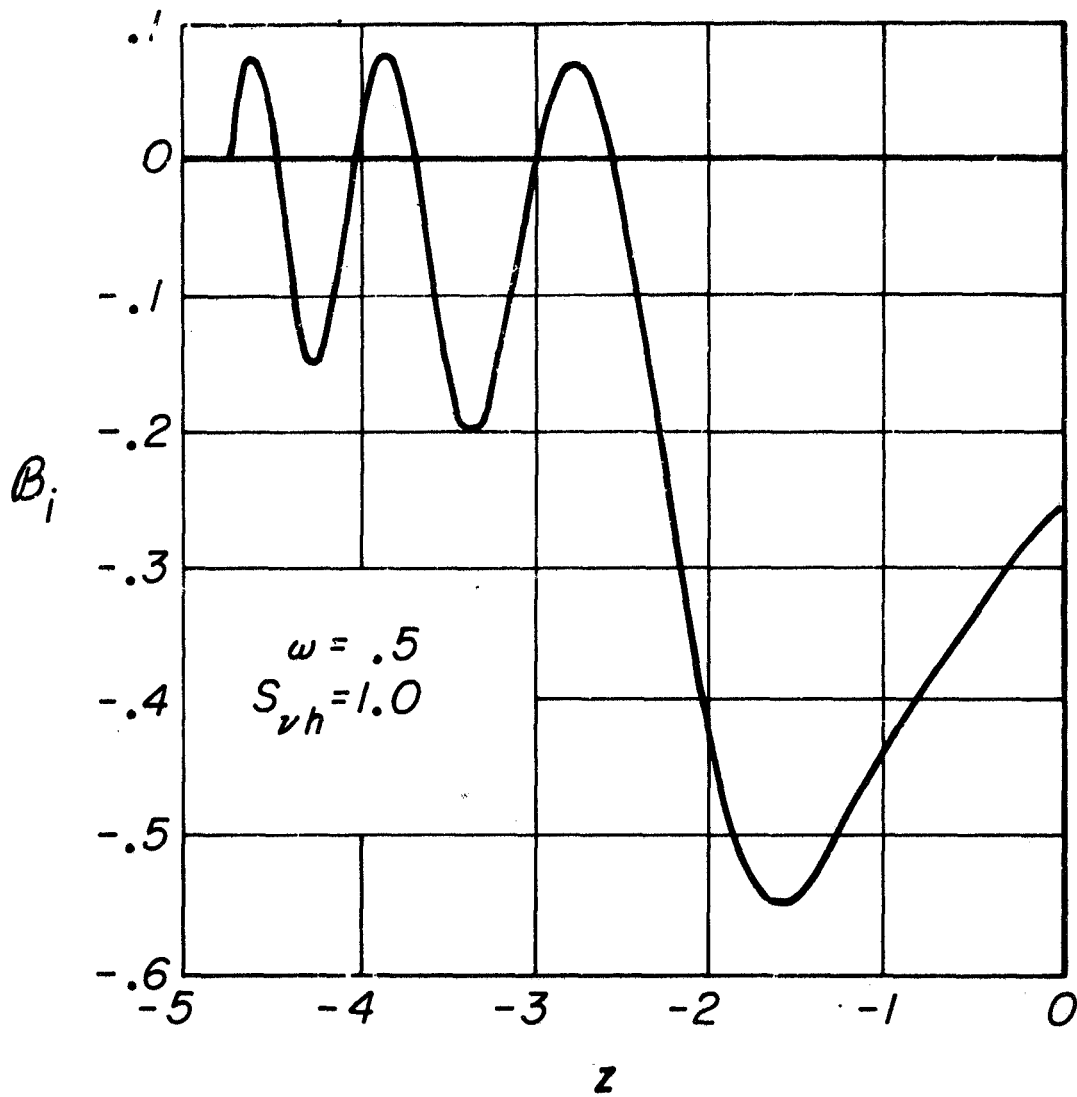


Figure 10. Imaginary Part of Radial Velocity Admittance Coefficient Versus Axial Distance

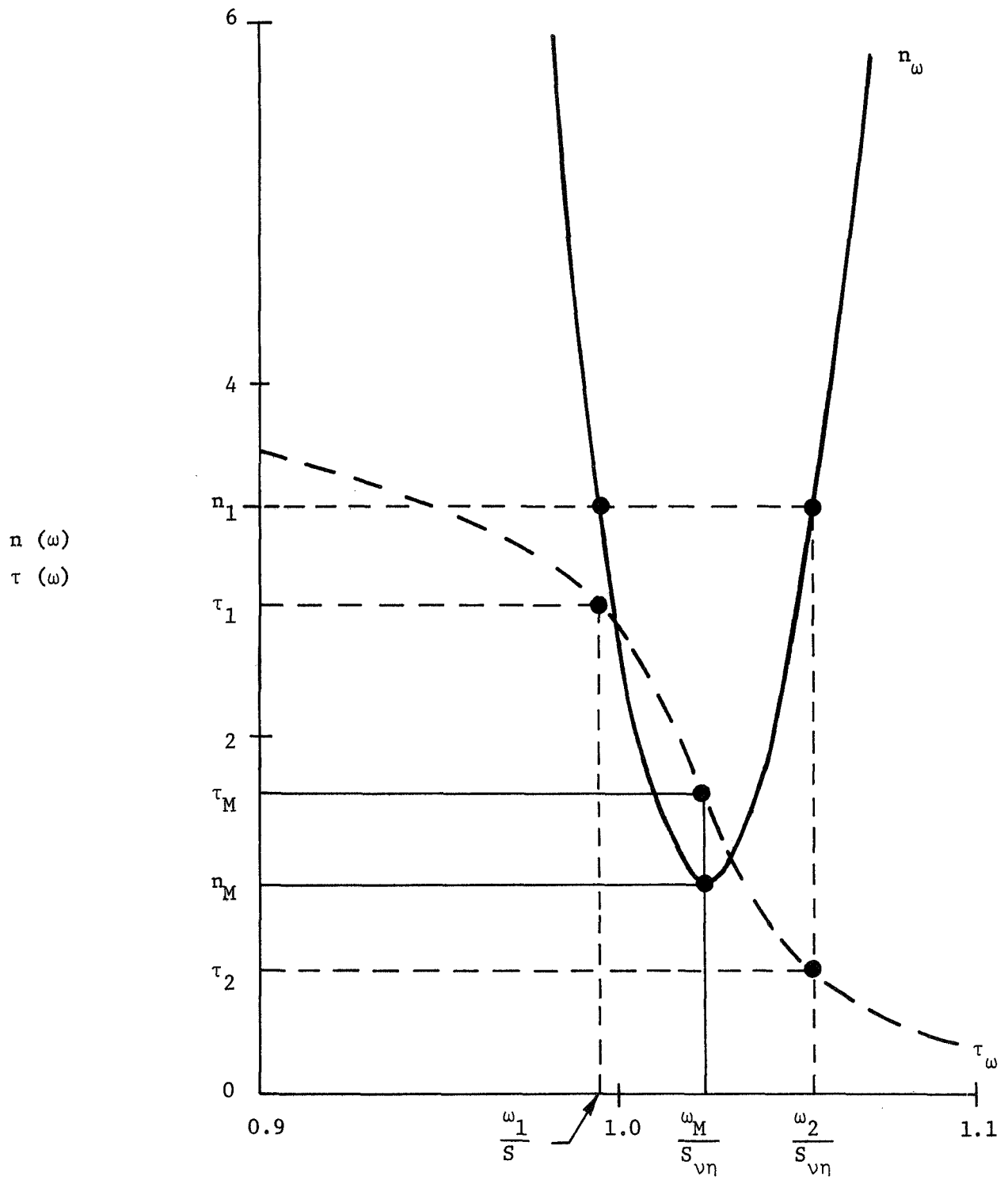


Figure 11. Typical Solutions of (ω) and $\tau(\omega)$

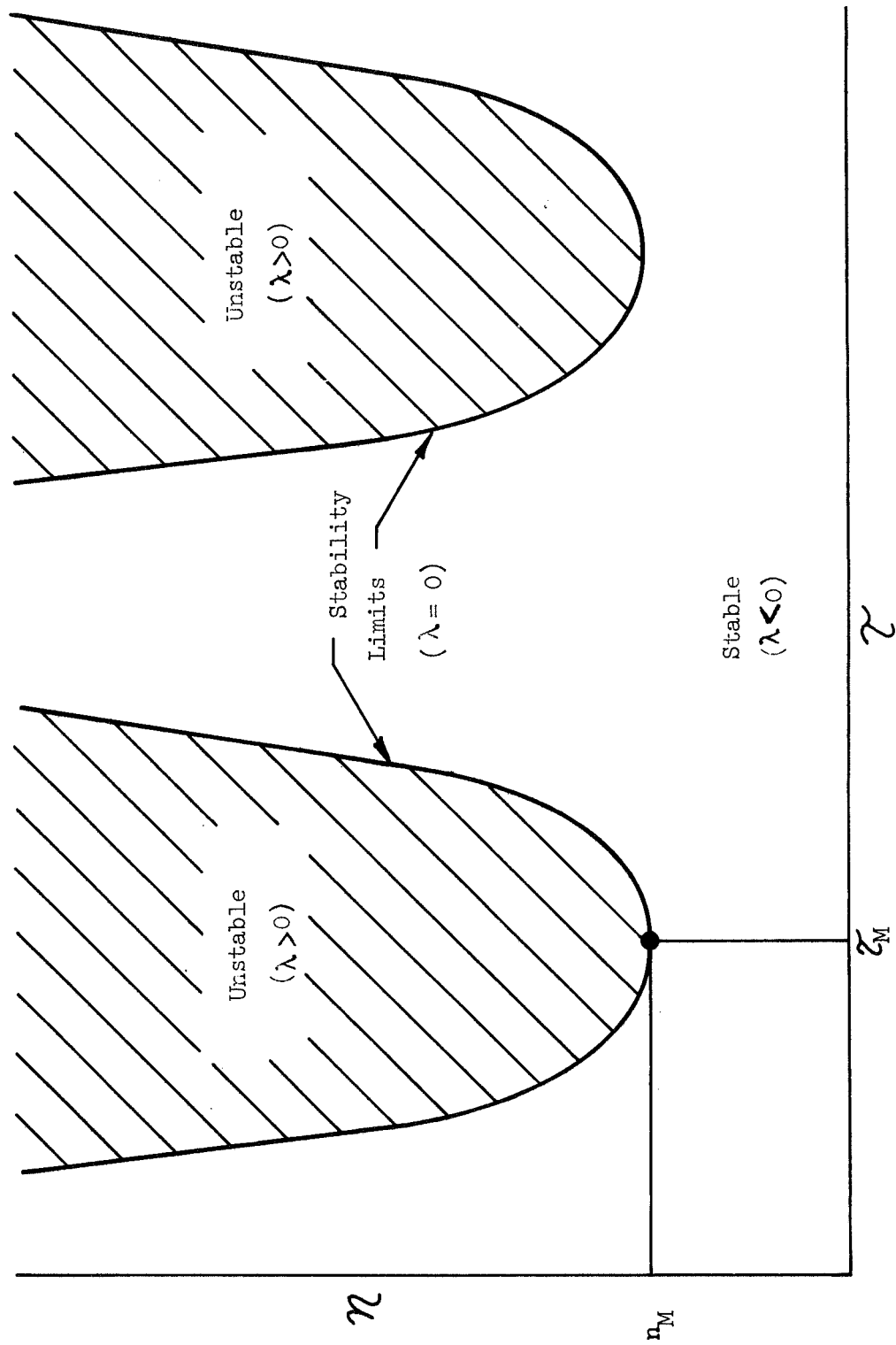


Figure 12. Stable and Unstable Regions on the η , ζ -Plane

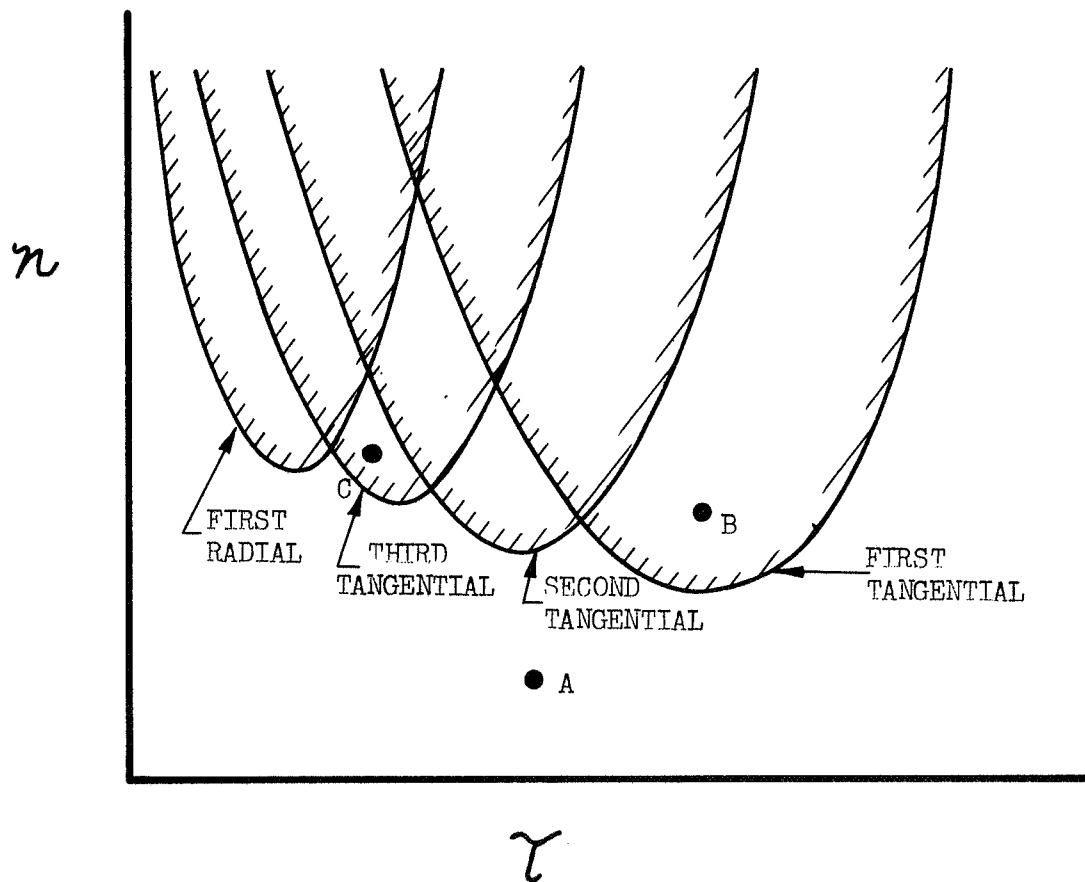


Figure 13. Relationship of Various Transverse Modes on the η , τ -Plane

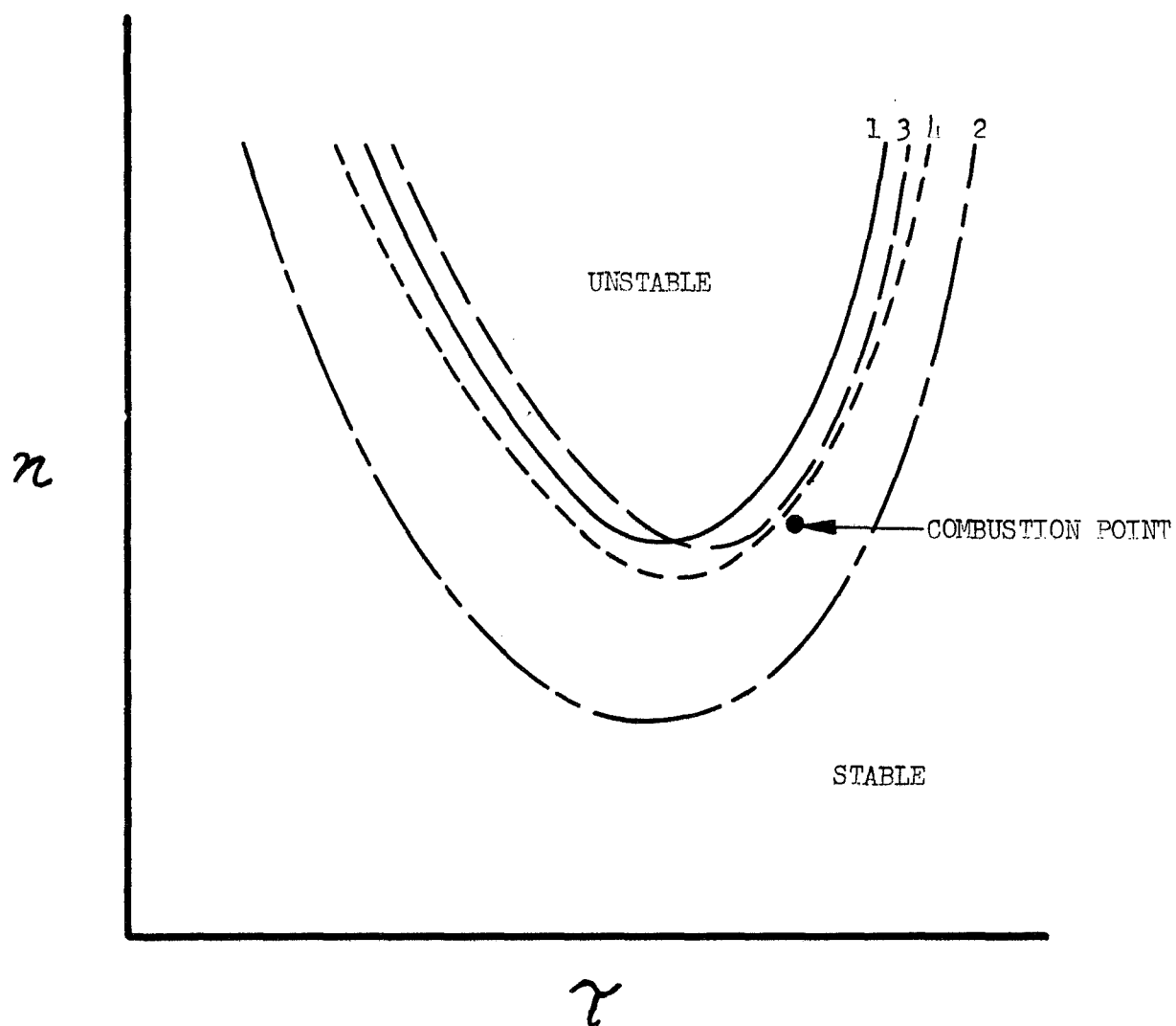


Figure 14. The Shift of the Stability Zone due to Nonlinear and Velocity Effects

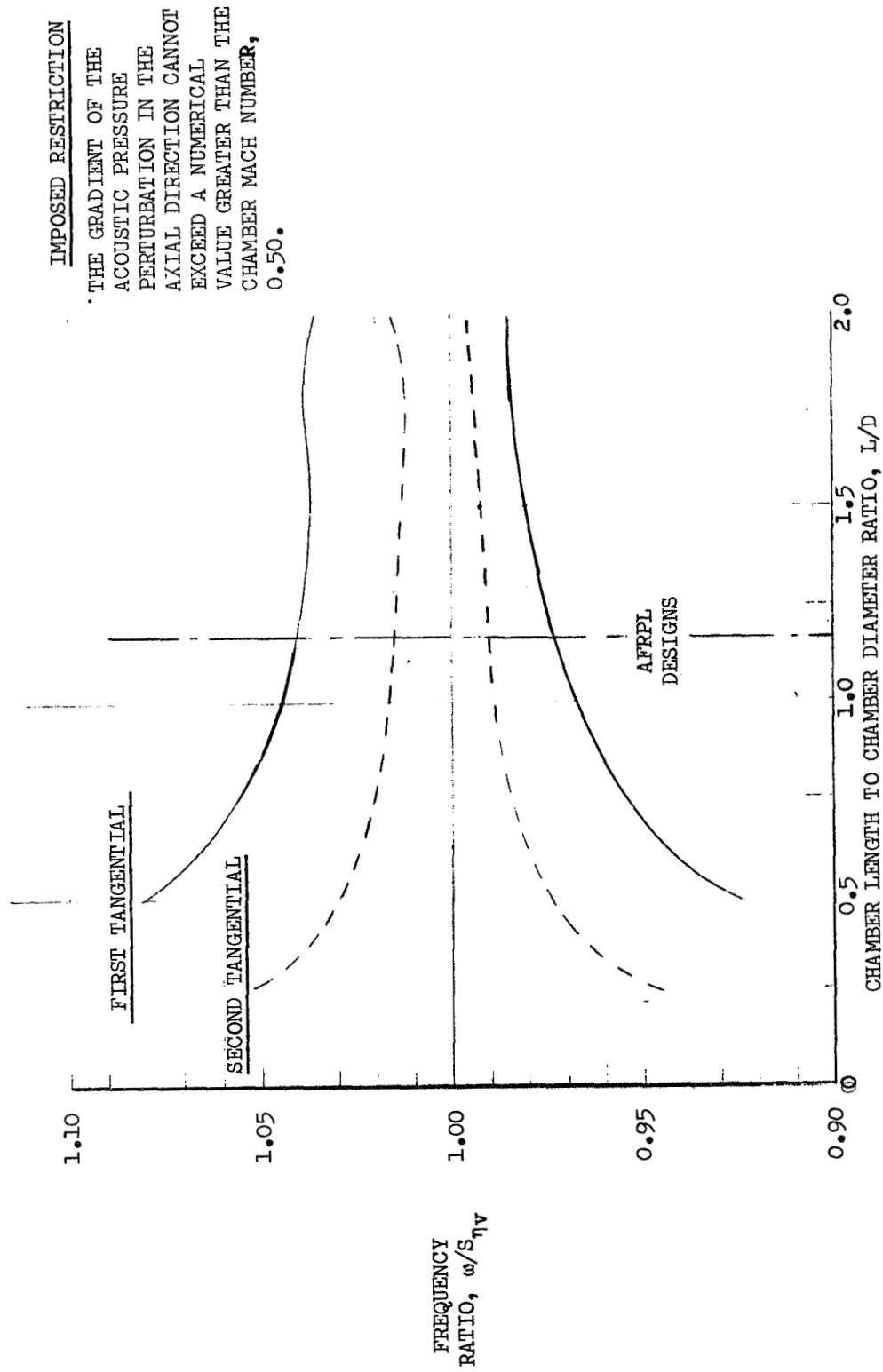


Figure 15. Applicable Frequency Ranges of Linear, Transverse Mode Sensitive Time Lag Model

DISTRIBUTION LIST

	<u>Copies</u>
NASA Headquarters Washington D.C., 20546 Attn: Chief, Liquid Propulsion Technology, RPL Office of Advanced Research and Technology	2
NASA Headquarters Washington D.C., 20546 Attn: Mr. A. O. Tischler, RP	1
NASA Headquarters Washington D.C., 20546 Attn: Mr. Vincent L. Johnson, Director Launch Vehicles and Propulsion, SV Office of Space Sciences and Applications	1
NASA Headquarters Washington D.C., 20546 Attn: Dr. A. Gessow	1
NASA Headquarters Washington D.C., 20546 Attn: Director Advanced Manned Missions, MT Office of Manned Space Flight	1
NASA Marshall Space Flight Center Huntsville, Alabama, 35812 Attn: Purchasing Office, PR-RC	1
NASA Marshall Space Flight Center Huntsville, Alabama, 35812 Attn: Scientific and Technical Information Branch, MS-IP	1
NASA Marshall Space Flight Center Huntsville, Alabama, 35812 Attn: Patent Office, CC-P	1
NASA Marshall Space Flight Center Huntsville, Alabama, 35812 Attn: Technology Utilization Office, MS-T	1
NASA Marshall Space Flight Center Huntsville, Alabama, 35812 Attn: Mr. Robert Richmond, R-P&VE-PAC	8

Report 20672-PIF

DISTRIBUTION LIST (cont.)

	<u>Copies</u>
NASA Marshall Space Flight Center Huntsville, Alabama, 35812 Attn: Mr. Rex Bailey, R-P&VE-PAC	1
NASA Marshall Space Flight Center Huntsville, Alabama, 35812 Attn: Mr. Keith Chandler, R-P&VE-PA	1
NASA Ames Research Center Moffett Field, California 94035 Attn: Technical Librarian for Dr. H. J. Allen, Director	1
Air Force Plant Representative Office Aerojet-General Corporation P.O. Box 2048 Sacramento, California 95809 Attn: Mr. D. F. Schafer	1
NASA Goddard Space Flight Center Greenbelt, Maryland 20771 Attn: Technical Librarian for Merland L. Moseson, Code 620	1
NASA Lewis Research Center 21000 Brookpark Road Cleveland, Ohio 44135 Attn: Dr. Richard Priem	1
NASA Lewis Research Center 21000 Brookpark Road Cleveland, Ohio 44135 Attn: Mr. E. W. Conrad	1
NASA Lewis Research Center 21000 Brookpark Road Cleveland, Ohio 44135 Attn: Mr. W. Tomazic	1
NASA Lewis Research Center 21000 Brookpark Road Cleveland, Ohio 44135 Attn: Technical Librarian for Dr. Abe Silverstein, Director	1

Report 20672-PIF

DISTRIBUTION LIST (cont.)

	<u>Copies</u>
NASA Jet Propulsion Laboratory California Institute of Technology 4800 Oak Grove Drive Pasadena, California 91103 Attn: Technical Librarian for Robert F. Rose, Propulsion Division, 38	1
NASA Jet Propulsion Laboratory California Institute of Technology 4800 Oak Grove Drive Pasadena, California 91103 Attn: Mr. Henry Burlage, Jr.	1
NASA Jet Propulsion Laboratory California Institute of Technology 4800 Oak Grove Drive Pasadena, California 91103 Attn: Mr. Jack H. Rupe	1
NASA Langley Research Center Langley Station Hampton, Virginia 23365 Attn: Technical Librarian for Floyd L. Thompson, Director	1
NASA Manned Spacecraft Center Houston, Texas 77001 Attn: Technical Librarian for Robert R. Gilruth, Director	1
NASA Manned Spacecraft Center Houston, Texas 77001 Attn: Mr. J. G. Thibodaux, EP	1
NASA John F. Kennedy Space Center Cocoa Beach, Florida 32931 Attn: Technical Librarian for Dr. Kurt H. Debus, Director	1
Scientific and Technical Information Facility P.O. Box 33 College Park, Maryland 20740	24
Advanced Research Projects Agency Washington 25, D.C. Attn: Technical Librarian for Dr. D. E. Mock	1

Report 20672-PIF

DISTRIBUTION LIST (cont.)

	<u>Copies</u>
Defense Documentation Center Headquarters Cameron Station, Bldg. 5 5010 Duke Street Alexandria, Virginia 22314 Attn: Technical Librarian for TISTA	1
Picatinny Arsenal Dover, New Jersey 07801 Attn: Technical Librarian for Mr. I. Forsten, Chief, Liquid Propulsion Laboratory, SMUPA-DL	1
Rocket Research Laboratories Edwards Air Force Base Edwards, California 93523 Attn: Technical Librarian	1
Rocket Research Laboratories Edwards Air Force Base Edwards, California 93523 Attn: Mr. Richard R. Weiss, RPRR	1
U. S. Army Missile Command Redstone Arsenal, Alabama 35809 Attn: Technical Librarian for Gen. Zierdt	1
U. S. Army Missile Command Redstone Arsenal, Alabama 35809 Attn: Dr. Walter W. Wharton, AMSMI-RRK	1
U. S. Naval Ordnance Test Station China Lake, California 93557 Attn: Technical Librarian for Chief, Missile Propulsion Division, Code 4562	1
Chemical Propulsion Information Agency Johns Hopkins University Applied Physics Laboratory 8621 Georgia Avenue Silver Spring, Maryland 20910 Attn: Technical Librarian for Mr. Neil Safeer	1

DISTRIBUTION LIST (cont.)

	<u>Copies</u>
Chemical Propulsion Information Agency Johns Hopkins University Applied Physics Laboratory 8621 Georgia Avenue Silver Spring, Maryland 20910 Attn: Mr. T. W. Christian	1
ARL Wright-Patterson AFB Dayton, Ohio 45433 Attn: Mr. K. Scheller, Bldg. 450	1
Air Force Systems Division Air Force Unit Post Office Los Angeles 45, California Attn: Col. Clark, Technical Data Center	1
Arnold Engineering Development Center Arnold Air Force Station Tullahoma, Tennessee Attn: Dr. H. K. Doetsch	1
Bureau of Naval Weapons Department of the Navy Washington, D.C. Attn: Mr. J. Kay, RTMS-41	1
Headquarters Air Force Office of Scientific Research Propulsion Division Washington, D.C. Attn: Dr. Bernard T. Wolfson	1
Department of the Navy Office of Naval Research Washington, D.C. 20360 Attn: Mr. R. O. Jackel	1
RTNT Bolling Field Washington, D.C. 20332 Attn: Dr. L. Green, Jr.	1

Report 20672-PIF

DISTRIBUTION LIST (cont.)

	<u>Copies</u>
Aerojet-General Corporation P.O. Box 15847 Sacramento, California 95809 Attn: Technical Librarian for Mr. R. Stiff	1
Aerojet-General Corporation P.O. Box 15847 Sacramento, California 95809 Attn: Mr. J. M. Mc Bride	1
Sacramento State College Engineering Division 600 J Street Sacramento, California 95819 Attn: Dr. Fred H. Reardon	1
Aerospace Corporation P.O. Box 95085 Los Angeles, California 90045 Attn: Technical Librarian for Mr. J. C. Wilder	1
Aerospace Corporation P.O. Box 95085 Los Angeles, California 90045 Attn: Mr. O. W. Dykema	1
Aerospace Corporation P.O. Box 95085 Los Angeles, California 90045 Attn: Dr. W. G. Strahle	1
Aeronautronic Philco Corporation Ford Road Newport Beach, California 92663 Attn: Technical Librarian for Mr. D. A. Carrison	1
Astropower Laboratory Douglas Aircraft Company 2121 Paularino Newport Beach, California 92663 Attn: Technical Librarian for Dr. George Moc	1

DISTRIBUTION LIST (cont.)

	<u>Copies</u>
Astrosystems International, Inc. 1275 Bloomfield Avenue Fairfield, New Jersey 07007 Attn: Technical Librarian for Mr. A. Mendenhall	1
Atlantic Research Corporation Edsall Road and Shirley Highway Alexandria, Virginia 22314 Attn: Technical Librarian for Mr. A. Scurlock	1
Arther D. Little, Inc. Acorn Park Cambridge, Massachusetts 02140 Attn: Technical Librarian for Dr. E. K. Bastress	1
Bell Aerosystems Company P.O. Box 1 Buffalo 5, New York Attn: Technical Librarian for Mr. W. M. Smith	1
Boeing Company P.O. Box 3707 Seattle, Washington 98124 Attn: Technical Librarian for Mr. J. D. Alexander	1
Curtiss-Wright Corporation Wright Aeronautical Division Wood-Ridge, New Jersey 07075 Attn: Technical Librarian for Mr. G. Kelly	1
General Electric Company Cincinnati, Ohio 45215 Attn: Technical Librarian for Mr. D. Suichu	1
Lockheed Missiles and Space Company Technical Information Center P.O. Box 504 Sunnyvale, California 94088 Attn: Technical Librarian for Dr. Y. C. Lee	1
The Marquardt Corporation 16555 Saticoy Street Van Nuys, California 91409 Attn: Technical Librarian for Mr. Warren P. Boardman, Jr.	1

Report 20672-PIF

DISTRIBUTION LIST (cont.)

	<u>Copies</u>
North American Aviation, Inc. Space and Information Systems Division 12214 Lakewood Boulevard Downey, California Attn: Technical Librarian for Mr. Bergen	1
Reaction Motors Division Thiokol Chemical Corporation Denville, New Jersey 07832 Attn: Technical Librarian for Mr. Arthur Sherman	1
Reaction Motors Division Thiokol Chemical Corporation Denville, New Jersey 07832 Attn: Technical Librarian for Mr. O. Mann	1
Space Technology Laboratories TRW Incorporated One Space Park Redondo Beach, California 90278 Attn: Mr. G. W. Elverum	1
Stanford Research Institute 333 Ravenswood Avenue Menlo Park, California 94025 Attn: Technical Librarian for Mr. Lionel Dickinson	1
TAPCO Division TRW, Incorporated 23555 Euclid Avenue Cleveland, Ohio 44117 Attn: Technical Librarian for Mr. P. T. Angell	1
Thiokol Chemical Corporation Redstone Division Huntsville, Alabama Attn: Technical Librarian for Mr. John Goodloe	1
United Aircraft Corporation Research Laboratories 400 Main Street East Hartford, Connecticut 06108 Attn: Technical Librarian for Mr. Erle Martin	1

DISTRIBUTION LIST (cont.)

	<u>Copies</u>
United Aircraft Corporation Research Laboratories 400 Main Street East Hartford, Connecticut 06108 Attn: Mr. D. H. Utvik	1
United Aircraft Corporation Research Laboratories 400 Main Street East Hartford, Connecticut 06108 Attn: Mr. R. H. Osborn	1
United Technology Center 587 Mathilda Avenue P.O. Box 358 Sunnyvale, California 94088 Attn: Technical Librarian for Mr. B. Adelman	1
Rocketdyne Division of North American Aviation 6633 Canoga Avenue Canoga Park, California 91304 Attn: Technical Librarian for Mr. S. Hoffman	1
Rocketdyne Division of North American Aviation 6633 Canoga Avenue Canoga Park, California 91304 Attn: Dr. Robert B. Lawhead	1
Rocketdyne Division of North American Aviation 6633 Canoga Avenue Canoga Park, California 91304 Attn: Mr. Robert Fontaine	1
Warner-Swasey Company Control Instrument Division 32-16 Downing Street Flushing, New York 11354 Attn: Mr. R. H. Tourin	1
Pratt and Whitney Aircraft P.O. Box 2691 West Palm Beach, Florida 33402 Attn: Technical Librarian for Mr. R. J. Coar	1

Report 20672-PIF

DISTRIBUTION LIST (cont.)

	<u>Copies</u>
Pratt and Whitney Aircraft P.O. Box 2691 West Palm Beach, Florida 33402 Attn: Mr. George Lewis	1
Rocket Research Corporation 520 South Portland Street Seattle, Washington 98108 Attn: Technical Librarian for Mr. Foy McCullough, Jr.	1
Defense Research Corporation P.O. Box 3587 Santa Barbara, California Attn: Mr. B. Gray	1
Multi-Tech Inc. Box 4186 No. Annex San Fernando, California Attn: Mr. F. B. Cramer	1
Geophysics Corporation of America Technical Division Burlington Road Bedford, Massachusetts 01730 Attn: Mr. A. C. Tobey	1
Polytechnic Institute of Brooklyn Graduate Center Route 110 Farmingdale, New York Attn: Dr. V. D. Agosta	1
Applied Physics Laboratory The Johns Hopkins University 8621 Georgia Avenue Silver Spring, Maryland 20910 Attn: Dr. W. G. Berl	1
Ohio State University Rocket Research Laboratory Department of Aeronautical and Astronautical Engineering Columbus, Ohio 43201 Attn: Dr. R. Edse	1

DISTRIBUTION LIST (cont.)

	<u>Copies</u>
Princeton University Forrestal Research Center Princeton, New Jersey Attn: Dr. I. Glassman	1
Princeton University Forrestal Research Center Princeton, New Jersey 08540 Attn: Mr. D. T. Harrje	1
University of Wisconsin Dept. Mechanical Engineering 1513 University Avenue Madison, Wisconsin 53705 Attn: Dr. P. S. Myers	1
Dartmouth University Hanover, New Hampshire Attn: Dr. P. D. McCormack	1
University of Michigan Aeronautical and Astronautical Engineering Laboratories Aircraft Propulsion Laboratory North Campus Ann Arbor, Michigan Attn: Dr. J. A. Nicholls	1
Institute of Engineering Research University of California Berkeley, California Attn: Dr. A. K. Oppenheim	1
Purdue University School of Mechanical Engineering Lafayette, Indiana Attn: Dr. J. R. Osborn	1
Massachusetts Institute of Technology Department of Mechanical Engineering Cambridge 39, Massachusetts Attn: Dr. T. Y. Toong	1

Report 20672-PIF

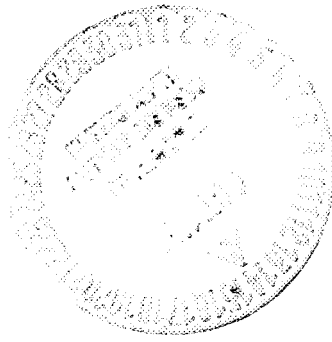
DISTRIBUTION LIST (cont.)

	<u>Copies</u>
Illinois Institute of Technology 10 W. 35th Street Chicago, Illinois Attn: Dr. P. T. Torda	1
The Pennsylvania State University Mechanical Engineering Department 207 Mechanical Engineering Blvd. University Park, Pennsylvania 16802 Attn: G. M. Faeth	1
Georgia Institute of Technology Aerospace School Atlanta, Georgia 30332 Attn: Dr. B. T. Zinn	1





AEROJET-GENERAL CORPORATION



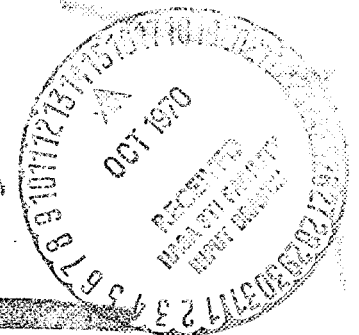
See N70-25301
N70-25301
DRF

A Reproduced Copy OF

Reproduced for NASA
by the
NASA Scientific and Technical Information Facility

61

PROPULSION DIVISION



STABILITY CHARACTERIZATION OF ADVANCED INJECTORS

Summary Final Report on Phase I of
Contract NAS 8-20672

Prepared for

MARSHALL SPACE FLIGHT CENTER
Huntsville, Alabama

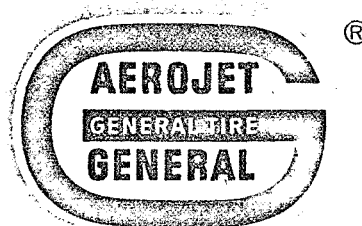
Report 20672-PISF

25 October 1962

LIBRARY COPY

NOV 18 1962

MAILED BY [illegible] and
HOUSTON, TEXAS



AEROJET-GENERAL CORPORATION

SACRAMENTO, CALIFORNIA



STABILITY CHARACTERIZATION OF
ADVANCED INJECTORS


Summary Final Report on Phase I of
Contract NAS 8-20672

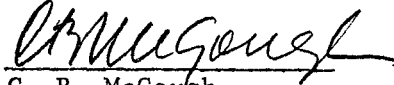
Prepared for
MARSHALL SPACE FLIGHT CENTER
Huntsville, Alabama

Report 20672-PISF

25 October 1968

Approved


J. M. McBride
Project Manager


C. B. McGough
Program Manager



AEROJET-GENERAL CORPORATION
A SUBSIDIARY OF THE GENERAL TIRE & RUBBER COMPANY

TABLE OF CONTENTS

	<u>Page</u>
I. Introduction	1
II. Summary	2
III. Task I: Analytical Model Development	4
A. Annular Combustor Analysis	4
B. Staged Combustion Model	5
IV. Task II: Annular Thrust Chamber Assembly Tests	7
V. Task III: Transverse Excitation Chamber Testing	10
VI. Conclusions	12

TABLE LIST

	<u>Table</u>
Steady State and Stability Test Results	1

FIGURE LIST

	<u>Figure</u>
Tangential Mode Acoustic Frequencies for Annular Chambers	1
Annular Coaxial Injector	2
Annular Thrust Chamber Assembly on Test Stand C-6	3
Transverse Excitation Chamber Assembly Schematic	4
Transverse Excitation Chamber Triplet Injector Hydroflow Pattern	5

I. INTRODUCTION

The purpose of Phase I of this program was to determine the stability characteristics of various injectors using high combustion chamber pressures with the cryogenic propellants, hydrogen and oxygen. Coaxial injectors for the most part were characterized under previous programs at Aerojet, NASA, and other government subcontractors. The remaining design feature to be evaluated on the coaxial injector was the effect of injection density on combustion stability. This effect was evaluated during the test portion of this program in an annular combustion chamber.

Combustion stability correlations based on Sensitive Time Lag Theory require an accurate definition of theoretical considerations. Consequently, part of the investigation necessary to advance current knowledge in combustion stability was the advancement of Sensitive Time Lag Theory. A refinement to the basic theory was the addition of terms to account for higher combustion chamber Mach numbers and an extension of the current model to include the toroidal or annular combustors.

As part of the experimental program an experimental tool, the "Transverse Excitation Chamber," was designed and the feasibility of using this tool to measure the frequency sensitivity of a particular injector demonstrated.

Many preliminary designs were evaluated prior to the selection of the designs fabricated and tested on this program.

Phase I was scheduled for 12 months of technical effort, but was extended to 15 months to include additional hardware fabrication.

II. SUMMARY

The stability characteristics of two injection concepts to be used in advanced injectors for high chamber pressure, hydrogen/oxygen systems were determined on this phase of the program. The two injection concepts tested were: coaxial with central oxidizer and 30° included angle fuel impingement; and triplet injectors with 60° included angle oxidizer-fuel-oxidizer pattern. Analytical model developments were advanced for the Sensitive Time Lag Theory, and a research tool termed "Transverse Excitation Chamber" was demonstrated.

Analytical model developments included expansion and refinement of the existing Sensitive Time Lag model to include annular combustion chambers and initiation of analyses to include feed system coupled pressure oscillations as encountered with the staged combustion system.

The second major task consisted of testing injector patterns in an annular thrust chamber. Injectors designed and fabricated for this task included one coaxial and two versions of one basic triplet element pattern. The coaxial injector was patterned after an injector tested on Contract NAS 8-11741, except that the injection density (total propellant flow rate per projected injector face area) was nearly doubled. The triplet injectors were patterned after a design being considered for NASA's Advanced Cryogenic Rocket Engine. The major difference between the two versions of this injection pattern is that one has nearly twice the injection density of the other. Seven tests on the coaxial injector were made under this task. Two triplet injectors were also fabricated.

The third major task consisted of the design, development, and demonstration of a research tool, the "Transverse Excitation Chamber." This combustor is a variable angle sector chamber that can be varied from 9 to 36° and is used to determine the relative sensitivity of injection elements to instability. Six tests conducted with this combustion chamber yielded preliminary results on its effectiveness as a research tool.

II, Summary of Program (cont.)

A detailed analysis of combustion stability data obtained during the testing of this program is included in this report, and correlations with results from tests conducted on other programs were made. Considerable injector design studies were conducted on this program.

III. TASK I: ANALYTICAL MODEL DEVELOPMENT

A. ANNULAR COMBUSTOR ANALYSIS

Analytical tasks on this program included the extension of the basic Sensitive Time Lag model for cylindrical combustion chamber to include annular chambers. A preliminary analysis for the gas-generator-fed staged combustion system was also made.

The analysis for the annular combustion chamber fits into the basic framework of the cylindrical chamber analysis; a few minor modifications are required. In the general solution of the pressure perturbation equation by using separation of variables technique the solution is:

$$P_o = P_o(z) \psi_o(r) \theta_o(\theta)$$

Three ordinary differential equations for $P_o(z)$, $\psi_o(r)$ and $\theta_o(\theta)$ are obtained.

The solution for the annular combustion chamber case is concerned with the solution of $\psi_o(r)$. The differential equation for $\psi_o(r)$ is a Bessel equation of the form: $\psi_{v\eta}(r) = AJ_v(S_{v\eta} \cdot r) + BY_v(S_{v\eta} \cdot r)$

where: J_v = Bessel function of the first kind
 Y_v = Bessel function of the second kind
 $S_{v\eta}$ = the transverse mode number

By considering the cylindrical chamber case and the inner wall for the annular case separately and solving these two relationships simultaneously one obtains the following result: .

$$J'_v(S_{v\eta}) Y'_v(S_{v\eta} R) - J'_v(S_{v\eta} R) Y'_v(S_{v\eta}) = 0$$

III, A, Annular Combustor Analysis (cont.)

The solution of this equation defines the transverse acoustic mode number, $S_{v\eta}$, for annular chambers. This equation has been solved in published literature and values of $S_{v\eta}$ are listed. Annular combustion chambers will alter the frequency of the transverse mode from the cylindrical case. The extent of this alteration is shown in Figure 1.

The configuration of the exhaust nozzle affects the nozzle admittance coefficient in much the same manner as for the cylindrical combustion chamber nozzle. The analysis for the annular nozzle is different primarily in the determination of the local contraction ratio. This is accomplished in the computer program by inputting both the inner and outer radii of the chamber and throat.

B. STAGED COMBUSTION MODEL

The system selected for the staged combustion model consists of (1) propellant feed system, (2) primary combustor, (3) secondary combustor, and (4) a turbine. The approach taken was to assume that the engine design parameters are given. The instability zones are then calculated for the secondary combustor, for assumed values of the primary combustion parameters (n_p, τ_p) and the total time lag of the hot gas τ_{FS} . The shift of the instability zones as these combustion parameters are varied shows the nature of the interaction between the two combustors.

The first-order analysis involves the following assumptions: the propellants are incompressible, the feed lines are short, the combustion is concentrated at the injector, and mean chamber Mach numbers are small.

As a general result of this analysis, it has been observed that the total time lag is from 6 to 10 times larger than the sensitive time lag.

III, B, Staged Combustion Model (cont.)

Consequently, for frequencies of interest to high frequency instability, the effects of the feed system terms will tend to average over the finite length of the combustion zone. Since the total time lag includes the time required for atomization, vaporization, mixing, and heating of the propellants, some interaction is likely in high pressure engines -- particularly in the secondary combustor.

IV. TASK II: ANNULAR THRUST CHAMBER ASSEMBLY TESTS

Annular thrust chamber assembly hardware consisted of three major components: (1) injector with attached axial centerbody, (2) combustion chamber, and (3) annular nozzle. Of the injectors designed for the annular combustion chamber, three were fabricated and one tested. A 600-element triplet injector to deliver 60,000 lb thrust with a total propellant weight flow of 180 lb/sec was fabricated, and a 200-element triplet injector to deliver 20,000 lb thrust with 60 lb/sec total propellant weight flow was also fabricated. To evaluate the effect of injection density on stability a 54-element coaxial injector was designed, fabricated, and tested for comparison with injectors previously built on Contract NAS 8-11741. This injector with the centerbody attached is shown in Figure 2 and again in Figure 3 as assembled prior to testing.

The combustion chamber and centerbody were ablatively cooled and both centerbody and chamber converged to form a throat. Two pyrotechnic igniters, three pulse guns, eight high-frequency pressure transducers and three static pressure transducers were located on the combustion chamber.

Tests were conducted at mixture ratios from 4 to 6 and chamber pressures of from 1500 to 2500 psia at a constant propellant weight flow of 180 lb/sec. Table 1 shows the results from this testing.

Each instability pattern observed during the annular testing was nearly identical in its form and was initiated by the 20-grain charge, using a tangential pulse gun. The peak-to-peak overpressures of these instabilities ranged from 800 to 2000 psi. The frequency was approximately 2500 Hz, depending on the acoustic velocity value for each test condition.

Test No. 7, using 200°R hydrogen, experienced -- in addition to its high-frequency instability -- a low-frequency (500 Hz) oscillation which

IV, Task II, Annular Thrust Chamber Assembly Tests (cont.)

attained an amplitude of 750 psi. Except for one brief occurrence of a low frequency (100 Hz and 100 psi) instability on Test No. 3, there was no other indication of a coupling between the feedlines and the combustion process. It should be pointed out that the large pressure drops across the injector face due to the small orifice design result in significant hydraulic resistances in the circuit.

The effect of chamber Mach number was evaluated in this series of tests by comparing results with test results from Contract NAS 8-11741. The two Mach numbers used were 0.176 and 0.29.

This verification of the Mach number as an important correlating parameter, together with the work of NASA's Lewis Research Center, has led to the selection of six design parameters as being important in combustion stability evaluations. These parameters are functionally related by the following formula:

$$f_s = 4550 \left(\frac{M_c}{d_i} \right)^{0.15} \frac{(P_c/P_{\text{critical}})^{1/3}}{F}$$

where:	f_s	=	Sensitive frequency (hz)
	M_c	=	Chamber Mach Number
	d_i	=	Injection orifice diameter of least volatile propellant, inches
	P_{critical}	=	Critical pressure of least volatile time controlling propellant, psia
	P_c	=	Chamber pressure, psia
	F	=	Function of the velocity ratio and impingement angle. This function is not defined for the nonimpinging showerhead coaxial element.

IV, Task II, Annular Thrust Chamber Assembly Tests (cont.)

This formula may be used by a designer in his preliminary work to develop an injector configuration whose sensitive frequency is displaced from the first tangential acoustic mode of the thrust chamber. These first order estimates may then be combined with the analytical results of the sensitive time lag computer program to obtain a more detailed engine configuration. Of prime importance is the overall trends which may be observed from changes in any of the six design parameters.

V. TASK III: TRANSVERSE EXCITATION CHAMBER TESTING

The concept of a transverse excitation was originated at Aerojet on a Company-sponsored Independent Research and Development program to evaluate transverse modes of pressure oscillation (tangential instabilities) and simulate the pressure/velocity effects as experienced in a rocket combustion chamber. The transverse excitation chamber tested on this program is described in the following paragraphs.

The excitation chamber consisted of three principal parts: (1) chamber, (2) nozzle, and (3) injector inserts. The chamber is a 36° sector of a circle 2-1/4 inches in height. A drawing of this chamber is shown in Figure 4. The 36° sector of the 30-inch radius results in a fundamental acoustic frequency in the transverse mode at 1800 Hz. The smallest chamber angle was 9° , which results in a chamber acoustic frequency of 7000 Hz. The height of the chamber (2.17) inches limits the associated acoustic frequency to greater than 13,000 Hz. A single chamber design was used and the chamber angle was varied by inserting steel wedges in the combustion zone to achieve the desired angle. The O-ring-sealed chamber lid is removable to facilitate various injection concepts; ablative liners and throats were used to protect the areas most vulnerable to erosion.

Two triplet injectors were designed and fabricated for testing. One was an 11-element triplet, and the other was a three-element triplet similar to the 11-element triplet design in all but the orifice diameters. The purpose of the larger orifice size was to determine the effect of orifice diameter or thrust per element on combustion stability. Only the 11-element injector inserts were tested during this program. A photo of the 11-element injector is shown in Figure 5.

Testing of the transverse excitation chamber was conducted to measure the growth rates of spontaneous instabilities or decay rates of pulsed pressure perturbations.

V, Task III, Transverse Excitation Chamber Testing (cont.)

Mixture ratios of around 4 and chamber pressures of 1300 to 1400 psi were evaluated during the test series. Two of the three valid tests (in three tests the fuel valve was inoperative) attained these conditions and both experienced spontaneous instabilities. One test exhibited a growth rate of 650 db/sec, while the other test had two distinct growth periods. The first, occurring at the onset of the instability, had a 600 db/sec rate, while the second growth period came after thermal ignition of the 40 grain pulse charge had disrupted the initial instability. Its growth rate was 330 db/sec.

From the data obtained, the indication is that over the frequency range of 3000 to 4500 Hz the triplet element shown in Figure 3 has a peak response at 3300 Hz (see Figure 4) at the specified steady state conditions. This peak response frequency, when related to τ by the relationship

$$\tau = \frac{1}{2f}$$

compares favorably with previous correlations of τ for this type of injector.

VI. CONCLUSIONS

1. The use of combustion chamber Mach number as a stability correlating factor was examined and was found to have a relatively minor effect which appears to be related to the sensitive frequency as follows:

$$f_s = 4550 \left(\frac{M_c}{d_i} \right)^{0.15} \frac{(P_c/P_{crit})^{0.33}}{F}$$

f_s	=	Sensitive frequency
M_c	=	Chamber Mach Number
d_i	=	Injection orifice diameter of least volatile propellant (inches)
P_{crit}	=	Critical pressure of least volatile propellant (psia)
P_c	=	Chamber pressure, (psia)
F	=	Function of the velocity ratio and impingement angle

2. For the annular chamber tests, all recorded high frequency instabilities were pure first tangential modes pulsed at a comparatively low shock level (20 grains). This indicates that, for the operating parameters, the combustion process was close to its spontaneous oscillation regime.

3. The incidence of pure modes rather than the mixed modes noted with previous tests with a cylindrical chamber indicates a higher value for the sensitive time lag (τ) and, correspondingly, a lower sensitive frequency value (since $\tau = \frac{1}{2f}$). This conclusion is logical when the annular chamber design is considered (see Figure 2). Placing the centerbody in the injector has two effects: (1) the centerbody acts as an effective barrier against the radial modes, and (2) the integrated effect of propellant injection (mass distribution) is over larger radial distances -- or in a zone of greater tangential acoustic mode sensitivity.

VI, Conclusions (cont.)

4. The fact that lower pulse charges triggered instability does not necessarily indicate a reduction in pressure interaction index (the sensitive time lag term, n). This apparent increased combustion sensitivity could be due to the fact that pure modes are initiated at lower n values than are the combined modes. In fact it is analytically theorized that the pressure interaction index, n , was approximately the same for both the cylindrical and the annular chamber coaxial injection test phases (that is equal to approximately 0.5).

5. The excitation chamber has potential as a stability rating tool which will give many inexpensive tests and will evaluate many single parameter characteristics of an injection pattern. A complete spectrum of frequencies can be evaluated; short duration tests are adequate to evaluate an injector. Injector modules are inexpensive and easily replaced; the removable chamber lid permits testing of long injection elements (i.e., tubelet or HIPERTHIN), servicing of the combustion chamber protective coating, and removal and replacement of wedge inserts.

6. It is recommended that dynamic high frequency transducers be flush mounted for proper wave description.

7. It is recommended that the transverse excitation chamber as a research tool be used extensively to evaluate the effect on combustion stability of the various injection parameters (i.e., injection velocities, velocity ratio, fuel temperature orifice chambers, injection distribution, etc.) on a variety of injection concepts (i.e., triplets, quadlets, coaxial, HIPERTHIN, etc.). These tests should serve as a single parameter variation test and should evaluate a range of design and test conditions to determine optimum operating conditions for combustion stability and performance for a given injector design.

VI, Conclusions (cont.)

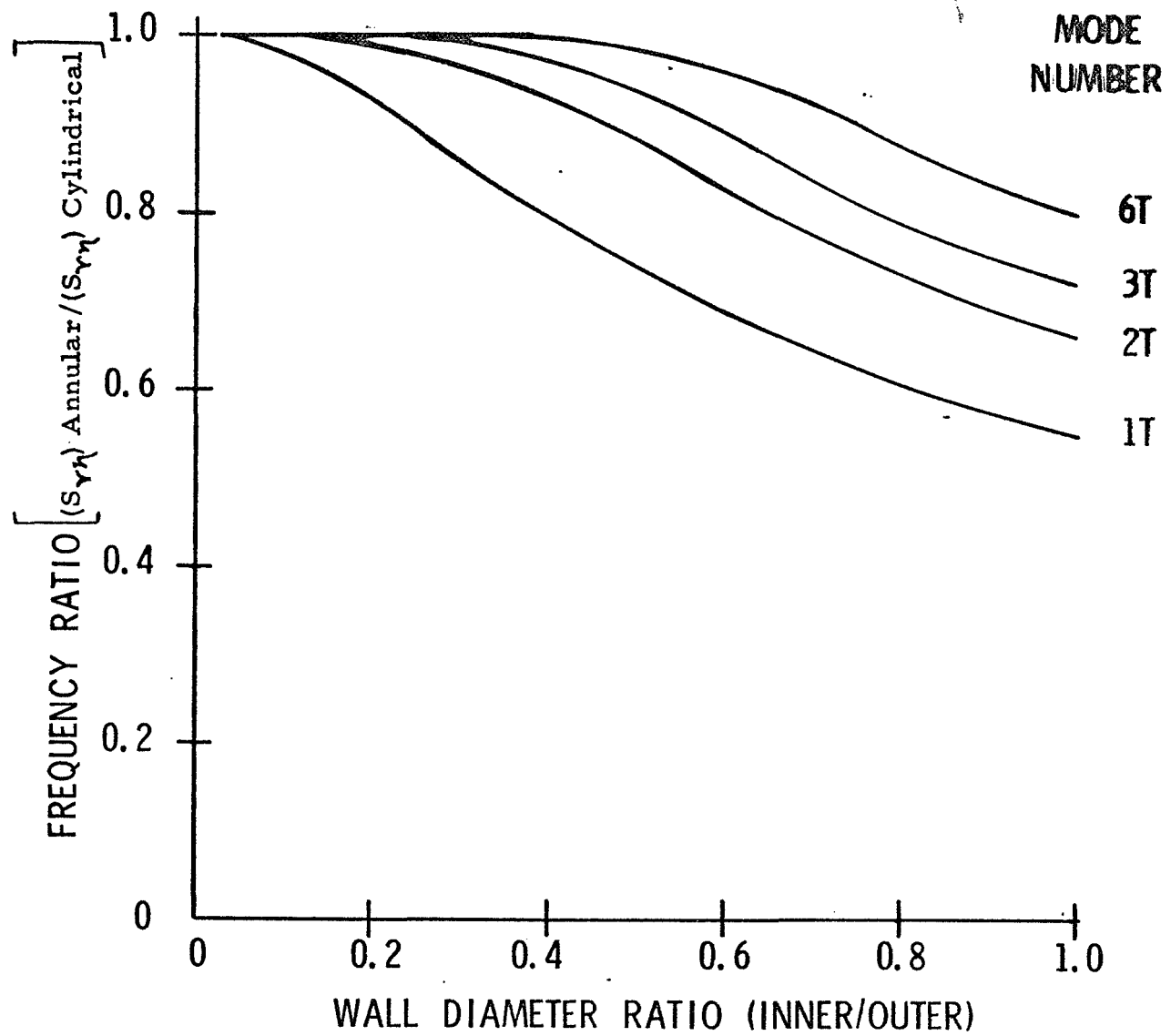
8. It is recommended that a limited number of verification tests be conducted using conventional cylindrical or annular combustion chambers to evaluate the injectors tested in the transverse excitation chamber in pulse rated stability tests. These tests should serve as demonstration tests to determine correlations between conventional injectors and excitation chamber results.

TABLE 1
STEADY STATE AND STABILITY TEST RESULTS

OPERATING CONDITION PARAMETERS										STABILITY PARAMETERS				
Test No.	Time, sec	Mixture Ratio	Velocity Ratio	Chamber Pressure, psia	Hydrogen Temperature, °F	Avg. Mach No.	High Frequency		Cause SP. or P.	Grain Size/ Pulse Ampl.	Stability	Low Frequency		REMARKS
							Frequency, Hz	Amplitude, psi (peak-to-peak)				Frequency, Hz	Amplitude, psi (peak-to-peak)	
001	1.016	6.05	3.44	1575	83.4	0.29	2400	800	IT	*P	20/960	*S	--	
	1.210	5.86	3.61	1532	82.9									
	1.608 (FS-2)	6.62	3.14	1417	80.6									
002	1.140	5.82	3.39	1425	75.5	0.29	2450	1300	IT	P	20/250	S	--	Oxidizer flow measurement erratic at FS-2.
	1.575	5.96	3.27	1467	76.5									
	1.944 (FS-2)	SEE REMARKS		1378	76.6									
003	0.970	3.94	16.50	413	98.3		NO RECORDS					U	100	Ox. valve malfunctioned.
	1.140	3.70	16.06	454	99.0							S	--	
	1.495	4.06	13.01	452	90.1						20			
	1.577	3.15	16.14	462	94.1						40			
	1.693	3.97	17.44	445	104.5						80			
	2.001 (FS-2)	3.20	14.39	454	85.5									
004	0.996	5.92	3.47	2345	96.9	0.176	2500	1000	IT	P	20/1000	S	--	
	1.475	4.57	4.10	2395	80.1									
	1.596 (FS-2)	5.78	3.18	2494	79.4									
005	SEE REMARKS	4.88	26.37	456	172.0		NO RECORDS					S	--	Ox. valve malfunctioned. Average data used.
006	0.900	3.39	6.13	2285	102.5	0.176	2700	2000	IT	P	20/225	S	--	
	1.186	3.72	4.84	2302	78.5									
	1.245 (FS-2)	3.76	4.76	2221	77.8									
007	0.900	6.53	6.73	1221	143.5	0.177	SEE REMARKS					U	500	High frequency pressure instruments sustained damage; however, the data (wave forms) recorded were similar to the previous unstable tests.
	1.086	6.93	6.75	1419	167.8							U	750	
	1.462 (FS-2)	7.15	7.01	1317	175.4									

*P = pulsed, S = stable, Q = unstable

Table 1



Tangential Mode Acoustic Frequencies for Annular Chambers

Figure 1

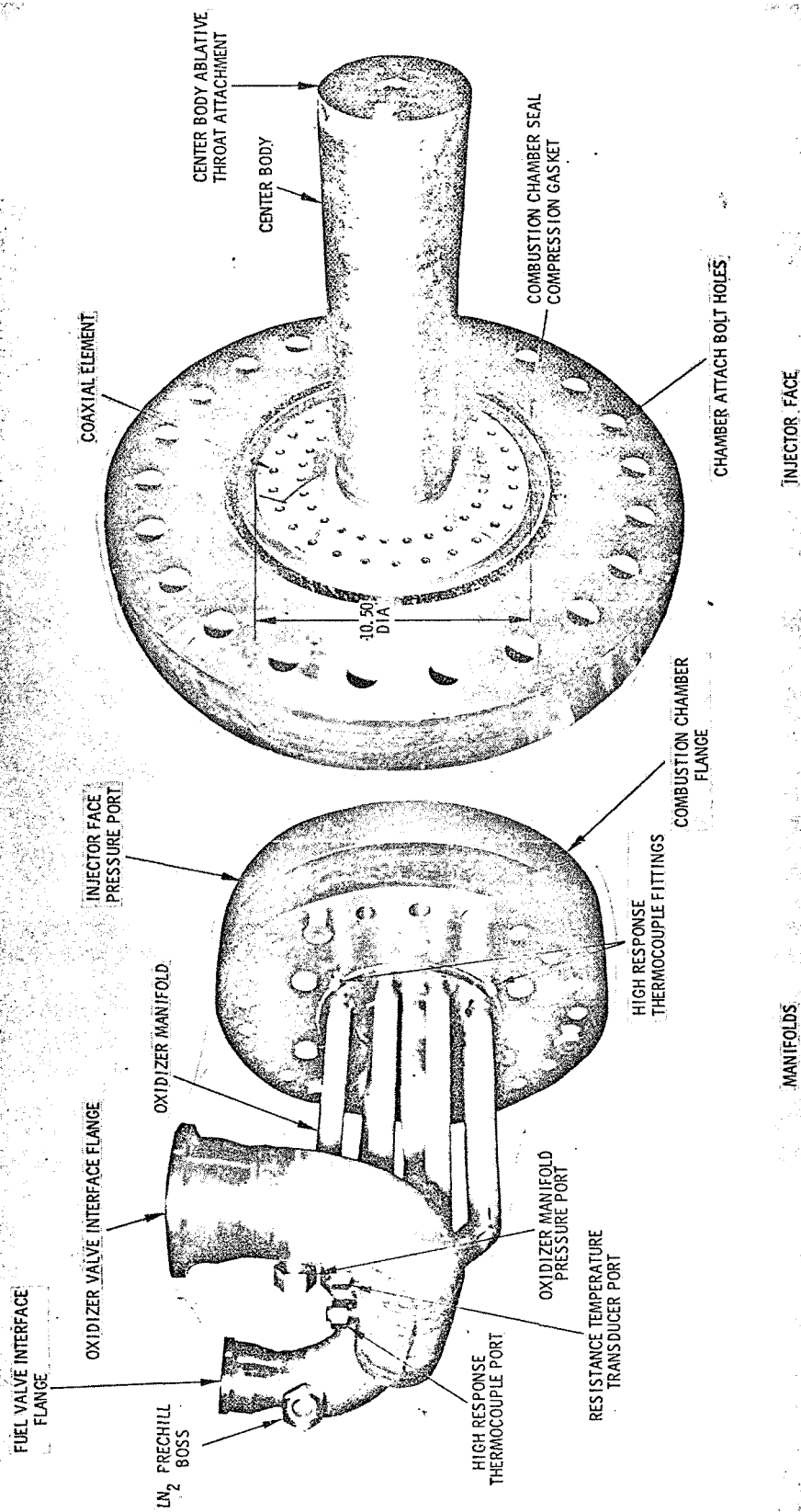


Figure 2

Annular Coaxial Injector

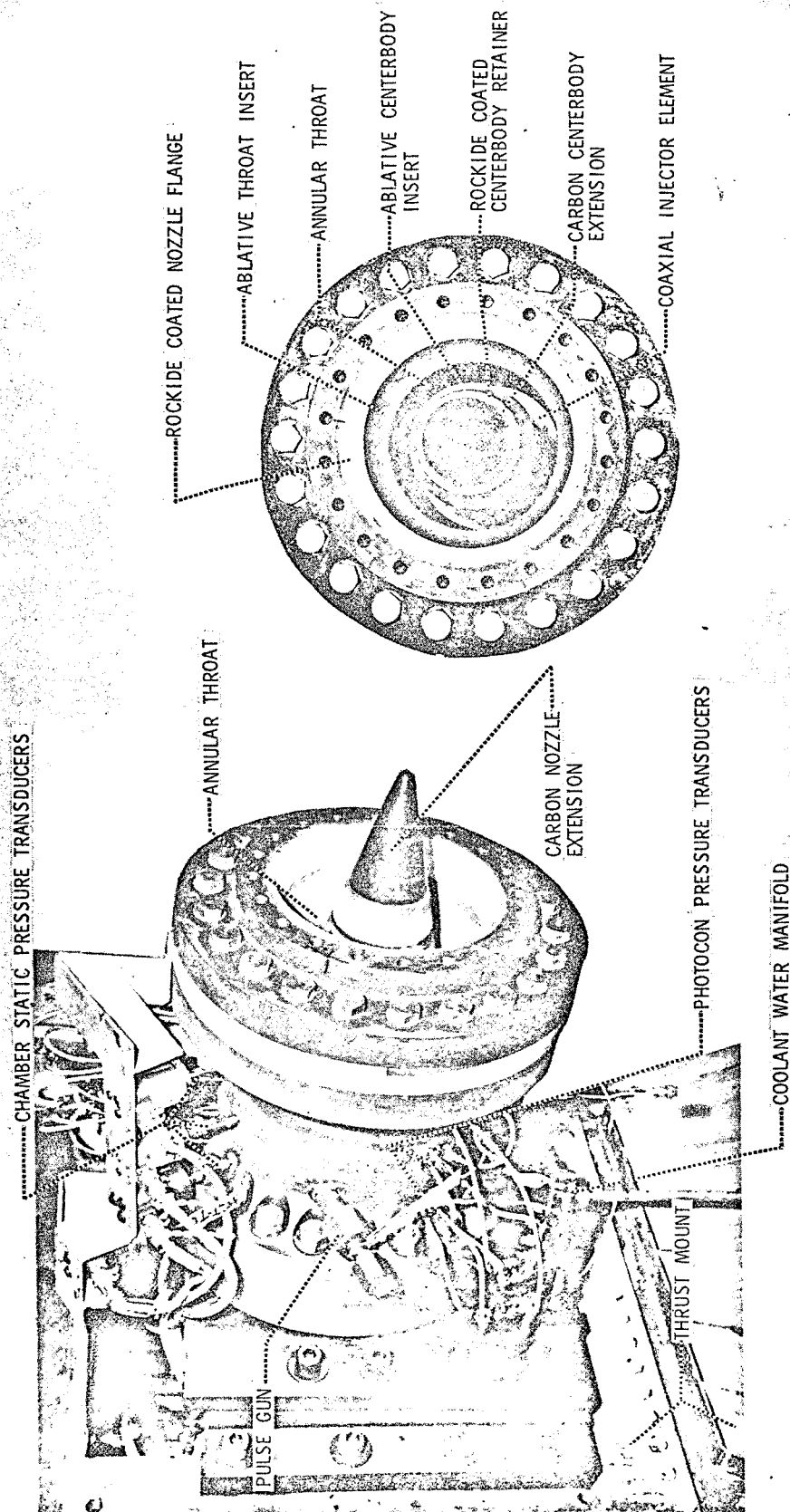
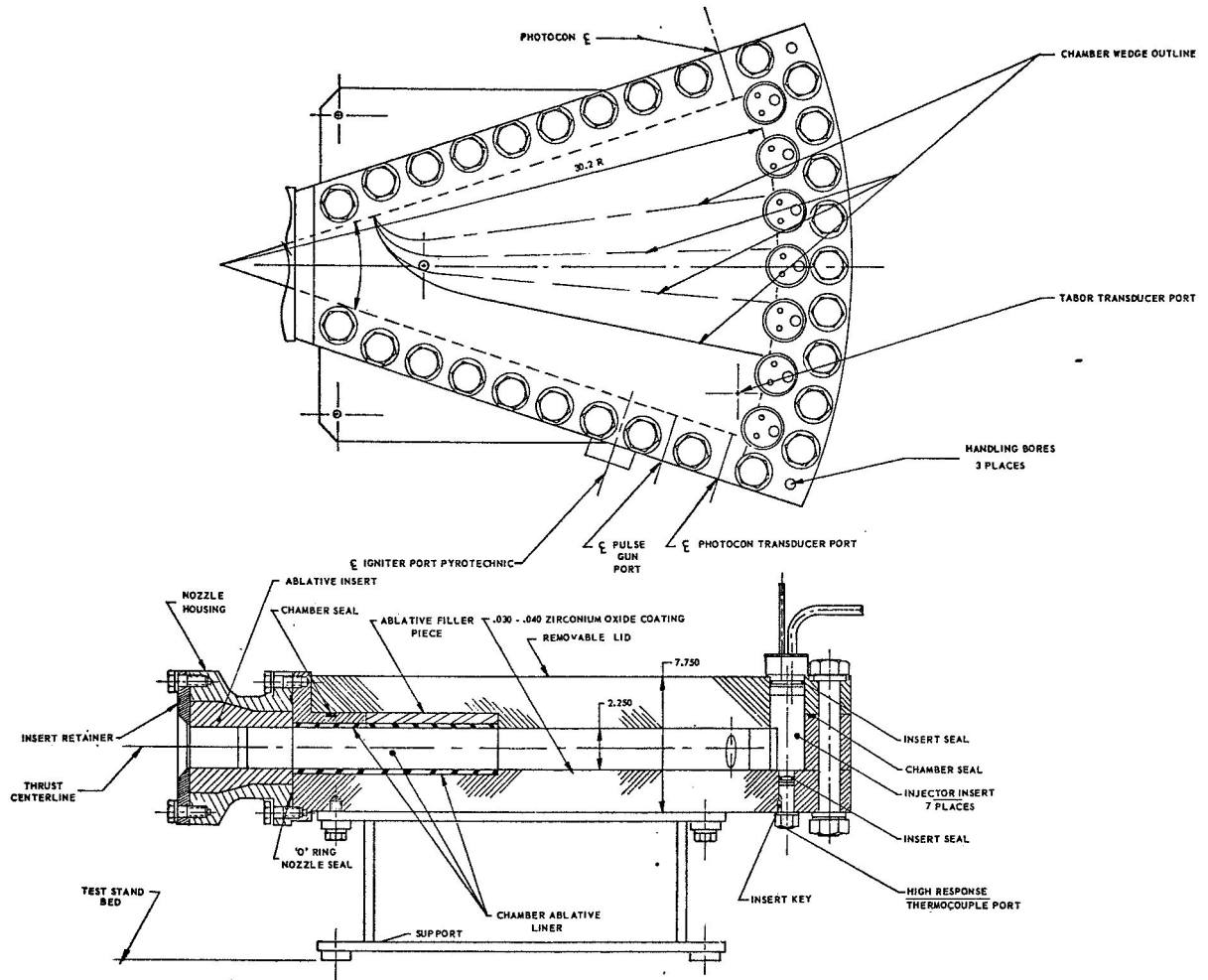


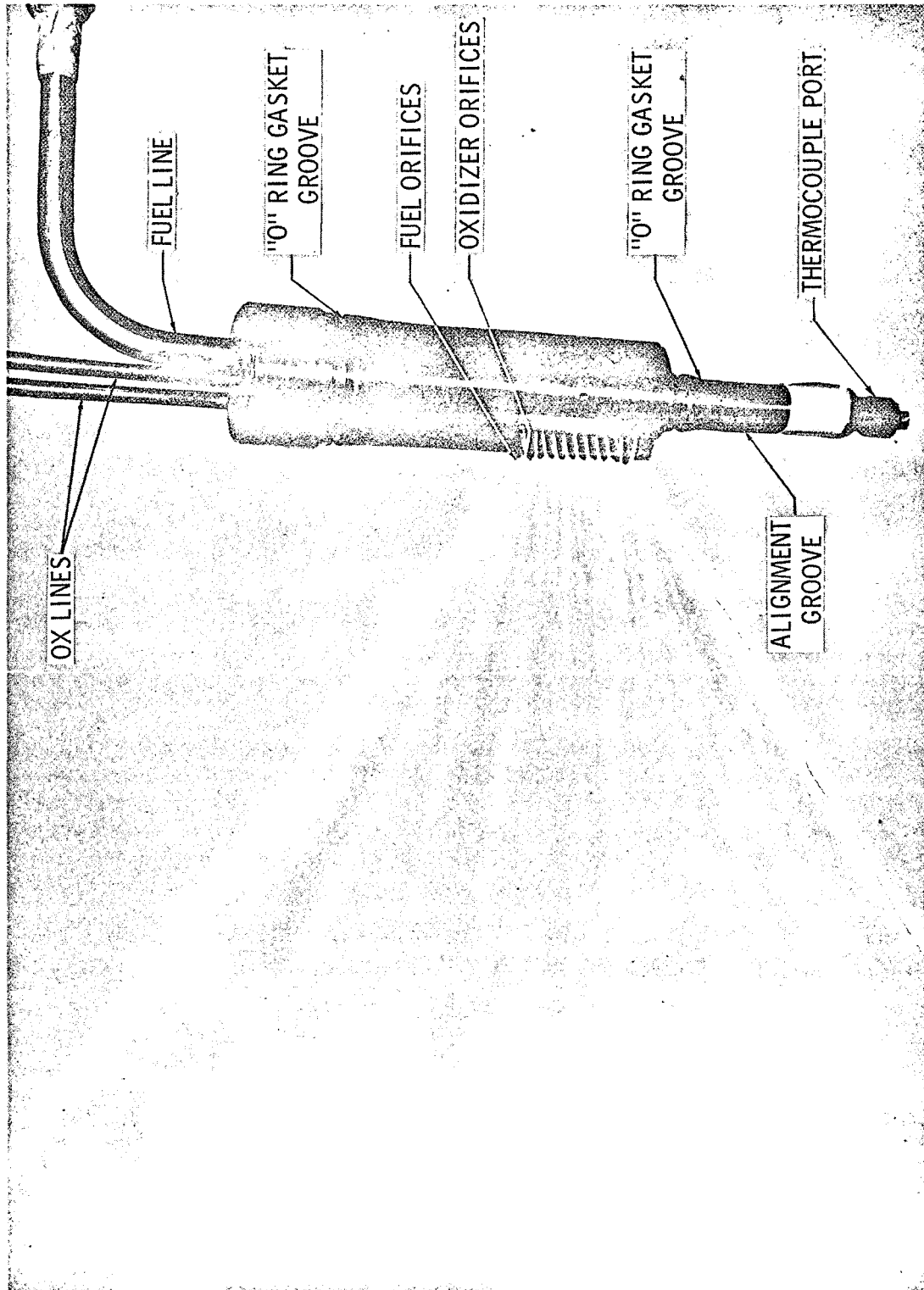
Figure 3

Annular Thrust Chamber Assembly on Test Stand C-6



Transverse Excitation Chamber Assembly Schematic

Figure 4



Transverse Excitation Chamber Triplet Injector Hydroflow Pattern

Figure 5